Formability and Springback Analysis of Aluminum/Polypropylene/Aluminum Sandwich Laminates

by

Caroline K Kella

A dissertation submitted in partial fulfillment
of the requirements for the degree of
Doctor of Philosophy
(Mechanical Science and Engineering)
in the University of Michigan - Dearborn
2022

Doctoral Committee:

Professor Pankaj K. Mallick, Chair
Associate Professor Jian Hu
Associate Professor German Reyes-Villanueva
Assistant Professor Lei Chen

Caroline Karishma Kella

ckkella@umich.edu

ORCID iD: 0000-0002-1474-0048

Dedication

This dissertation is dedicated to the loving memory of my mother.

I would also like to dedicate this dissertation to my husband for his unwavering support and encouragement without which this work would not have been possible.

Acknowledgements

I would like to express my deepest gratitude to my advisor Dr. Pankaj Mallick for his unwavering patience, motivation, and support. Dr. Mallick's guidance and insights helped me greatly in pursuing research and in writing this dissertation. I could not have asked for a better mentor for my doctoral studies, Thank you.

I would also like to thank my doctoral committee: Dr. German Reyes-Villanueva, Dr. Lei Chen and Dr. Jian Hu for their valuable time and advice.

I thank my fellow colleagues Kishore Reddy and Monish Ramakrishnan for the interesting discussions and brain storming sessions that made this research experience enriching.

I would like to thank the staff at UM-Dearborn and MSEL lab technicians for their prompt technical assistance. Thanks to Shawn Simone and Matthew Brown for their kind cooperation in carrying out the experimental work

Lastly, I would like to thank the rest of my family and friends who encouraged me to pursue my research interests.

Table of Contents

List of Tables

List of Figures

List of Appendices

Abstract

The advancement in vehicle fuel efficiency brings about an increasing need to develop lightweight materials of equal or better mechanical properties compared to those of traditionally used materials. To meet this need, hybrid materials are being developed in which two or more different materials are combined to produce better structural performance than the original material themselves. One such hybrid material is a sandwich laminate, which is made of two thin skins of a high modulus material, such as a steel or an aluminum alloy, and a low density core of a lower modulus material, such as a polymer. The application of metal/polymer/metal sandwich laminates results in increased flexural stiffness per unit weight, higher flexural strength, and in some cases, vibration and noise abatement. Because of these advantages, they are being considered for many automotive body panel and structure applications to achieve significant weight reduction. Although a few studies have been published on the mechanical properties and formability of metal/polymer/metal sandwich laminates, continued growth in usage of such materials requires additional knowledge of their formability, springback characteristics, and failure modes during press forming operations.

The objective of this research is to address the challenges of formability and springback of sandwich laminates made of aluminum skins and a polypropylene core with various thickness combinations. The effect of the polypropylene core on the formability of sandwich laminates is studied and compared to the formability of aluminum-aluminum laminates and monolithic aluminum sheets. The predicted forming limit curves are validated by comparing them to published experimental forming limit curves.

The springback behavior of aluminum/polypropylene/aluminum laminates after draw bending of a U-channel is studied. Various process parameters such as die and punch radius, friction and blank holder force are studied to understand their effect on springback behavior of sandwich laminates. For accurate prediction of springback by finite element method, simulation parameters such as model type, material models and number integration points are studied. The springback results predicted by simulation are validated by comparing them to experimental springback values. The residual stress distribution through the thickness of the sandwich laminate of different thickness combinations is also studied and compared with the stress distribution in a single aluminum sheet of equal thickness.

The various combinations of Al/PP/Al laminates studied in this research have lower weight than single aluminum sheets of equivalent bending stiffness. Their formability and springback are either equivalent or slightly lower than single aluminum sheets of equivalent thickness. For better formability and springback of the sandwich laminate, its core to skin thickness ratio can be adjusted, albeit with some sacrifice in weight savings.

Chapter 1 - Introduction

1.1 BACKGROUND

As the automotive industry continues to progress toward electric vehicles (EV), the need for new and unique material combinations that offer low weight along with suitable mechanical properties and crash resistance has accelerated. Since vehicles with internal combustion engines are going to remain on roads for the next few decades to come, there is also a more urgent need for reduced fuel consumption in order to protect the environment. To achieve the targeted fuel efficiency, the most effective way has proven to be reduction in vehicle weight by using lightweight materials [1]. According to a Massachusetts Institute of Technology (MIT) study published by Bandivadekar et al. [2], lighter materials can reduce fuel consumption, by about 7 % for every 10 % of reduced vehicle weight; thereby reducing the GHG (greenhouse gas) emissions.

Current materials for vehicle body construction are mostly steels and aluminum alloys. The future vehicles may include a combination of materials, such as sandwich laminates and hybrid materials of different types, since they can be designed to not only provide weight reduction, but also improvements in other features, such as reductions in vibrations and noise. A market analysis report on NVH (noise, vibration and harshness) reduction products is presented in Ref. [3]. As per this report, the trend of NVH material usage in the industry shows an increasing use of hybrid materials, including foam laminates, molded rubber, metal laminates and few others. This is because the focus of automotive manufacturers is leaning more towards noise control and acoustic management based on changing customer needs.

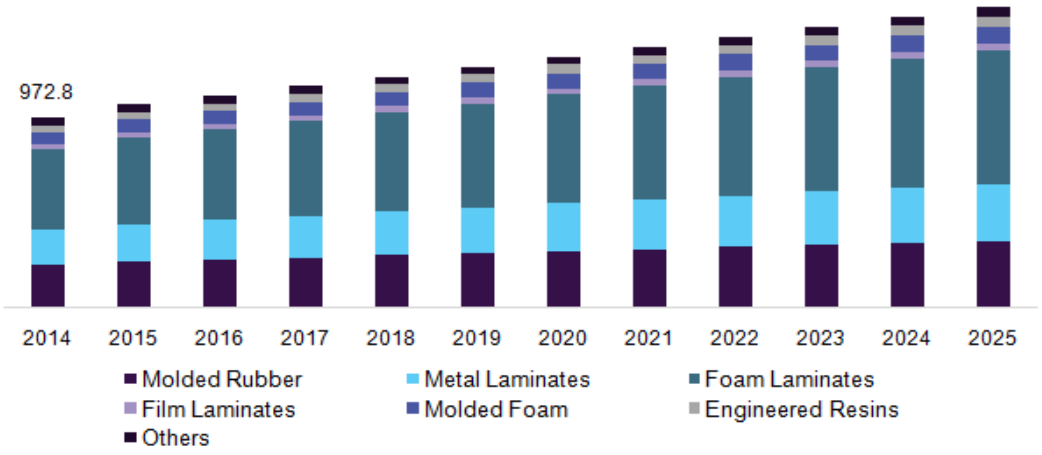

Figure 1.1: U.S automotive NVH materials market by product 2014-2025 **[3]**

Sandwich laminates belong to a class of hybrid materials in which two or more different materials are combined in a laminated form to achieve properties and structural performance that are superior to those of the materials being combined. One form of these sandwich laminates consists of three layers in which the skin layers are usually made of a high strength, high modulus material such as aluminum, steel or a fiber reinforced composite and the core layer is made of a low specific weight material such as a thermoplastic polymer, a corrugated sheet metal or a honeycomb structure (metallic or non-metallic) [4]. A reinforcement material, such as a metal mesh or glass fibers, may be used in the core to provide local strengthening of the material. Some of the metal components of a car that can be replaced with such sandwich structures are seat tub, seat-storage tub, wheelhouse, dash panel, cowl plenum, front and rear floor panels.

Sandwich laminates were known to be manufactured initially in 1924 using plywood and balsa [5]. Today there are several commercially available sandwich laminates, such as Hylite, ARALL, CARALL, Smart steel and GLARE, some of which are already being used in aircraft and automotive structural components. In most sandwich materials, the outer skins carry the tensile and compressive stresses, while the inner polymer layer transfers the shear stresses thus preventing

buckling. High weight saving capabilities of metal/polymer/metal sandwich laminates prove their usefulness in naval and aviation applications. A commercially available sandwich material, Hylite made of aluminum/polypropylene/aluminum, shows 30% weight reduction in comparison to monolithic aluminum and 65% weight reduction in comparison to traditional steel for the same stiffness [6]. High damping of vibrations is also achieved by shear deformation of the polymer core. GLARE, another sandwich laminate is used in the aviation industry due to its high damage tolerance and fire resistance [7]. Use of GLARE in the fuselage panels on the Airbus A380 has shown 30% weight reduction. A few of these laminates and their advantages are listed in Table 1.1

Table 1.1 : Composition and advantages of different sandwich materials

Sandwich Laminate	**Skin Material**	**Core Material**	**Primary advantage over the Core Material**
Hylite	Aluminum	Polypropylene	Improved stiffness
ARALL	Aluminum	Kevlar fiber/epoxy composite	Improved fracture resistance
CARALL	Aluminum	Carbon fiber/epoxy composite	Improved fracture resistance
Smart steel	Low carbon steel	Viscoelastic	Improved vibration response
GLARE	Aluminum	Glass fiber/epoxy composite	Improved fracture resistance
Bondal	Steel	Polyolefin	Improved sound damping

In general, metal/polymer/metal sandwich laminates have higher flexural stiffness to weight ratio due to the skins being separated by the core thickness. Among them are aluminum/polypropylene/aluminum laminates and steel/polypropylene/steel laminates that have

found applications in body panels, such as hoods, trunks, and dashboards, where their improved stiffness to weight ratio has contributed to significant weight reduction. In effect, such sandwich laminates can be modelled as wide-flanged I-beams in which the skins act as flanges and resist the bending load and the core acting as the web resists the shear deformation. The flexural stiffness and flexural stiffness-to-density ratio of the laminates can be represented by the following equations.

$$\text{Flexural stiffness} \approx \frac{\boldsymbol{btd^2E_s}}{\mathbf{2}} \qquad \text{Eq. 1.1}$$

$$\text{Flexural stiffness-to-weight ratio} = \left(\frac{\boldsymbol{E_s}}{\boldsymbol{\rho_s}}\right)\boldsymbol{d} \qquad \text{Eq. 1.2}$$

where, E_s is the modulus of the skin material, ρ_s is its density of the skin material, b and t are the skin width and skin thickness, respectively, and d is the core thickness. Equations 1.1 and 1.2 show that the presence of the core in the laminate increases its flexural stiffness as well as flexural stiffness-to-weight ratio. Furthermore, the overall material performance index for flexural stiffness $\frac{E^{\frac{1}{3}}}{\rho}$ is higher for the sandwich laminate compared to the skin material. Other advantages of metal/polymer/metal sandwich laminates over the skin material are their high strength-to-weight ratio, superior vibration and sound damping, thermal insulation, and crash energy absorption.

Roll bonding is the most common manufacturing process for producing metal/polymer/metal laminates. In this process, a stack of two layers of the skin material and a layer of the polymer core is pulled through a set of rollers (Figure 1.2) where the skins and the core are bonded together to form a continuous laminated sheet. Since weak bonding between the skins and the core may lead to delamination, their surfaces are carefully prepared before stacking. The surface preparation may include surface cleaning, chemical surface treatment, and application

of thin adhesive layers. In addition, preheating the skins and the core before they enter the space between the rollers, or the use of heated rollers may be required to improve bonding. If an adhesive is used, the rollers must be heated to cure the adhesive. The pressure from the rollers during roll bonding causes the core layer to penetrate through the microscopic surface pores and microcracks normally present on the metal skins to further increase the bonding between them. Some adhesives, such as epoxy, become brittle after curing and result in reduced formability of the entire sandwich panel. For sandwiches produced by warm roll bonding, thermoplastic polymers are better for forming as they become soft and easily formable when heated. Roll bonding may result in thickness reduction of 40%-75%, which alters the mechanical properties of the individual materials because of cold work, and also increases the density of the sandwich. However, bond strength may increase with greater thickness reduction due to increase in contact pressure [8].

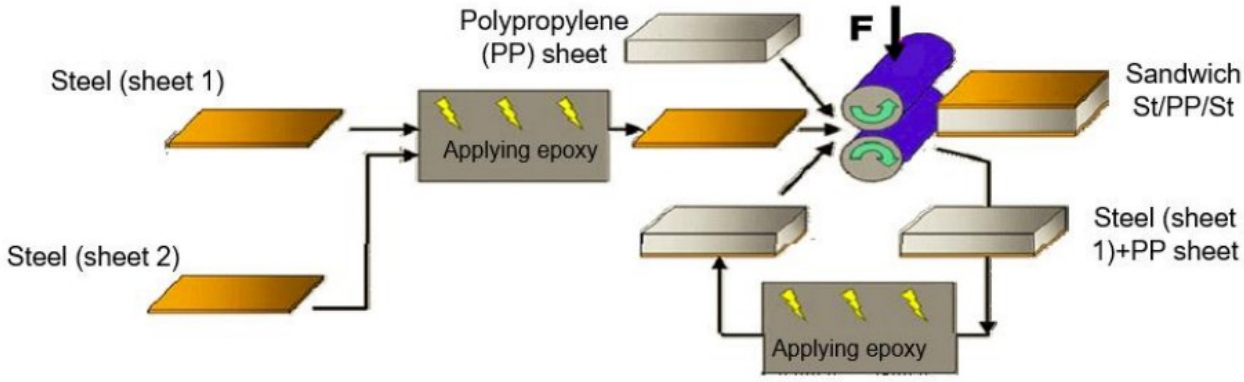

Figure 1.2: Roll bonding process for making metal/polymer/metal laminates [4]

One major concern in the application of metal/polymer/metal sandwiches is the possibility of delamination at the interfaces between the skins and the core material. The resistance to delamination depends on the strength of the bond between them. One test for determining the bond strength between the layers is the T-peel test (Figure 1.3) in which one end of the sandwich

is pulled while the other end remains fixed. The peel strength (α_s) is measured as the ratio of the average pulling load (P) to the bond width (w), $\alpha_s = \frac{P}{w}$ [6] . Surface roughness also plays an important role to assist good bonding between the metal skins and polymer layer. Higher surface roughness results in better bonding, while a very rough surface can result in poor permeability and void formation.

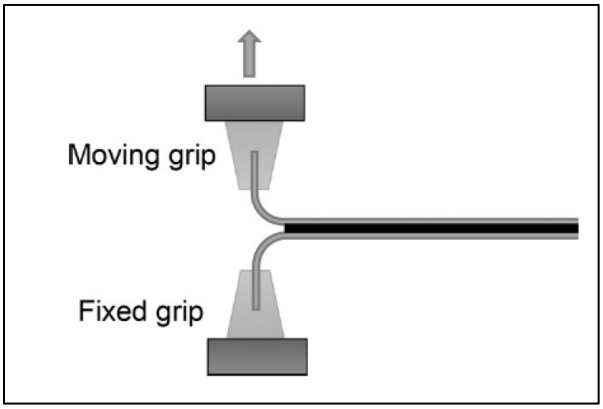

Figure 1.3: T-peel test setup for determining bond strength between the polymer core and metal skins in a metal/polymer/metal laminate **[6]**

The production of automotive body panels and structural components using metal/polymer/metal sandwich laminates requires the knowledge of their formability in stamping operations. Forming behavior of sandwich laminates has been studied by using the Erichsen Index, or by determining the forming limit curves using the Nakazima test or other experimental test methods. In a comparative study between monolithic stainless steel (AISI SS316L) and its corresponding sandwich material (AISI SS316L/PP–PE/AISI SS316L), a near equal measure of formability was achieved [9]. In a study by Somayajulu [10] to determine the forming limit curves for aluminum/polypropylene/aluminum and monolithic aluminum, it was shown that the sandwich laminate had a higher forming limit in some cases. However, in this study, the sandwich material was considerably greater in thickness compared to the monolithic aluminum sheets.

The stamped parts, which in many cases may have intricate deep-drawn or stretch-bent shapes, must be produced with tight dimensional tolerances, minimal wrinkles, low surface defects and no splits. The large difference in mechanical properties of the skin and the core materials may result in multiple forming issues and types of failure that are not observed in stamping monolithic steels and aluminum alloys. These failure modes may include delamination at the skin-core interfaces, fracture within the polymer core, wrinkling of skin layers, etc. Fracture in monolithic steels and aluminum alloys is observed through the entire thickness, whereas in sandwich materials the crack propagation is resisted by the presence of the core polymer.

Liu and Xue [11] showed that the rule of mixtures can be applied to metal/polymer/metal laminates to determine the mechanical properties of the sandwich material as they were in good agreement with the mechanical properties attained by experiment. In Ref. [12], the properties of a steel/polymer/steel sandwich were experimentally determined by conducting tensile tests using digital image correlation (DIC) to obtain the data, since the polymer core shows strain localization. The material properties were obtained for two skin thicknesses (0.49 and 0.24 mm) combined with core thicknesses of 0.2, 0.3, 0.6, 1 and 2 mm. The experimentally determined drawing force was compared to the drawing forces obtained by analytical and numerical solutions. With increasing core thickness, the mechanical properties of the sandwich laminate proportionally decreased. Normal anisotropy (r) and strain hardening exponent (n) decreased with increasing core thickness. The study proves the validity of the rule of mixtures (ROM) for sandwich panels, by comparing the ROM curves with those of the curves obtained by experiments. Increasing core thickness did not increase the strain to failure, indicating that the core layer does not have a strong influence in forming. The tensile properties for aluminum/polypropylene/aluminum sandwich laminates have been tested by Shin et al. [1]. The yield strength and ultimate tensile strength lie between the

respective values of the skin (Aluminum) and core (polypropylene). The sandwich laminates show improved total elongation (%) in comparison to the aluminum sheet.

Successful application of sandwich laminates requires a clear understanding of the choice of material combinations, layer thicknesses and interface conditions that influence the forming and springback characteristics of such laminates. In-depth knowledge of these sandwich laminates in manufacturing complex shapes is required if they are to be used on large-scale, high-volume applications such as in the automotive industry. The proposed research focuses on studying, validating and developing the numerical solutions for formability and springback for metal/polymer/metal laminates.

In this research, the forming behavior of a metal-polymer-metal laminate made of AA5182 aluminum skins and a polypropylene core is considered. AA5182 has good formability coupled with high corrosion resistance, and most importantly, high weight saving capabilities. It is one of the aluminum alloys used in automobile body structure components. The thermoplastic core, polypropylene, is fairly inexpensive in comparison to other polymers, has a good balance of modulus and strength, and is not moisture sensitive. Its melting point is between 165 and 170^{o}C, and it is mechanically stable up to 145^{o}C, a temperature close to that used in paint baking ovens. Although the properties and mechanical behavior of monolithic materials are well known, the behavior of sandwich laminates as a system may be very different under similar loading conditions.

1.2 OBJECTIVES

The objective of this dissertation is to perform a numerical study on the forming behavior of aluminum/polypropylene/aluminum (Al/PP/Al) sandwich laminates comprised of AA5182 aluminum skins and a thermoplastic polypropylene core. Forming behavior includes formability, springback and residual stress patterns generated after springback. Another objective of this study

is to determine influence of design, material and process parameters on the forming behavior of the Al/PP/Al laminates. Among these parameters are core thickness, skin thickness, aluminum skin properties, blank holder force, die and punch radius, etc. Different thickness combinations of the skin and core layers are considered. Formability is characterized by forming limit curves and springback is characterized by the change in shape of U-channels after draw-bending. The accuracy of predicted forming limit curves and springback by finite element analysis is evaluated in comparison to experiments.

1.3 METHODOLOGY

Figure 1.4 shows a flow chart describing the methodology used in this research. The formability study is conducted by simulating the forming behavior of the Al/PP/Al laminates in Nakazima formability tests. The springback and residual stress studies are conducted by simulating the draw-bending operation to form U-channels following Numisheet‘93 recommendations. All simulations are performed using LS-DYNA, a non-linear finite element software commonly used for structural and manufacturing process analysis of metals, polymers and composites. Different computational parameters such as material models, through-thickness integration points and model types are studied and compared to the experiments to provide the optimal parameters for accurate predictions of springback of Al/PP/Al laminates. Some process parameters such as punch and die radius, die-punch gap, blank holder force, friction and their influence on the springback of Al/PP/Al laminates along with how they differ from that of monolithic metal counterparts is reported.

Finite element analysis is performed to first understand the formability and springback of single layer aluminum AA5182 alloy, followed by adding a polypropylene layer between two aluminum skins and gradually increasing the core thickness to skin thickness ratio. Two different

AA5182 aluminum skins are considered, an annealed soft skin and a cold-worked hard skin. Variations in the thickness of the polymer layer and skin layers and their effects on formability and springback and residual stresses are studied. The finite element models include modelling the laminate as a composite material as well as modelling each layer individually assuming perfect bonding between each laminate layer.

In the final phase of the research, experiments were conducted to draw-bend Al/PP/Al sandwich laminate panels into U-channels by the process described in Numisheet '93 to measure springback and sidewall curl. The results of the computational models are validated against those obtained from experiments. The results of this research are used to draw inferences on how the current models can be extended for use in industry for more complex scenarios.

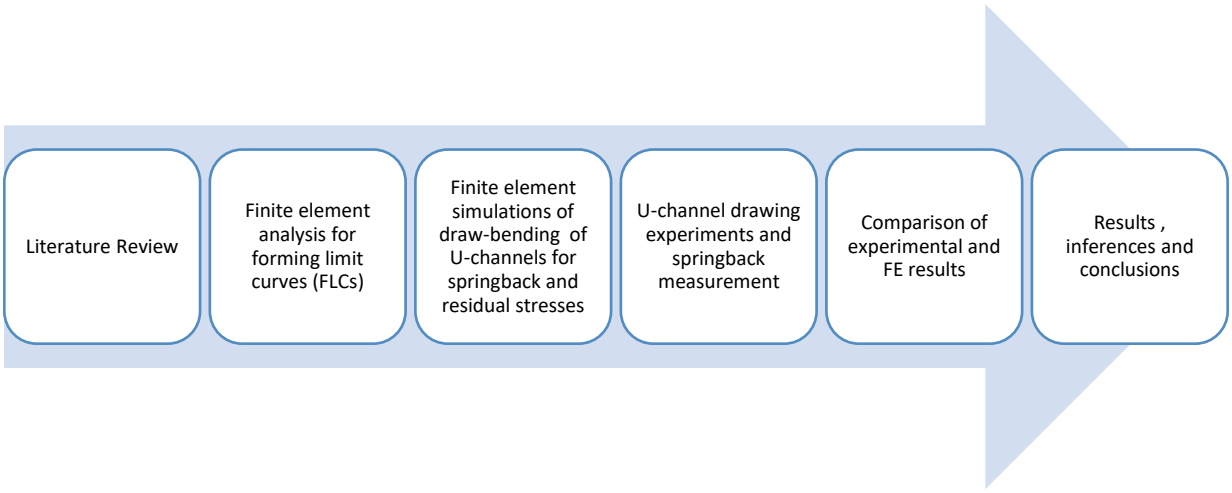

Figure 1.4: Flow chart describing the research methodology

1.4 Chapter Distribution

The dissertation is divided into the following chapters.

- Chapter 2: This chapter presents a review of the existing literature on formability and springback of sheet materials. Some of the different methods of numerically and

theoretically determining forming limit curves for steel and aluminum materials are summarized. In addition, a brief summary of the various procedures for measuring and quantifying springback of metals is also presented.

- Chapter 3: Formability analysis of AA5182, AA5182/AA5182 laminates, and AA5182/polypropylene/AA5182 laminates is presented in this chapter. A finite element analysis process for determining forming limit curves for single aluminum sheets, two layered Al/Al laminates and Al/PP/Al laminates is developed. The predicted FLCs are validated by published experimental data. A comparison between the different laminate configurations and their effect on limit strains is made and conclusions are drawn on the role of the polypropylene core on formability.
- Chapter 4: In this chapter, springback of sandwich laminates at the end of a draw-bending process to form U-channels is studied. A comparison between the springback behavior of single aluminum sheets and sandwich laminates of equivalent thickness are made. The finite element model is validated by experimental work. A study on several computational and process parameters and their effect on springback behavior of Al/PP/Al sandwich laminates is conducted.
- Chapter 5: This chapter focuses on the residual stress distributions through the thickness of U-channels upon elastic recovery (springback) after the draw-bending force is released. It also includes the forming stress distributions induced by the draw-bending process. The stress distributions are determined at different locations of the formed part along with their variations with different sandwich thickness combinations, punch radius and die radius. The residual stresses of Al/PP/Al laminates are compared to the residual stresses of monolithic aluminum AA5182.

- Chapter 6: Conclusions. Based on the results of the numerical and experimental work conducted in Chapters 3, 4 and 5, a summary of drawn inferences as well as the scope for future work is presented in this chapter.

1.5 REFERENCES

[1] K. S. Shin, K. J. Kim, S.W. Choi and M. H. Rhee, "Mechanical properties of Aluminum/Polypropylene/Aluminum sandwich sheets," *Metals and Materials,* vol. 5, no. 6, pp. 613-618, 1999.

[2] A. Bandivadekar, K. Bodek, L. Cheah, C. Evans, T. Groode, J. Heywood, E. Kasseris, M. Kromer and M. Weiss, "On the road in 2035 : Reducing transportation's petroleum consumption and GHGs emissions," Massachusetts Institute of Technology, 2008.

[3] Grand View Research, "Automotive Noise, Vibration & Harshness Materials Market Size, Share & Trends Analysis Report By Product (Molded Rubber, Metal, Foam & Film Laminates, Molded Foam, Engineering Resins) By Application, By End-use, & Segment Forecasts, 2018 - 2025," https://www.grandviewresearch.com/industry-analysis/automotive-nvh-materials-market/segmentation.

[4] L. Librescu and T. Hause, "Recent developments in the modeling and behavior of advanced sandwich constructions: a survey," *Composite Structures,* vol. 48, no. 1-3, pp. 1-17, 2000.

[5] B. Castanie, C. Bouvet and M. Ginot, "Review of composite sandwich structure in aeronautic applications," *Composites Part C: Open Access,* 2020. https://www.sciencedirect.com/science/article/pii/S2666682020300049

[6] F. Federico, "Lightweight metal/polymer/metal sandwich composites for automotive applications," M.S. Thesis, University of Windsor, Windsor, 2017.

[7] H. Palkowski and G. Lange, "Creation of Tailored High-Strength, Hybrid Sandwich Structures," *Advanced Materials Research,* vol. 22, pp. 27-36, 2007.

[8] S. Mousa, "Roll bonding of metal-polymer-metal sandwich," Ph.D. Dissertaion, Iowa State University, 2017.

[9] H. Palkowski, O. A. Sokolova and A. Carrad`o, "Sandwich Materials," in *Encyclopedia of Automotive Engineering*, John Wiley and Sons, 2015, pp. 3183-3200.

[10] T. S. Somayajulu, "Vibration and formability characteristics of aluminum-polymer sandwich materials," D.Eng. Dissertation, University of Michigan, 2004.

[11] G.-J. liu and W.Xue, "Formability of AA5052/polyethylene/AA5052 sandwich sheets," *Transactions of Nonferrous Metals Society of China,* vol. 23, no. 4, pp. 964-969, April 2013.

[12] M. Harhash, R. Rogin, S. Hartmann and H. Palkowski, "Experimental characterization , analytical and numerical investigations of metal / polymer / metal sandwich composites – Part 1 : Deep drawing," *Composite Structures,* vol. 202, no. June, pp. 1308-1321, 2018.

Chapter 2 - Literature Review

Formability and springback are the two major manufacturing issues in the production of sheet metal parts with fewer forming defects and high dimensional accuracy. Both these topics have been studied experimentally, analytically, and numerically because of their importance to the metal forming industry. Many of these studies have been done with low carbon steels; however, because of greater use of advanced high strength steels, such as dual phase (DP) steels, and aluminum alloys, studies on their formability and springback are also appearing in literature. Comparatively, there are only a few studies on the same topics related to metal/polymer /metal laminates. In this chapter, existing literature on different approaches to determine the formability of sheet metals are briefly summarized. There are numerous ways to quantify formability and springback. A few of those methods and some standardized procedures are explained. The best practices in determining springback of monolithic materials are compared.

2.1 FORMABILITY

2.1.1 Experimental methods to determine formability of metals

Formability of a sheet metal is defined as its ability to undergo plastic deformation without failure. Banabic [1] divided the methods of determining formability into four classes: (1) methods based on mechanical tests, (2) methods of limiting dome height and (3) methods based on forming limit diagrams, and (4) methods based on simulations. An early mechanical test for measuring formability is called the Erichsen test which is performed by stretching a 90 mm blank with a 20 mm diameter spherical punch (Figure 2.1). The depth of punch indentation just before fracture,

called the Erichsen index (IE), is considered a measure of formability. This test is not considered very accurate as the specimen is not firmly held in place and the blank size is very small.

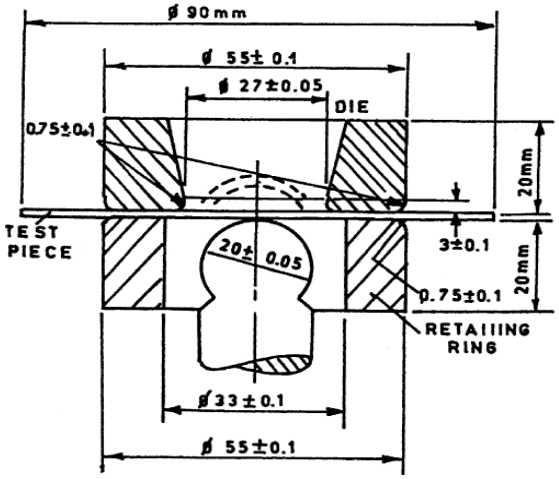

Figure 2.1: Experimental setup for Erichsen test [1]

Hecker [2] established a similar method with different tool dimensions and lubrication to overcome the inaccuracy of formability index measured by the Erichsen method. Hecker's test consists of a hemispherical punch and blanks that are much larger than those used in Erichsen test. His test also includes a lock bead to firmly hold the blank in place. The formability measure in Hecker's test is similar to that in the Erichsen test, which is the depth of punch penetration just before fracture.

To further improve the measure of formability, Ghosh [3] developed the limiting dome height (LDH) test in which rectangular blanks of different widths are clamped firmly over lock beads and stretched using a hemispherical punch of 101.6 mm in diameter. The blanks are gridded with 2.54 mm diameter circles that become deformed when they are stretch formed. Minor strains at failure are calculated from the changes in dimeters of these circles in the necked or fractured area of the blanks. The dome height at the maximum load is plotted against the minor strain at

failure to represent the formability limit. An example of the specimen dimensions used for LDH test is shown in Figure 2.2.

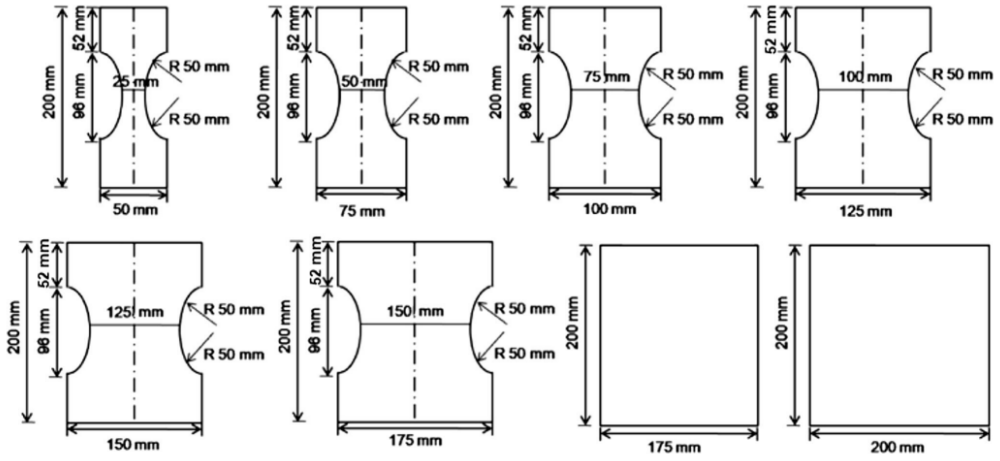

Figure 2.2: Dimensions of the specimens for LDH test [4]

The forming limit diagram (FLD) or forming limit curve (FLC), is most commonly used in sheet metal forming for predicting forming behavior of sheet metals. FLD is defined in Ref. [5] as a graphical representation of the limit strains up to which a sheet metal can be formed in different modes of deformation. As shown in Figure 2.3, it is plotted between two in-plane principal strains (usually referred to as major and minor strains) measured or calculated on the surfaces of the formed part. For successful forming of any sheet metal part, the strain states on the part are expected to be in the safe forming region as indicated in Figure 2.3. Several sheet metal products were formed successfully by using the FLC as a measure of formability. Hence, the forming limit diagram (FLD) is the most used method of evaluation of formability.

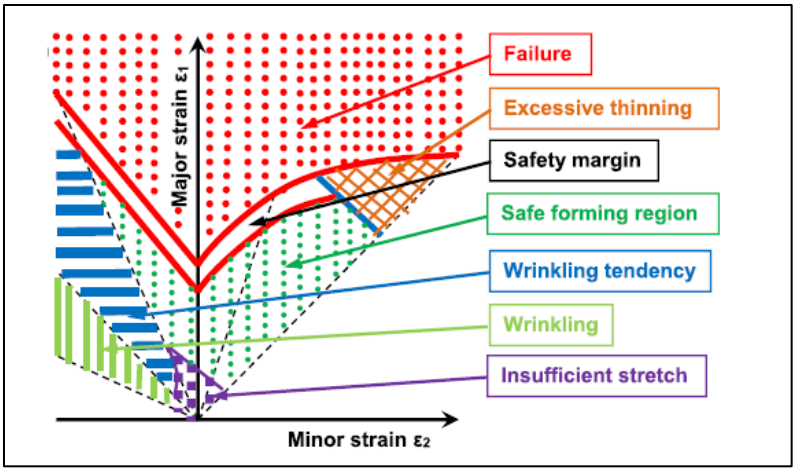

Figure 2.3: Typical forming limit diagram with different defect zones [6]

The forming limit diagram can be determined experimentally by several different test methods. Uniaxial tension tests conducted on specimens of different widths and different shapes can be used to determine the negative side of the FLC (minor strain $\varepsilon_2 < 0$) and hydraulic bulge tests with varying dimensions of elliptic dome shapes can be used to attain different strain paths on the positive side of FLC (minor strain $\varepsilon_2 > 0$). There are other methods used to determine the forming limit diagram. One method was by Keeler [7] and Goodwin [8], which is based on the determination of principal strains by measuring the strains at failure using sheet metal parts with circular grids marked on them. The circular grids deform into ellipses at the end of the forming process. Their major and minor dimensions are measured and compared with the diameter of the initial circular grids to determine the maximum principal strains. Keeler's method can be used to obtain major-minor strain curve in biaxial stretching of the sheet specimens where $\varepsilon_1 > 0$ and $\varepsilon_2 > 0$ and forms the tension-tension region of the forming limit curve. Goodwin obtained the curve on the tension-compression region where $\varepsilon_1 > 0$ and $\varepsilon_2 < 0$ using tensile specimens of different widths and thicknesses. Together the two curves constitute the forming limit diagram. Figure 2.4 shows

the different strain paths that can be attained by varying either the specimen dimensions or the punch diameter.

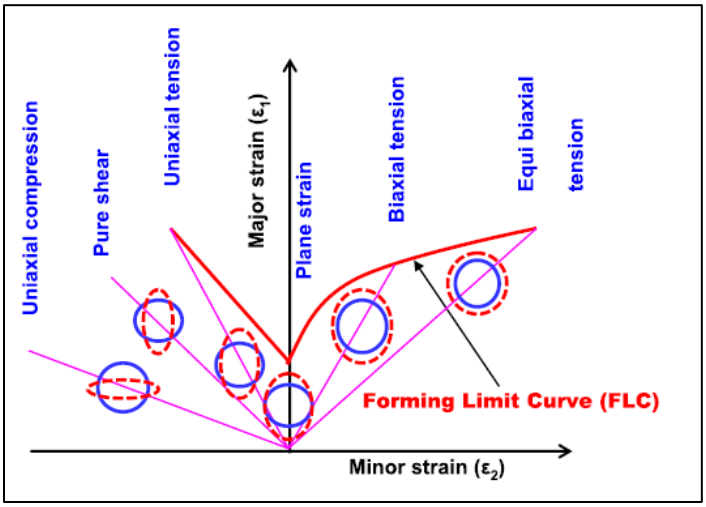

Figure 2.4: Different strain states on the forming limit diagram [6]

The Nakazima test (Figure 2.5) is an out-of-plane bend-stretching test and uses a hemispherical punch to carry out the experiments on flat sheet specimens required to plot the necessary forming limit diagrams. Specimens of varying widths as shown in Figure 2.6 are used to attain different strain paths.

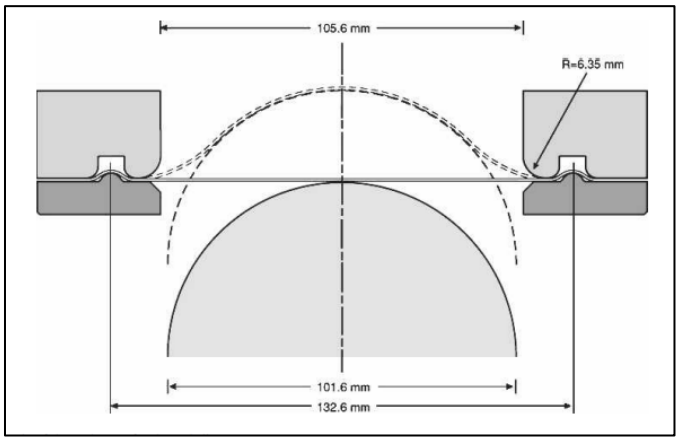

Figure 2.5: Nakazima tool setup and dimensions [9]

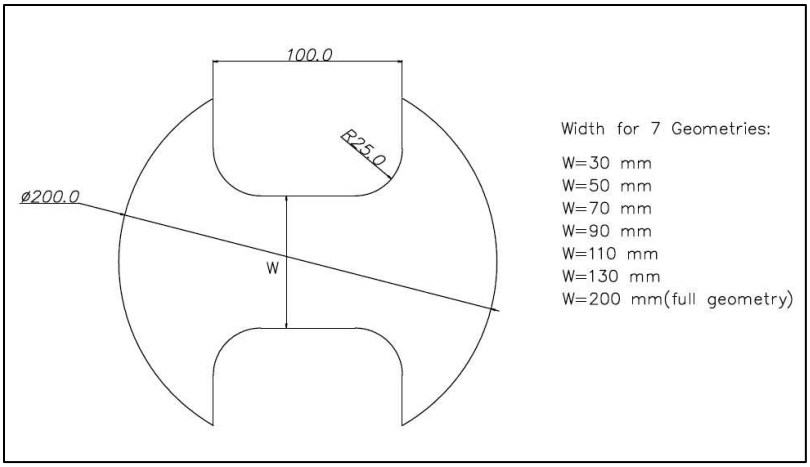

Figure 2.6: Nakazima blank specimen dimensions [10]

Marciniak test also known as in-plane test uses a flat-bottomed hollow circular punch to draw cups as shown in Figure 2.7. In this test, a carrier blank with a circular hole is used between the punch and the sheet blank to reduce the possibility of tearing in the cup wall near the bottom of the cup. Rectangular, circular, and elliptic blanks of different cross-sectional dimensions are used to obtain different strain paths. Zhu and Gang [11] stated that this test is sensitive to internal defects in materials that can cause premature failure, and therefore it must be conducted with care to attain reliable results. In comparing the FLCs determined by Marciniak and Nakazima tests, Huang and Shi [12] concluded that thickness of the sheet has a greater effect on FLCs determined by the Nakazima method when compared to the FLCs determined by the Marciniak method.

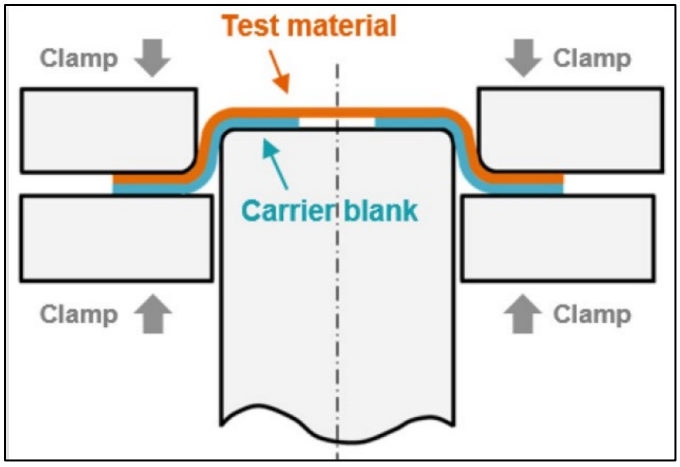

Figure 2.7: Marciniak deep drawing test set up to determine FLC [12]

2.1.2 Methods to determine forming limit curves using finite element method

The numerical determination of FLC is based on the evolution of strains with time [13]. Finite element programs are used to simulate deep drawing or punch stretching experiments with varying blank sizes to attain different strain paths. These blank shapes allow to capture uniaxial, plane stain, pure shear, and biaxial strain states.

As the circle grid method is more cumbersome to use in numerical simulation, a few different methods were proposed to numerically determine the FLC of a material using finite element software. A study is conducted by Li et al. [14] to numerically determine the forming limit curve of AA5182-O for a 1 mm thick sheet. First the elements that show localized necking are identified. Then the elements near the necked elements are studied to identify the behavior of major (ε_1) and minor (ε_2) strains. Elements that showed constant ε_1 and ε_2 after necking as shown in Figure 2.8 are used to define the limit strains. This study also shows that as the friction condition changes the area where necking occurs moves away from the pole.

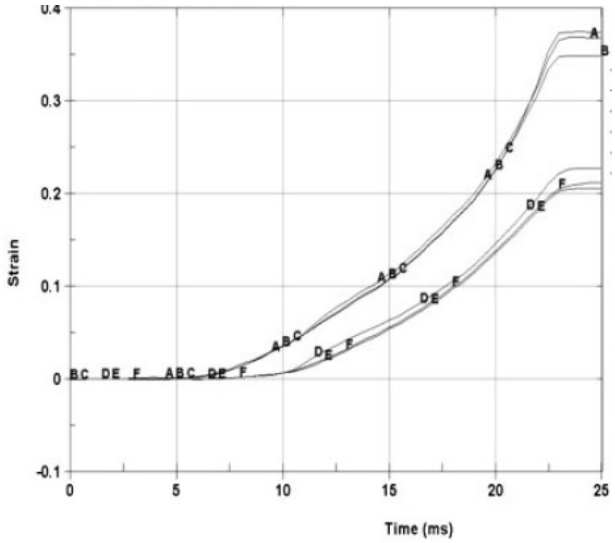

Figure 2.8: Plot of major and minor strain history for un-necked elements [14]

Hashemi et al. [15] studied different methods to determine the onset of necking using hemispherical die stretching methods for low carbon steels. The SDM criterion or second derivative of the major strain criteria identifies the major strain paths of elements over the duration of the simulation and is studied to identify the point of inflection. This point indicates the onset of necking and the major and minor strains at that point are used as forming limits. The SDT criterion uses the acceleration or second time derivative of the thickness strain to identify the point of necking. Lastly, the PEEQ method uses the second derivative of effective plastic strain history to identify the onset of necking. The FLCs determined using all three methods are compared and show no difference (Figure 2.9).

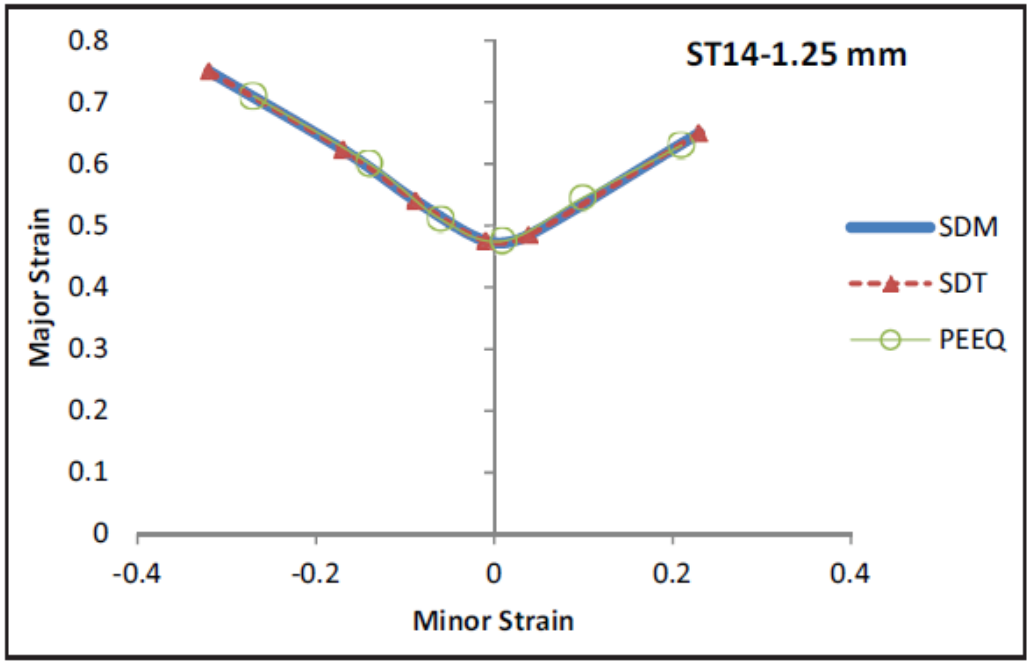

Figure 2.9: FLCs obtained by SDT, SDM and PEEQ necking criteria [15]

A review on the factors controlling the forming limit curves by Paul [6] shows that nonlinear strain paths were seen when a hemispherical punch from the Nakazima test method, when compared to the linear strain paths obtained using the flat-bottomed punch in Marciniak. Material properties such as strain hardening exponent, coefficient of anisotropy and total elongation are shown to have a linear relationship with the FLC_0 (plane strain). The study also shows that formability improves with increasing temperature and decreasing strain rate.

Strain path non-linearity was also addressed by Zhang et al. [16]. The strain paths obtained by using low friction condition (high lubrication) and high friction (dry lubrication) are compared. It is concluded that friction condition has significant influence on the location of fracture while it has a small effect on the linearity of the strain path.

The effect of friction on the FLC for two different steels is studied in Ref. [17] , it was concluded that changing friction does not have a strong influence on the left-hand side of the FLD

(ε_2 <0) while the right-hand side of the FLC changes from balanced biaxial strain path to a plane strain path as friction increased.

Habibi et al. [18] included the M-K model in the Nakazima test (out-of-plane test) method using finite element simulation to determine the forming limit curve. This is done by including a groove or defect region in the uniaxial stretch specimen at different angles. Localized necking was defined as the point where the strain in the grove area was 10 times more than the strain in the safe area. The study concludes that without the inclusion of bending effect, the predicted FLC would be far from the experimental FLD.

The effect of isotropic and kinematic hardening models on sheet metal formability was studied by Butuc et al. [19] for DC06 steel without changing yield criteria (Barlat 2000). Swift law and Voce law with and without kinematic hardening are compared. The right side of the FLD was not affected by the selection of hardening law. The Swift law with and without kinematic hardening over predicts the left side of the FLC and the Voce law with and without kinematic hardening under predicts the FLCs. These models were also compared with a microstructural hardening model which predicted results closest to the experiment.

2.1.3 Theoretical determination of forming limit curves

There are several theoretical models to determine FLCs for monolithic sheet metals, some of which are discussed in this section. Swift's model for determining FLC follows the Considere´ criteria which states that necking occurs when the strain is equal to the strain hardening exponent ($\varepsilon = n$) for a material that follows the Ludwik- Holloman strain hardening law, $\sigma = K\varepsilon^n$. The limit strains were found by analyzing a sheet loaded in perpendicular directions.

Hill's localized instability theory suggests that necking occurs in the direction of zero elongation (i.e., sheet thinning is responsible for necking) [1] . The limit strains for Hill's model are calculated using Equations 2.1 and 2.2

$$\boldsymbol{\varepsilon_1^*} = \frac{\frac{\partial f}{\partial \sigma_1}}{\frac{\partial f}{\partial \sigma_1}+\frac{\partial f}{\partial \sigma_2}}\boldsymbol{n} \qquad \text{Eq 2.1}$$

$$\boldsymbol{\varepsilon_2^*} = \frac{\frac{\partial f}{\partial \sigma_2}}{\frac{\partial f}{\partial \sigma_1}+\frac{\partial f}{\partial \sigma_2}}\boldsymbol{n} \qquad \text{Eq 2.2}$$

This model only depends on the hardening coefficient of the material.

Another theoretical model to determine FLD is the Marciniak and Kuczynski (M-K) [20] model. This model represents the non – homogeneity of the specimen by a structural defect in the form of a groove, in the direction of zero-elongation. The model is characterized by an imperfection ratio (*f*), which is the ratio of the thickness of the uniform region (A) to the thickness of the groove region (B) as depicted in Figure 2.10. When the strain ratio of the two areas is very high then a localized necking occurs in region B.

$$\boldsymbol{f} = \frac{\boldsymbol{t_A}}{\boldsymbol{t_B}} \qquad \text{Eq 2.3}$$

By applying a force balance to the two thickness regions and using a suitable yield criterion, the limit strains are attained when the strain in region A is insignificant in comparison to the strain in region B. The strain paths are varied by changing the inclination of the structural defect from 0° to 90°. By assuming the homogeneity of a sandwich panel and attaining the material constants through rule of mixtures, these theories can be extended to obtain FLCs for metal/polymer/metal sandwiches.

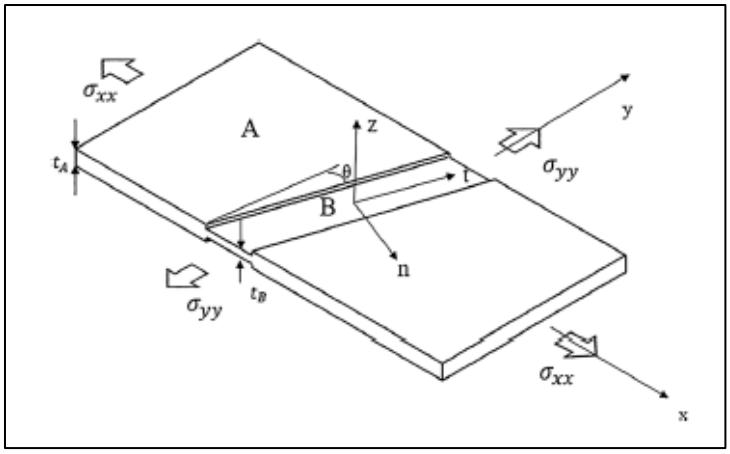

Figure 2.10: M-K Model Specimen [13]

In a study by Chen et al. [21] the formability of AA5182 was determined by using the M-K model with three different yield criteria – Barlat 1989, Yld200 and Hill's 1948. The study shows that the FLCs obtained from using Barlat 1989 model and Yld2000 model are in strong agreement with the experimental data. It was also concluded that the increase in formability due to the increase in strain hardening exponent is negligible for aluminum alloys.

The prediction of forming limit curves for monolithic metals has been comprehensively understood but their behavior when combined with other materials to form hybrid materials requires more extensive studying, which is the aim of this research.

2.2 SPRINGBACK

Springback is a deviation from the designed shape that occurs in a formed part due to elastic recovery after the forming force is removed and is measured as a change in angle or other dimensional deviations. Figure 2.11 shows the recovery of elastic strain that causes springback for a specimen is loaded up to an arbitrary point A (beyond the yield strength of the material) and then unloaded. The elastic recovery causes the final part to deviate from the desired part dimensions and often leads to problems in assembly and secondary forming operations such as trimming or flanging. Based on the complexity of the formed geometry, process parameters, material

properties, type of lubrication and tolerance requirements, it can often be difficult to control this phenomenon. Theoretically, simple solutions derived from mechanics of materials can be used to calculate this angle of deviation. However, since most stamped parts are complex, more advanced numerical solutions are required. For monolithic materials under pure bending, a simple solution can predict quite accurately, the angle of elastic recovery, based on residual stress calculation.

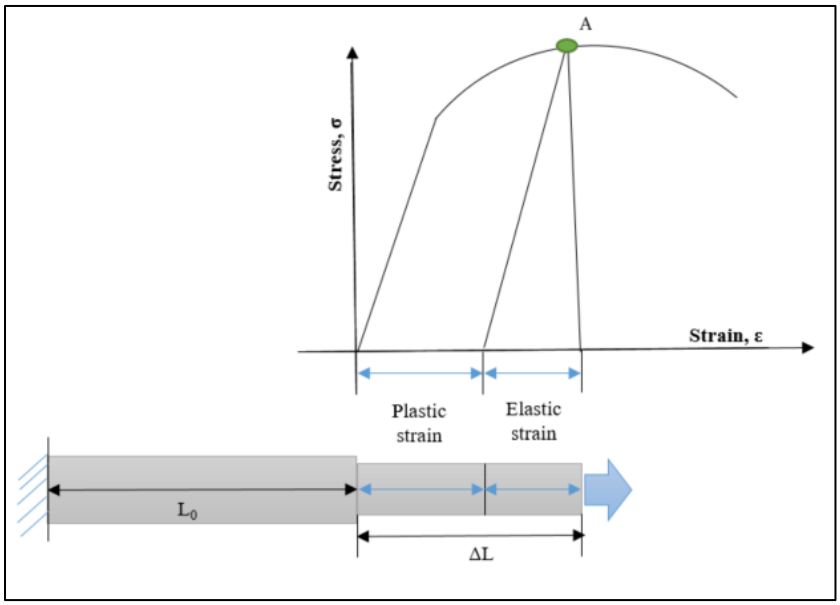

Figure 2.11: Elastic recovery in a specimen loaded beyond the yield point

In metals, this phenomenon has been studied for several years and is treated by a method of compensation or by increasing tension during bending (stretch-bending). Compensation is a method of cutting the tools by the amount of measured springback to achieve a final part within the accepted tolerance. Compensation can be expensive and result in multiple recuts and is mainly dependent on the accuracy of springback measurement. Hence, the goal is often to understand the causes and influencing factors to reduce springback during the manufacturing process instead of dealing with it after the final part is formed. Stretch bending or tension-superposed forming can result in reducing the stress differential between the inner and outer layers thus causing a lower and more controllable springback angle [22].

2.2.1 Computational parameters influencing springback

Accurate prediction of springback using numerical analysis leads to less re-cuts in die tryout and prototyping, which leads to material savings that further leads to reduced cost and cycle time. Several computational factors such as material models, through-thickness integration, element formulation, type of analysis (implicit/explicit), forming parameters, and friction models can strongly influence the final results of measured springback as shown in Ref. [23].

In Ref. [24], Wagoner et al. reviewed the influence of plastic constitutive equations, variable Young's modulus, through-thickness integration, and different material models on springback. Hardening model determines how the material strain hardens as plastic strain increases, while yield criteria describes the increment of plastic strain when yielding occurs. It has been proved repeatedly that both these models must be chosen appropriately based on the material being used, the number of bending/unbending cycles and availability of accurate model parameters. Inclusion of Bauschinger effect in the simulation of forming and especially springback is shown to be important by Gau and Kinsel [25]. The final stress state can be significantly different if pure isotropic hardening is assumed, which in turn influences the calculation of residual stresses, thereby modifying the springback angle. For complex forming simulations, the direction of strain path changes along with total plastic strain strongly influence the calculation of springback. In Figure 2.12, it can be seen that, the two-surface hardening model (Yoshida-Uemori model) shows strong agreement with experimental results while the model with pure isotropic hardening and pure kinematic hardening shows maximum deviation.

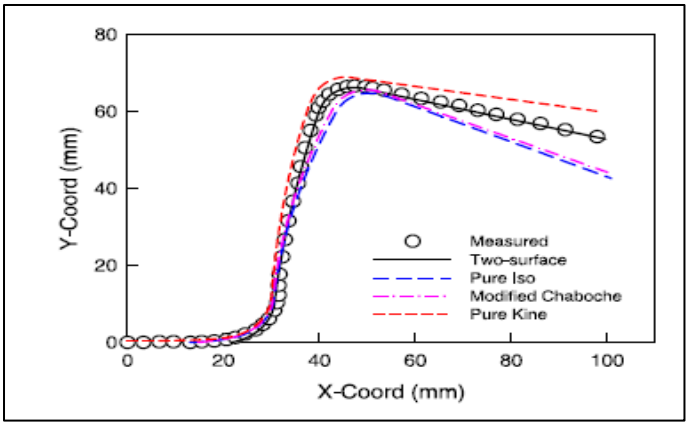

Figure 2.12: Springback based on type of hardening models [25]

From simple isotropic yield criteria (Von Mises) to very complex and repeatedly revised Hill and Barlat models are available to represent yield surfaces. In a study by Hou et al. [26], the three anisotropic yield criteria, Hill48, Barlat89 and Barlat2000 are compared in FE simulation to the experimental yield loci of AHSS (DP980) obtained through biaxial tension tests. The Barlat2000 model gives the most accurate representation of the yield surface especially for larger plastic strain ranges (Figure 2.13). In that same study results show that for smaller die radius, the springback values predicted are least accurate when simple isotropic hardening is used with less complex yield criteria (Hill 48) and the predictions are much closer to experiments when Barlat 2000 is used with Y-U hardening model.

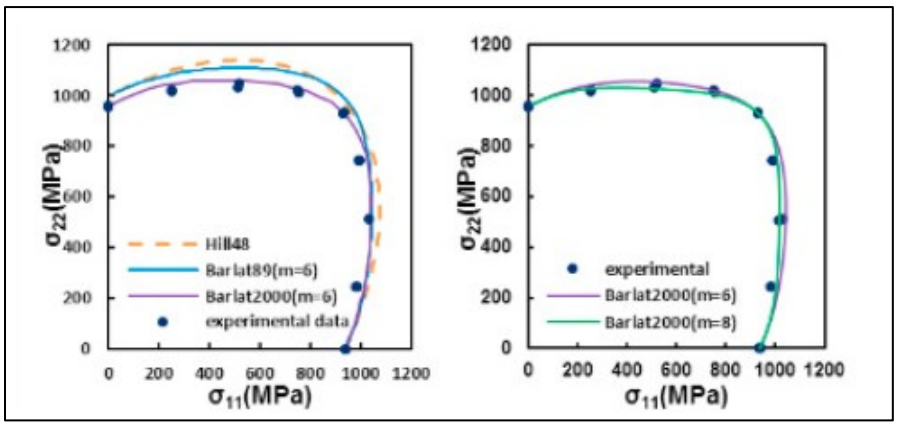

Figure 2.13: Yield Surface developed with different yield criteria [26]

Other simulation parameters such as minimum number of integration points through the thickness have been debated on, in the past 25 integration points were recommended around the year 2002 by Wagoner et al. [24] , however commercial software today recommends using 7-9 points based on the thickness of the material to accurately capture stress

Some of the other computational parameters to be checked for better springback predictions are, mesh refinement around tight radii, good aspect ratio for the mesh and artificial mass scaling to reduce run time. The fully integrated element formulation is recommended for forming and springback in LS-DYNA finite element software by Maker and Zhu [27] .

Sheet forming is treated as a quasi-static process since the effects of acceleration are negligible. An implicit or explicit analysis can be used for forming, however most research uses explicit time integration scheme for forming simulations as it is computationally less expensive and can produce equally accurate results when the time step size is calculated logically. In the research conducted by Jock et al. [28] springback of a simple U-drawing for DP780 is simulated with both explicit and implicit methods in ABAQUS finite element software, while the forming process is run with dynamic explicit solution. The results obtained however do not show much difference as can be seen in Figure 2.14. However, this was attributed to the particular software solution used as well as the hardening model that has been newly implemented in this particular study.

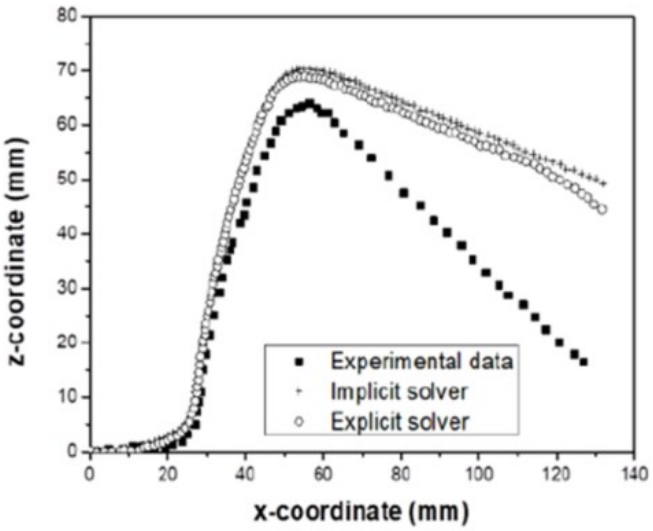

Figure 2.14: Springback results for explicit and implicit solver [28]

Since springback is a purely static process, presently several researchers recommend the use of one step implicit solutions for simple parts. While more complex parts can use multi-step implicit solution for non-linear springback.

2.2.2 Analytical solutions for springback

Analytical solutions for springback of monolithic steel and aluminum has been studied over several years. Although the challenge in forming new types of DP steels and TRIP steels continue to pose problems to the industry, research has been successfully implemented to obtain solutions to a great extent.

An equation to predict springback by Gardiner [29] for a material under pure bending was given in 1957. This equation assumes that the material is elastic-perfectly plastic, and the neutral axis is located at the midthickness of the sheet. The strain distribution is also assumed to be linear and is proportional to the distance from the neutral axis.

$$K_s = \frac{R_i}{R_f} = 4\left(\frac{R_i * \sigma_0}{E' * \mathbf{t}}\right)^3 - 3\left(\frac{R_i * \sigma_0}{E' * \mathbf{t}}\right) + 1 \qquad \text{Eq 2.4}$$

In Equation 2.4, R_i refers to the initial bend radius and R_f is the final radius after springback, as shown in Figure 2.15. σ_0 is the yield strength of the material , E' refers to the Young's modulus of the material in plane strain condition and t is the thickness of the sheet material.

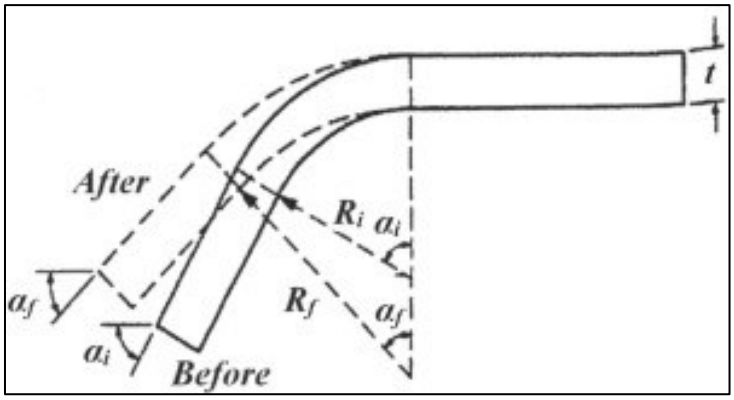

Figure 2.15 Springback after wiper die bending

Kumar et al. [30] provided a modification to Equation 2.4 by considering modified Ludwik stress-strain relation i.e. the material strain hardens and is no longer treated as perfectly plastic. Considering the equation for Young's modulus based on plane strain and along with strain hardening exponent (n) a more complex equation for springback is given in Equation 2.5,

$$K_s = \frac{R_i}{R_f} = 1 - \frac{3(1-\vartheta^2)}{(n+2)(\frac{3}{4})^{\frac{n+1}{2}}} \left(\frac{\sigma_0}{E}\right)\left(2\frac{R_i}{t_0}\right)^{(n-1)} \quad \text{Eq 2.5}$$

An analytical model for springback based on strains, contrary to the most commonly used bending theory, is proposed by Yi [31]. The model predicts springback angle based on the strain differential for the outer and inner layer of the beam and does not require knowledge of the stress distribution through the thickness.

$$SB = (\epsilon_l - \epsilon_u)/\epsilon_l \quad \text{Eq 2.6}$$

Equation 2.6 is a proposed solution where ϵ_l is the strain difference between the outer and inner surfaces when the specimen is loaded and ϵ_u is the strain difference when the specimen is in

unloaded condition. The strain values ϵ_l , ϵ_u are defined based on whether the inner and outer layers are both in elastic state, plastic state or one in elastic with the other layer in plastic state. This model is studied for mild steel, DP780, TRIP780 and an aluminum alloy for varying sheet thickness and die radii. The results show strong agreement with the springback prediction from the bending model for all cases considered, however it has not been validated by experiment. While this model has not yet been extended to sandwich panels, there may be a loss of accuracy as the effect of the core polymer is overlooked.

2.2.3 Current practices in experimental analysis of springback

Different setups are used to model the forming and springback process experimentally. Commonly used experiments to measure springback are air bending, wipe-bending, V-bending, U-bending and cylindrical bending. Some of these are summarized in this section. The main difference is these methods is caused by the stress distribution induced through the thickness of the materials.

A draw-bend test developed by Carden [22] consists of a metal sheet placed over a fixed or free roller, while being displaced at a constant speed from one end and the other end is under an opposing constant force to allow a tension superposed on bending (Figure 2.16). Springback is measured as the angle change in the drawn sheet with load to the sheet without any applied load.

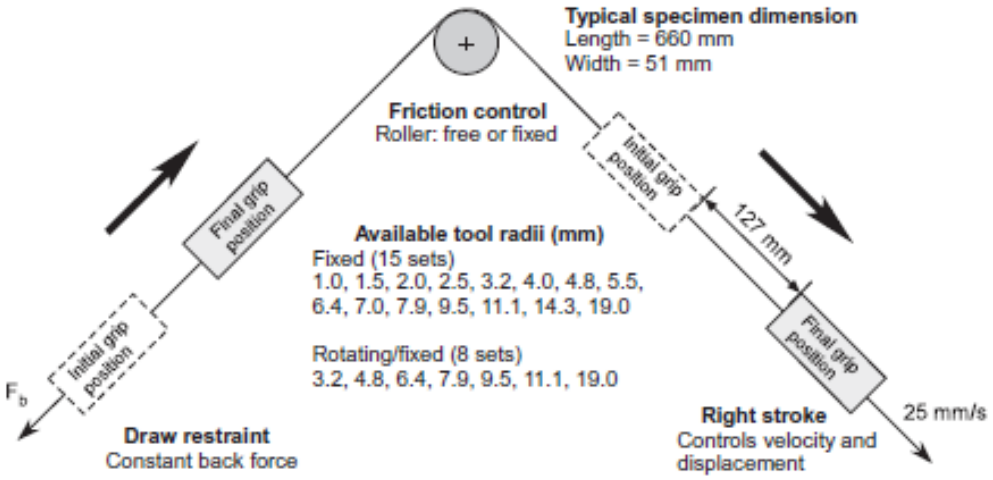

Figure 2.16: Draw-bend test setup [17]

The Numisheet '93 [32] benchmarking conducts experiments using a U-shaped lower die along with a blank holder holding the sheet at a recommended force depending on the material being drawn. The punch moves at constant velocity drawing the sheet into the U-cavity. At the end of forming, the forming load is released and springback is measured as the angle change along the side walls or flanges. A schematic of the setup is shown in Figure 2.17 (a).

Springback tests on formed shapes that are similar to industrial applications are also available. One example is the benchmarking set up in Numisheet 2005 [33] that uses the forming of a cross member using a three-piece die. Additionally, Numisheet 2014 [34] defines a test to measure the springback in AHSS and an aluminum alloy after a draw, restrike and trimming operation. It includes using a rectangular draw die (Figure 2.17 (b)) drawn to a particular depth with large tool radius first and then drawn by sharper tool radius to a greater depth in a restrike die setup. The final part is trimmed and springback is measured along the walls.

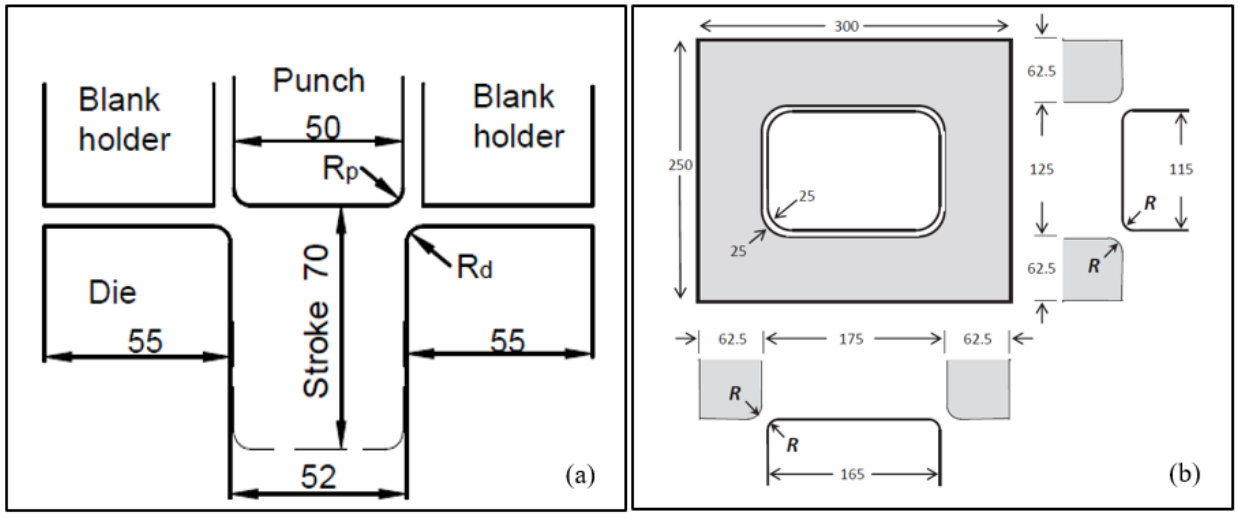

Figure 2.17: Schematic of the tool setup for springback measurement in (a) Numisheet 93 (b) Numisheet 2014

To measure the springback behavior in automotive panels the formed part is often placed on a fixture and is clamped in the locations of assembly, after which a go or no-go gauge indicates if springback is within the tolerance limits. Clamping locations can cause change in the springback angles and must be chosen carefully, in simulation these locations prevent rigid body rotations and translations. Several processing parameters influence springback phenomenon and its measurement experimentally. Some of them include blank holder force, type of drawbead, tool wear, type of lubrication, tool radius etc. These factors influence different materials differently**.**

In an experimental study of springback by Stein [35]**,** a channel part is used with constant die radius and binder tonnage. The rolling direction of the blank is placed perpendicular to the length of the channel. The springback is measured for different materials, DQSK (draw quality, special killed steel), bake hardened steel (BH33) and 6000 series aluminum alloy. Due to the lower elastic modulus of aluminum alloys a much greater springback affect is observed. By varying the sheet thickness for DQSK it was observed that the thicker sheet showed lesser springback. The study also concludes the altering the lubrication for the aluminum alloy affects the restraining force, which in turn influences the strain distribution causing a change in springback values.

From the literature reviewed in Section 2.2.2 it is evident that the material model used for finite element simulations is crucial in achieving accurate results or springback measurement. Therefore, this research explores four different material models available in commercial FE software, with different combinations of yield criteria and hardening rules. The theory, governing equations and assumptions behind each material model is briefly described in Section 2.3.

2.3 Description of Material Models Used in Finite Element Simulations

2.3.1 Hill 1948 yield criterion

Hill proposed a yield criterion for anisotropic materials assuming that the material has three orthogonal planes of symmetry, the yield surface is expressed as Equation 2.7.

$$2f(\sigma_{ij}) = F(\sigma_{22}-\sigma_{33})^2 + G(\sigma_{33}-\sigma_{11})^2 + H(\sigma_{11}-\sigma_{22})^2 + 2L\sigma_{23}^2 + 2M\sigma_{31}^2 + 2N\sigma_{12}^2 = 1 \qquad \text{Eq 2.7}$$

Here, 1 is parallel to the rolling direction of the sheet metal, 2 is parallel to the transverse direction and 3 is parallel to the normal direction. F, G, H, L, M and N are material constants related to the anisotropy of the material. F, G and H are defined as functions of tensile yield stresses in the directions of the principal axes of anisotropy, by the following relations.

$$\left.\begin{aligned} 2F &= \left(\frac{1}{\sigma_{y^2}} + \frac{1}{\sigma_{z^2}} - \frac{1}{\sigma_{x^2}}\right) \\ 2G &= \left(\frac{1}{\sigma_{Z^2}} + \frac{1}{\sigma_{X^2}} - \frac{1}{\sigma_{Y^2}}\right) \\ 2H &= \left(\frac{1}{\sigma_{X^2}} + \frac{1}{\sigma_{Y^2}} - \frac{1}{\sigma_{Z^2}}\right) \end{aligned}\right\} \qquad \text{Eq 2.8}$$

and L, M and N can be expressed in terms of the shear yield stresses (R, S, and T) in the directions of anisotropy,

$$\left.\begin{aligned} 2L &= \frac{1}{R^2} \\ 2M &= \frac{1}{S^2} \\ 2N &= \frac{1}{T^2} \end{aligned}\right\} \quad \text{Eq 2.9}$$

Equations 2.8 and 2.9 show that this yield criterion depends on three tensile yield stresses and three shear yield stresses of the material. Hill's yield model is widely used because all of its parameters have a physical meaning, and it has simple assumptions. Using the relationships between anisotropy coefficients and the parameters *F*, *G* and *H* in this model and assuming a plane stress condition for sheet metals, while the principal directions of the stress tensor coincide with the anisotropy axes, Equation 2.7 reduces to Equation 2.10.

$$\sigma_1^2 - \frac{2r_0}{1+r_0}\sigma_1\sigma_2 + \frac{r_0(1+r_{90})}{r_{90}(1+r_0)}\sigma_2^2 = \sigma_0^2 \quad \text{Eq 2.10}$$

In Equation 2.8, knowledge of only 3 mechanical parameters (r_0, r_{90} and σ_0) is necessary to define the yield condition.

2.3.2 Barlat 1989 yield criterion

This material model developed in 1989 by Barlat and Lian [36], also known as Barlat89, uses Lankford parameters to model the yielding behavior of materials with planar anisotropy under plane stress conditions. It is governed by Equation 2.11. It also assumes that the material follows an isotropic hardening rule so that its yield surface expands with increasing strain hardening with its center remaining fixed.

$$f = a\,|k_1 + k_2|^M + a|k_1 - k_2|^M + c|2k_2|^M = 2\sigma_e^M \quad \text{Eq 2.11}$$

where, f = yield function and,

$$k_1 = \frac{\sigma_{xx}+h\sigma_{yy}}{2} \quad \text{Eq 2.12}$$

$$k_2 = \sqrt{\left(\frac{\sigma_{xx}-h\sigma_{yy}}{2}\right)^2 + p\tau_{xy}^2} \quad \text{Eq 2.13}$$

where *a*, *c*, *h* and *p* are material parameters defined by Equations 2.14-2.16, *M* = exponent of Barlat's yield surface, and σ_e = yield strength of the material.

Barlat and Lian have shown that the material parameters *a*, *c*, *h* and p can be written in terms of Lankford parameters as shown below.

$$a = 2 - c = 2\left[1 - \sqrt{\left(\frac{R_0}{1+R_0}\right)\left(\frac{R_{90}}{1+R_{90}}\right)}\right] \quad \text{Eq 2.14}$$

$$h = \sqrt{\left(\frac{R_0}{1+R_0}\right)\left(\frac{R_{90}}{1+R_{90}}\right)} \quad \text{Eq 2.15}$$

The calculation of *p* is not straightforward and requires an iterative procedure using Equation 2.14 in which *g(p)* is a non-linear function of *p* and σ_{45} is the tensile stress on a specimen tested at a 45° angle to the rolling direction.

$$g(p) = \frac{2M\sigma_e^M}{\left(\frac{\partial f}{\partial \sigma_{xx}}+\frac{\partial f}{\partial \sigma_{yy}}\right)\sigma_{45}} - 1 - R_{45} \quad \text{Eq 2.16}$$

In Equations 2.14, 2.15 and 2.16, R_0, R_{45} and R_{90} are the Lankford parameters determined by conducting uniaxial tension tests in 0°, 45° and 90° directions to the rolling direction. Since *a* and *c* are related as shown in Equation 2.7, Barlat89 has only three independent parameters, namely *a*, *h,* and *p*.

Barlat89 is known to give better predictions of the yield behavior of aluminum alloys when compared to Hill48 and also contains fewer parameters to be determined [1]. They are the three

Lankford parameters, namely R_o, R_{45} and R_{90}, and the parameter M which is an exponent of the Barlat's yield surface. For aluminum, which is an FCC metal, the recommended value of M is 8. Barlat89 is limited in some ways, as the material parameters hold no significance as those in Hill48, and in some cases, cannot accurately predict biaxial yield stress.

2.3.3 Barlat 2000 yield criterion

Barlat 2000 yield criteria is a more complex criteria for anisotropic materials under plane stress conditions, described to overcome the shortcomings of Barlat 1989, 1991 and 1994 models. Examples of these shortcomings are inaccuracies in predicting biaxial stress values, blank earring in deep drawing, and difficulty of implementing numerical solutions because of complex calculations of equivalent stresses [1] .The improved yield function in Barlat 2000 is expressed by a combination of two isotropic functions,

$$\Phi = \Phi'(X') + \Phi''(X'') = 2\sigma^a \qquad \text{Eq 2.17}$$

$$\text{where, } \Phi' = |S1 - S2|^a$$

$$\Phi'' = |2S_2+S_1|^a + |2S_1+S_2|^a \qquad \text{Eq 2.18}$$

In Equations 2.17 and 2.18, S_1 and S_2 are principal deviatoric stresses, 'a' is the exponent controlling the shape of the yield surface based on the crystallographic (FCC/BCC) structure of the material. For aluminum alloys, the value of 'a' is generally assumed to be 8. X is the linearly transformed stress tensor (**X = C. s**,) and

$$X' = L'.\sigma \text{ And } X'' = L''.\sigma$$

where L' and L" are defined as,

$$\begin{bmatrix} L'_{11} \\ L'_{12} \\ L'_{21} \\ L'_{22} \\ L'_{66} \end{bmatrix} = \begin{bmatrix} 2/3 & 0 & 0 \\ -1/3 & 0 & 0 \\ 0 & -1/3 & 0 \\ 0 & 2/3 & 0 \\ 0 & 0 & 1 \end{bmatrix} \begin{bmatrix} \alpha 1 \\ \alpha 2 \\ \alpha 7 \end{bmatrix} \quad \text{Eq 2.19}$$

$$\begin{bmatrix} L''_{11} \\ L''_{12} \\ L''_{21} \\ L''_{22} \\ L''_{66} \end{bmatrix} = 1/9 \begin{bmatrix} -2 & 2 & 8 & -2 & 0 \\ 1 & -4 & -4 & 4 & 0 \\ 4 & -4 & -4 & 1 & 0 \\ -2 & 8 & 2 & -2 & 0 \\ 0 & 0 & 0 & 0 & 1 \end{bmatrix} \begin{bmatrix} \alpha 3 \\ \alpha 4 \\ \alpha 5 \\ \alpha 6 \\ \alpha 8 \end{bmatrix} \quad \text{Eq 2.20}$$

Barlat 2000 material model requires 8 coefficients, namely α_1, α_2, α_3, α_4, α_5, α_6, α_7 and α_8 to be determined by conducting uniaxial tension and biaxial tension-tension experiments. The properties required are 3 uniaxial yield stresses (σ_0, σ_{45}, and σ_{90}), 3 coefficients of uniaxial anisotropy (r_0, r_{45}, and r_{90}), biaxial yield stress σ_b and coefficient of biaxial anisotropy r_b.

2.3.4 Yoshida-Uemori hardening model

In the year 2002, Yoshida and Uemori [37] proposed a two-surface hardening model that describes the transient Bauschinger effect, work hardening stagnation and permanent softening effect. The Yoshida-Uemori model, henceforth referred to as Y-U model, can be easily implemented with any existing anisotropic yield criteria. The inner surface of the Y-U model represents kinematic hardening, and the outer bounding surface represents isotropic-kinematic hardening (Figure 2.18).

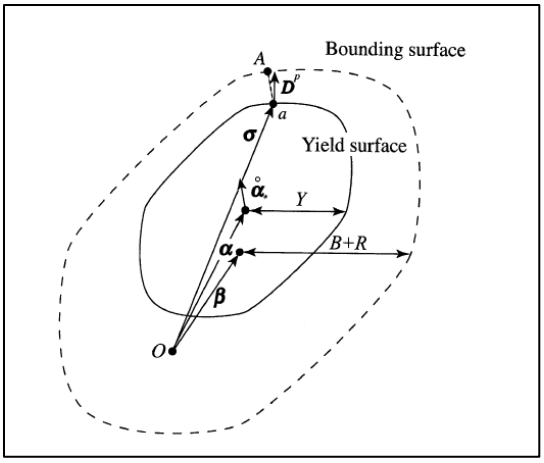

Figure 2.18: Yoshida-Uemori two-surface hardening model [37]

With the Y-U model, predicted forming limits and springback values are very close to the experimental results when compared with most other isotropic and kinematic hardening models [37]. The inner yield surface is given by Equation 2.21, where α denotes the back stress

$$f = \varphi(\sigma - \alpha) - Y = 0 \qquad \text{Eq 2.21}$$

and the equation of the outer bounding surface is expressed as,

$$F = \varphi(\sigma - \beta) - (B + R) = 0 \qquad \text{Eq 2.22}$$

where, β is the center of the bounding surface, B is the initial size and R is the isotropic hardening component. Isotropic hardening of the bounding surface is represented as

$$\dot{R} = k\,(R_{sat} - R)\dot{p} \qquad \text{Eq 2.23}$$

In Equation 2.23, R denotes yield stress at large strain, R_{sat} is the saturated value. k is a material parameter controlling the rate of isotropic hardening, and $\dot{\boldsymbol{p}}$ is the effective plastic strain rate. Kinematic hardening of the bounding surface is defined by Equation 2.24.

$$\dot{\beta} = k\,(\tfrac{2}{3}\mathrm{b}(\sigma - \alpha) - \beta)\dot{p} \qquad \text{Eq 2.24}$$

and *b* describes the movement of the bounding surface. The relative motion of the yield surface on the bounding surface is defined by

$$\alpha^* = \alpha - \beta \quad \text{Eq 2.25}$$

$$\dot{\alpha}^* = C\left[\frac{a}{Y}(\sigma - \alpha) - \sqrt{\frac{a}{\alpha^*}}\right]\dot{p} \quad \text{Eq 2.26}$$

$$a = B + R - Y \quad \text{Eq 2.27}$$

C is a material parameter controlling the rate of kinematic hardening. Lastly *h*, a parameter controlling the work hardening stagnation is chosen between 0 and 1.The detailed derivation of these equations can be found in [37].

The Y-U model requires 7 parameters (*Y*, *C*, *B*, *Rsat*, *b*, *k*, and *h*) and these parameters can be identified using uniaxial tension-compression tests, the components are shown in Figure 2.19 and the method of calculation is described in Ref [38] Since this process can be cumbersome and the uniaxial tension–compression tests are difficult to control due to the specimen buckling phenomenon during compression, optimization tools such as LS-OPT (an optimization tool from LSDYNA) are used to identify all 7 parameters by optimization techniques.

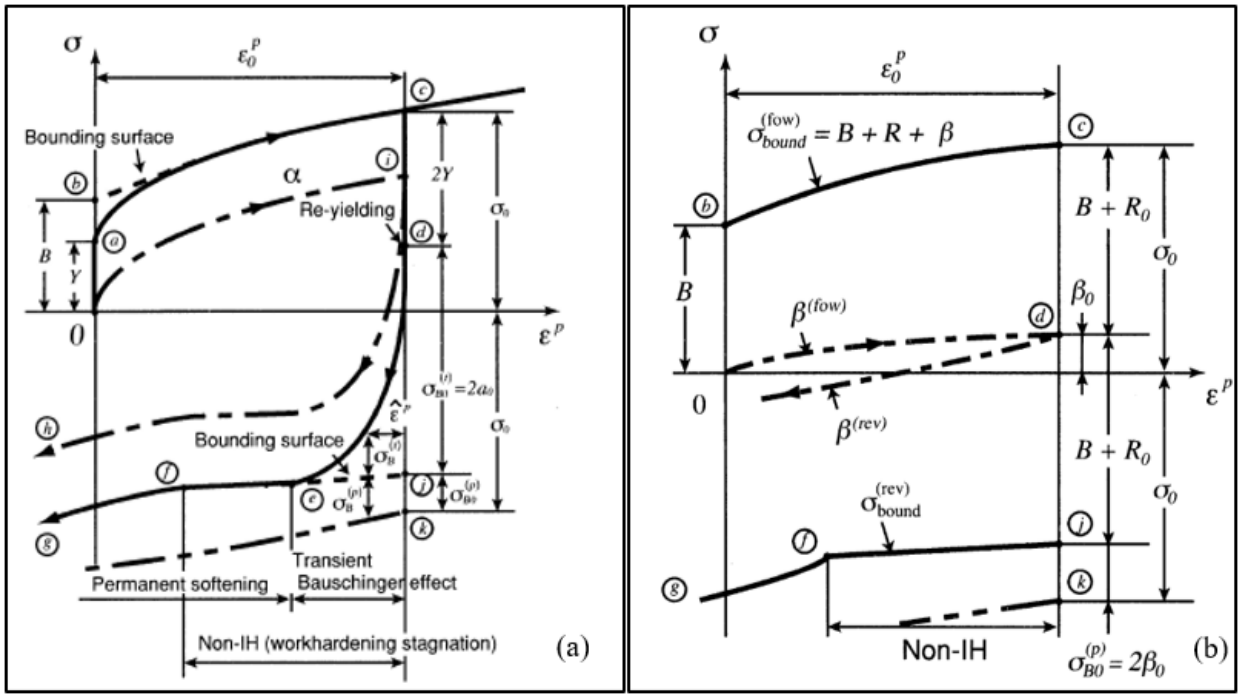

Figure 2.19: Parameter determination of Y-U model from tension-compression test data (a) motion of yield surface (b) motion of bounding surface

In LS-DYNA the commercial FE software used in this research includes material model Mat_125 which uses YU hardening model with Hill 48 yield criterion, material model Mat_226 which has Barlat 89 yield criteria in combination with YU hardening model. Mat_36 uses isotropic hardening combined with Barlat 89 yield criterion. Material model Mat_133 uses Barlat 2000 yield criteria and can be used with either isotropic hardening rule or kinematic hardening rule.

2.4 CONCLUSION

This chapter has briefly discussed the methods of determining formability and springback of monolithic sheet metals. Combining monolithic sheet metals with polymers in sandwich laminate constructions alters the mechanical behavior of the component materials in forming and other operations. Robust industrial applications of these sandwich laminates require not only more knowledge on their mechanical behavior, but also their forming and springback characteristics.

2.5 REFERENCES

[1] D. Banabic, Sheet Metal Forming Processes: Constitutive Modelling and Numerical Simulation, Berlin: Springer , 2010.

[2] S. Hecker, "A simple technique for determining forming limit curves," *Sheet Metal Industries ,* vol. 52, 1975.

[3] A. Ghosh, "The effect of lateral drawing-in on stretch formability," *Metals Engineering Quarterly,* pp. 53-64, 1975.

[4] B. H. Vadavadagi, H. Bhujle and R. K. Khatirkar, "Role of texture and microstructural developments in the forming limit diagrams of family of interstitial free steels," *Journal of Materials Engineering and Performance,* vol. 30, no. 11, p. 8065–8078, 2021.

[5] D. E. Hardt, "Closed-loop sheet metal forming processes," *IFAC proceedings Volumes,* vol. 25, no. 28, pp. 187-192, 1992.

[6] S. Paul, "Controlling factors of forming limit curve: A review," *Advances in Industrial and Manufacturing Engineers,* vol. 2, 02 2021.

[7] S. P. Keeler, "Circular grid system -A valuable aid for evaluating sheet metal formability," in *SAE Technical Paper 680092*, 1968.

[8] G. Goodwin, "Application of strain analysis to sheet metal forming problems in the press shop," *La Metallurgia Italiana,* vol. 60, pp. 764-774, 1968.

[9] X. Duan, M. Jain and D. S. Wilkinson, "Development of a heterogenous microstrucurally based finite element methof for the prediction of forming limint diagram for sheet material," *Metuallurgical and Material transactions, A,* vol. 37 A, pp. 3489-3501, 2006.

[10] B. Sanay, "Prediction of plastic instability and forming limits in sheet metal forming," MS Thesis, Middle East Technical University , 2010.

[11] Z. Chen and G. Fang, "Determination of forming limit for aluminium alloy sheet eliminating the interferences of through-thickness stress and non-linear strain path," *IOP Conference Series: Materials Science and Engineering,* vol. 418, 2018.

[12] L. Huang and M. F. Shi, "Forming Limit Curves of Advanced High strength Steels: Experimental Determination and Emperical Prediction," *SAE International Journal of Materials and Manufacturing,* vol. 11, no. 4, pp. 409-418, 2018.

[13] D. Lumelskyj, J. Rojek, L. Lazarescu and D. Banabic, "Determination of forming limit curve by finite element simulations," *Procedia Manufacturing,* vol. 27, pp. 78-82, 2019.

[14] B. li, T. J. Nye and P. Wu, "Predicting the forming limit diagram of AA5182-O," *Journal of Strain Analysis for Engineering Design ,* vol. 45, pp. 255-273, 2010.

[15] R. Hashemi, H. Mamusi and A. Masoumi, "A simulation- based approach to the determination of forming diagrams," *Proceedings of the Institution of Mechanical Engineers, Part B: Journal of Engineering Manufacture.,* vol. 228, no. 12, pp. 1582-1591, 2014.

[16] L. Zhang, J. Min, J. E. Carsley, T. B. Stoughton and J. Lin, "Experimental and theoretical investigation on the role of friction in Nakazima testing," *International Journal of Mechanical Sciences,* vol. 133, pp. 217-226, 2017.

[17] G. Manikandan, R. K. Verma and P. Biswas, "Effect of friction in stretch forming and its influence on the forming limit curve," *Proceedings of the Institution of Mechanical Engineers, Part B: Journal of Engineering Manufacture.,* vol. 229, no. 6, pp. 973-981, 2015.

[18] M. Habibi, R. Hashemi, A. Ghazanfari, R. Naghdabadi and A. Assempour, "Forming limit diagrams by including the M-K model in finite element simulation considering the effect of bending," *Proceedings of the Institution of Mechanical Engineers, Part I: Journal of Materials:Design and Application ,* vol. 232, no. 8, 2016.

[19] M. C. Butuc, C. Teodosiu, F. Barlat and J. J. Gracie, "Analysis of sheet metal formability through isotropic and kinematic hardening models," *European Journal of Mechanics A/Solids ,* vol. 30, pp. 532-546, 2011.

[20] Z. Marciniak and K. Kuczynski, "Limit strain in the processes of stretch-forming sheet metal," *International Journal of Mechanical Sciences ,* vol. 9, pp. 609-620, 1967.

[21] J. Chen, P. Gong and L. Yang, "Forming Limit Evaluation for AA5182 Aluminum Alloy," *Journal of Materials Engineering and Performance,* vol. 29, pp. 1176-1184, 2020.

[22] W. D. Carden, L. M. Geng, D. K. Matlock and R. H. Wagoner, "Measurement of springback," *International Journal of Mechanical Sciences,* vol. 44, no. 1, pp. 79-101, January 2002.

[23] L. Chen, "Finite element simulation of springback in sheet metal forming," *Applied Mechanics and Materials,* Vols. 50-51, pp. 615-618, January 2011.

[24] R. H. Wagoner, H. Lim and M. G. Lee, "Advanced issues in springback," *International Journal of Plasticity ,* vol. 45, pp. 3-20, June 2013.

[25] J.-T. Gau and G. L. Kinzel, "An experimental investigation of the influence of the Bauschinger effect on springback predictions," *Journal of Materials Processing Technology,* vol. 108, no. 3, pp. 369-375, 2001.

[26] Y. Hou, J. Min, J. Lin, Z. Liu, J. E. Carsley and T. B. Stoughton, "Springback prediction of sheet metals using improved material models," *Procedia Engineering,* vol. 207, pp. 173-178, 2017.

[27] B. Maker and X. Zhu, "Input parameters for springback simulation using LS-DYNA," Livermore Software Technology Corporation , 2001.

[28] M. Yetna N'Jock, B. Houssem, C. Labergere, K. Saanouni and Y. Zhenming, "Explicit and implicit springback simulation in sheet metal forming using fully coupled ductile damage and distortional hardening model," in *AIP Conference Proceedings*, 2018.

[29] F. Gardiner, "The spring back of metals," *Transactions of the American Society of Mechanical Engineers,* vol. 79, no. 1, pp. 1-7, 1957.

[30] S. K. Patel, R. K. Lal, J. Dwivedi and V.P.Singh, "Springback analysis in sheet metal forming using modified ludwik stress-strain relation," *International Scholarly Research Notices,* vol. 2013, pp. 1-11, 2013.

[31] H. K. Yi, D. W. Kim, C. J. Van Tyne and Y. H. Moon, "Analytical prediction of springback based on residual differential strain during sheet metal bending," *Proceedings of the Institution of Mechanical Engineers, Part C: Journal of Mechanical Engineering Science,* vol. 222, pp. 117-129, 2008.

[32] A. Makinouchi, NUMISHEET'93: proceedings of the 2nd International Conference Numerical Simulation of 3-D Sheet Metal Forming Processes : verification of simulation with experiment, Isehara, Japan, 1993.

[33] T. Buranathiti and J. Cao, "Numisheet2005 benchmark analysis on forming of an automotive underbody cross member: Benchmark 2," in *NUMISHEET 2005: 6th International Conference and Workshop on Numerical Simulation of 3D Sheet Metal Forming Processes*, Detroit, 2005.

[34] J. E. Carsley, C. Xia, L. Yang, T. B. Stoughton, S. Xu, S. E. Hartfield-Wünsch, J. Li and Z. Chen, "Benchmark 2 – Springback of a Draw /Re-draw panel," in *NUMISHEET 2014 : The 9th International Conference and Workshop on Numerical Simulation of 3D Sheet Metal Forming Processes*, Melbourne, 2014.

[35] J. J. Stein, "The effect of process variables on sheet metal springback," *Body Manufacturing, Assembly and Advanced Manufacturing,* vol. 5, p. 334, 1998.

[36] F. Barlat and K. Lian, "Plastic behavior and stretchability of sheet metals. Part I: A yield function," *International Journal of Plasticity,* vol. 5, no. 1, pp. 51-56, 1989.

[37] F. Yoshida and T. Uemori, "A model of large-strain cyclic plasticity and its application to springback simulation," *Interntional Journal of Mechanical Sciences,* vol. 45, no. 10, pp. 1687-1702, 2003.

[38] F. Yoshida and T. Uemori, "A model of large-strain cyclic plasticity describing the Bauschinger effect and workhardening stagnation," *Internation Journal of Plasticity ,* vol. 18, pp. 661-686, 2002.

Chapter 3 - Formability Analysis of Aluminum-Aluminum and Aluminum/Polypropylene/Aluminum Laminates

Prediction of forming limits of monolithic metals, such as steels and aluminum alloys, is a well-developed area of research and numerous publications exist on both numerical and experimental determinations of their forming limit diagrams. However, their forming behavior when combined with other materials has so far not received much attention and requires more in-depth research. Chapter 3 focuses on the forming behavior of aluminum/polypropylene/aluminum symmetric sandwich laminates and aluminum/aluminum laminates and compares them with the forming behavior of the aluminum used in these laminates. Their forming limit curves (FLCs) are determined through numerical simulations and then compared to the previously published experimental data.

3.1 Review of Literature on Formability of Metal/Polymer/Metal Laminates

There are a limited number of studies available in literature on the formability of metal/polymer/metal laminates. DiCello [1] presented forming limit diagrams of steel/polypropylene/steel laminates with various thickness combinations of low carbon steel skins and polypropylene core and compared them with monolithic low carbon steel and AA5182-O aluminum alloy. The formability of the laminate was found to be lower than that of the steel, but higher than that of the aluminum alloy. For example, the limit strain in plane strain condition (FLC_0) of a 1 mm thick laminate was 0.33 compared to 0.45 for a 0.9 mm thick steel and 0.23 for a 0.9 mm thick aluminum alloy. Another experimental study by Link [2] on the forming limit diagrams of steel/polypropylene/steel laminates generated by limiting dome height (LDH) shows

that the formability of the laminates is equivalent to or slightly superior to the formability of the steels used in their skins. It is influenced more by the formability of the steel than by the core thickness.

Somayajulu [3] conducted an experimental study using punch-stretching method to obtain forming limit diagrams of AA5182/polypropylene/AA5182 sandwich laminates. Both soft (annealed) and hard (cold-worked) AA5182 alloy were used as the skin material. This study shows that the FLC_0 of the sandwich laminates is slightly higher than that of the monolithic soft and hard AA5182. It also shows that increasing the polypropylene core thickness results in better formability on the tension-compression side of the forming limit diagram of sandwich laminate with hard AA5182 skins, whereas no such pattern was observed with soft AA5182 in the skins.

Liu et al. [4] used finite element analysis to study the forming behavior of AA5052/polyethylene/AA5052 laminates. They used the Gurson-Tvergaard-Needleman (GTN) damage model to simulate the forming process and a cohesive zone model to simulate the interface condition between the skins and the core layer. Their finite element results show that the forming limit of the sandwich laminates is higher than that of the monolithic aluminum and increases with increasing thickness of the polyethylene core. The forming limits were also experimentally determined using the Nakazima test method and were found to be lower than the predicted forming limits.

Palkowski et al. [5] used the Nakazima test method to determine the FLCs of 1 mm thick 316L stainless steel sheet and 1.6 mm thick sandwich laminate sheet with the same stainless steel in the skins and a polypropylene copolymer in the core. The total skin thickness was 1 mm, the same as the monolithic sheet. Their results show that the sandwich laminate has a lower formability

near the plane strain region, but about the same formability as the monolithic sheet in the deep drawing (tension-compression) and biaxial stretch conditions.

A study of the forming behavior of a steel/polypropylene/steel (SPS) sandwich composite with different skin and core thickness combinations in a deep drawing operation is reported by Harhash et al. [6]. In this study, the strain fields on the outer layers of the monolithic steel and the SPS laminate are compared. The SPS laminate shows a gradual increase in the major strain value at the outer punch corner radius as the cup is drawn to its full depth. The monolithic steel, on the other hand, does not show any such increase in the major strain at the punch corner radius. Cracking tendency of the sandwich panels were studied by comparing the strain state of the panel with its FLC and the results show that cracking was only found in the SPS panel with 2 mm core thickness. The finite element model over predicts the strain distribution in comparison with the experimental results of the SPS laminate. In the case of the drawn cups, both materials show very little thinning, while it becomes more prominent close to the punch radius. With increasing core thickness, more thinning is observed at the punch corner radius of the sandwich laminates. Thickening is observed in the flange areas. In SPS panels, the outer steel layer shows more thickness reduction compared to the inner steel layer. The core layer thins out at a faster rate with increasing core volume fraction.

Kim et al. [7] developed the forming limit diagrams (FLDs) of an AA5182/polypropylene/AA5182 sandwich laminate using both theoretical and experimental methods. For the theoretical FLDs, they used the modified Marciniak-Kuczynski theory, and to account for planar anisotropy of AA5182, they used both Hill 1948 and Barlat 2000 yield functions. For the experimental FLD, they used the Erichsen test method. In their study, the predicted FLD is higher than the experimental FLD, and the FLD determined by using the Barlat

yield function is closer to the experimental FLD than the Hill yield function. The forming limit of the sandwich laminate of 1.2 mm thickness with 0.2 mm thick aluminum skin on each side of a 0.8 mm thick polypropylene core is higher than the monolithic AA5182 of 0.2 mm thickness even though the AA5182 sheet has a higher strain hardening exponent compared to the sandwich. However, a comparison between the predicted FLCs of monolithic AA5182 aluminum of 1 mm thickness with the sandwich of 1.2 mm thickness shows that they have very similar forming limit curves. Since both these sheets have the same bending stiffness, it is concluded that the polypropylene core does not have a very significant effect on improving the FLC.

This chapter focuses on the formability of single aluminum sheets, two layered aluminum laminates (Al/Al) and aluminum/polypropylene/aluminum (Al/PP/Al) sandwich laminates. First, the numerical model for single layer aluminum sheets is verified by comparing the simulated data with previously published data. The effect of thickness is studied for aluminum sheets ranging from 0.2 mm to 1.2 mm that match the skin thickness and total thickness of the sandwich laminates. Lastly, forming simulations on Al/PP/Al laminates are performed to identify the advantage of the presence of polypropylene core with different thickness combinations of the skin and core layers.

The formability of sandwich laminates is of more interest in this research. The published data referred to in this section show that the core layer thickness, yield strength and modulus play a major role in the limit strains for metal/polymer/metal laminates. More in-depth analysis is required to fully understand the formability of sandwich panels and the important factors influencing their forming limits. In this chapter, variation of the forming limit curves with respect to different thickness combinations of outer skins and inner core layer is determined to understand the effects of skin thickness and core thickness on the formability of Al/PP/Al sandwich laminates. In addition, formability of sandwich laminates is compared with that of monolithic aluminum

sheets of equivalent thickness. The materials in the sandwich laminates and the thickness combinations are the same as those used in the experimental formability study presented in Ref. [3].

3.2 MATERIAL PROPERTIES

For the purpose of this study, aluminum alloy AA5182 with two different temper conditions, namely AA5182-O (annealed) and AA5182-H18 (hardened by cold work), is used as the skin material and polypropylene (PP) is used as the core material to form Al/PP/Al sandwich laminates. AA5182 is widely used in automotive body panels because of its good formability, corrosion resistance and weldability. The mechanical properties of annealed AA5182-O are listed in Table 3.1 and properties for the hardened AA5182-H18 are listed in Table 3.8. The annealed aluminum is henceforth referred to as soft aluminum and written as SA5182, and the hardened aluminum is henceforth referred to as hard aluminum and written as HA5182.

Table 3.1: Mechanical properties of annealed (soft) AA5182 [8]

Property	**SA5182**	**Unit**
Density	2890	Kg/m^3
Modulus of elasticity	70	GPa
Yield strength	110.2	MPa
Poisson's ratio	0.33	-
R_0	0.699	-
R_{45}	0.776	-
R_{90}	0.775	-

For the purpose of validation of forming limit curves of Al/PP/Al laminates, a comparison is made with the experimental forming limit curves for the same sandwich laminate from Ref. [3]. The stress-strain curve for SA5182 used in the current study is taken from Ref. [8], and in Figure 3.1, it is compared with the stress-strain curve given in Ref. [3]. The curve from Ref. [8] is an extension to the uniaxial true stress-plastic strain data using Voce hardening law. The curve is plotted upto a plastic strain of 0.98 and used as an input to avoid numerical errors that can occur by allowing the finite element software to extrapolate the stress-strain curve. The two curves are in close agreement; therefore, it is reasonable to make comparisons between the numerical FLC determined in the current study and the experimental FLC presented in Ref. [3].

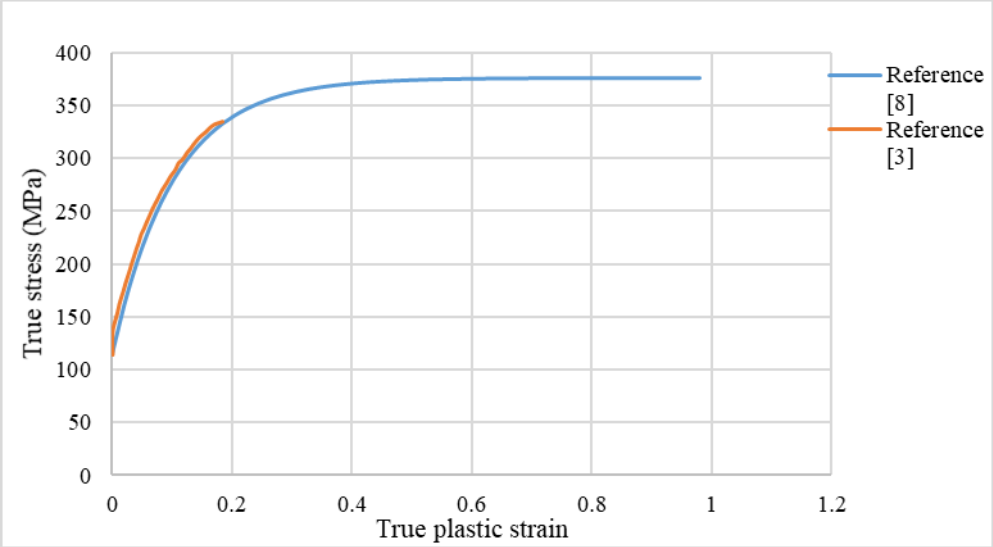

Figure 3.1: Plastic stress-strain curve for SA5182 (AA5182-O)

The true stress-strain curve for hardened aluminum (HA5182) is shown in Figure 3.2. It can be observed in this figure that the true strain at failure for HA5182 is only 0.0678 or 6.78%, whereas that for SA5182, it is 0.184 or 18.4 %. The strain hardening exponent (n) values as reported in Ref. [3] are 0.3 and 0.07, respectively.

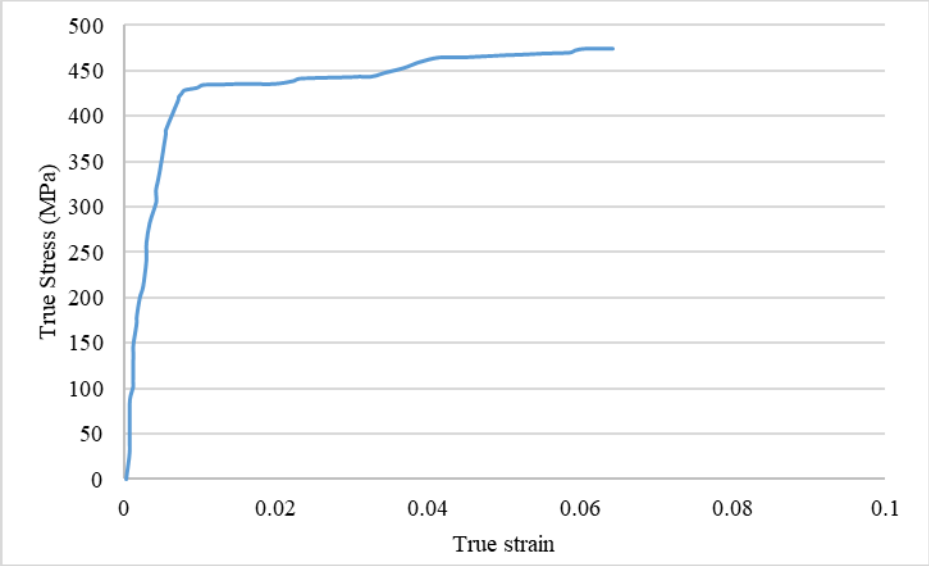

Figure 3.2: True stress-strain curve of HA5182 (AA5182-H18) [3]

The numerical simulations for formability analysis in Chapter 3 make use of two different material models for aluminum, Barlat 89 3-parameter model, known as Mat_36 in LS DYNA and Yoshida-Uemori (Y-U) model, known as Mat_125. These models are briefly described in Section 3.2.1. A comparison of the two models is made to understand the difference in predictions of forming limits.

The polymer in the core is a polypropylene, which has a density nearly one-third that of the aluminum in the skins. The properties of polypropylene are listed in Table 3.2. The stress-strain curve for polypropylene is defined in Figure 3.3 which is used as an input curve in modelling its behavior in the formability simulations.

Table 3.2: Mechanical properties of polypropylene [3]

Property	**Value**	**Units**
Density	900	kg/m^3
Modulus of elasticity	2.022	GPa
Yield Strength	26	MPa

Poisson's ratio	0.43	-

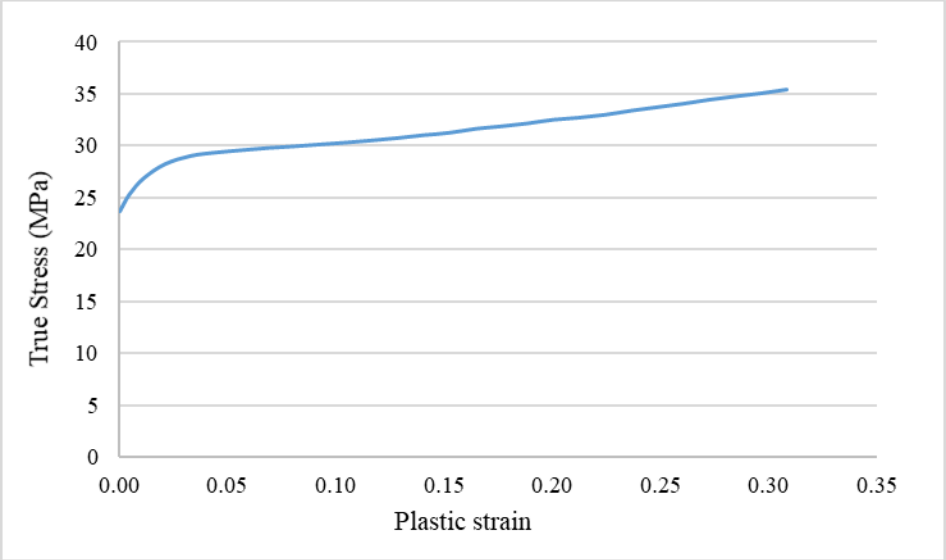

Figure 3.3: True plastic stress-strain curve of polypropylene at room temperature [3]

3.2.1 Material models used in finite element simulations

Material models hold significant importance in finite element simulations in accurately predicting formability of sheet metals. The two material models used for simulating the forming behavior of aluminum alloys are described in Chapter 2. Material model Mat_36 uses the isotropic hardening law combined with Barlat 1989 yield criteria and Mat_125 uses Yoshida-Uemori hardening combined with Hill 1948 yield criteria. The material model used for simulating the stress-strain behavior of polypropylene is a piecewise linear plasticity model, Mat_24, in LS-DYNA.

The Y-U model parameters for the annealed aluminum SA5182 are taken from LS-DYNA material library and are listed in Table 3.3. Since the Y-U model parameters for hardened aluminum HA5182 are not available, only the Barlat 89 model is used to determine the forming limit curves for HA5182 sandwich laminates. The Barlat 89 model parameters for HA5182 are listed in Section 3.7.

Table 3.3: Yoshida-Uemori material model parameters for SA5182 [9]

Property	Description	Value	Units
Rsat	Saturated value of yield stress at large strain	201.7	MPa
B	Initial size of isotropic bounding surface	122.3	MPa
Sb	Material parameter describing movement of bounding surface	16.5	
Y	Initial size of the yield surface	110.2	MPa
h	Material parameter controlling work hardening stagnation	0.16	
Sc	Material parameter controlling rate of kinematic hardening	577.5	
K	Material parameter controlling rate of isotropic hardening	12	

3.3 FINITE ELEMENT MODEL

The Nakazima test method is used to determine the FLCs with LS-DYNA's explicit solver. A hemispherical punch of constant-diameter is used to draw blanks of different widths in a round die. In this study, the punch diameter is 101.6 mm and the die opening diameter is 105.6 mm. The die corner radius is 6.35 mm and the blank holder diameter is 300 mm. A schematic of the setup in shown in Figure 3.4. By varying the specimen width, different strain paths are obtained and plotted on a true major strain vs. true minor strain diagram from uniaxial tension to pure biaxial strain conditions. The widths of the specimens modelled are 30 mm, 50 mm, 70 mm, 90 mm, 110 mm, 130 mm, and 200 mm. Out of these seven widths, the first four widths create strain paths on the tension-compression side of FLD and the last three widths create strain paths on the tension-tension side of FLD. The 90 mm width creates a plain strain condition, and the 200 mm width creates an equal biaxial tensile strain condition. Figure 3.5 shows the finite element mesh for different specimen widths built in LS-DYNA.

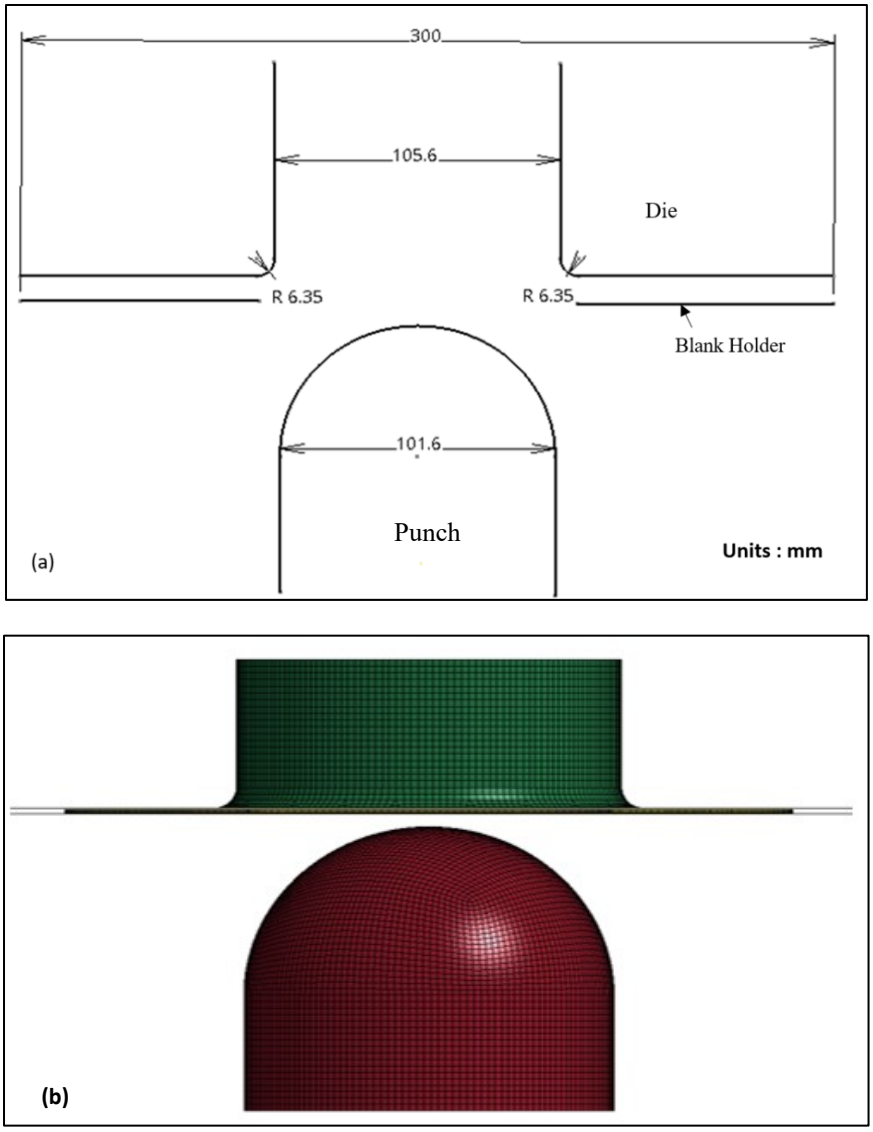

Figure 3.4: Punch, die and blank holder setup for determination of FLC (a) Nakazima test setup (b) Finite element model

The tools (die, punch and blank holder) and the sheet specimen (blank) are modelled as 2D surfaces using Belytschko-Tsay shell element formulation. For the blank, seven integration points are used through its thickness to capture the bending and drawing phenomenon accurately. The tools are set up as rigid bodies, while the blank is deformable. The tools use a mesh size of 2 mm by 2 mm and more refined meshes along the radius areas to capture the geometry more accurately. The blank mesh size is 1 mm by 1 mm.

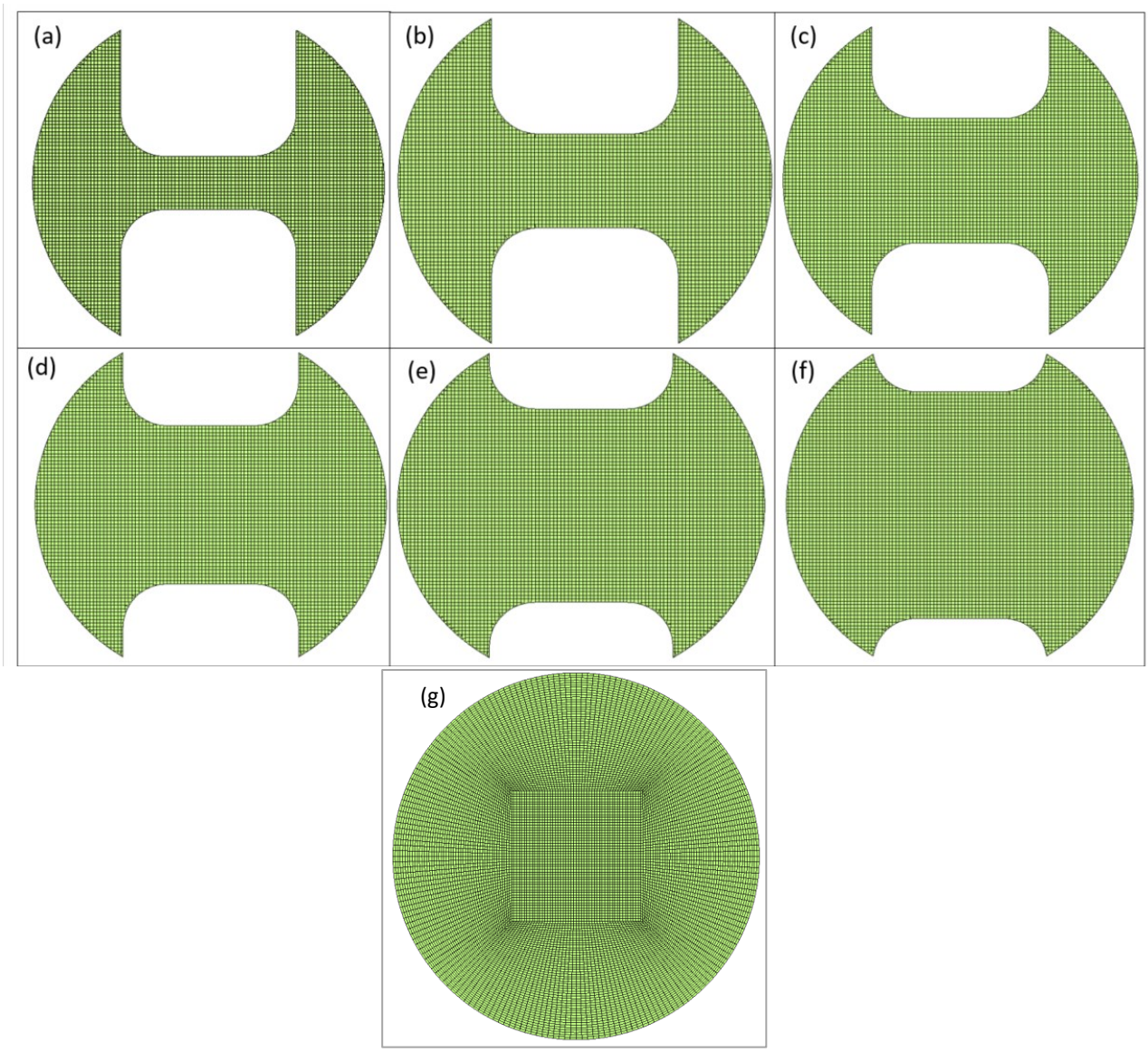

Figure 3.5: FE mesh for Nakazima specimens of varying width (mm) (a) W30 (b) W50 (c) W70 (d) W90 (e) W110 (f) W130 (g) W200

A penalty friction model is used with a coefficient of friction of 0.15 between all contacting surfaces of the blank, punch, die and blank holder. The die remains stationary, and the blank is held in place between the die and the blank holder with a blank holder force of 150 kN. The blank holder force is adjusted if needed to completely restrict sliding of the blank between the blank holder and the die, imitating the presence of a lock bead. The punch moves upward with a forming

velocity of 100 mm/sec. Since aluminum has a low strain rate sensitivity, a high punch speed is used to reduce the computation time. Mass scaling is used by maintaining the total energy ratio close to 1.

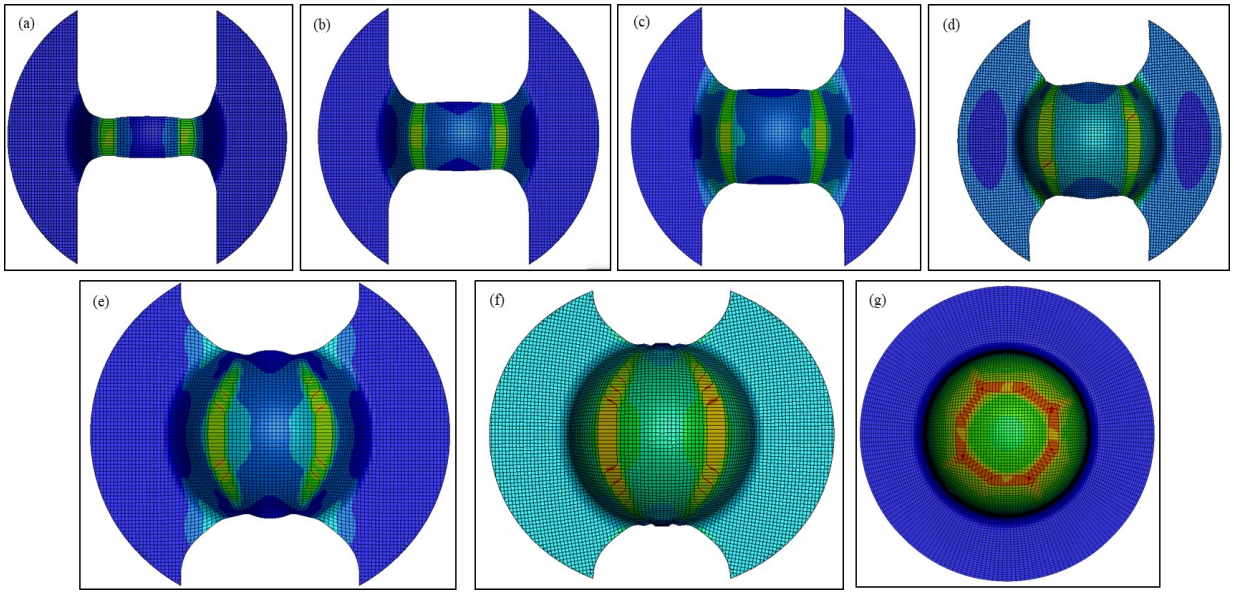

Figure 3.6: Nakazima specimens of varying widths (W) after necking (a) W30 (b) W50 (c) W70 (d) W90 (e) W110 (f) W130 (g) W200

Figure 3.6 shows the specimens of different widths when formed to failure by necking. When the specimen is stretched by the punch beyond the point of necking, it is observed that some elements close to the necked region show constant effective plastic strain and the necked elements show increasing effective plastic strain. Figure 3.7 shows the strain of one element each in the necked and un-necked regions. Each point on the FLC for a particular strain path is obtained by identifying the elements on the mesh closest to the necked area that record constant effective

plastic strain after necking. The average of six such un-necked elements, three on each side of the failed specimen, is used to calculate the limit major and minor strains.

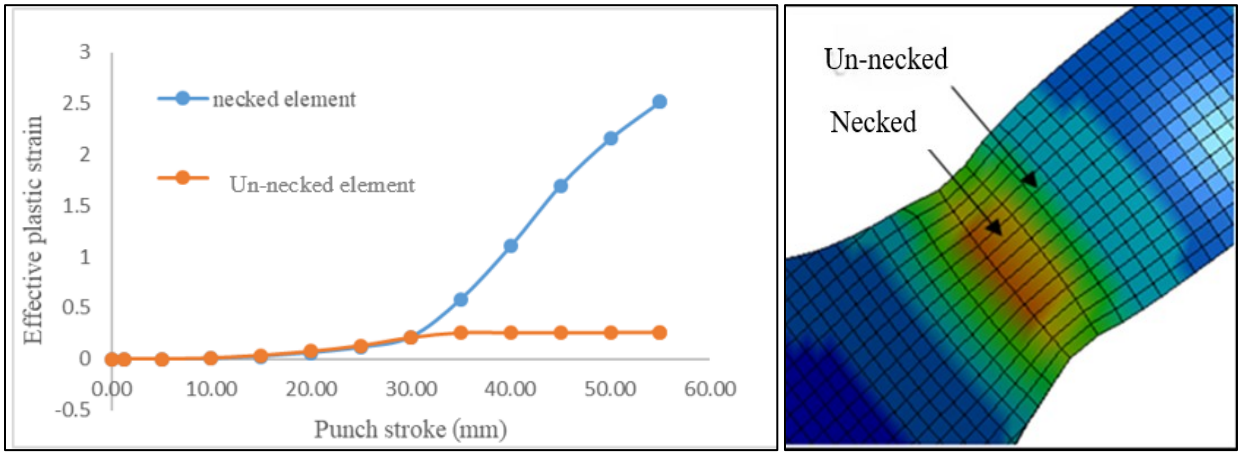

Figure 3.7: Comparison of effective plastic strains in the necked and un-necked elements (0.2 mm thick SA5182, W30 specimen)

The blank is deformed until failure by necking occurs. When the specimen starts to neck, a drop in the load curve is observed, indicating the onset of failure. The load-displacement curves for SA5182 single aluminum sheets of 0.2 mm thickness and four different specimen widths are shown in Figure 3.8. All of the specimens show a similar trend in the load-displacement curves. With increasing width of the blank, a higher punch load is recorded. A similar trend is observed for all the specimen widths.

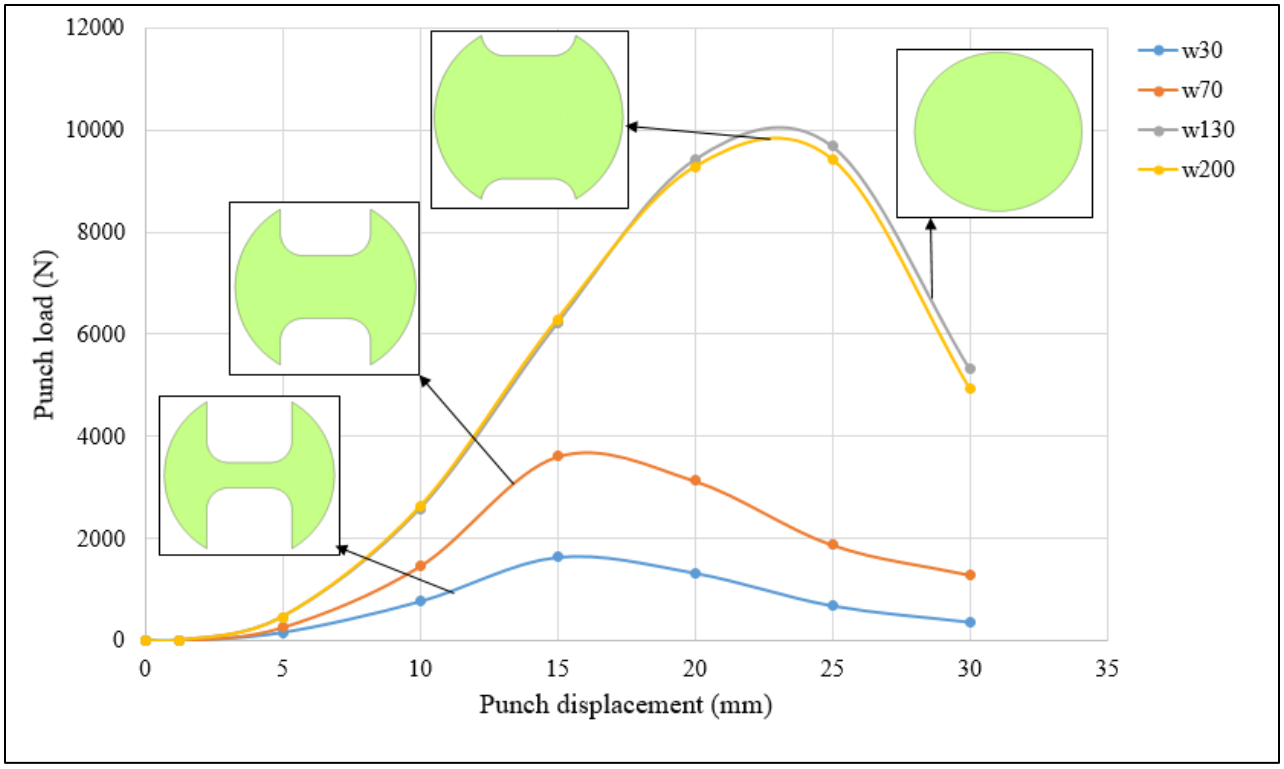

Figure 3.8: Load-displacement curves for 0.2 mm thick single aluminum SA5182 sheets with 30, 70, 130, and 200-mm widths

Based on the width of the specimen, the strain path of the un-necked elements during drawing varies. For each specimen, the strain history over the duration of the punch displacement is recorded. Figure 3.9 shows the different strain paths obtained for each specimen width for three different thicknesses, 0.2, 0.8 and 1.2 mm. The strain states along each strain path are recorded and a curve is fit through the final strain values to attain the forming limit curve (FLC).

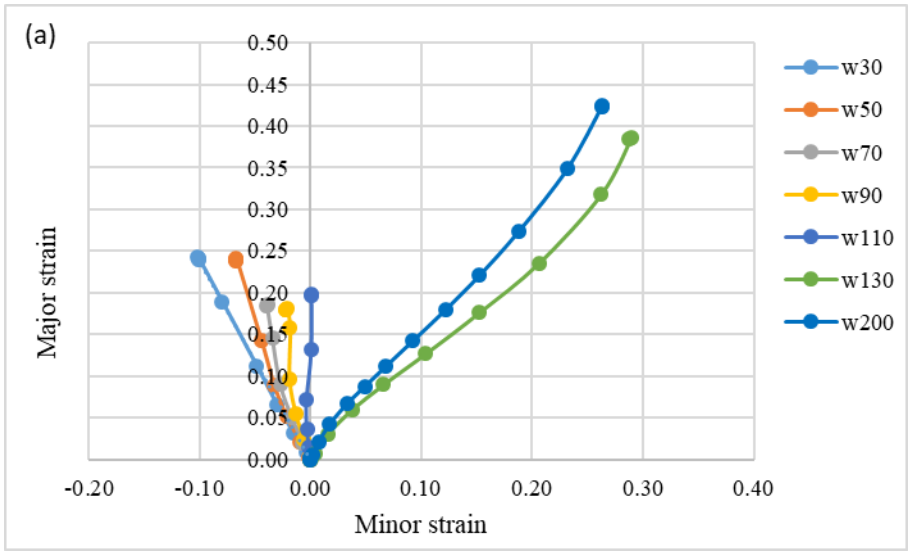
(a)
0.50
0.45
0.40
0.35
0.30
0.25
0.20
0.15
0.10
0.05
0.00
Major strain
-0.20
-0.10
0.00
0.10
0.20
0.30
0.40
Minor strain
w30
w50
w70
w90
w110
w130
w200

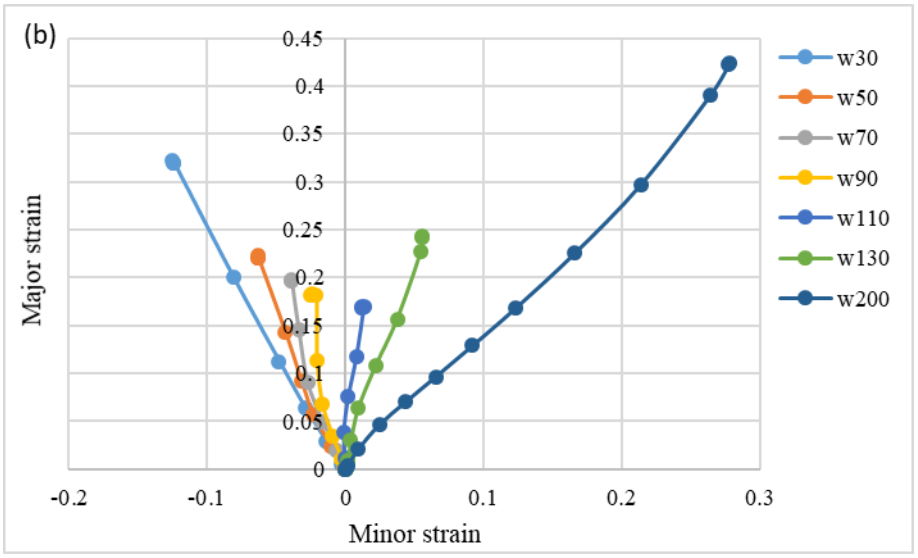
(b)
0.45
0.4
0.35
0.3
0.25
0.2
0.15
0.1
0.05
0
Major strain
-0.2
-0.1
0
0.1
0.2
0.3
Minor strain
w30
w50
w70
w90
w110
w130
w200

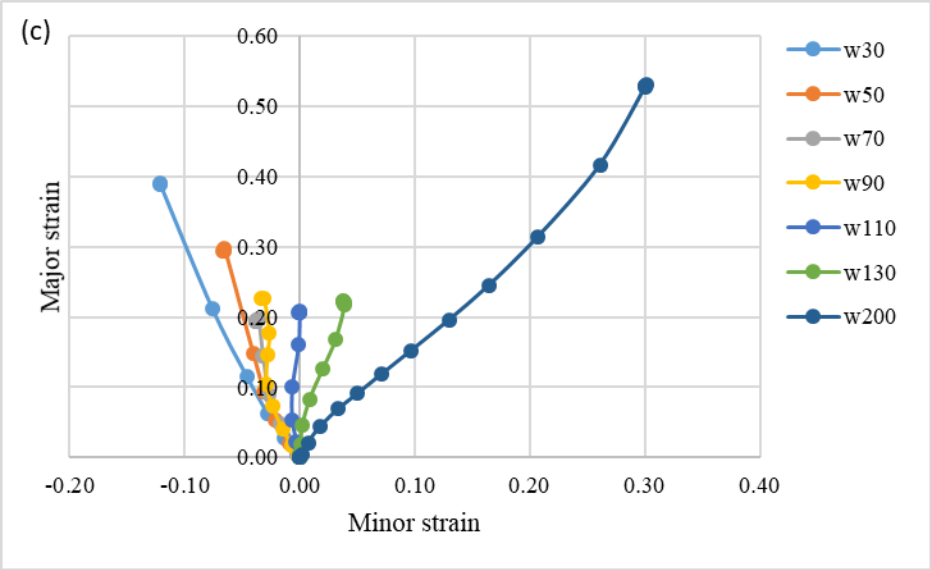

Figure 3.9: Strain paths of SA5182 for each specimen width for different sheet thicknesses (a) 0.2 mm (b) 0.8 mm (c) 1.2 mm

It can be observed in Figure 3.9 that the strain paths are not all linear, especially on the tension-tension side of the diagram. The non-linearity of strain paths in Nakazima tests has been observed by Ganapathy et al. [10] and is attributed to the presence of out-of-plane bending deformation [11]. The 0.2 mm thickness (Figure 3.9(a)) shows that the specimens with 130 mm and 200 mm widths have similar strain paths unlike the 0.8 mm and 1.2 mm sheet thicknesses.

The resulting FLCs for monolithic aluminum, aluminum-aluminum laminates and aluminum polypropylene sandwich laminates are recorded and compared in Section 3.4 through Section 3.6.

3.4 Forming Limit Curves for Monolithic Aluminum SA5182 Sheets

The forming limit curves for SA5182 modelled using Mat_125 material model (Yoshida-Uemori material model with Hill 48 yield criteria) for various thickness values, ranging from 0.2 mm to 2 mm, are plotted in Figures 3.10 and 3.11. The FLC curves are fitted through the strain limit data points obtained from numerical simulations of the Nakazima tests. Figure 3.10 shows the forming

limit curves for 0.2 mm, 0.22 mm and 0.24 mm thick aluminum sheets used in the skins of Al/PP/Al sandwich sheets. The forming limit curves in this figure show a small increase in formability with increase in thickness. The corresponding FLC_0 values (Table 3.4) do not show a significant increase, since the thickness are very close (increments of 0.02 mm).

Table 3.4: FLC_0 (plane strain condition) values for SA5182

Thickness (mm)	**FLC_0 (Curve)**
0.2	0.18
0.22	0.192
0.24	0.198

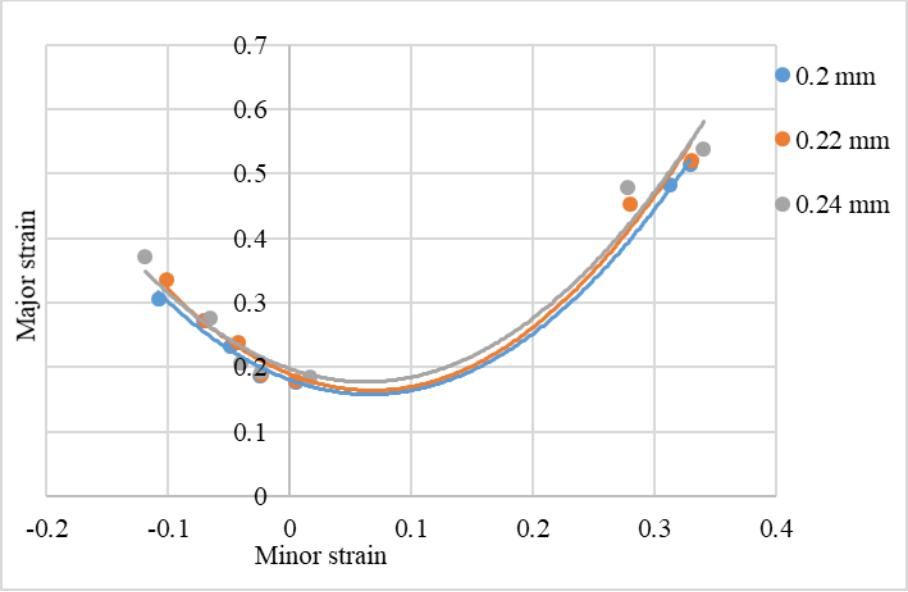

Figure 3.10: FLC curves for SA5182 sheets with 0.2, 0.22, 0.24 mm thicknesses

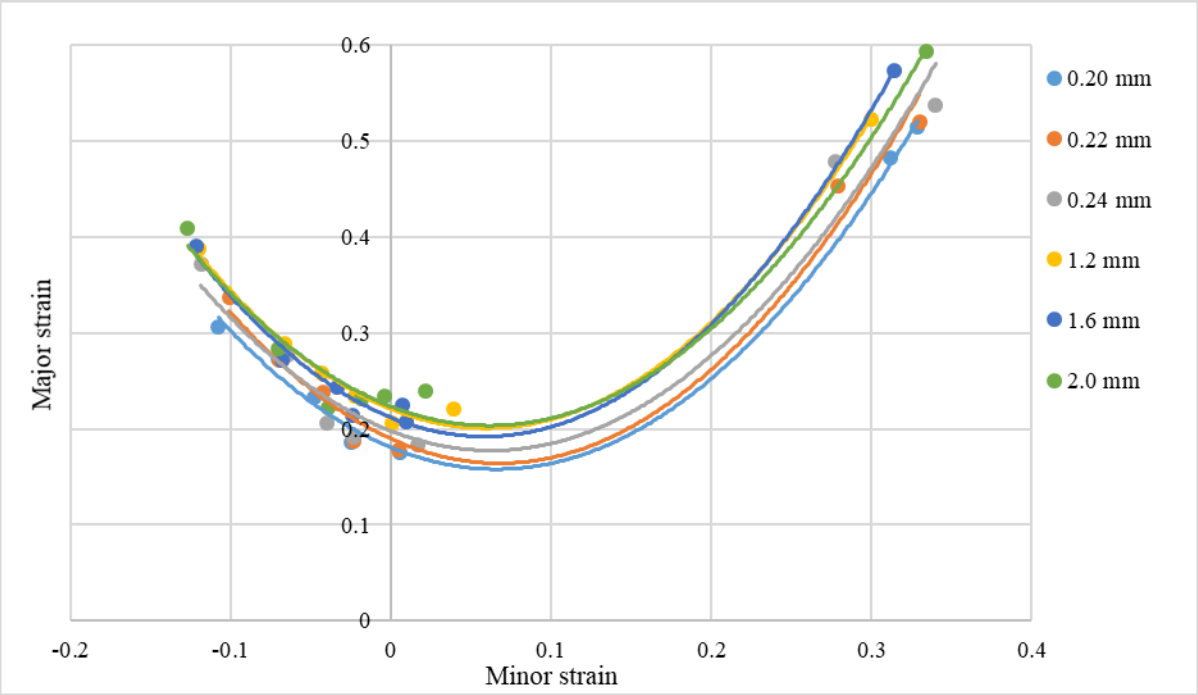

Figure 3.11: FLCs for SA5182 sheets of 0.2, 0.3, 0.4 and 1.2-mm thicknesses

Figure 3.11 shows FLCs for 0.2, 0.22, 0.24, 1.2, 1.6 and 2.0 mm sheet thicknesses. It is observed that the limit strain increases with increase in thickness, as expected. The forming limit curves for 1.2 mm, 1.6 mm and 2 mm thicknesses do not show much variation on the tension-compression side of the diagram. However, formability consistently increases with increase in thickness on the biaxial tension side of the diagram. The forming limit curve for 2 mm thickness shows the highest strain limits, indicating that thickness must be increased significantly to improve the FLC. The 1.6 mm thick sheet shows strain limits similar to the 2 mm thick sheet near the equibiaxial tension state.

It can be observed in Figure 3.10 that the limit strain state for equibiaxial stretch specimen (circular Nakazima specimen) is relatively high and does not show the major and minor strains to be equal. This is explained by looking at the strains at different locations on the drawn specimen. An equibiaxial strain state is recorded only in the elements at the pole of the formed circular

specimen and not in the necked area, which is located away from the pole. Since the highest possible strain state is used for defining the forming limit, the elements closest to the necked area that also exhibit constant effective plastic strain (EPS) post failure by necking are selected, and they exhibit higher strains than the elements at the pole. Figure 3.12 shows the EPS for the elements in two areas and their corresponding strain path in the FLC.

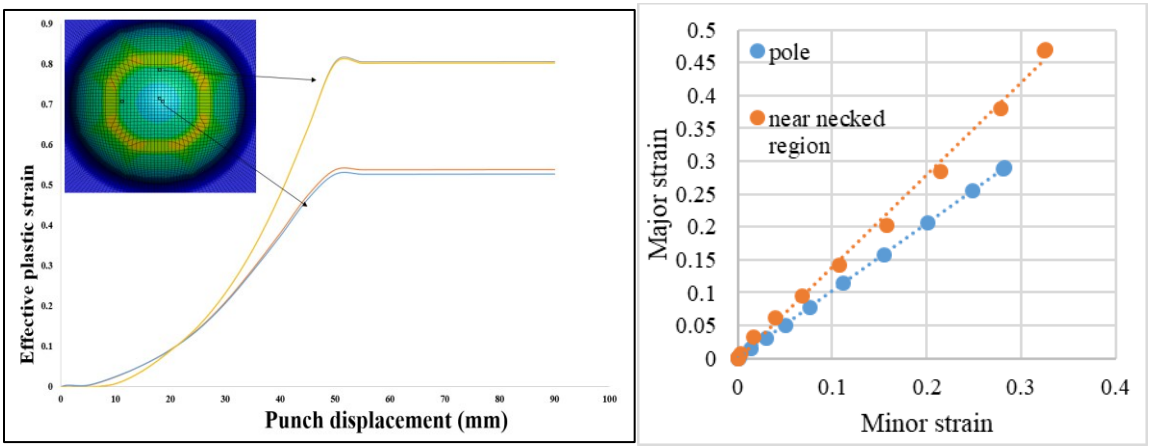

Figure 3.12: (a) Effective plastic strains and (b) major/minor strains in elements at the pole and near necked region of the circular specimen with 200 mm diameter

In all further results, the major and minor strains for equibiaxial stretch conditions are taken at the elements closest to the necked elements. The current finite element model predicts an FLC_0 value of approximately 0.18 for a sheet thickness of 0.2 mm which is in close agreement to the value obtained by Somayajulu [3]. Following this verification, the numerical model is extended to the rest of this study.

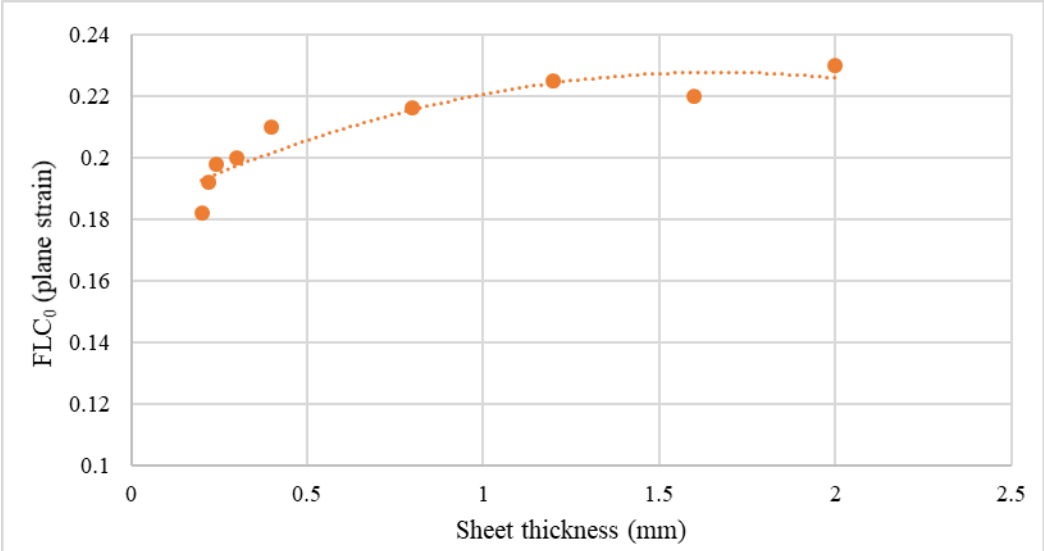

Figure 3.13: Variation of FLC_0 of monolithic SA5182 with increasing sheet thickness

Figure 3.13 plots the FLC_0 (plane strain) values for blank thickness ranging from 0. 2 mm to 2 mm. FLC_0 increases from 0.2 mm to 0.4 mm sheet thickness and then continues to increase at a lower rate up to a sheet thickness of 2 mm.

The forming limit curve for 0.24 mm thick single aluminum SA5182 sheet is compared to the experimental FLC determined in Ref. [3]. The forming limits on the tension-compression side of the FLD are close to the experimental values while the predicted forming limits on the tension-tension side are higher than the experimental values. (Figure 3.14)

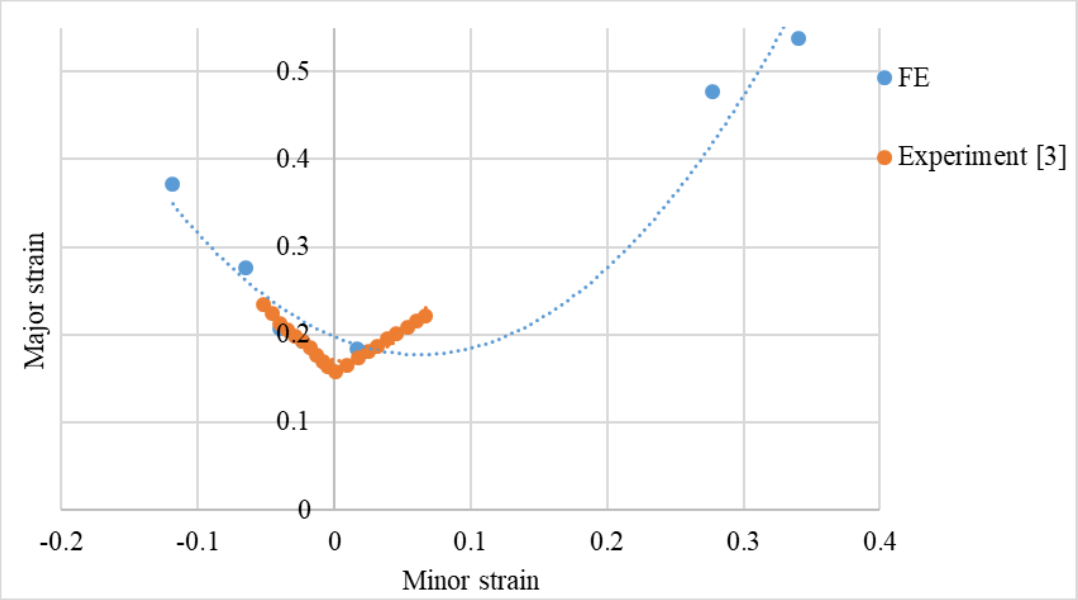

Figure 3.14: Comparison of experimental [3] and FE model results for a 0.24 mm thick SA5182

3.5 Forming limit curves of SA5182 Aluminum-Aluminum laminates

3.5.1 Description of the finite element model

An aluminum-aluminum laminate containing two layers of SA5182 aluminum sheets of equal thickness (0.22 mm each) is drawn to failure using the Nakazima test setup to determine its forming limit. Two different models are used. In the first model, the two sheets are assumed to be not fully bonded, but the friction between them plays a role in their formability. In the second model, the two sheets are assumed to be roll bonded so that there is no sliding between them during the forming operation. In the first model, three different dynamic friction coefficients between the two sheets, namely 0.30, 0.45, and 0.60, are used to determine their effect on the formability. For the roll-bonded laminate, perfect bonding is assumed between the two aluminum sheets and the nodes at the interface between them are tied. Both layers are modelled using Belytschko-Tsay shell elements with 5 integration points through their thicknesses. The tools are defined as rigid bodies and the two aluminum sheets have equal thickness of 0.22 mm each so that the laminate thickness

is 0.44 mm. The material model and other numerical parameters, such as the blank holder force and punch velocity, are identical to those mentioned in Section 3.3.

3.5.2 Results and discussion

The FLCs for the upper and lower layers of the aluminum-aluminum laminate are drawn separately in Figures 3.15 and 3.16. A polynomial curve of second degree is fit to the seven data points obtained for each laminate specimen representing a different load path. Figure 3.15 shows the effect of friction coefficient on the forming limits of the upper aluminum layer and Figure 3.16 shows the effect of friction coefficient on the forming limits of the lower aluminum layer in the aluminum-aluminum laminate. Both upper and lower aluminum sheets in the laminate are 0.22 mm thick. It is observed that there is very little difference in the FLCs with friction coefficients of 0.3 and 0.45, and the FLC with friction coefficient of 0.6 friction is much lower than the other two FLCs. Also, the strain limits for the upper as well as the lower aluminum layers show a greater difference on the tension-tension side of the FLC than on the tension-compression side.

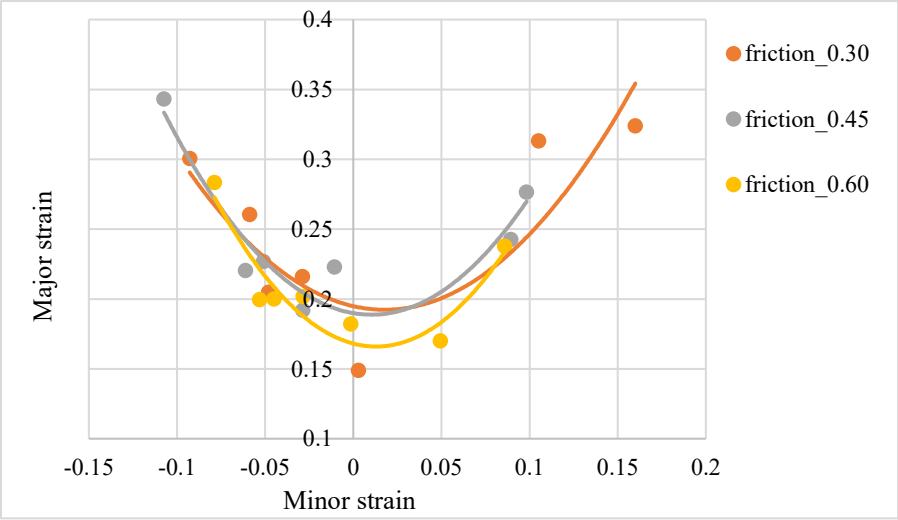

Figure 3.15: Effect of friction coefficient at the interface between the two layers of 0.44 mm thick aluminum-aluminum laminate on the FLCs of the upper aluminum layer

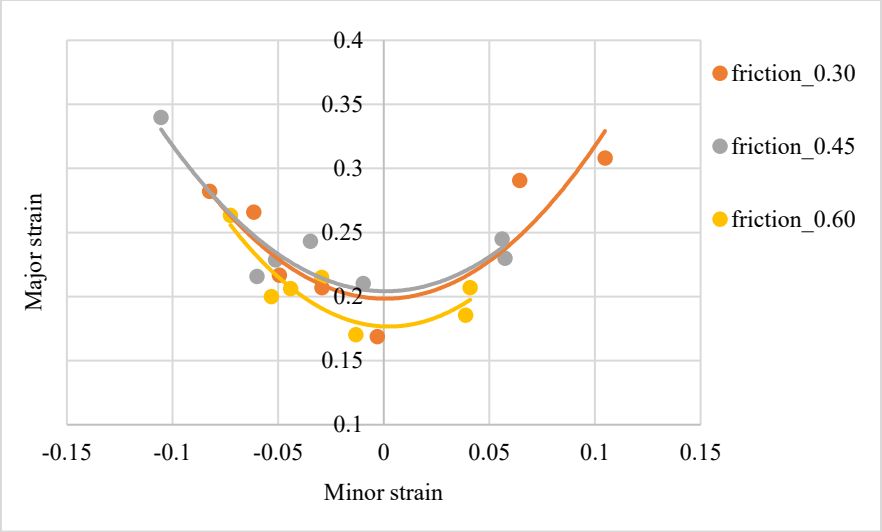

Figure 3.16: Effect of friction coefficient at the interface between the two layers of 0.44 mm thick aluminum-aluminum laminate on the FLCs of the lower aluminum layer

The major and minor strains in equibiaxial tension condition decreases with increasing friction coefficient, thereby reducing the formability of the aluminum–aluminum laminate. Additionally, the percentage of thickness reduction at the same location is higher for the upper aluminum sheet in comparison to the lower aluminum sheet irrespective of the friction condition (Table 3.5). The thickness reduction is examined for the elements close to, but outside of the necked area.

Table 3.5: Comparison of thickness reduction between the upper and lower aluminum sheets for different friction conditions

Friction condition between aluminum layers	**% Thickness reduction in the unnecked elements close to the necked area**	
	Upper Al layer	**Lower Al layer**
0.30	15.0	12.6
0.45	16.6	16.4
0.60	15.2	14.6

Figures 3.17, 3.18 and 3.19 compare the forming limit curves of the upper and lower aluminum layers at each condition of friction. The lower layers show an overall higher limiting

strain. This means that the formability of the laminate as a whole is controlled by the upper layer since its forming limit is more conservative.

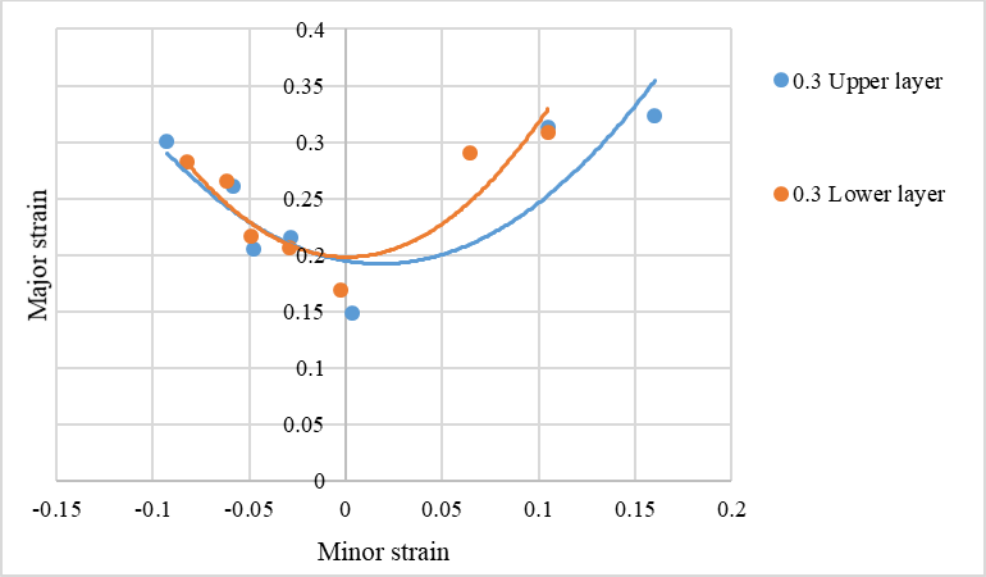

Figure 3.17: Comparison of FLCs of upper and lower aluminum layers (coefficient of friction = 0.30) in the Al-Al laminate

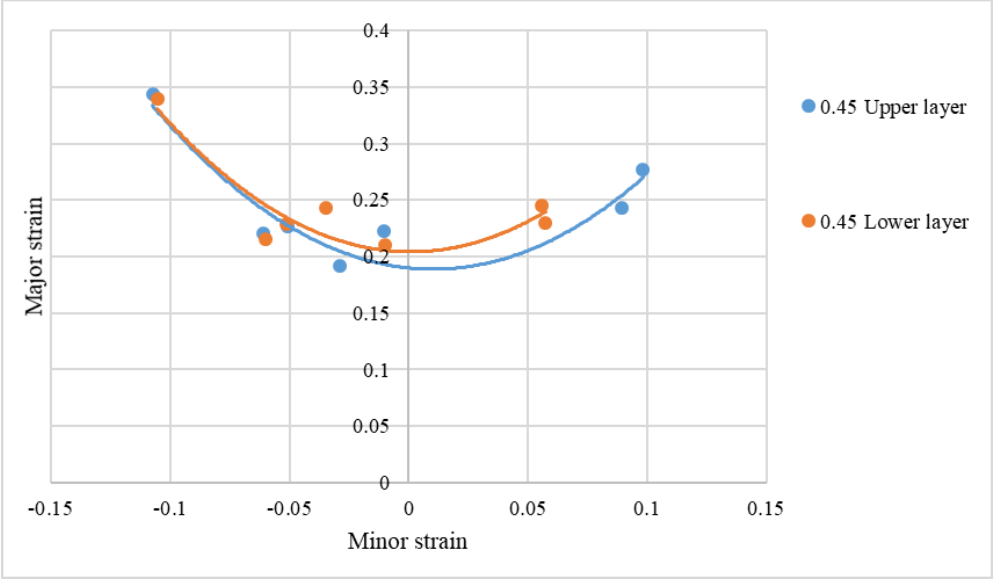

Figure 3.18: Comparison of FLCs of upper and lower aluminum layers (coefficient of friction = 0.45) in the Al-Al laminate

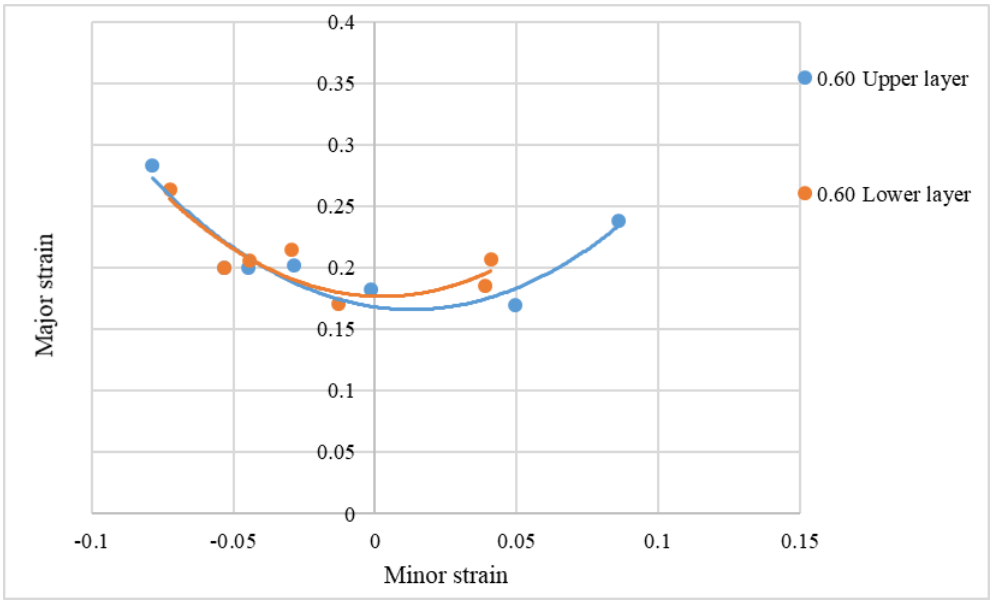

Figure 3.19: Comparison of FLCs of upper and lower aluminum layers (coefficient of friction = 0.60) in the Al-Al laminate

Lastly, a case with the two aluminum sheets of 0.22 mm thickness each and perfect bonding between them is simulated by using the tied contacts in LS-DYNA. The forming limit curve of a 0.44 mm thick single aluminum sheet is compared to the FLC of the bonded two-layered aluminum laminate of equivalent thickness in Figure 3.20. It can be seen that strain limit in plane strain condition (FLC_0) is higher for the aluminum-aluminum laminate with perfect bonding between its layers. On the biaxial stretch side, both FLCs are nearly equal; however, on the tension-compression side, the laminate has a higher forming limit.

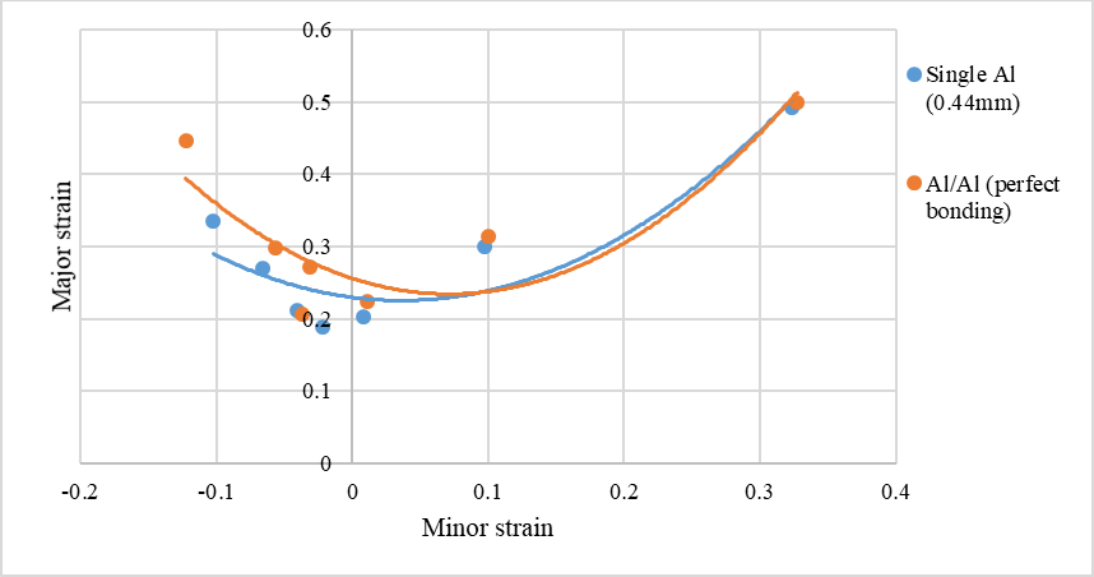

Figure 3.20: Comparison of FLCs of a 0.44 mm thick a perfectly bonded aluminum-aluminum laminate and a single aluminum sheet of equivalent thickness

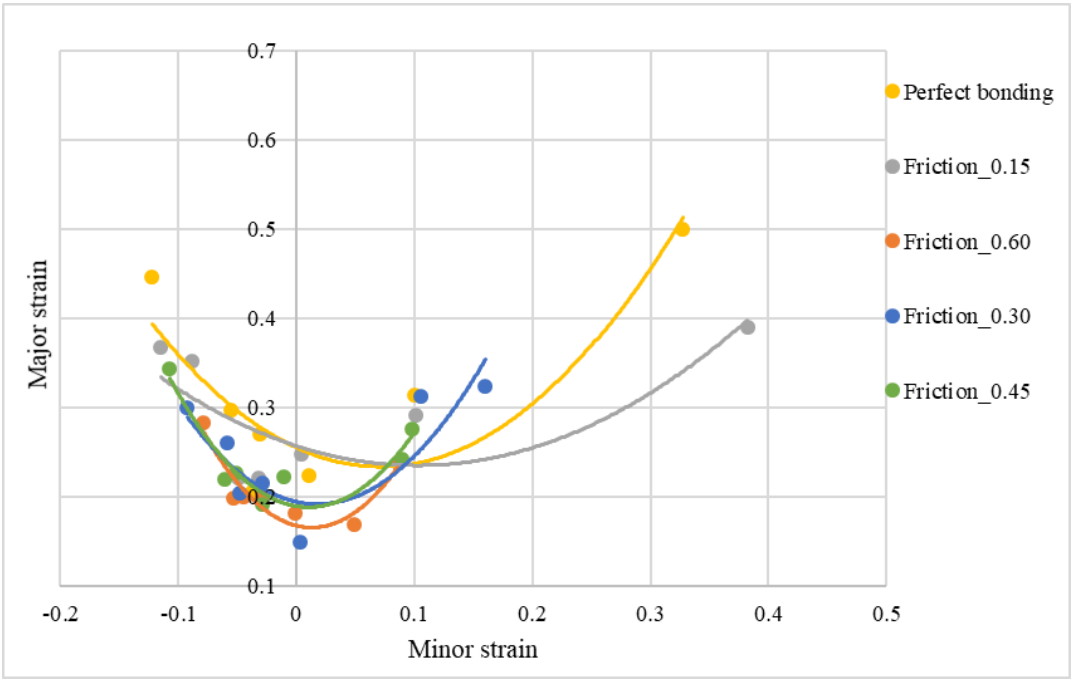

Figure 3.21: Comparison of FLCs of Al-Al laminates with different conditions of bonding between aluminum sheets

From Figure 3.21, it can be seen that the bonding between the layers of the aluminum laminate play an important role in the forming limit curve. It is observed that the highest FLC_0 is

obtained for two aluminum sheets with tied contact (representing perfect bonding), the curve developed with friction condition of 0.15 also shows an almost equal FLC_0 to the tied condition, however the curve at all other strains shows lower limits.

3.6 Forming Limit Curves of SA5182/PP/SA5182 Sandwich Laminates

3.6.1 Description of the finite element model

The finite element model for SA5182/PP/SA5182 sandwich laminates is similar to the model described in Section 3.3 with additional finite element meshes to represent each material layer. The outer aluminum skins are represented by Belytschko-Tsay shell elements and the inner polypropylene core layer is represented by quadrilateral solid elements. Figure 3.22 shows the finite element mesh of the sandwich laminate for 0.8 mm and 1.6 mm core thicknesses. For the 0.8 mm core thickness, only one layer of solid elements is used, while for the 1.6 mm core thickness, two layers of solid elements are used. Tied contact model from LS-DYNA is used between the aluminum skins and the inner polymer core. To simulate perfect bonding between the skin and the core layers, the top nodes of the solid elements are tied to the upper aluminum skin nodes, while the bottom nodes of the solid elements are tied to the bottom aluminum skin nodes.

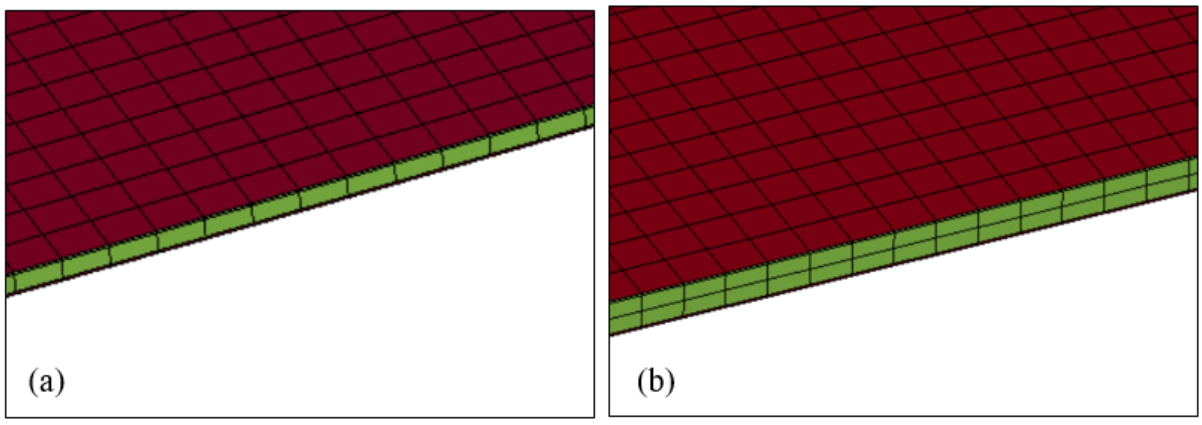

Figure 3.22: Finite element meshing for Al/PP/Al blank with shell – solid –shell elements:
(a) core thickness = 0.8 mm (b) core thickness = 1.6 mm

The punch, die and blank holder are modelled as rigid bodies. The aluminum layers are modelled in LS-DYNA with material model Mat_125 which uses Yoshida-Uemori's kinematic hardening model for transversely anisotropic materials and is suitable for sheet metal forming simulations in all thickness variation cases. Later, material model Mat_36 is also used to study the effect of material model selection on the FLC of sandwich laminates. The polypropylene layer is modelled using material model Mat_24, a piecewise linear plasticity model.

The penalty friction model is used with a coefficient of friction of 0.15 between all contacting surfaces. The die remains stationary, and the blank is held in place between the die and the blank holder with a blank holder force of 150 kN. The punch moves upward with a velocity of 100 mm/sec. Strain rate sensitivity of the aluminum alloy is not considered.

3.6.2 Forming limit curves for SA5182/PP/SA5182 sandwich laminates

FLCs are calculated by forming the sandwich laminate blanks of various widths to failure. Strain limits from uniaxial tension to biaxial stretch are obtained by identifying the elements close to the necked area with constant strain after necking. It is observed that the failure areas in all three layers of the laminate are close to each other due to the assumption of perfect bonding (tied contact) between them. The forming limit curves for different thickness combinations of skin and core thicknesses listed in Table 3.6 are determined. The FLC of the upper aluminum skin is used as the FLC for the entire sandwich, since it has the lowest strain limits arising from maximum stretching.

Table 3.6: Thickness combinations of SA5182/PP/SA5182 laminates

	Outer skin layer (mm)	**Core polymer (mm)**	**Inner skin layer (mm)**	**Total thickness (mm)**
1.	0.24	0.8	0.24	1.28
2.	0.24	1.6	0.24	2.08
3.	0.22	0.8	0.22	1.24
4.	0.22	1.6	0.22	2.04
5.	0.20	0.8	0.20	1.20

6.	0.20	1.6	0.20	2.00
7.	0.25	1.9	0.25	2.40

In Figure 3.23 the load vs. punch displacement curve of a 1.2 mm thick sandwich laminate (0.2/0.8/0.2 mm) is compared to the load vs. punch displacement curves of 1.2 mm thick and 0.4 mm thick single SA5182 sheets. The blank width is 30 mm for all three sheets. The load for 1.2 mm thick SA5182 is much higher in comparison to the 1.2 mm thick sandwich laminate. The load increase with displacement of 0.4 mm thick SA5182 is the same as that of the sandwich laminate with total aluminum skin thickness of 0.4 mm up to 30 mm displacement. The peak loads for both single aluminum sheets occur at 40 mm punch displacement, while the punch load for the sandwich peaks at 50 mm punch displacement. The peak punch load for the 1.2 mm thick single aluminum sheet is significantly higher than the 1.2 mm thick laminate with 0.2 mm thick aluminum skins on each side of the 0.8 mm polypropylene core.

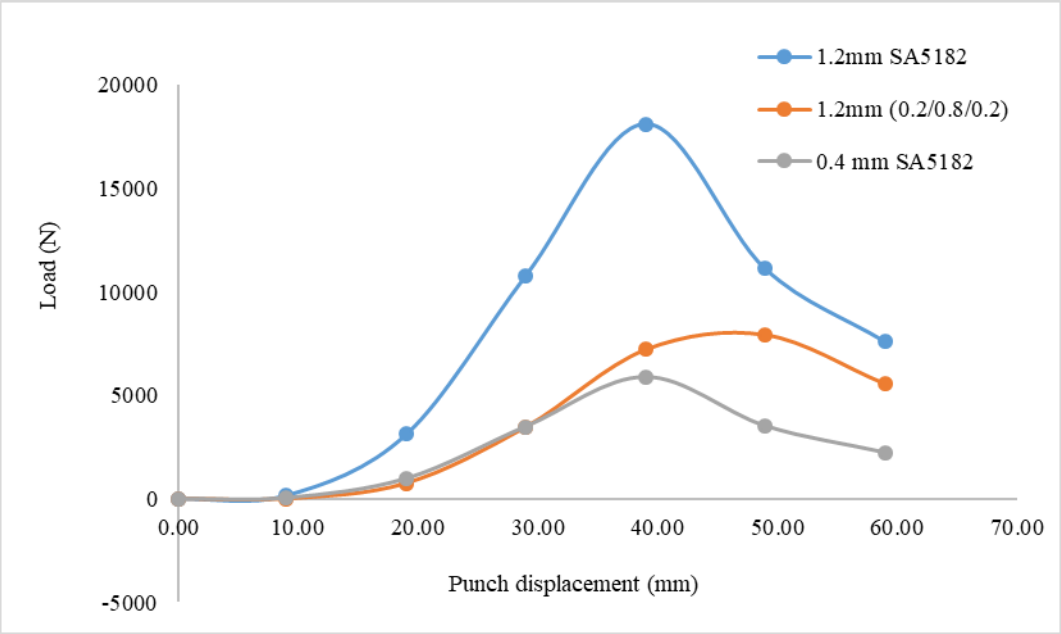

Figure 3.23: Load-punch displacement curves compared for single aluminum sheets (0.4 mm and 1.2 mm thicknesses) and a sandwich laminate with 1.2 mm thickness and 0.4 mm aluminum skin thickness

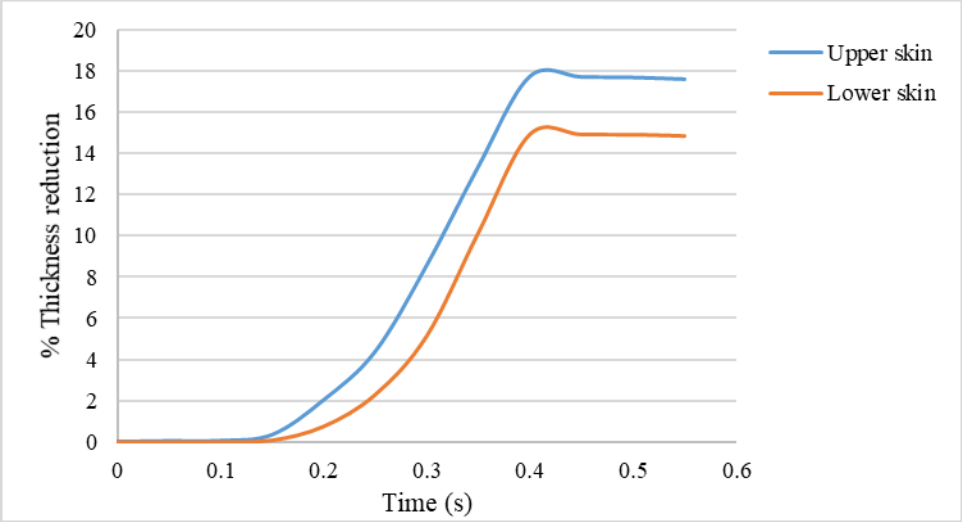

Figure 3.24: Comparison of thickness reduction of the two skins in the 0.2/0.8/0.2 Al/PP/Al laminate

The percentage thickness reduction at the same location for the upper and lower skins of the 0.2/0.8/0.2 mm sandwich laminate is compared in Figure 3.24. It can be seen that the upper skin shows more thinning in comparison to the lower skin. Similar thinning behavior is observed for all sandwich laminates.

A polynomial fit curve is added to the data points to achieve the forming limit curve for each thickness combination which is shown in Figures 3.25 and 3.26. For a constant core thickness of 1.6 mm (Figure 3.25), it can be seen that the limit strains increase with increase in skin thickness. For a constant core thickness of 0.8 mm (Figure 3.26), there is not much variation in limit strains. By comparing the FLCs in Figure 3.25 and 3.26, it can be observed that the highest formability limit is obtained with the 0.25/1.9/0.25 sandwich which has a skin thickness of 0.25 mm and a core thickness of 1.9 mm.

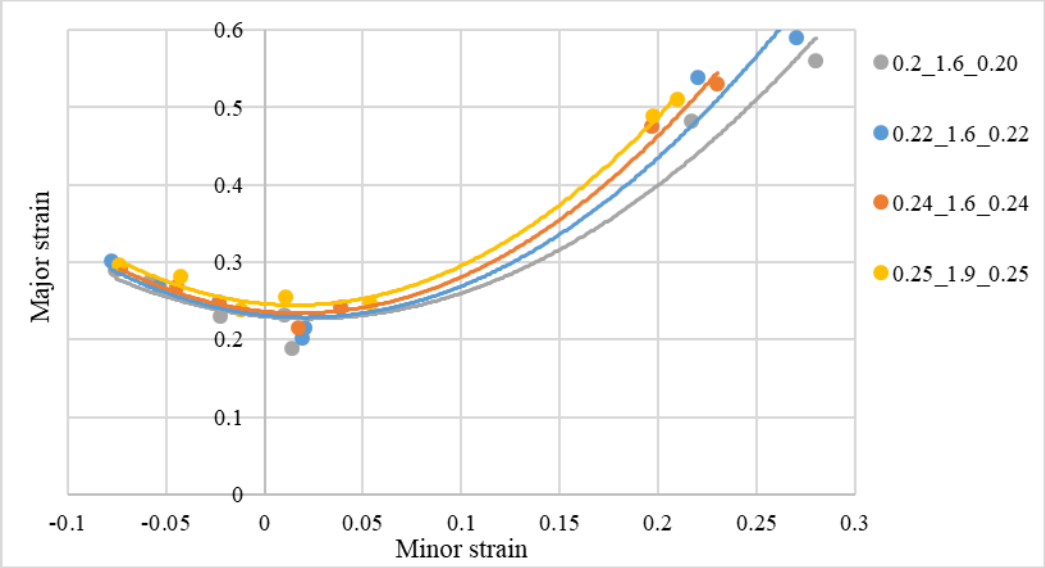

Figure 3.25: Forming limit curves of SA5182/PP/SA5182 laminates with increasing skin thickness (core thickness = 1.6 mm and 1.9 mm)

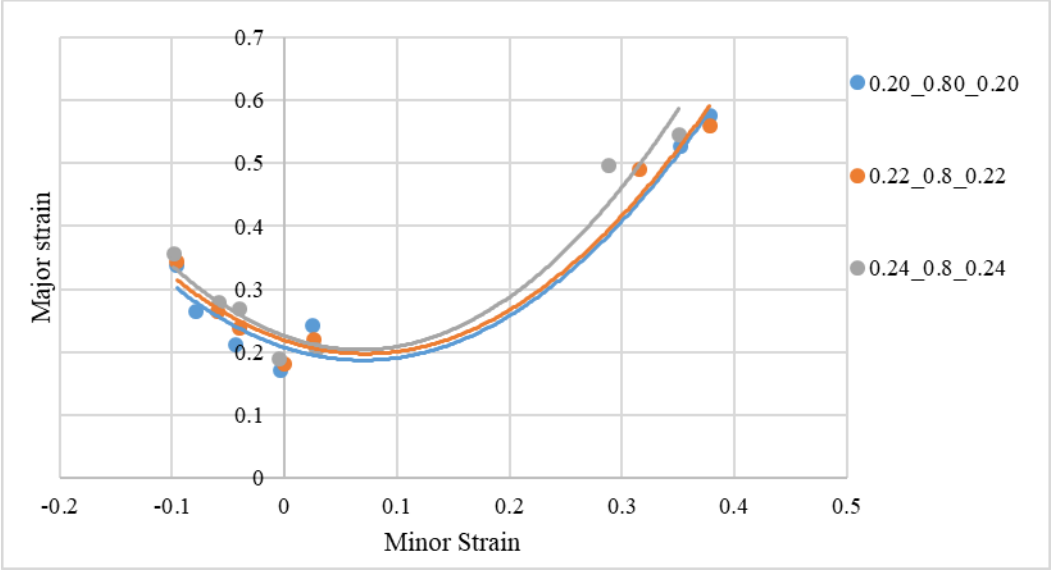

Figure 3.26: Forming limit curves of SA5182/PP/SA5182 laminates with increasing skin thickness (core thickness = 0.8 mm)

The effect of core thickness is further explored by plotting the FLCs for three different skin thicknesses, namely 0.2, 0.22 and 0.24 mm, in Figure 3.27. The core thicknesses are 0.8 and 1.6 mm. In each case where the skin thickness is kept constant, it can be seen that the laminate with

the thicker core has a much higher forming limit curve on the tension-tension side (biaxial stretch conditions). The forming limits on the tension-compression side show no significant difference.

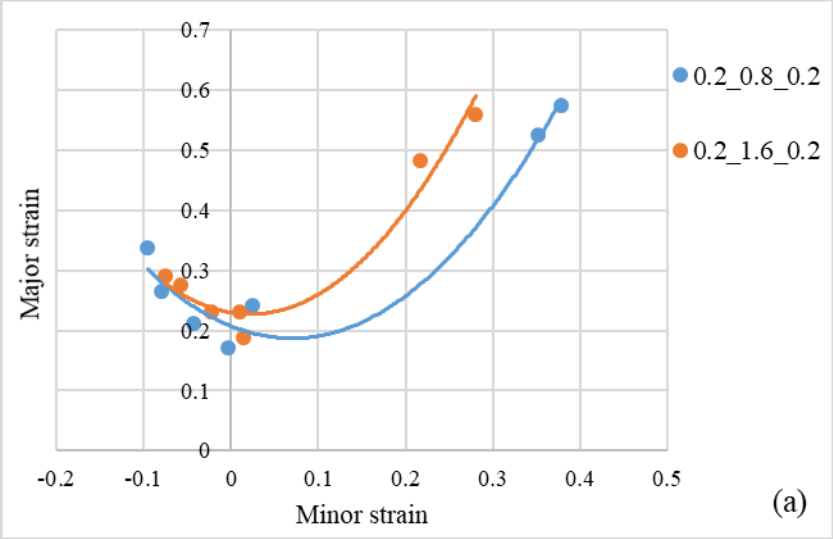

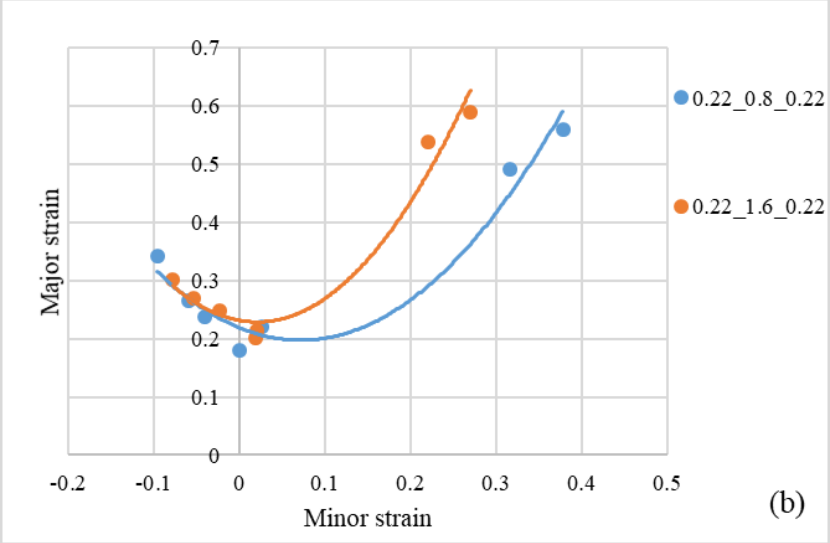

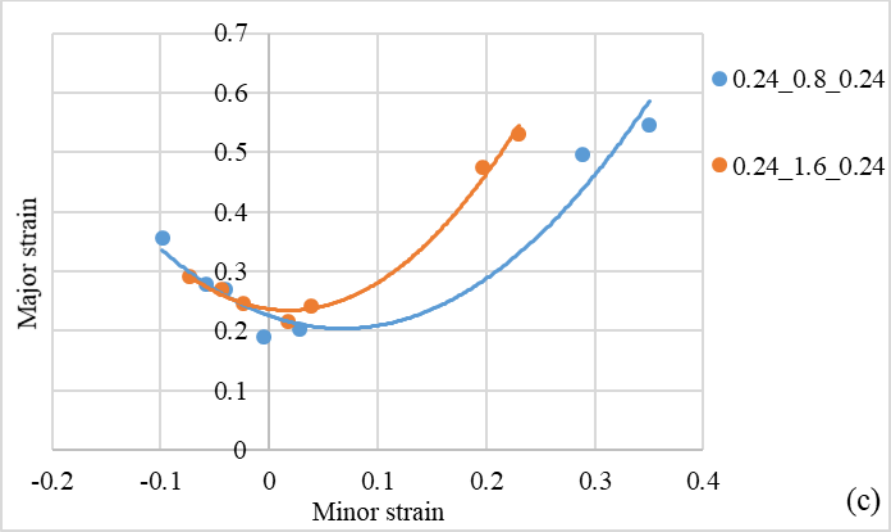

Figure 3.27: Effect of core thickness on the FLCs of SA5182/PP/SA5182 laminates with constant skin thickness of (a) 0.2 mm (b) 0.22 mm (c) 0.24 mm

The forming limit curves experimentally determined for three different sandwich thickness combinations in Ref. [3] are compared in Figure 3.28 with the finite element results obtained in this research. It can be observed in this figure that the predicted FLCs of the sandwich laminates with 0.8 mm core thickness are very close to the experimental counterparts; however, for the sandwich laminate with 1.9 mm core thickness, the experimental curve shows lower or more conservative forming limits under all strain conditions. While the limit strains on the tension-compression side of the FLC show closer values to the experiment, the finite element model prediction on the tension-tension side are much higher.

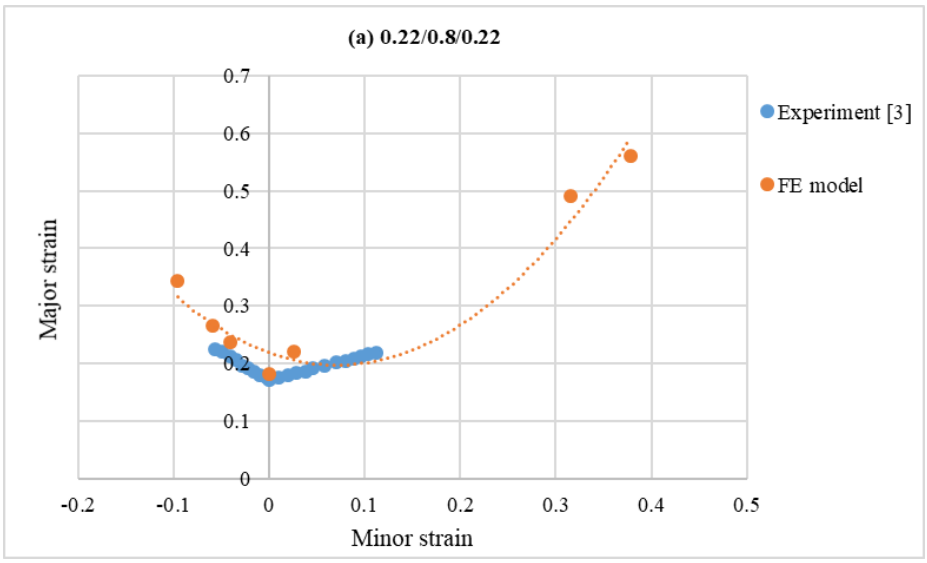
(a) 0.22/0.8/0.22
Major strain
Minor strain
Experiment [3]
FE model
0.7
0.6
0.5
0.4
0.3
0.2
0.1
0
-0.2
-0.1
0
0.1
0.2
0.3
0.4
0.5

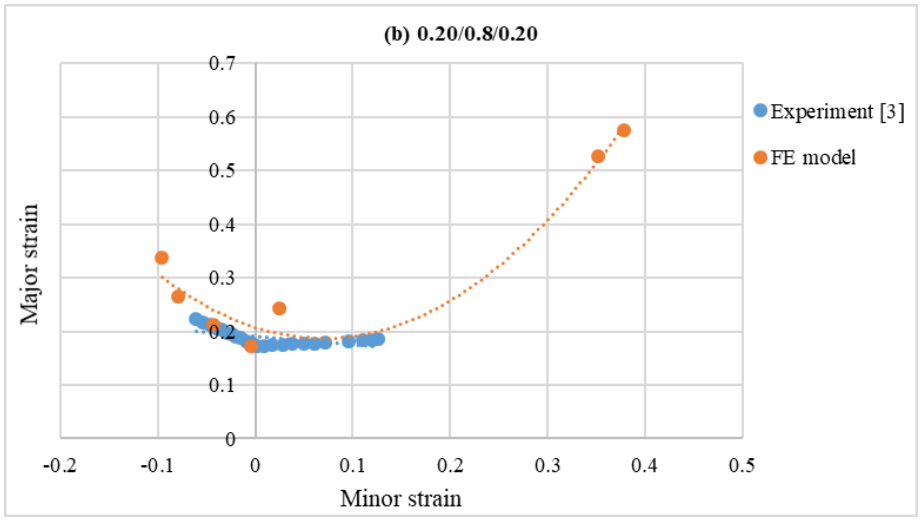
(b) 0.20/0.8/0.20
Major strain
Minor strain
Experiment [3]
FE model
0.7
0.6
0.5
0.4
0.3
0.2
0.1
0
-0.2
-0.1
0
0.1
0.2
0.3
0.4
0.5

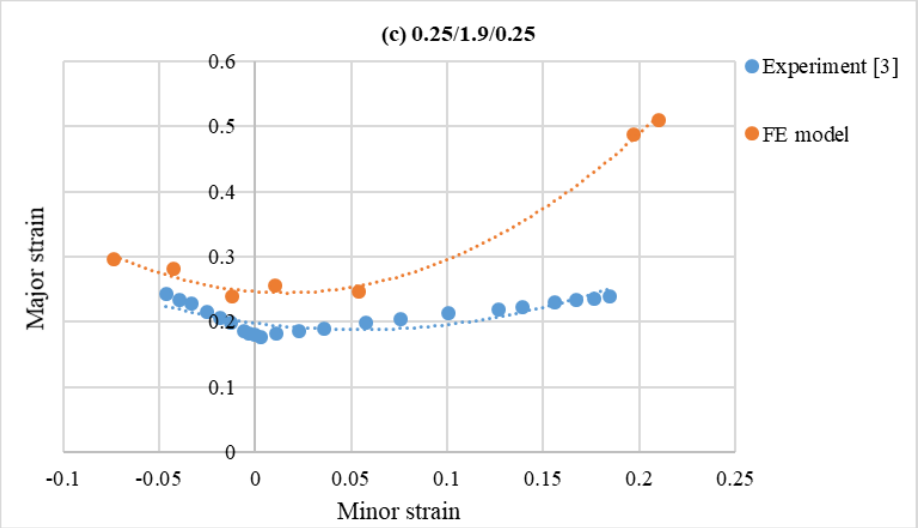

Figure 3.28: Comparison of experiment [3] and finite element model prediction of forming limit curves SA5182/PP/SA5182 laminates: (a) 0.22/0.8/0.22 mm, (b) 0.2/0.8/0.2 mm and (c) 0.25/1.9/0.25 mm

In general, FLC_0 represents the minimum limit strain on an FLC diagram, and it occurs with the plane strain specimen for which the minor strain is zero. Due to the non-linearity of the strain paths, the Nakazima plane strain specimen of 90 mm width does not show the exact value of FLC_0 (i.e., the minor strain is not zero when the specimen fails by necking). Therefore, the FLC_0 is determined as the intersection of the fitted forming limit curve with the major strain axis for each case. Table 3.7 shows limit strains as predicted with the W90 specimens as well as the FLC_0 values obtained from the curve fit. In comparing the single aluminum sheet of 0.22 mm , the Al/Al laminate with 0.22 mm thickness in each layer and the 0.22/0.8/0.22 mm Al/PP/Al laminate, it can be seen that the Al/Al laminate shows the highest FLC_0. The FLC_0s of the Al/PP/Al laminates are higher than those of the single Al sheets.

Table 3.7 Comparison of FLC_0 and W90 strains for single aluminum, Al/Al and the Al/PP/Al laminates

Single Al					
Thickness (mm)			**Minor strain**	**Major strain**	**FLC_0**
			W90 Specimen		*From FLC curve*
0.2			-0.0247	0.186	0.18
0.22			-0.0234	0.188	0.192
0.4			-0.019	0.193	0.21
1.2			-0.0227	0.234	0.225
Al-Al					
			Minor strain	**Major strain**	**FLC_0**
0.22/0.22 (*Tied condition*)			0.0108	0.2238	0.25
Al-PP-Al					
Skin (mm)	**Core (mm)**	**Total (mm)**	**Minor strain**	**Major strain**	**FLC_0**
0.2	0.8	1.2	-0.0039	0.172	0.209
0.22	0.8	1.24	-0.0001	0.181	0.219
0.2	1.6	2	0.0140	0.1884	0.23
0.22	1.6	2.04	0.0193	0.2022	0.23

3.7 FORMING LIMIT CURVES FOR HA5182 AND HA5182/PP/HA5182 SANDWICH LAMINATES

The forming limits of HA5182 aluminum sheets and sandwich laminates with HA5182 aluminum skins are studied in this section. HA5182 shows a much lower forming limit in comparison to SA5182, primarily due to its extremely low '*n*' value, which is 0.07 compared to 0.3 of SA5182. The finite element model remains the same as in Section 3.3. Barlat 89 material model is used to model the HA5182 aluminum skins, since the material properties required to use Yoshida-Uemori material model are not available for HA5182. The material properties for HA5182 including the plastic strain ratios required for Barlat 89 model are listed in Table 3.8.

Table 3.8: Mechanical properties of HA5182 used for Barlat 89 model [3]

ρ (Kg/cm^3)	E (GPa)	Poisson's ratio	K (MPa)	n	Y (MPa)	R0	R45	R90	M
2890	69.6	0.33	581	0.07	425	0.51	0.95	0.98	8

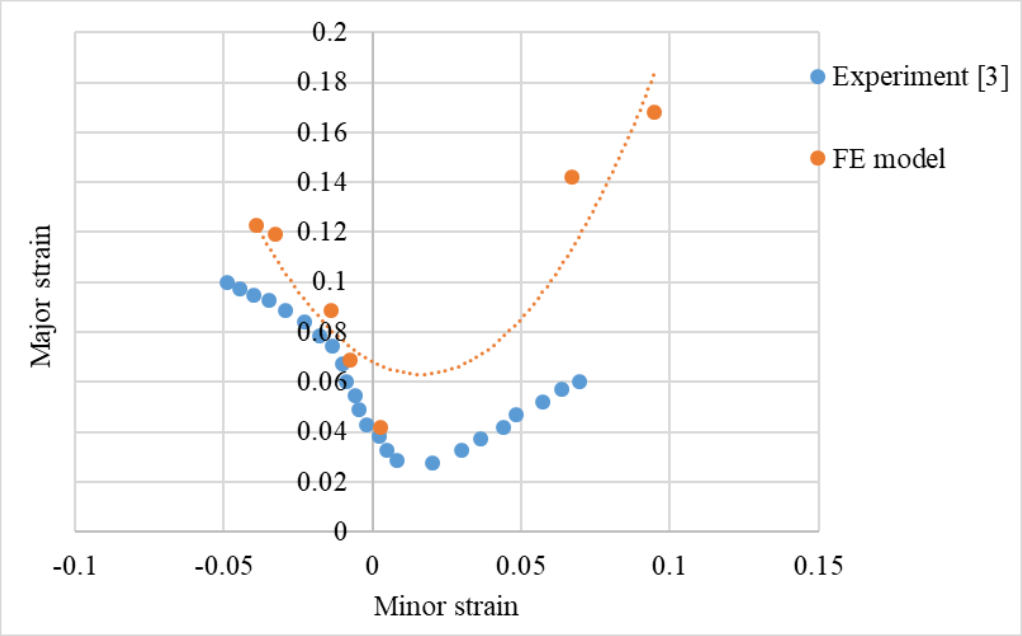

Figure 3.29: Comparison of FLCs determined by experiment [3] and finite element simulation for 0.2 mm thick HA5182

In Figure 3.29, the predicted forming limit curve for monolithic HA5182 (0.2 mm thickness) is compared with the experimental curve taken from Ref [3]. The predicted FLC exhibits higher limit strain values than the experimental FLC. The values on the tension-compression side of the predicted FLC is in close agreement to the experimental FLC.

The forming limit curves for sandwich laminates made with HA5182 aluminum skins are shown in Figures 3.32 and 3.33. The Barlat 89 model is used to model the aluminum skins. The thickness combinations are 0.2/0.8/0.2 mm and 0.2/1.6/0.2 mm.

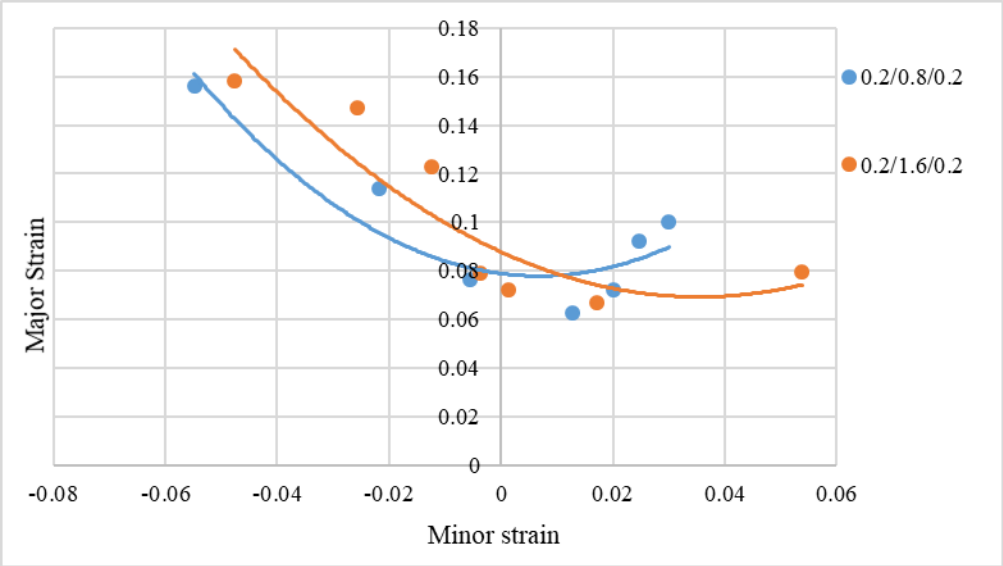

Figure 3.30: Comparison of FLCs of HA5182/PP/HA5182 with 0.2/0/8/0.2 mm and 0.2/1.6/0.2 mm thickness combinations

Figure 3.30 compares the forming limit curves for two thickness configurations of the HA5182/PP/HA5182 sandwich laminates. It can be seen that increasing the core thickness form 0.8 mm to 1.6 mm at a constant skin thickness of 0.2 mm improves the forming limits only on the tension-compression side of the curve. The sandwich laminate with higher core thickness shows lower forming limits on the tension-tension side of the forming limit diagram. This behavior is identical to the experimental FLCs compared for the same hard skin sandwich thickness configurations in Ref. [3].

Figure 3.31 compares the forming limit curves of two sandwich laminates with the 0.2/0.8/0.2 mm thickness combination, one with HA5182 as the skin material and the other with SA5182 skins. Both models use Barlat 89 material model for the aluminum skins and piecewise linear plasticity model for the polypropylene core. The sandwich laminate with HA5182 skins shows much lower forming limits in comparison with the sandwich with SA5182 skins.

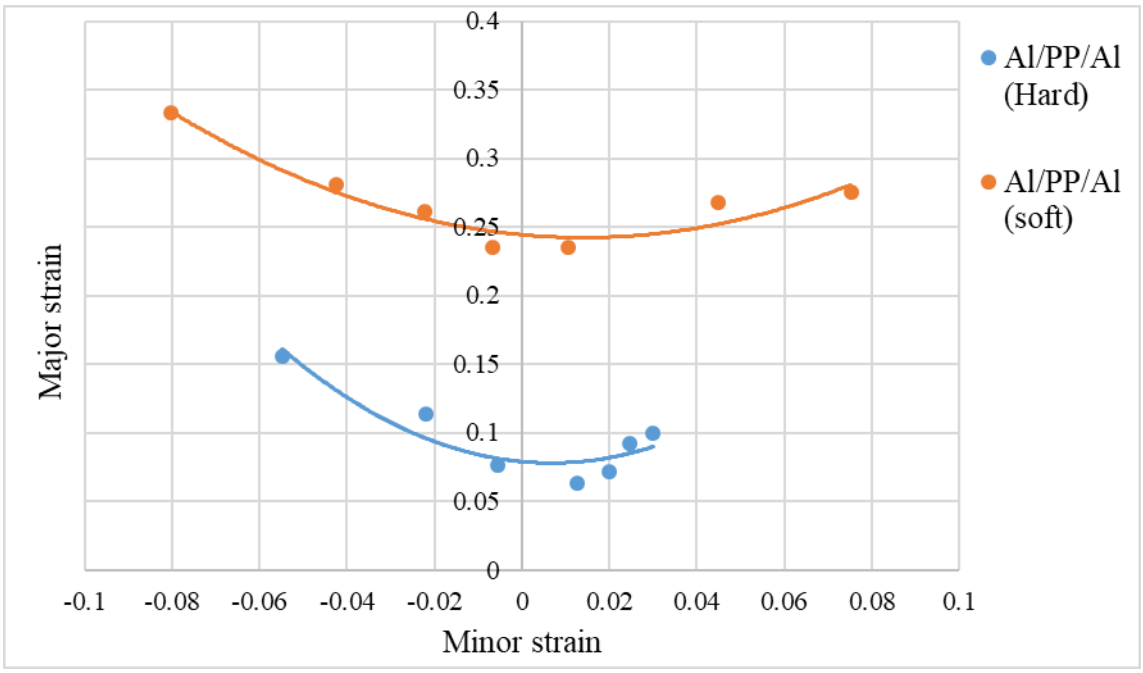

Figure 3.31: Comparison of predicted FLCs for 0.2/0.8/0.2 mm sandwich laminates with HA5182 and SA5182 aluminum skins

In Figures 3.32 and 3.33, the forming limit curves predicted by the finite element simulations in this study are compared with the experimental forming limit curves for the same sandwich laminates. The experimental curves are taken from Ref [3]. Although the experimental FLC_0s and the predicted FLC_0s are very close, the predicted FLCs are higher than the experimental FLCs.

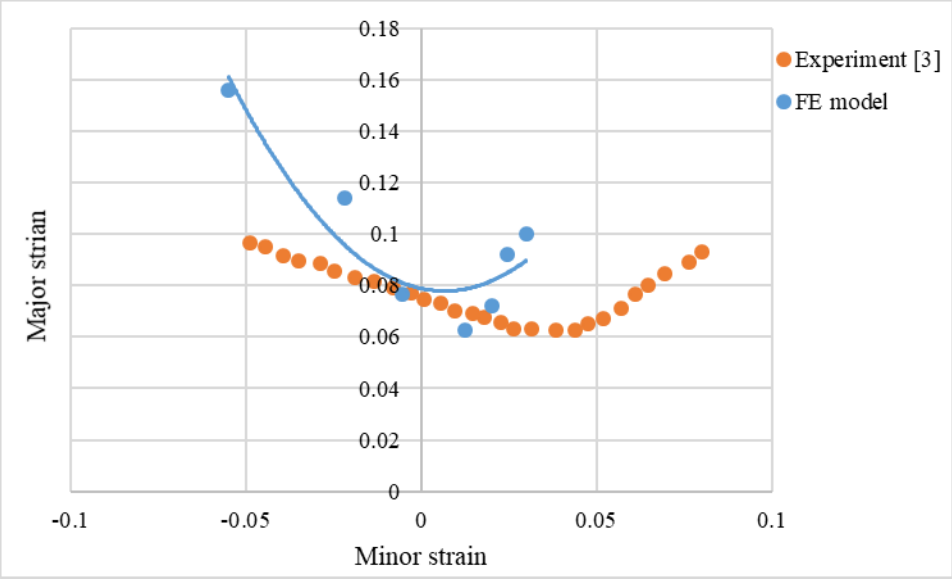

Figure 3.32: Comparison of FLCs determined by finite element simulation and experiment for HA5182/PP/HA5182 (0.2/0.8/0.2 mm thickness)

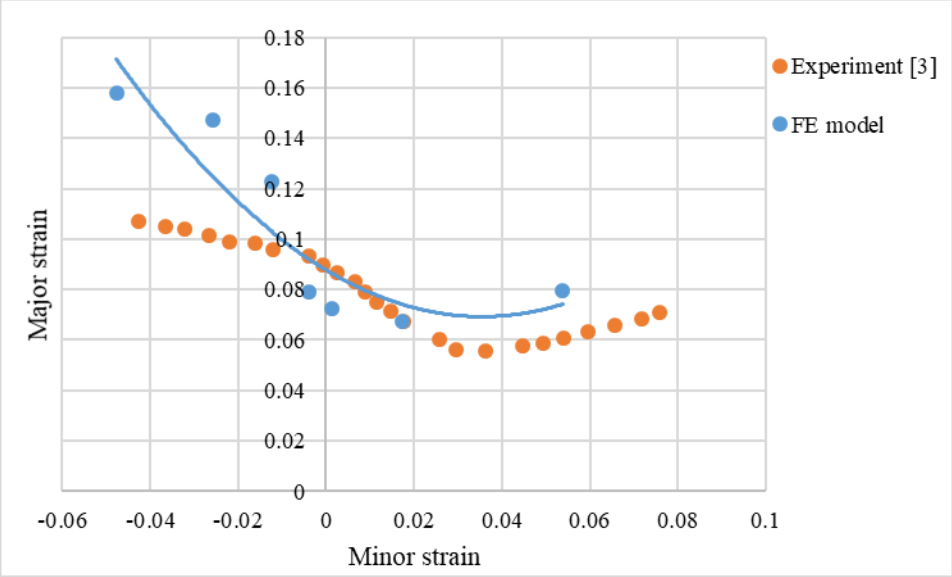

Figure 3.33: Comparison of FLCs determined by finite element simulation and experiment for HA5182/PP/HA5182 (0.2/1.6/0.2 mm thickness)

3.8 Concluding Remarks

The forming limit curves are obtained by numerical simulations for single aluminum sheets, two-layered aluminum laminates, and aluminum-polypropylene-aluminum sandwich laminates. FLCs

are determined by the Nakazima method using blank specimens of widths ranging from 30 mm to 200 mm. The elements exhibiting constant effective plastic strain closest to the necked area are used to evaluate the forming strain limits. The major and minor strains in these elements are plotted for each specimen width to draw the firming limit curves.

- For single aluminum sheets it is observed that the limit strain increases with increase in thickness, as expected. The forming limit curves do not show much variation on the tension-compression side of the diagram but shows consistent increase with increase in thickness on the tension-tension side of the forming limit diagram.
- For aluminum-aluminum laminates with reduced bonding between the two layers, the limit strain decreases with increasing coefficient of friction between the layers. The limit strains for upper and lower layers show more variation on the tension-tension side compared to the tension-compression side. The upper layer shows a more conservative FLC, and is therefore the FLC of the Al-Al laminate is considered to be the FLC of the upper layer.
- When aluminum–aluminum laminates are compared to a single aluminum sheet of equivalent thickness, the model using two layers with perfect bonding shows a higher FLC on the tension-compression side of the curve as well as a higher FLC_0 value. No difference is observed on the biaxial stretch side of the FLC.
- For constant skin thickness of the soft Al/PP/Al sandwich laminates, doubling the core thickness does not have any significant effect on the tension-compression side of the FLC. Higher core thickness shows higher limit strain values only on the tension-tension side of the FLC.

- For a constant core thickness, increasing the skin thickness by a very small value, such as 0.02 mm, shows a small overall improvement in the FLCs of soft Al/PP/Al sandwich laminates.
- Comparing the forming limit curves for single aluminum of 0.2 mm thickness and sandwich laminate (0.2/0.8/0.2 mm), the presence of the polypropylene core shows some improvement in the $FLC_{0.}$
- Similarly, comparing 0.22 mm single SA5182 sheet with the 0.22/0.8/0.22 mm sandwich laminate, some improvement is observed in the $FLC_{0.}$
- The formability of hard Al/PP/Al laminates compared to monolithic hard aluminum shows a minor improvement, which can be attributed to the presence of the polypropylene core.
- The formability of hard Al/PP/Al laminates is much lower than that of soft Al/PP/Al laminates of equivalent thickness combination.
- The finite element model shows fairly close but consistently higher predictions in forming limit strains when compared to the experimental FLCs obtained from previously published data for annealed as well as cold worked aluminum sandwich laminates

3.9 REFERENCES

[1] J. Dicello, "Steel-Polypropylene-Steel Laminate -A New Weight Reduction Material," SAE Paper No. 8800078, *Society of Automotive Engineers*, Detroit, 1980.

[2] T. M.Link, "Formability and performance of steel-plastic-steel laminated sheet materials," SAE Technical Paper 2001-01-0079, *Society of Automotive Engineers*, Detroit, 2001.

[3] T. S. V. Somayajulu, "Vibration and formability characteristics of aluminum polymer sandwich materials," *D.Eng, Dissertation, University of Michigan ,* 2004.

[4] J. Liu, W. Liu and W. Xue, "Forming limit diagram prediction of AA5052/polyethylene/AA5052 sandwich sheets," *Materials and Design,* vol. 46, pp. 112-120, 2012.

[5] H. Palkowski, O. A. Sokolova and A. Corrad`o, "Sandwich materials," in *Ecyclopedia of Automotive Engineering* , John Wiley and Sons, pp. 3183-3200, 2015,.

[6] M. Harhash, R. R. Gilbert, S. Hartmann and H. Palkowski, "Experimental characterization, analytical and numerical investigations of metal/polymer/metal sandwich composites- Part 1: Deep drawing," *Composite Structures ,* vol. 202, pp. 1308-1321, 2018.

[7] K. Kim, D. Kim, S.-H. Choi, K. Chung, K. S. Shin, F. Barlat, K. H. Oh and J. Youn, "Formability of AA5182/polypropylene/AA5182 sandwich sheets," *Journal of Materials Processing Technology,* vol. 139, pp. 1-7, 2003.

[8] T. B. Stoughton, M. F. Shi, G. Huang and J. W. Yoon, "Material characterizations for benchmark 1 and benchmark 2," in *NUMISHEET 2014: The 9th International Conference and Workshop on Numerical Simulation of 3D Sheet Metal Forming Processes: Part A Benchmark Problems and Results and Part B General Papers*, 2014.

[9] LS DYNA, "MAT125_AA5182-O_NUMI2014," LSDYNA , 2014.

[10] M. Ganapathy, R. K. Verma and P. Biswas, "Effect of friction in stretch forming and its influence on the forming limit curve," *Procedings of the Institution of Mechanical Engineers, Part B: Journal of Engineering Manufacture,* vol. 229, 2014.

[11] S. Paul, "Controlling factors of forming limit curve: A review," *Advances in Industrial and Manufacturing Engineering ,* vol. 2, 2021, Article 100033.

Chapter 4 - Springback Behavior of Aluminum/Polypropylene/Aluminum Sandwich Laminates

The springback of metals after forming has been widely studied for decades using numerical and experimental methods. Many of these springback studies involve aluminum alloys. This chapter aims to understand the springback behavior of aluminum-polypropylene-aluminum laminates as they are being used increasingly in automotive and other applications because of their weight saving potential. A finite element model of the draw bending of a U-channel based on Numisheet '93 benchmark study [1] is built using LS-DYNA. First, the model is validated and studied for springback prediction of single AA5182-O (SA5182) aluminum alloy sheets, and then it is extended to the study of the springback behaviors of SA5182/Polypropylene/SA5182 containing AA5182-O or soft aluminum (SA) skins and HA5182/Polypropylene/HA5182 sandwich laminates containing AA5182-H18 or hard aluminum (HA) skins.

4.1 Review of Literature on Springback of Metal/Polymer/Metal Sandwich Laminates

The springback of sandwich panels is a far more complex problem compared to the springback of monolithic panels and not much literature is published in this area. Lui and Wang [2] proposed an analytical model to predict the springback and sidewall curl of metal-polymer-metal laminates after wiper die bending. This model gives a measure for the angle of deviation along with sidewall curl that is observed after laminate bending. This is attributed to the large difference in the properties of the metal skins and the polymer core in the laminates. In this approach, beam bending is treated as a combination of a curved beam bending and a straight beam bending. The curved

beam model is used to calculate the springback angles of the inner and outer skins without the influence of the polymer core. Since these two springback angles are not equal, an interfacial shear stress is developed in the polymer layer. The angular rotation that results from the sidewall curl is calculated using the deflection equation of a straight cantilever beam under shear load. Due to this rotation, the springback of the laminate is higher than the springback based on a single layer model given by Gardiner [3]. Using this combined model, it is shown that the springback of a laminate of a given thickness increases with increasing polymer core thickness and decreases with increasing die radius. Ito et al. [4] derived equations for free bending and springback back behavior of asymmetric metal polymer sandwich laminates, assuming that the polymer layer contains only elastic strains. The asymmetry arises from using skins of two different thicknesses. Additionally, different cases based on the level of propagation of the plastic stress through the thickness of the skins are considered.

Another investigation conducted on steel/polymer/steel panel proposes a model for springback based on 3 point bending experiments [5]. The springback angle is defined as the difference between the final bent angle α_f to the initial angle α_i as shown in Figure 4.1.

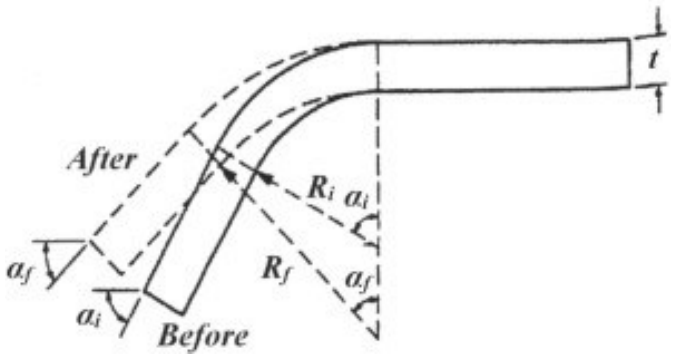

Figure 4.1: Schematic of bending process [6]

This model is simple compared to the previously discussed analytical solutions and has been validated by experimental results to give reasonably accurate predictions. With varying core

thickness value, the effect of (σ/E) ratio is recorded to show that its effect is almost negligible up to a core thickness of 0.6 mm. Increasing the thickness/radius ratio leads to smaller springback values. For a constant core thickness, springback increases with increasing bending angle, and for a constant bending angle, springback reduces with increasing core volume fraction. Figure 4.2 shows a comparison between the experimental and numerical springback values for various core and skin thickness combinations and shows that the FE model results are close to the experimental values. Results also show that the larger the area of specimen in contact with the punch radius the lesser is the amount of springback. For asymmetric sandwich laminates, the thicker the steel sheet that was in contact with the punch, lesser is the springback angle irrespective of the core thickness. More testing can be done to check if these statements hold true when the skin material is swapped out for aluminum.

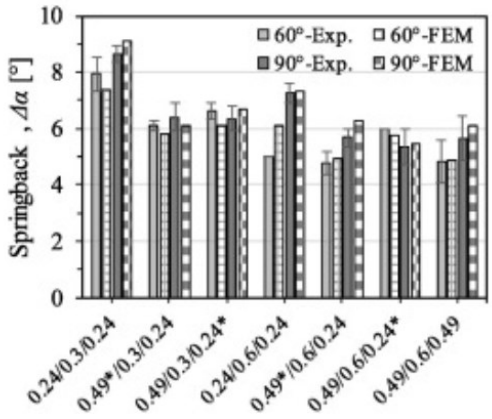

Figure 4.2: Experimental and numerical springback results [5]

In Ref. [7], the springback behavior of aluminum/polymer/aluminum sandwich laminates in free bending was studied with three different grades of aluminum alloys as the skin material and three different polymers as the core material. It was observed that the springback angle decreases with increasing core thickness and is much higher with the skin material having the highest yield strength compared to that having the lowest yield strength. The core material has much less effect

on the springback angle than the skin material. Another study by Ahmed and Chatti [8] compares a semi analytical model to calculate springback of steel/polyurethane/steel panels. The polyurethane core is a foam core. Springback was calculated as the difference between the radius of neutral axis before and after unloading. The springback calculated by analytical model shows a decrease as the core thickness increases. However, the experimental and numerical models shows a much smaller decrease in springback. Additionally a simple equation for calculating springback using corrected Young's modulus at large plastic strains is also proposed and this equation predicts values of springback closer to experiment. Mohammadi et.al [9] studied the V-die bending of Al3105/polypropylene/Al3105 sandwich sheets. They proposed an analytical model that calculates springback as a sum of the springback in the punch-sheet contact area and springback along the length of the sandwich panel. When compared to numerical and experimental work, the analytical model showed significantly higher values of springback.

The published studies on the springback of metal-polymer-metal laminates mostly involves free bending. The current work focuses on the springback behavior of aluminum-polypropylene-aluminum sandwich laminates under draw bending conditions. In draw bending operations, the sheet blank first undergoes bending-unbending deformation around the die corner as it is pulled into the die cavity and then a significant stretching deformation as the final shape of the part is being formed. As the part is released from the die, its sidewalls and flanges exhibit springback due to elastic strain recovery. Also, instead of remaining straight, the sidewalls become curved, which is called sidewall curl.

4.2 SPRINGBACK OF SINGLE SA5182 ALUMINUM SHEETS

4.2.1 Finite element model

Springback of single SA5182 aluminum sheets is studied using the draw-bend setup for forming U-channels defined in Numisheet '93 [1]. A quarter model is built in LS-DYNA applying symmetric conditions to reduce computation time. The model consists of a rigid die, punch, blank holder and a deformable blank similar to Figure 4.3. The gap between the die and the punch is 1 mm. The aerial dimensions of the blank are 350 mm x 35 mm (175 mm x 17.5 mm for the quarter model). The thickness of the blank is 0.81 mm. A total blank holder force of 2450 N is applied (a reduced value of 612.5 N is used for the quarter model). The blank is drawn to a depth of 70 mm with a punch velocity of 200 mm/sec. The tools and the blank are modelled using fully integrated 4-noded quadrilateral shell element formulation (type 16 in LS-DYNA) recommended for springback simulations by Maker and Zhu [10]. The mesh size is 1 mm by 1 mm for both the blank and the tools. Adaptive meshing with a maximum refinement of four levels is used to refine the mesh over the die and punch corner radii.

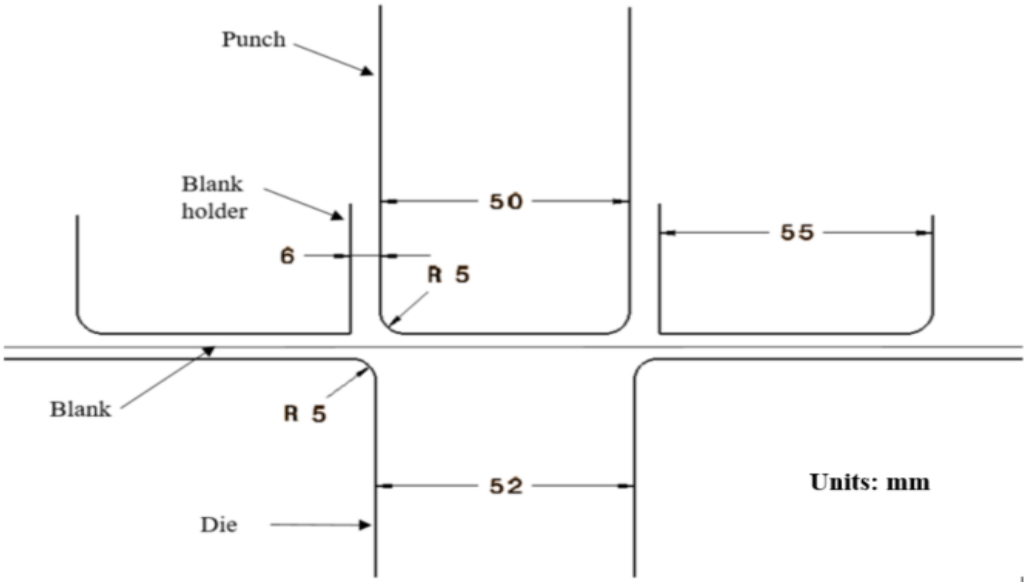

Figure 4.3: Dimensions of the draw-bend setup for forming U-channel according to Numisheet '93 [1]

In Ref. [11], the effect of the number of integration points on the springback of aluminum sheets using Numisheet '93 standards [1] is studied. The results show that with 5 integration points, the wall angle θ_1 shows zero error and the flange angle θ_2 shows minimal error. However, the thickness of the sheet is not mentioned. Recommendations have been made by Wagoner et al. [12] to use up to 25 integration points for accurate springback values; however, another study [13] shows that integration points beyond an optimal value of 7 can reduce the accuracy of springback prediction. To understand the bending and springback behavior of monolithic aluminum sheets in draw-bending simulations, 9 integration points through the sheet thickness are used in this study. The process of selecting a model for accurate springback values and stress distributions is described in Appendix A. The deformed aluminum blank mesh after it has reached the 70 mm draw depth is used as an input file for an implicit springback simulation.

Springback is characterized by measuring the change in shape along the side wall and the flange. The angular changes in the sidewall and the flange are measured by the wall angle θ_1 and the flange angle θ_2, respectively (Figure 4.4). The description of θ_1 and θ_2 along with the standard

procedure given in Numisheet‘93 [1] is followed to make these measurements uniform as shown in Figure 4.4. In addition to the wall and flange angles, the curvature of the wall of the formed U-channel, referred to as the sidewall curl, is measured by its radius ρ. The radius of curvature is measured by the radius of a curve fitted through three points A, B and C as shown in Figure 4.4. Here, C is the midpoint between A and B. In this study, the springback angles θ_1 and θ_2 are measured in CATIA V5 using the meshes at the end of the springback simulation obtained from LS-DYNA.

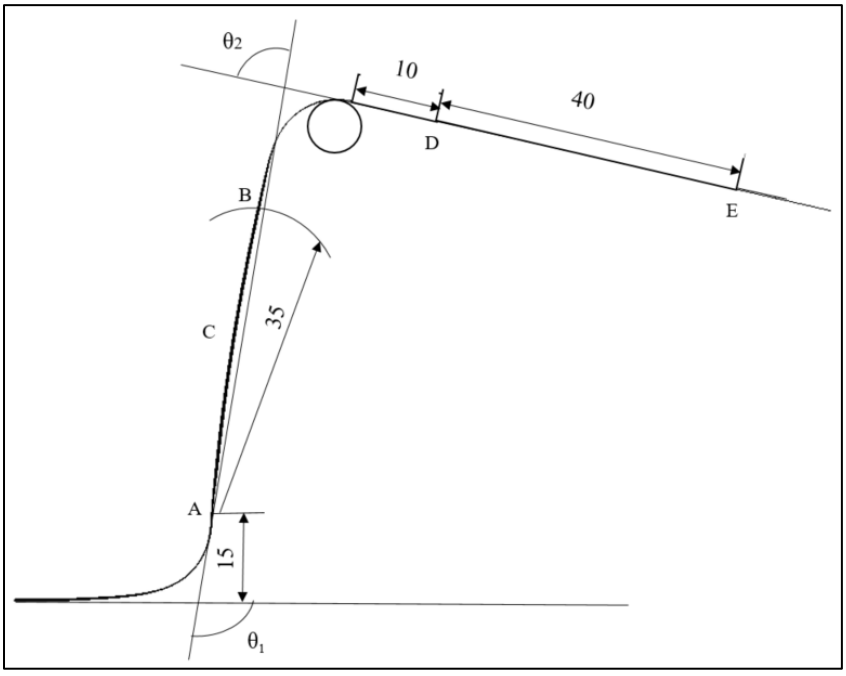

Figure 4.4: Springback measurements for a drawn U-channel according to Numisheet‘93
(All dimensions are in mm)

Four material models from LS-DYNA are compared in this study for their applicability for springback prediction of aluminum alloys. They are Mat_125 (YU hardening with Hill 48), Mat_36 (Barlat 89 with isotropic hardening), Mat_226 (YU hardening model with Barlat 89) and Mat_133 (Isotropic hardening with Barlat 2000). The theoretical description of each model is made in Chapter 2. To make exact comparisons between the material models, the uniaxial stress

strain data obtained from a simulation of a uniaxial tension test conducted based on ASTM-E8 standards for AA5182-O with material model Mat_226 is used as the input curve for material models Mat_36 and Mat_133.

In Ref. [14], Mat_125 and Mat_133 were used to compare θ_1 and θ_2 with the experimental values for an inverted U channel. This study was applied for different grades of steel and shows that Mat_125 gives closer predictions to the experiments. It also shows that the side wall curl was better captured by Mat_125. In Numisheet 2005 [15], springback predictions for a crossmember with an aluminum AA5182-O modelled by using Mat_226 show closest values to the experimental results in comparison to Mat_125 and other material models.

The four material models are now used to evaluate the springback of an SA5182 blank of dimensions of 350 mm x 35 mm with a thickness of 0.81 mm. The results obtained for the wall angle (θ_1) and the flange angle (θ_2) are listed in Table 4.1 and are compared to the range of the experimental values given in Ref. [1].

Table 4.1: Springback of single SA5182 as predicted by different material models (sheet thickness = 0.81 mm, die and punch corner radii = 5 mm)

Material card (LS-DYNA)	**Material model**	**Wall angle θ_1(°)**	**Flange angle θ_2(°)**
Numisheet 93	----	101.5-116	68.5-77.5
Mat_226	YU* + Barlat 89	107.167	78.245
Mat_133	IH**+ Barlat 2000	109.725	69.26
Mat_125	YU + Hill 48	106.092	77.204
Mat_36	IH+ Barlat 89	109.745	68.035

**YU – Yoshida –Uemori, **IH – isotropic hardening*

The contours of the U-Channels after springback as predicted by the four material models are compared in Figure 4.5. From Table 4.1, it can be seen that all material models predict wall angle ($\boldsymbol{\theta_1}$) values within the expected range shown in Numisheet '93 [1]. The difference between

them is in the prediction of the flange angle (θ_2). The flange angle predicted by material model Mat_226 is slightly higher than the range in Numisheet '93, while the flange angles predicted by Mat_36 is lower than the range in Numisheet '93. Material models 125 and 226 produce wall angles close together, while material models 133 and 36 produce wall angles very close together. Overall, the stiffest response to springback is obtained by material model 226 (Yoshida-Uemori hardening model combined with Barlat 89 yield surface) while the most flexible response to springback is obtained with material models 36 and 133. These results are in agreement with the results presented by Zhang et.al. [16]. Considering the bending and unbending cycle that occurs in the process of forming the U-channel as the material passes over the die radius, the YU hardening model is considered more appropriate to capture the Bauschinger effect more accurately. Although this capability is present in both Mat_226 and Mat_125, Barlat89 yield criterion used in Mat_226 is recommended over Hill48 used in Mat_125 for modelling aluminum alloys [17]. Based on the discussion presented in this section, all further springback analyses for SA5182 aluminum alloy sheets will be conducted with Mat_226.

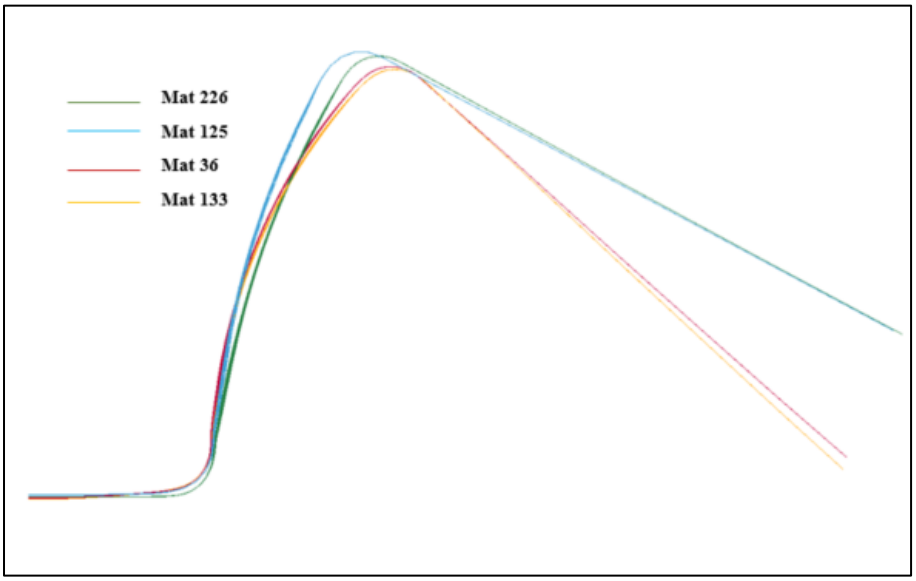

Figure 4.5: Comparisons of springback for single SA5182 obtained by using different material models in LS-DYNA

4.2.2 Effect of sheet thickness

In this section, the effect of sheet thickness on the springback of SA5182 is studied by considering a thickness range of 0.2 mm to 1.2 mm in steps of 0.2 mm. The blank size has the aerial dimensions of 320 mm x 35 mm. A blank length of 320 mm is used instead of 350 mm to match the blank length used in the springback experiments described later in the chapter. The punch diameter is 50 mm, and the die-punch gap is adjusted based on the sheet thickness so that there is no ironing as the U-channel is formed.

The results presented in Table 4.2 and Figure 4.6 show that as the sheet thickness increases from 0.2 mm to 1.2 mm, the springback of the SA5182 aluminum sheets shows a stiffer response. The wall angle reduces, while the flange angle increases with increasing sheet thickness. The radius of curvature controlling the sidewall curl also increases when the sheet thickness increases. The U-channel profiles after springback are shown in Figure 4.8.

Table 4.2: Effect of sheet thickness on springback of single SA5182 sheets
(For die and punch radius = 5 mm)

Thickness (mm)	**Die-Punch Gap (mm)**	**Bending Stiffness ($N\text{-}mm^2$)**	**θ_1 (°)**	**θ_2 (°)**	**ρ (mm)**
0.20	0.5	1633.33	118.283	67.63	62.818
0.40	1.0	13066.67	111.553	71.297	95.157
0.60	1.5	44100.00	108.532	72.635	105.894
0.80	1.5	104533.33	106.584	80.22	131.119
1.00	1.5	204166.67	102.294	81.865	145.004
1.20	1.5	352800.00	98.639	83.017	194.21

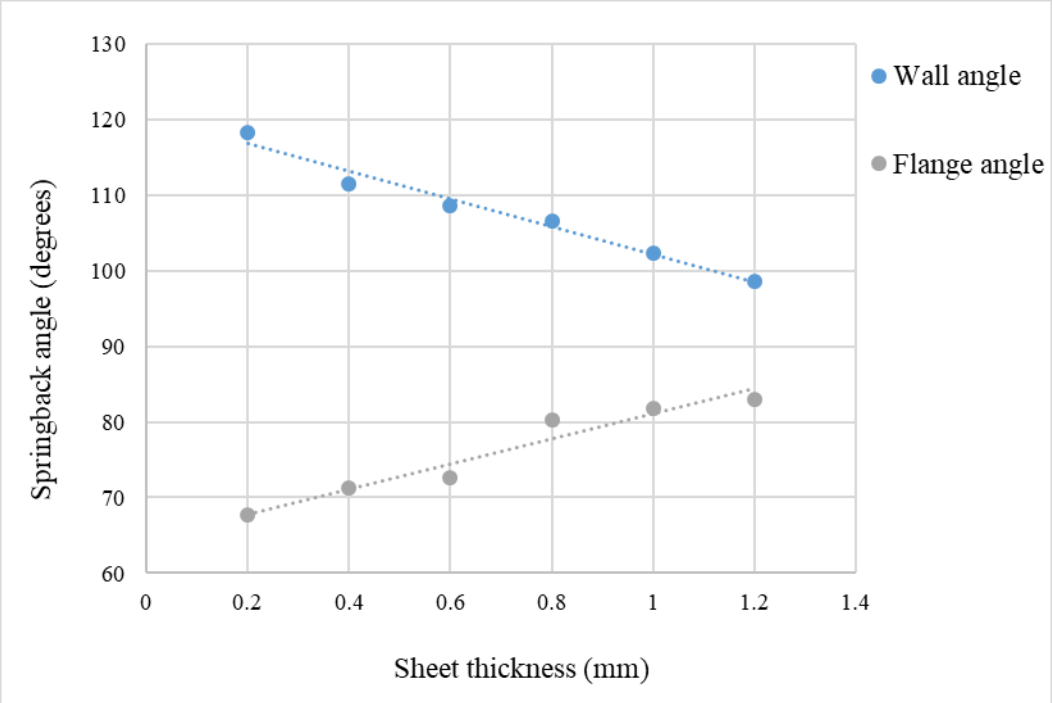

Figure 4.6: Effect of sheet thickness on the springback angles of SA5182

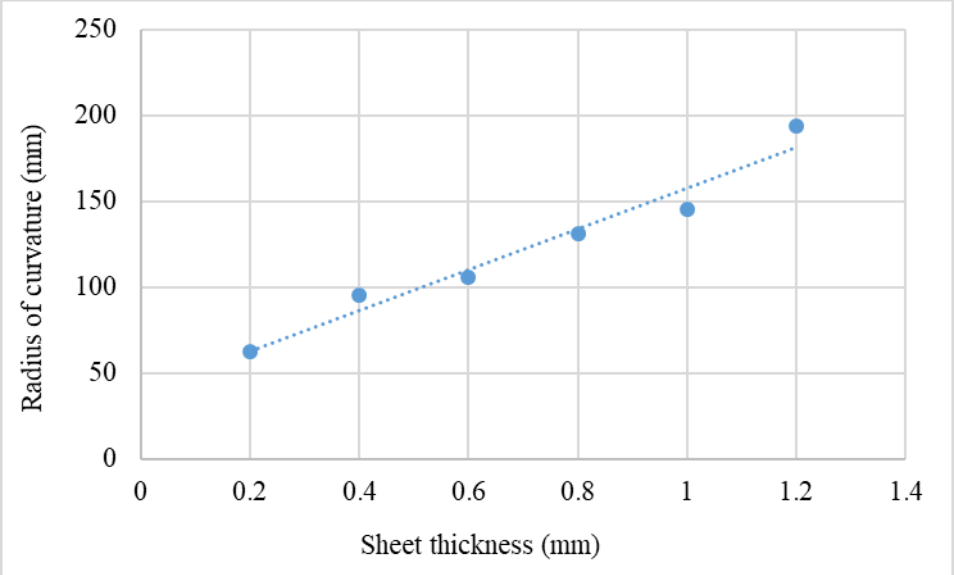

Figure 4.7: Variation of radius of curvature of the wall with sheet thickness for SA5182

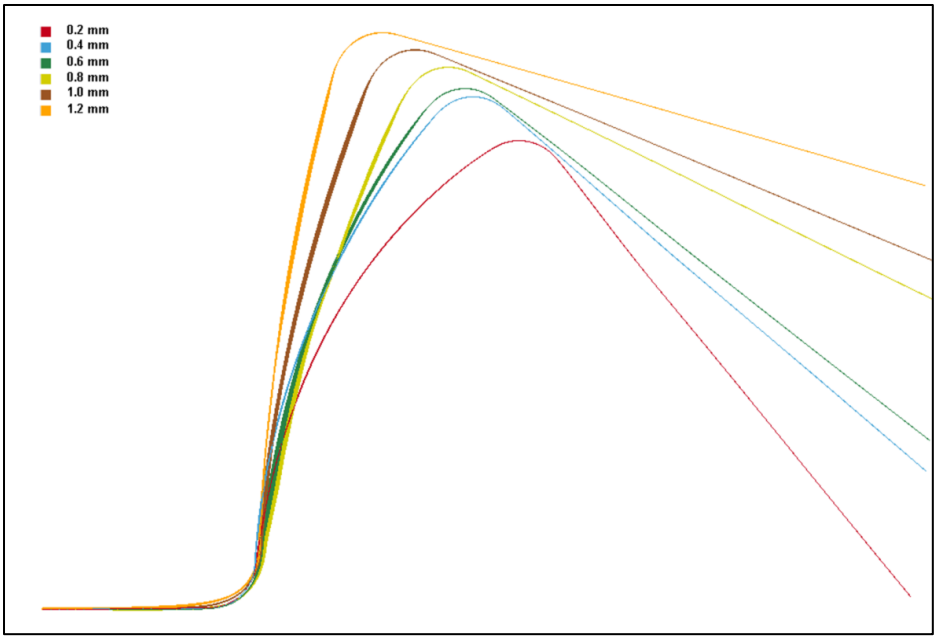

Figure 4.8: Springback profiles of single SA5182 sheets with thickness ranging from 0.2 mm to 1.2 mm

Since springback after U-channel forming involves bending deflection of its walls and flanges, the effect of sheet bending stiffness on the springback angles and the radius of curvature is considered. The bending stiffness of single aluminum sheets is calculated using Equations 4.3 and 4.4.

$$Bending\ stiffness \propto EI \qquad \text{Eq. 4.3}$$

$$Second\ moment\ of\ area,\ I = \frac{bt^3}{12} \qquad \text{Eq. 4.4}$$

where b is the width of the sheet, which for the U-channels is 35 mm, and t is the thickness of the sheet.

The springback angles are plotted against the bending stiffness of the SA5182 sheets with different thicknesses in Figure 4.9. It can be seen in this figure that the wall angle decreases, and the flange angle increases with increasing bending stiffness until it reaches a value of 200000 N-mm^2. At higher bending stiffnesses, the springback angles do not show much variation. However, as can be seen in Figure 4.10, the radius of curvature of the wall increases with increasing bending

stiffness, indicating that there is less wall curl, even at bending stiffnesses higher than 200000 N-mm^2.

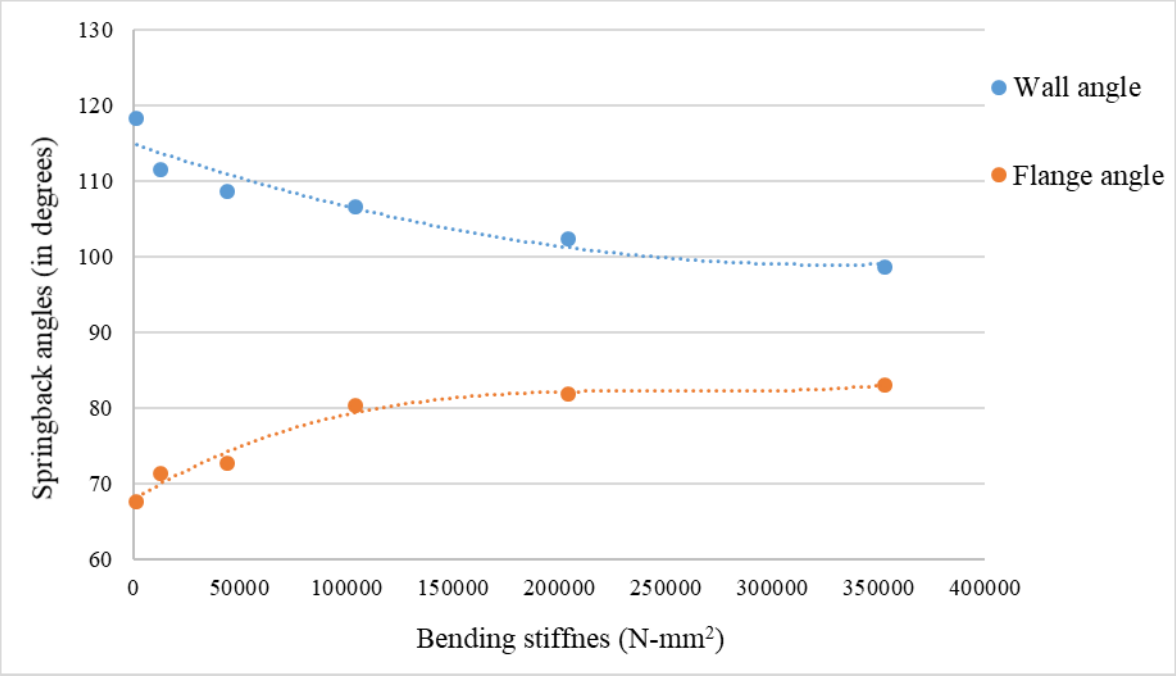

Figure 4.9: Wall angle and flange angle vs. bending stiffness of single SA5182 sheets

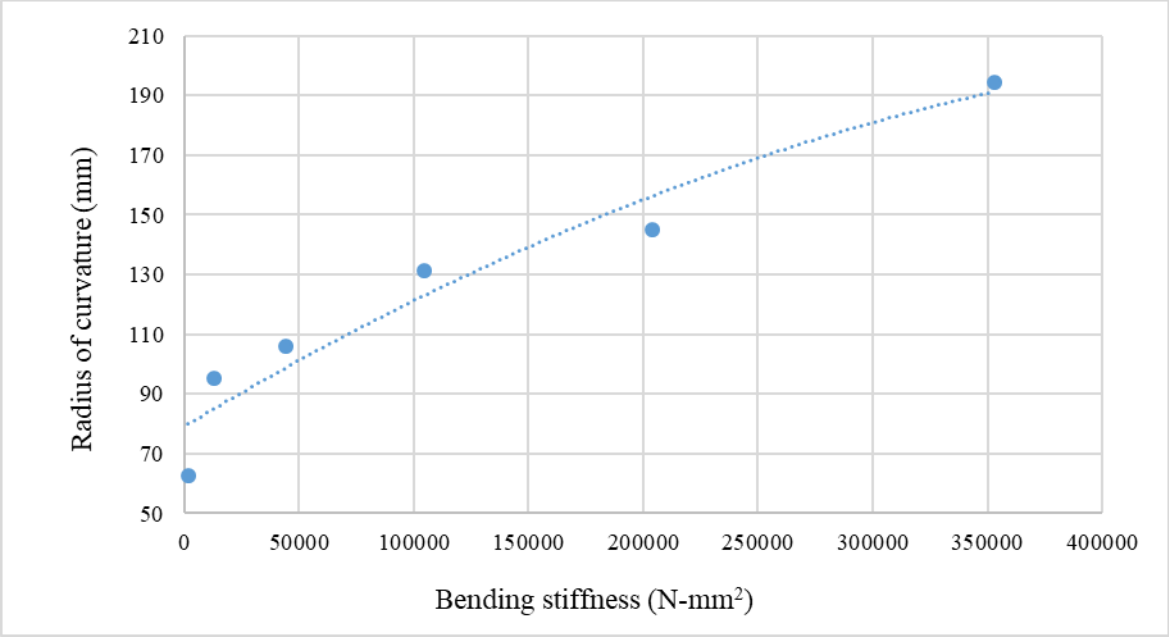

Figure 4.10: Variation of radius of curvature of the wall of SA5182 sheets with bending stiffness

The distributions of effective plastic strain on the upper surface of the formed U-channels with different sheet thicknesses of aluminum SA5182 are plotted in Figure 4.11(a) and (b) for die/punch radii of 5 mm and 8 mm, respectively. The effective plastic strains increase with increasing sheet thickness, and their peak values occur along the wall close to the die and punch radii. The effective plastic strains for the 1.0 mm and 1.2 mm aluminum sheet reduces when the die and punch radii are increased from 5 mm to 8 mm (Figure 4.11 (b))

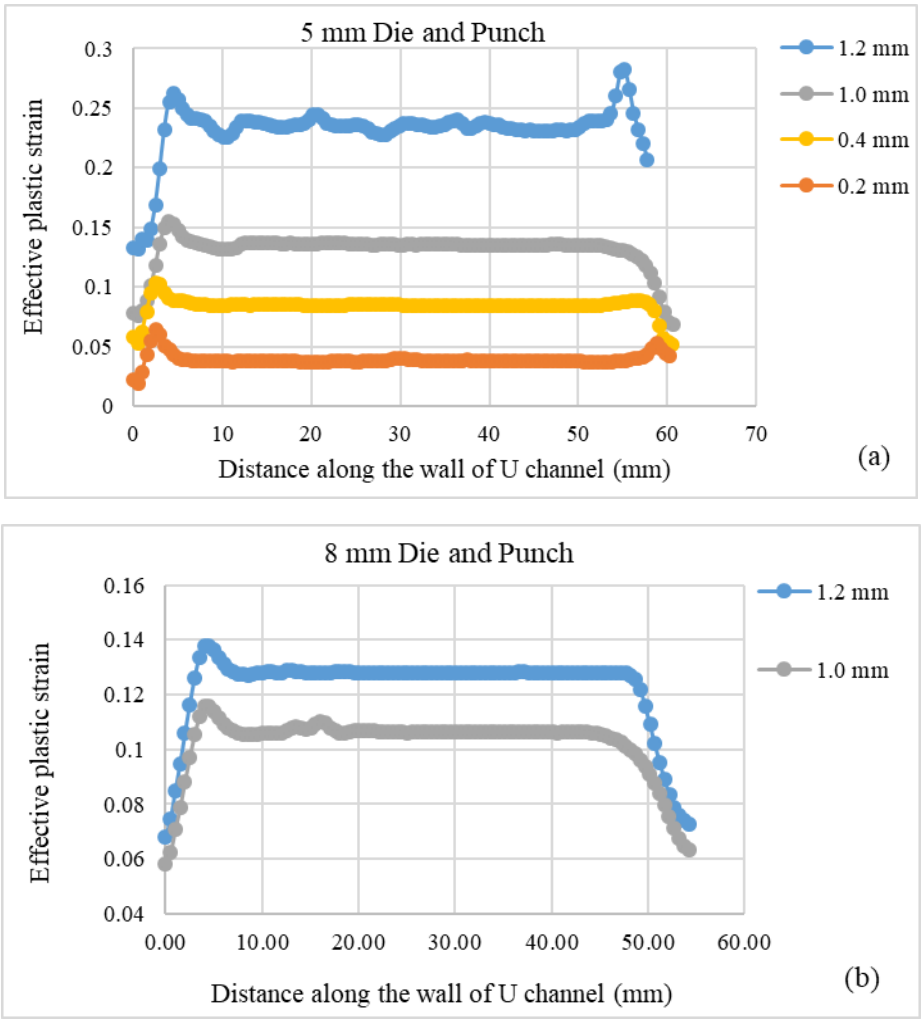

Figure 4.11: Effective plastic strains along the wall of drawn U-channels of single aluminum sheets for (a) 5 mm die and punch radii (b) 8 mm die and punch radii

Table 4.3: Springback values with die and punch radius 8 mm

Sheet Thickness (mm)	Die and punch radius = 8 mm		
	θ_1 (°)	θ_2 (°)	ρ(mm)
0.8	102.097	84.495	246.543
1	101.676	84.71	259.64
1.2	98.888	85.269	290.165

In Table 4.2, the springback values are listed for a die-punch radius of 5 mm. Table 4.3 shows the springback values for a die-punch radius of 8 mm. Comparing the two sets of springback values in Tables 4.2 and 4.3, it can be observed that while the wall and flange angle variations are similar, there is a large increase in the radius of curvature of the wall with increase in die-punch radii from 5 mm to 8 mm. This means that the side wall curl is reduced significantly as the radii of the die and punch are increased.

4.3 SPRINGBACK OF SA5182/POLYPROPYLENE/SA5182 SANDWICH LAMINATES

The springback of SA5182/Polypropylene/SA5182 laminates is assessed by using the same setup as shown in Figure 4.3. The aerial dimensions of the blank are 320 mm x 35 mm. The laminate thickness is in the range of 1.2 to 2.6 mm and is made of various combinations of aluminum skin thicknesses of 0.2, 0.22, 0.24 and 0.25 mm. The polypropylene core thicknesses are 0.8, 1, 1.6, 1.9 and 2.2 mm. These sandwich laminates are available commercially and their stress-strain characteristics have been studied previously by Somayajulu [18].

The material properties of polypropylene at room temperature and a strain rate of 10 s^{-1} are used for the springback evaluation. They are 2443 MPa for elastic modulus, 25 MPa for yield strength and 0.43 for Poisson's ratio. The true stress vs. plastic strain is calculated using the stress-strain relationship from Ref. [19] and is shown in Figure 4.12.

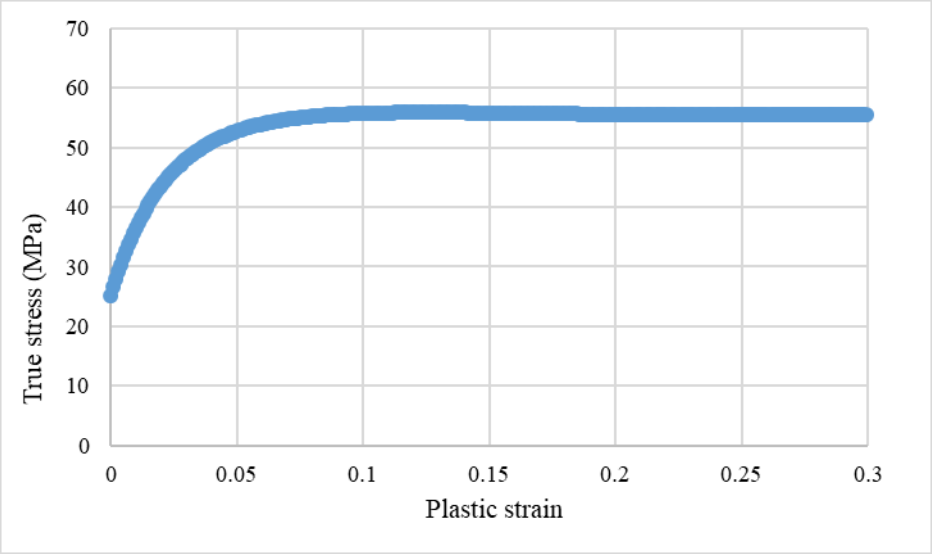

Figure 4.12: True stress vs plastic strain curves for polypropylene at 10 per sec strain rate

A quarter model of the die-punch setup is built in LS-DYNA to save computation time. Since U-channel draw-bending experiments conducted with 0.2/0.8/0.2 mm sandwich laminates in a die-punch setup with 5 mm die-punch radii have shown early cracking at the punch corners at a draw depth of 8 mm (Figure 4.13), it was decided to use 8 mm die-punch radii for all springback simulations with sandwich laminates. The finite element simulation shows that with a die-punch radius of 5 mm, the aluminum outer skins of the 0.2/0.8/0.2 mm sandwich laminate configuration reach plastic strain values at the punch corner radius that are higher than the failure strain of SA5182 (Table 4.5). As a result, failure is expected to occur at the punch corner of the U-channel. Therefore, to study the springback behavior of the sandwich laminates, the die and punch radii are both increased to 8 mm.

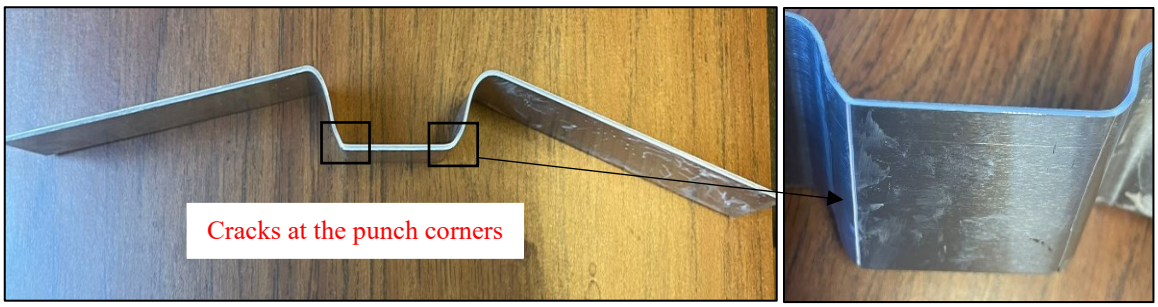

Figure 4.13: Cracks at the punch corners of a 0.2/0.8/0.2 (mm) Al/PP/Al sandwich specimen in a draw-bending experiment using 5 mm die-punch radii

Table 4.4: Effective plastic strains at the through-thickness integration points during draw-bending of a sandwich laminate with 0.2/0/8/0.2 thickness combination

	Upper aluminum skin (0.2 mm thickness)			**Polypropylene core (0.8 mm thickness)**				**Lower aluminum skin (0.2 mm thickness)**		
Integration point	1	2	3	4	5	6	7	8	9	10
Effective plastic strain	0.263	0.259	0.251	0.09	0.03	0.00	0.03	0.249	0.258	0.36

4.3.1 Finite element model

The finite element model for the sandwich laminates is similar to the setup for monolithic aluminum sheets described in Section 4.2, with the exception that the aluminum/polypropylene/aluminum sandwich blank is modeled with Part_Composite shell elements available in LS-DYNA. Unlike the traditional method that requires a separate mesh for each material, Part_Composite allows the use of a single shell mesh within which individual layers of the sandwich laminate are defined by their thickness and integration points. It is recommended and commonly used for modeling composite materials with multiple layers of different properties. Figure 4.14 shows the Part_Composite model of the aluminum/polypropylene/aluminum laminates used in this study. The aluminum skin on each side of the laminate is divided into three layers of equal thickness and the polypropylene core is divided into four layers of equal thickness.

The integration points are located at the center of each layer thickness. Thus, the aluminum skins are defined by 3 integration points each and the polypropylene layer is defined by 4 integration points. The Part_Composite elements use trapezoidal integration rule. Adaptive mesh is used in the model with up to 4 levels of refinement to capture the die and punch radii more accurately.

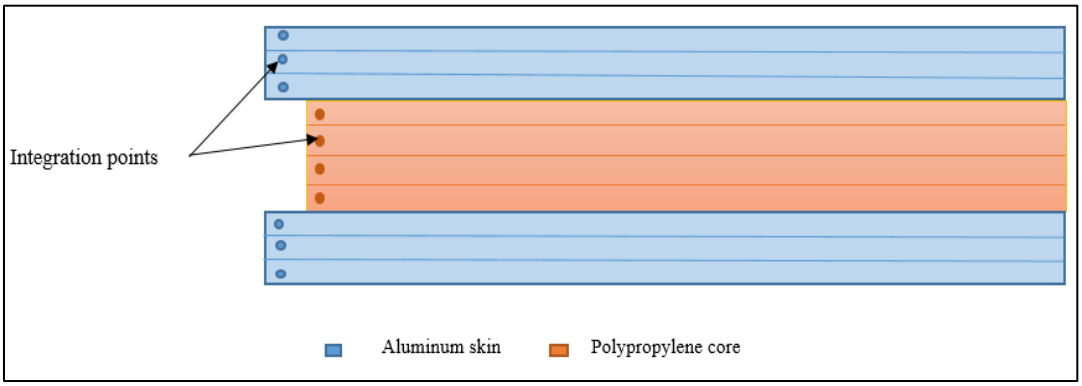

Figure 4.14: Part composite setup – location of integration points

4.3.2 Effect of laminate thickness

The springback in the wall is represented by the wall angle θ_1 and springback in the flange is represented by the flange angle θ_2, and the radius of curvature ρ represents the sidewall curl. The measurements of θ_1, θ_2 and ρ for the U-channels after springback are made as described in Section 4.2. The springback values obtained for different thickness combinations of aluminum skins and polypropylene core are recorded in Table 4.5. The wall angle θ_1 is directly influenced by the total thickness of the sandwich laminate, while the flange angle θ_2 is more dependent on the sidewall curl in the U-channel**.** A large value of radius of curvature indicates reduced sidewall curl.

Table 4.5: Springback measurements for Al/PP/Al sandwich laminates (with 8 mm die and punch radii)

Al/PP/Al Thickness combination (mm)	Laminate thickness (mm)	Die-punch gap (mm)	θ_1 (°)	θ_2 (°)	ρ(mm)
0.20/0.8/0.20	1.2	1.5	103.9	82.206	179.582
0.22/0.8/0.22	1.24	1.5	103.106	82.415	179.436
0.24/0.8/0.24	1.28	1.5	103.069	83.023	183.116
0.24/1.0/0.24	1.48	1.7	100.188	84.18	224.928
0.20/1.6/0.20	2.0	2.3	98.314	83.983	258.614
0.22/1.6/0.22	2.04	2.3	97.65	85.3	302
0.24/1.6/0.24	2.08	2.3	96.998	86.2	329
0.24/1.9/0.24	2.38	2.6	97.709	84.25	251.503
0.25/1.9/0.25	2.4	2.62	97.122	84.784	296.124
0.24/2.2/0.24	2.68	2.9	98.604	84.016	245.51

From Table 4.5, it can be seen that at a constant core thickness, increasing the skin thickness, even by very small values, changes the springback values significantly. It must also be noted that by increasing the thickness of the polypropylene core the sidewall curl is also reduced. From Figure 4.15 it can be seen that the wall angle θ_1 decreases with increasing laminate thickness and the flange angle θ_2 shows an increasing trend with increasing laminate thicknes. However, as the laminate thickness becomes very high, changes in both wall and flange angles become relatively small.

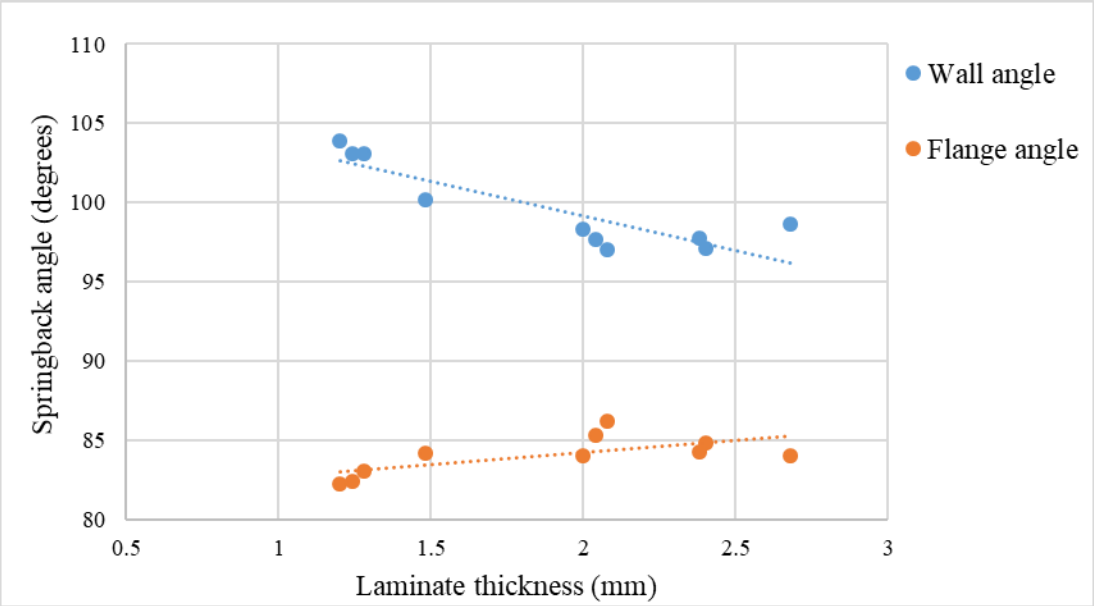

Figure 4.15: Variation of wall and flange angle with laminate thickness

In Figure 4.16, the radius of curvature is plotted against the laminate thickness. There is an increase in sidewall curl up to a laminate thickness of 2 mm after which it shows a decreasing trend.

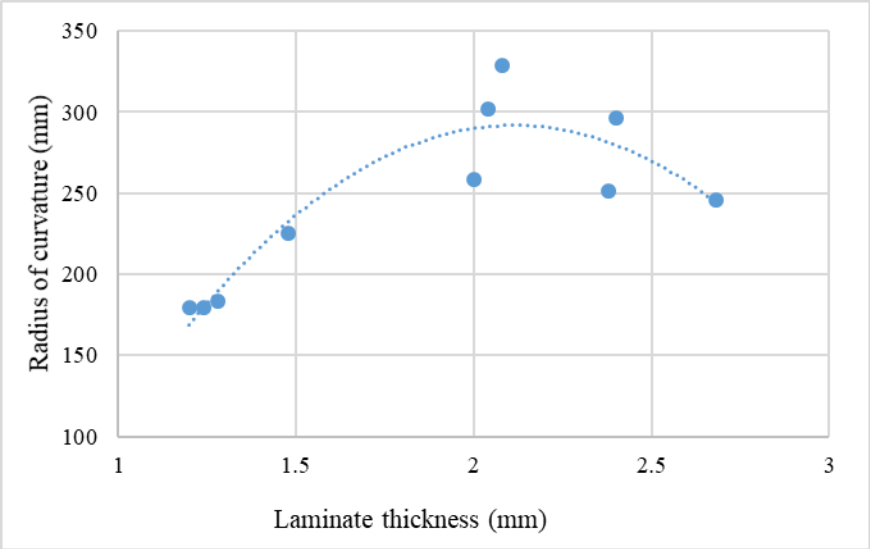

Figure 4.16: Variation of radius of curvature of the wall with laminate thickness

The shape of the U-channels after springback, compared for laminates with 0.8 mm core thickness and skin thickness of 0.2 mm, 0.22 mm and 0.24 mm. Figure 4.17 shows the improvement in springback behavior with increasing laminate thickness as well as increasing skin thickness.

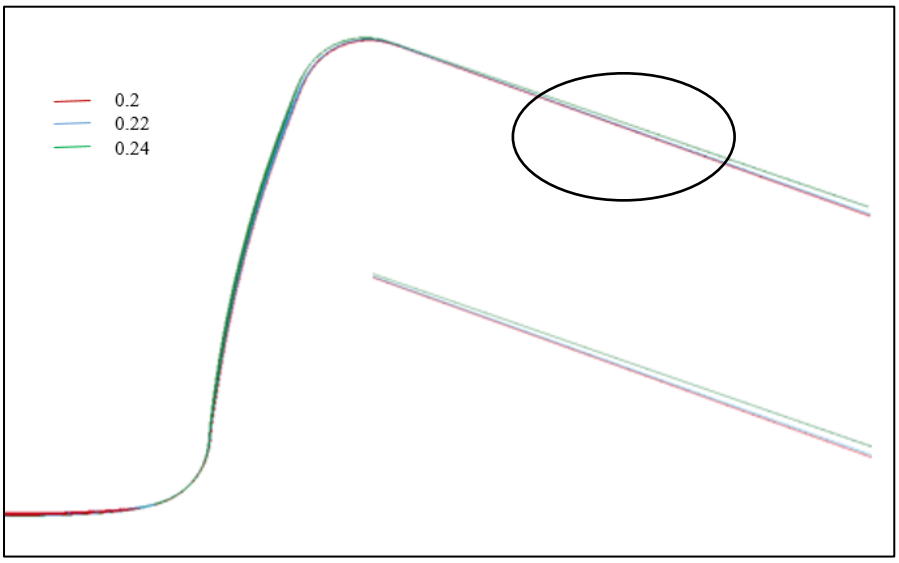

Figure 4.17: Springback shapes for 0.8 mm core thickness, with skin thicknesses of 0.2 mm,0.22 mm and 0.24 mm

The springback variation of Al/PP/Al laminates cannot be explained solely as a function of laminate thickness, since it is also dependant on the volume fraction of each component material and the overall stiffness of the sandwich laminate. Therefore, further comparisons are made to study the springback behavior with laminate stiffness. For a given symmetric 3-layered laminate of skin thickness (t) and core thickness (d), the bending stiffness EI is calculated using Equation 4.5 taken from [20].

$$EI_{Laminate} = E_s\left(\frac{bt^3}{6}\right) + 2bE_s t\left\{\frac{d+t}{2}\right\}^2 + E_c\left(\frac{bd^3}{12}\right) \quad \text{Eq. 4.5}$$

Table 4.6: Bending stiffness of Al/PP/Al laminates

Skin thickness, t (mm)	Core thickness, d (mm)	Skin stiffness	Core stiffness	Laminate stiffness (N-mm^2)
0.2	0.8	248266.67	3648.21	251914.88
0.22	0.8	284735.73	3648.21	288383.95
0.24	0.8	323635.20	3648.21	327283.41
0.24	1	457699.20	7125.42	464824.62
0.2	1.6	797066.67	29185.71	826252.37
0.22	1.6	897039.73	29185.71	926225.44
0.24	1.6	1001011.20	29185.71	1030196.91
0.24	1.9	1352047.20	48873.23	1400920.43
0.25	1.9	1422020.83	48873.23	1470894.07
0.24	2.2	1756003.20	75871.44	1831874.64

The bending stiffness calculated for each thickness combination is listed in Table 4.6. The graph plotted between wall angle and bending stiffness in Figure 4.18 shows that wall angle decreases with increasing bending stiffness up to a laminate stiffness of 11.5 x 10^6 N-mm^2 and then starts to show an increase. In comparing the wall angles of the single aluminum sheet and Al/PP/Al laminate with the same bending stiffness it can be seen that the laminate shows greater springback. Similarly, the flange angles for the Al/PP/Al laminates are lower than the flange angles of the single SA5182 sheets for the same bending stiffness. The flange angles are plotted against laminate stiffness in Figure 4.19. It can be seen that flange angle increases with bending stiffness, reaches a maximum and then decreases. The radius of curvature of the wall also increases with increasing bending stiffness up to a laminate stiffness of 11.5 x 10^6 N-mm^2 and then decreases (Figure 4.20). These results show that single aluminum sheets with equal bending stiffness as Al/PP/Al laminates have better springback performance.

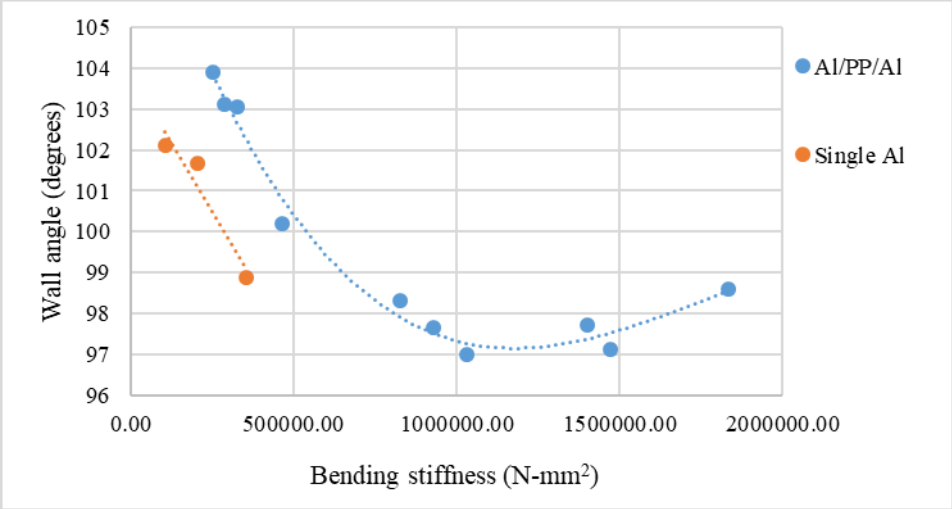

Figure 4.18: Wall angle vs. bending stiffness of single Al and Al/PP/Al laminates

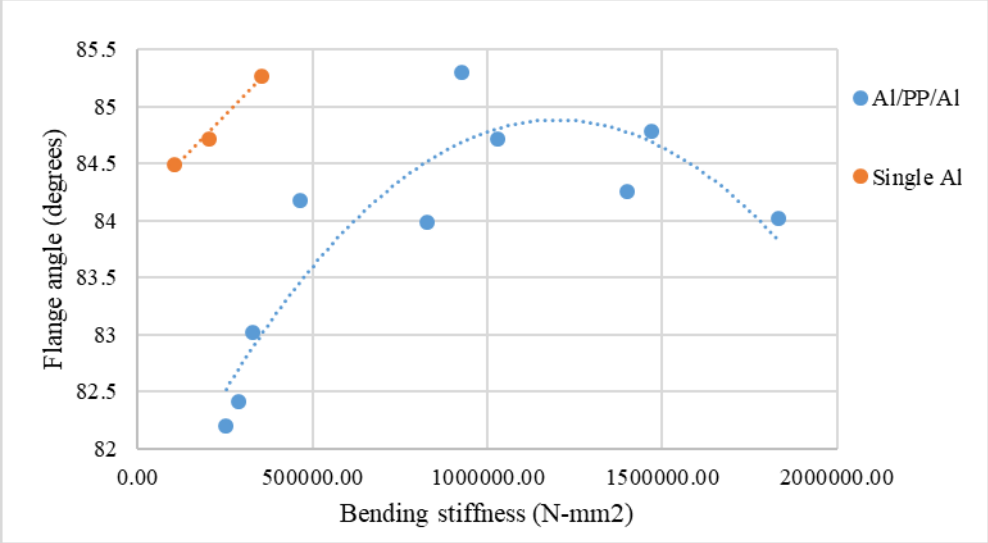

Figure 4.19: Flange angle vs bending stiffness of single Al and Al/PP/Al laminates

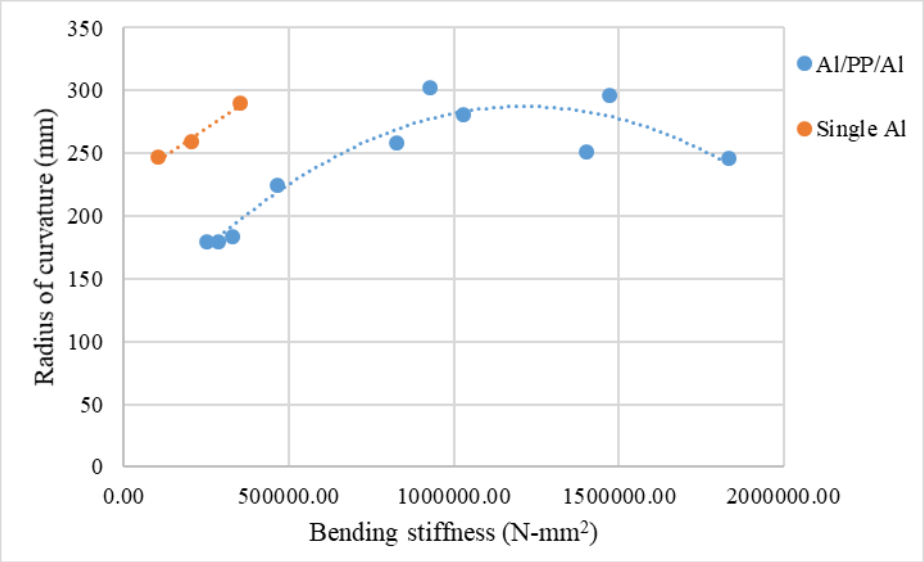

Figure 4.20: Radius of curvature vs bending stiffness of single Al and Al/PP/Al laminates

In comparing the springback values of single aluminum sheet and the sandwich laminates (Table 4.7), it can be seen that the 0.2/0.8/0.2 mm laminate has a lower bending stiffness and shows a greater degree of springback compared to the single aluminum sheet of equal thickness. The 2 mm thick sandwich laminate with 0.2/1.6/0.2 mm thickness combination has springback values close to those of the 1.2 mm thick single aluminum sheet. Its bending stiffness is higher than twice the bending stiffness of the single aluminum sheet. Thus, the springback response of sandwich laminates will be higher than that of the single sheet aluminum if they have the same thickness. For equal springback response, the bending stiffness of the sandwich laminate must be higher to that of the single sheet aluminum.

Table 4.7: Comparison of springback angles and radius of curvature for U-channels of a single aluminum sheet and sandwich laminates

		Bending stiffness (N-mm²)	**θ_1 (°)**	**θ_2 (°)**	**ρ (mm)**
Single Al	1.2	352800	98.888	85.269	290.165
Al/PP/Al	0.2/0.8/0.2	251914.88	103.9	82.206	179.582
Al/PP/Al	0.2/1.6/0.2	797066.67	98.314	83.983	258.614

4.3.3 Effects of skin and core thicknesses

To understand the effect of the skin and core thickness individually, Figures 4.21- 4.24 are plotted. It can be seen that at a constant core thickness, the U-channel shows reduced springback behavior in both wall and flange angles with increasing skin thickness. Figures 4.21 and 4.22 also show that the wall angle is significantly lower with 1.6 mm core thickness, while the flange angle is significantly higher with 1.6 mm core thickness, both indicating that springabck decreases with increasing core thickness.

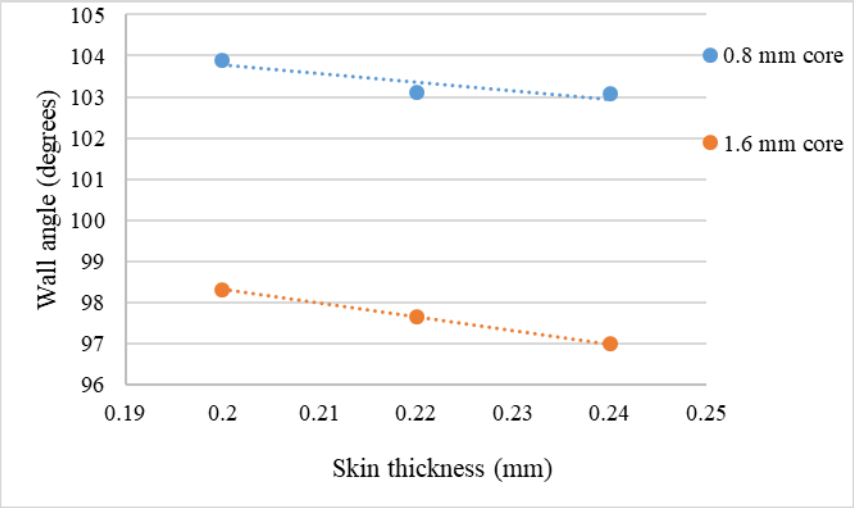

Figure 4.21: Wall angle with varying skin thickness for laminates with 0.8 mm and 1.6 mm core thickness

In Figures 4.21 and 4.22, the slope of the trendlines with core thickness of 1.6 mm is higher. This shows that springback angles are more sensitive to increasing skin thickness when the polypropylene layer is thicker.

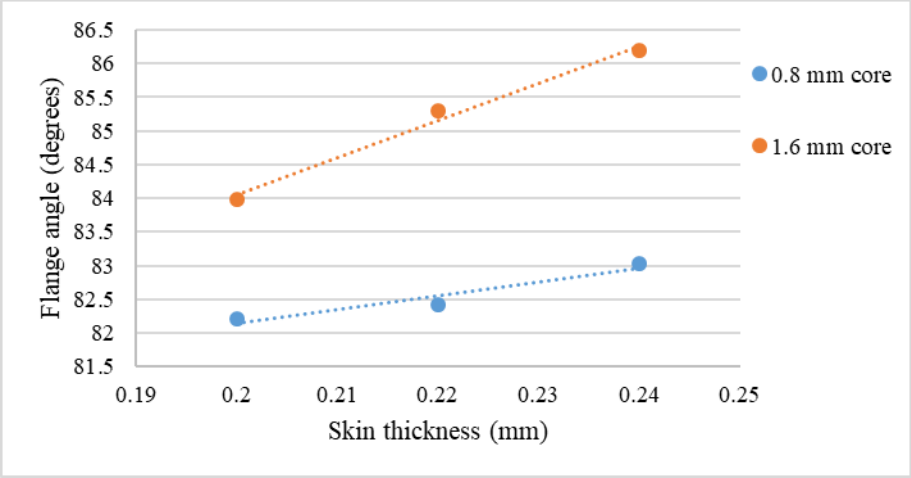

Figure 4.22: Flange angle with varying skin thickness for laminates with 0.8 mm and 1.6 mm core thickness

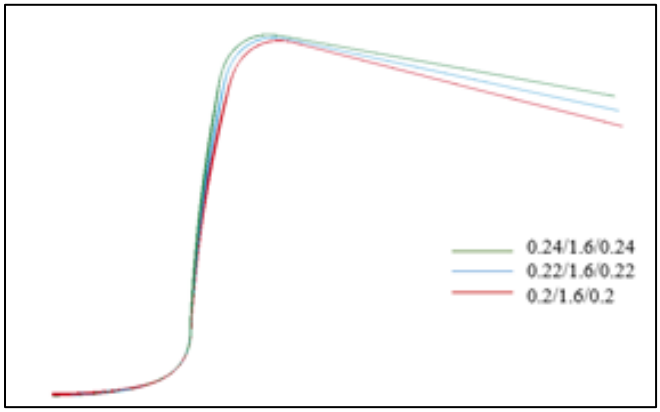

Figure 4.23: Shapes of U-channels after springback, with 0.2, 0.22, 0.24 mm skin thickness and a constant core thickness of 1.6 mm

The beneficial effect of increasing skin thickness can be seen in the shapes of U-channels (Figure 4.23) at the end of the springback simulation for 0.2, 0.22 and 0.24 mm skin thicknesses with the core thickness maintained at a constant value of 1.6 mm.

The effect of core thickness is demonstrated in Figures 4.24 and 4.25. When the core thickness is doubled by increasing it from 0.8 mm to 1.6 mm, the springback in the flange angle of the U-channel changes by an average of 2.61°. Similarly, the wall angle shows an increasing trend, and therefore, lower springback with increasing core thickness at constant skin thickness.

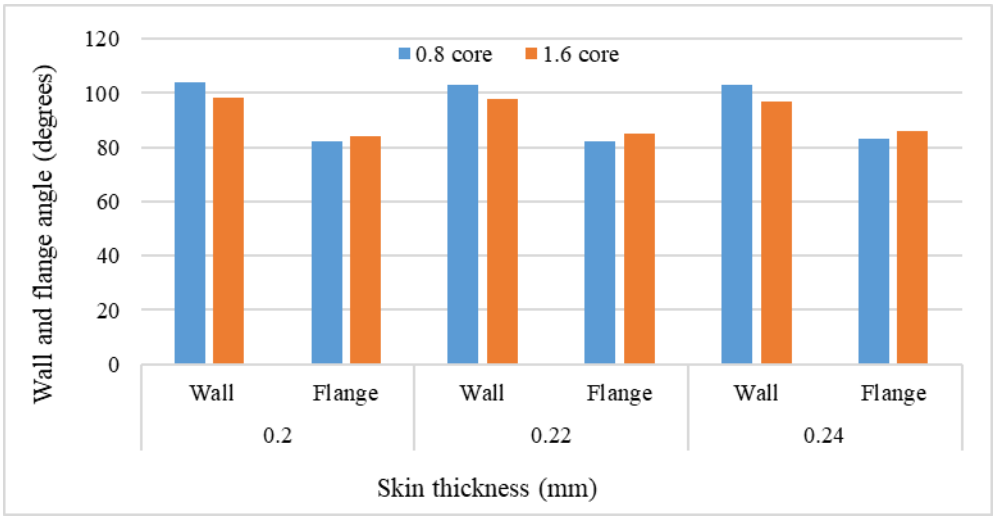

Figure 4.24: Effect of core thickness (0.8 mm and 1.6 mm) on wall angle and flange angle

Although increasing the core thickness shows an overall improvement in springback behavior, i.e., the wall angle reduces and the flange angle increases, it is true only up to a certain core thickness. In Figure 4.25 (a), the wall and flange angles for constant skin thickness of 0.24 mm are plotted against core thicknesses of 0.8, 1.0, 1.6, 1.9 and 2.2 mm. Increasing the core thickness above a value of 1.6 mm shows an increase in the wall angle and a decrease in the flange angle.

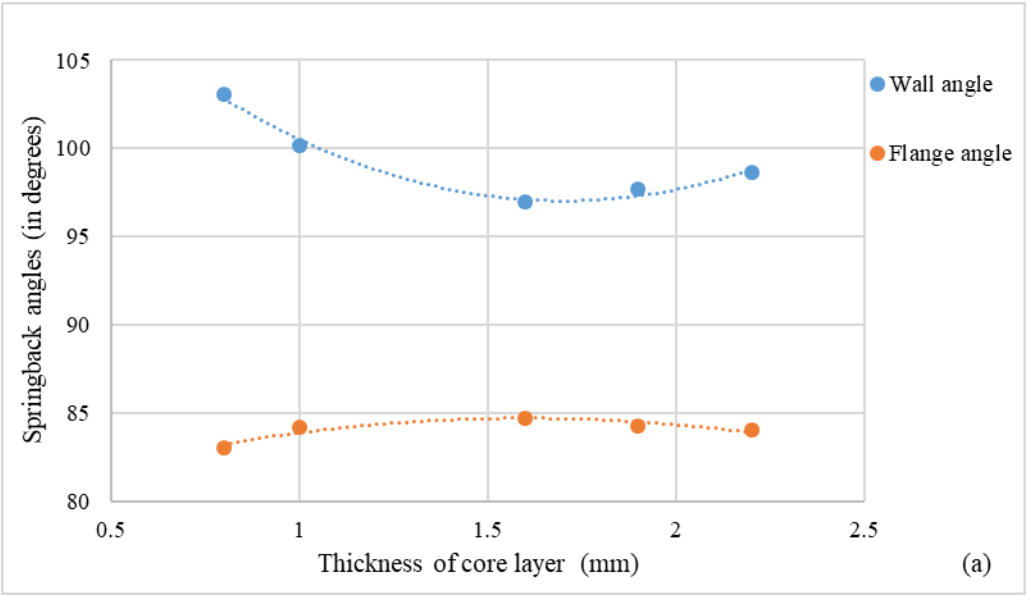

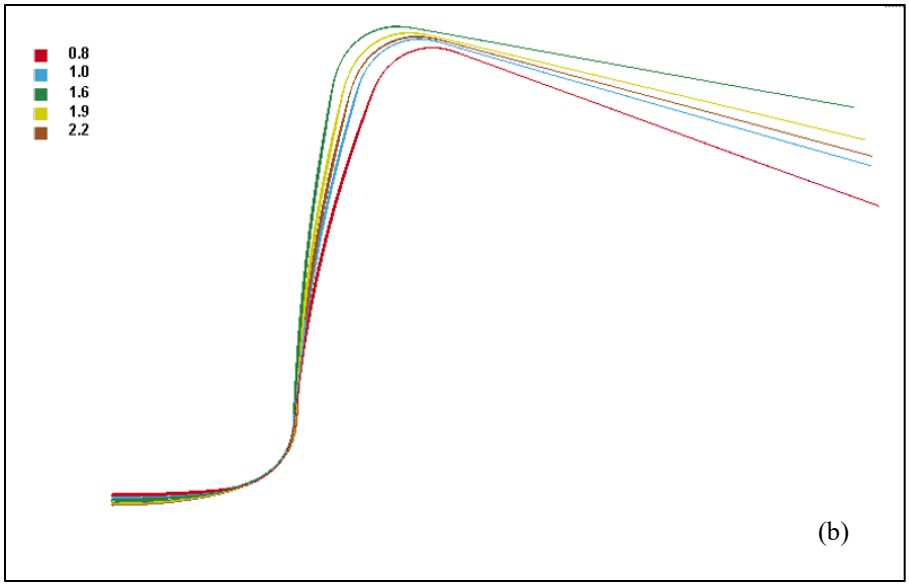

Figure 4.25: Effect of increasing core thickness at a constant skin thickness of 0.24 mm on (a)springback angles vs. core thickness (b) U-channel profiles

The change in springback behavior at higher than 1.6 mm core thickness is further investigated and found to occur due to very high plastic strains in the outer aluminum skins for the thicker sandwich laminates with core 1.6 mm and higher.

The effective plastic strains (EPS) in each layer of the sandwich laminates with skin thickness of 0.24 mm and varying core thicknesses of 0.8, 1.0, 1.6 and 1.9 mm are plotted in Figure 4.26. It can be seen that EPS values for the laminates with 0.8 mm and 1.0 mm core thickness are low. The 1.6 mm core sandwich shows high plastic strains in the lower skins, while the 1.9 mm core thickness sandwich shows much higher plastic strains in both upper and lower aluminum skins (Figure 4.26 (a)) that has led to excessive thinning. Therefore, the reversing trend in wall and flange angles with core thickness is probably due to high plastic strains in the lower and upper skins of the sandwich laminates with core thickness greater than 1.6 mm.

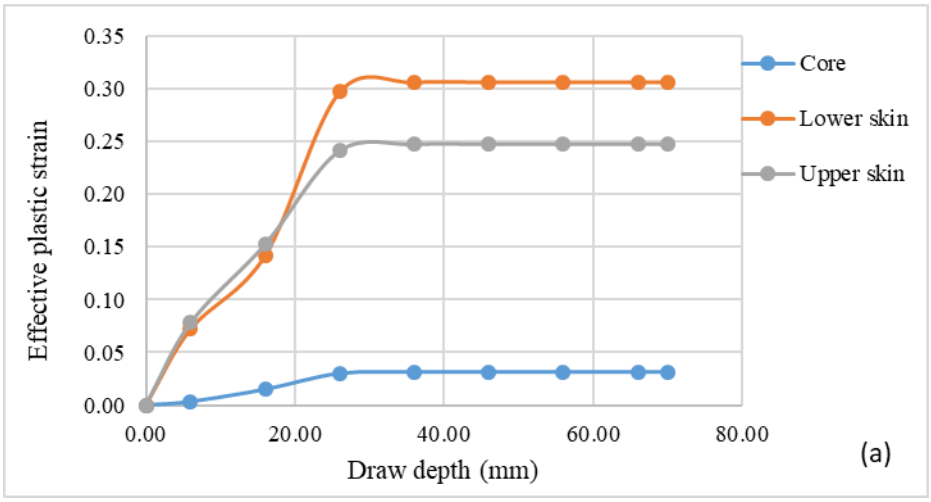
0.35
0.30
0.25
0.20
0.15
0.10
0.05
0.00
Effective plastic strain
0.00
20.00
40.00
60.00
80.00
Draw depth (mm)
Core
Lower skin
Upper skin
(a)

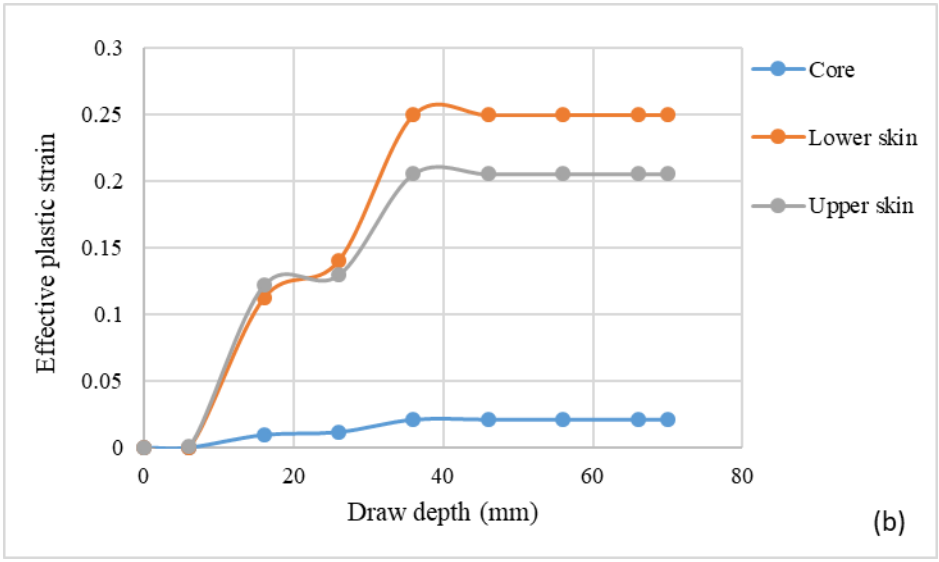
0.3
0.25
0.2
0.15
0.1
0.05
0
Effective plastic strain
0
20
40
60
80
Draw depth (mm)
Core
Lower skin
Upper skin
(b)

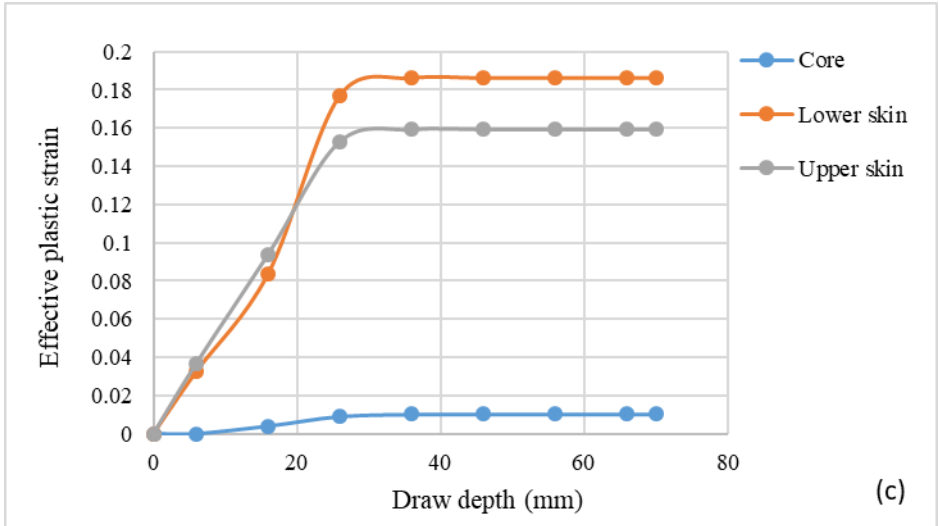
0.2
0.18
0.16
0.14
0.12
0.1
0.08
0.06
0.04
0.02
0
Effective plastic strain
0
20
40
60
80
Draw depth (mm)
Core
Lower skin
Upper skin
(c)

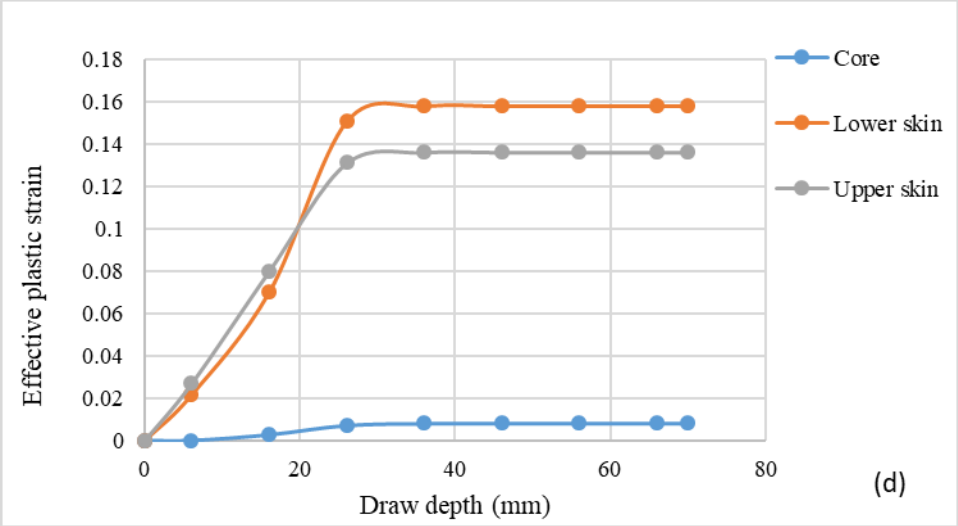

Figure 4.26: Effective plastic strains in sandwich laminates at the end of 70 mm draw depth. The thickness combinations are (a) 0.24/1.9/0.24 mm (b) 0.24/1.6/0.24 mm (c) 0.24/1.0/0.24 mm (d) 0.24/0.8/0.24 mm

4.3.4 Effect of punch radius

The effect of process parameters such as punch radius and die radius have been studied extensively for monolithic metals, some of the results can be seen in Refs. [21] and [22] .The effect of these parameters for sandwich laminates is studied in Sections 4.3.4 through 4.3.10.

First, the variation of punch radius is examined. To understand this, punch radii of 5 mm, 8 mm, 10 mm and 12 mm are modelled with a constant die radius of 8 mm in the numerical simulations. All other parameters remain the same as in the model described in Section 4.3.1. The wall and flange angles for each punch radius are plotted for three different laminate thickness combinations 0.2/0.8/0.2, 0.2/1.6/0.2 and 0.25/1.9/0.25 mm.

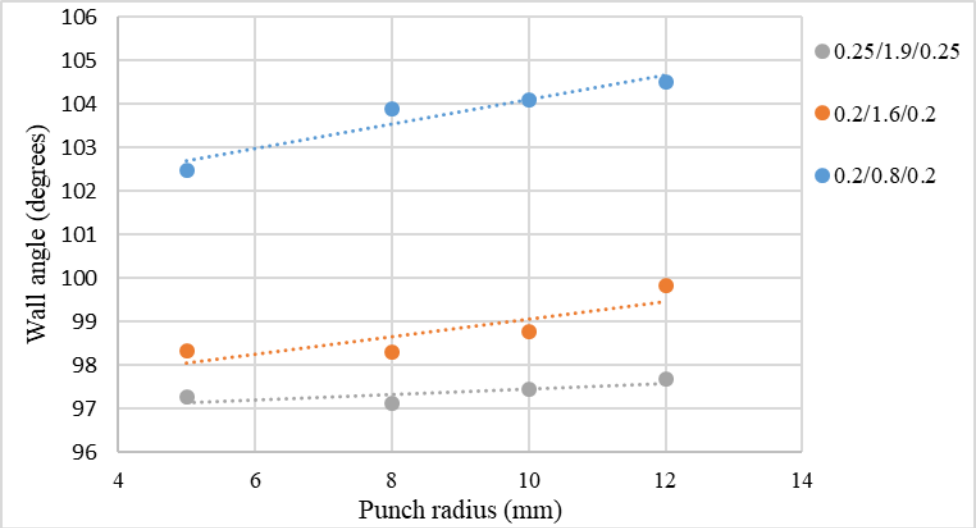

Figure 4.27: Effect of punch radius on wall angle after springback for three different sandwich laminate thickness combinations

In Figure 4.27 the wall angle shows an overall increasing trend with increasing punch radius. Changing of the punch radius has a more significant effect on the wall angle for sandwich laminates with a core thickness of 0.8 mm. The shapes of the sandwich laminate for different punch radii at the end of springback are shown in Figure 4.29.

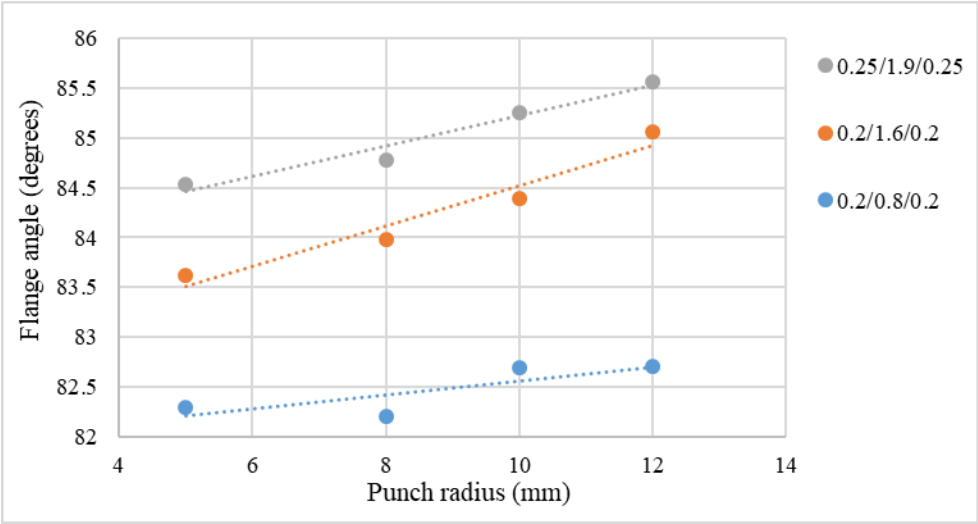

Figure 4.28: Effect of punch radius on flange angle after springback for three different sandwich laminate thickness combinations

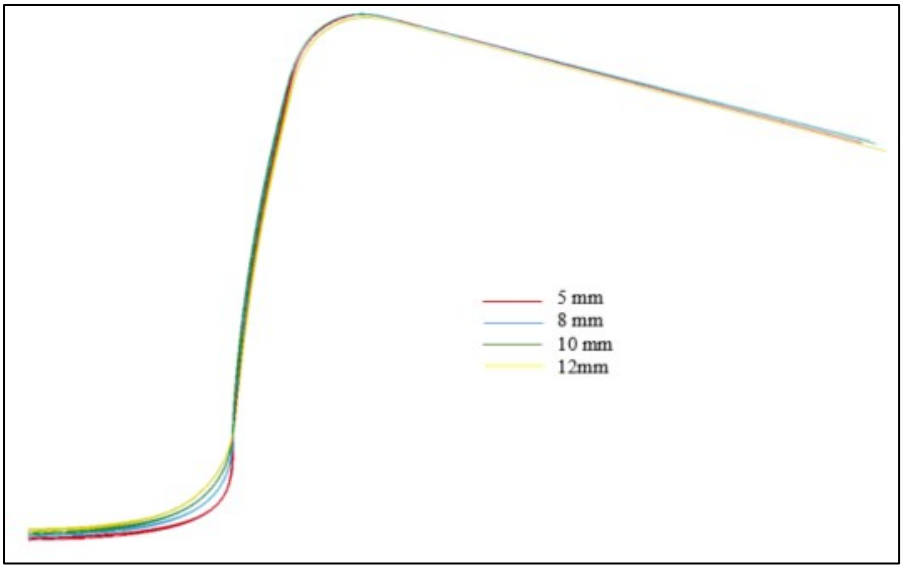

Figure 4.29: Springback profiles for 0.2/1.6/0.2 mm sandwich laminates with different punch radii

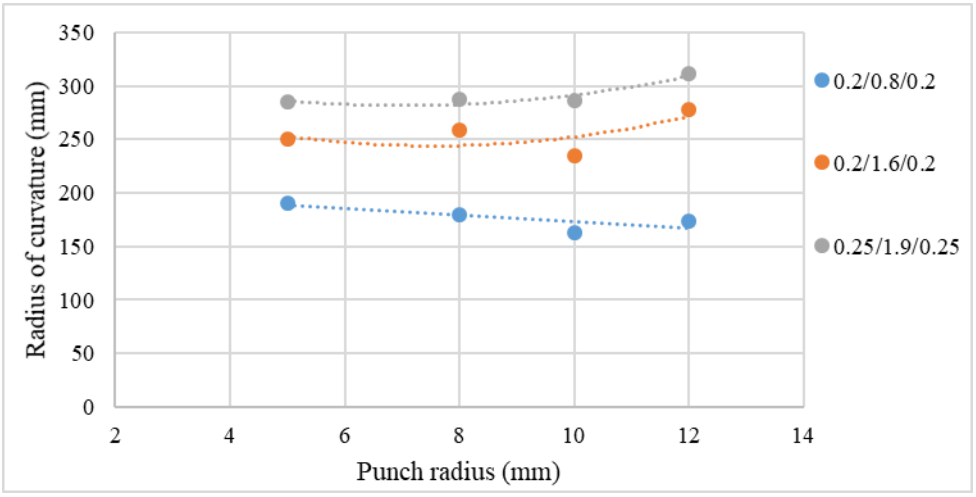

Figure 4.30: Effect of punch radius on radius of curvature for three different sandwich laminate thickness combinations

Increasing the punch radius shows an increase in flange angle (Figure 4.28) for all three thickness combinations of the sandwich laminate. Here, increasing the punch radius seems to have a greater effect on the flange angles for the laminates with thicker cores (1.6 mm and 1.9 mm). The radius of curvature shows a slight increase with punch radius for the 0.2/1.6/0.2 mm and 0.25/1.9/0.25 mm laminates but does not vary much for the 0.2/0.8/0.2 mm laminate (Figure 4.30).

4.3.5 Effect of die radius

The effect of die radius on the wall angle and flange angle values of the sandwich laminates is studied by maintaining a constant punch radius of 8 mm and varying the die radius in the range of 8 mm–12 mm. The load curves for each die radius for 0.2/0.8/0.2 mm sandwich laminate combination is plotted in Figure 4.31. The load curves give the punch load for a quarter blank setup and the load required to form the U channel is four times the predicted load in this figure.

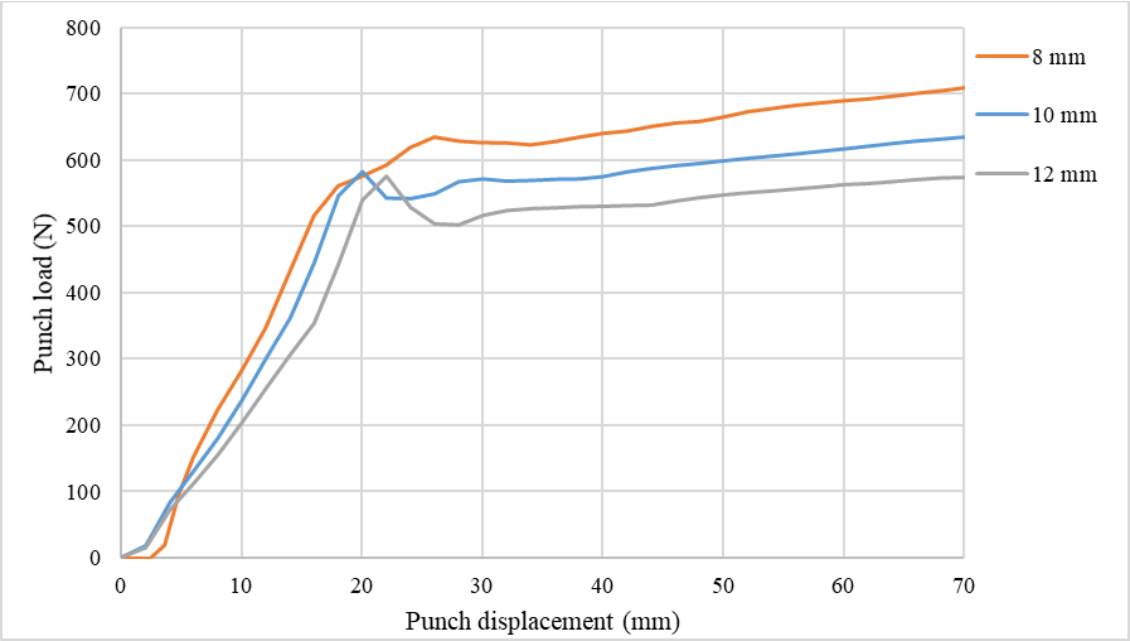

Figure 4.31: Punch load-displacement curve with increasing die radius (0.2/0.8/0.2 mm)

For all other thickness combination, the punch load variation with die radius shows a similar trend to Figure 4.31. As the die radius increases, the punch load decreases.

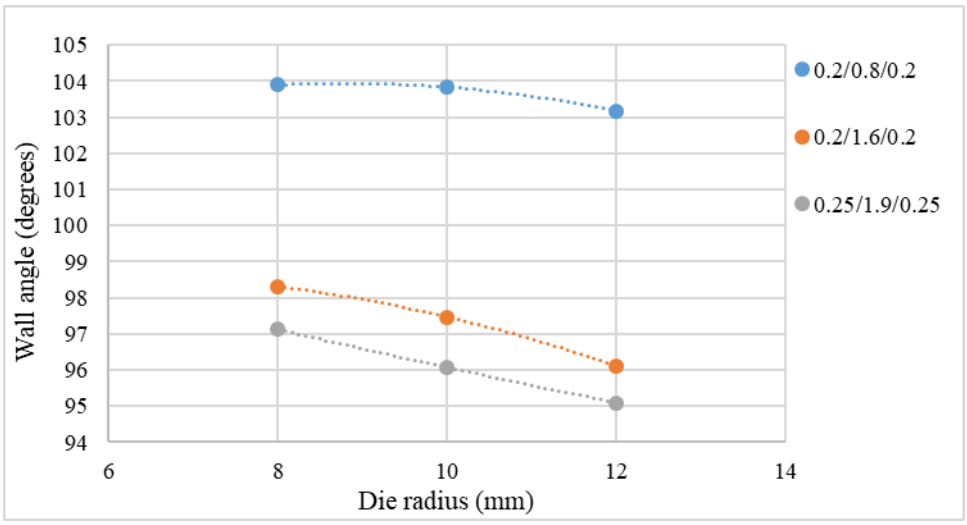

Figure 4.32: Effect of die radius on wall angles after springback for three different sandwich laminate thickness combinations

From Figure 4.32 it can be seen that as the die radius changes from 8 mm to 12 mm the wall angle decreases. More significant decrease is noted in the sandwich laminates with a thicker polypropylene core. It can also be seen that for all sandwich thicknesses, the flange angle increases with increasing die radius as shown in Figure 4.33. Another observation is that at a die radius of 10 mm and 12 mm, the sandwich laminates with 1.6 mm and 1.9 mm core show nearly equal flange angles. Similarly, the radius of curvature shows an increase with increasing die radius, indicating a decrease in sidewall curl. This reduction in sidewall curl is more prominent in the 0.2/1.6/0.2 and 0.25/1.9/0.25 (mm) sandwich laminates (Figure 4.34)

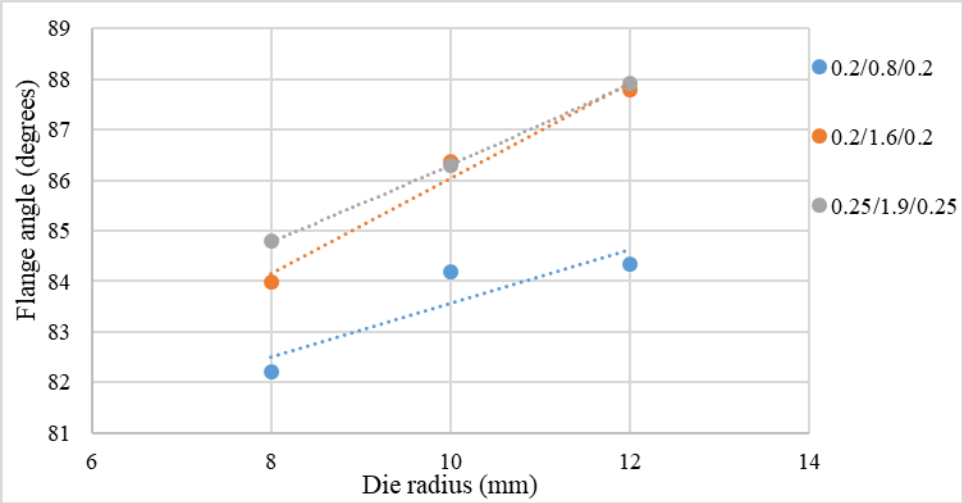

Figure 4.33: Effect of die radius on flange angle after springback for three different sandwich laminate thickness combinations

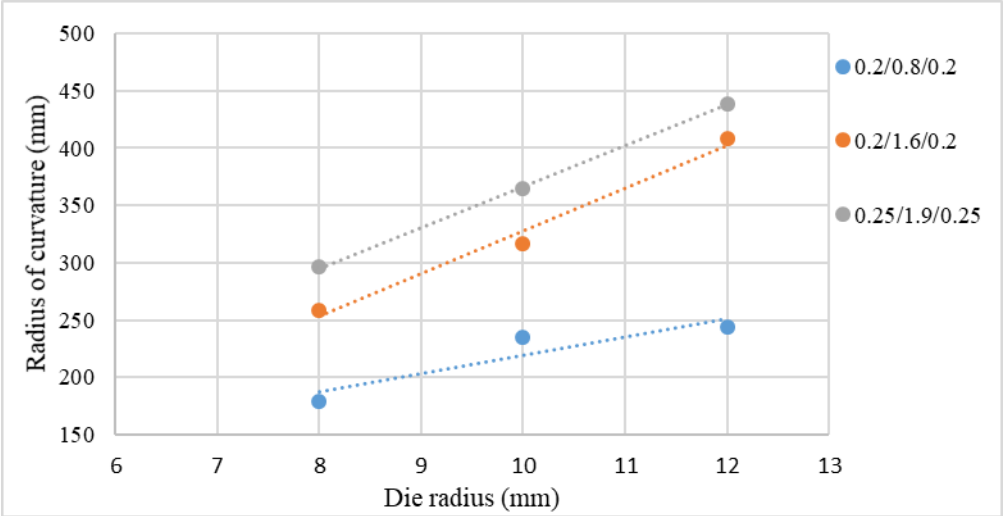

Figure 4.34: Effect of die radius on radius of curvature for three different sandwich laminate thickness combinations

The shapes of the U channel after springback for a laminate with 0.2/1.6/0.2 mm thickness combination is compared for different die radius values in Figure 4.35.

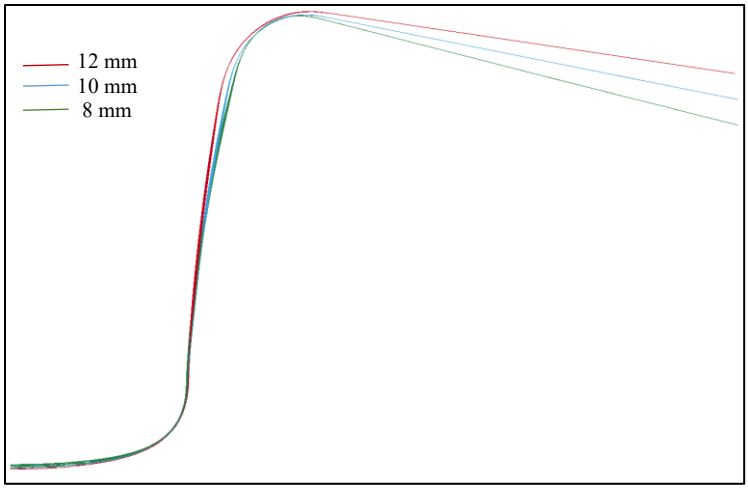

Figure 4.35: Springback profiles of U-channel for different die radii (0.2/1.6/0.2 mm)

4.3.6 Effect of punch-die gap

Die-punch gap has proven to be an important parameter in sheet metal forming processes. The effect of this parameter in draw bending of metals has been studied by Hu [23] and shows increasing springback behavior with increasing die-punch gap. In the current study, the gap between the punch wall and the die wall is adjusted such that there is no ironing; then for three different thickness combinations, an additional clearance of 0.1 mm to 0.3 mm is added. The difference between die-punch gap and sidewall clearance is shown in Figure 4.36.

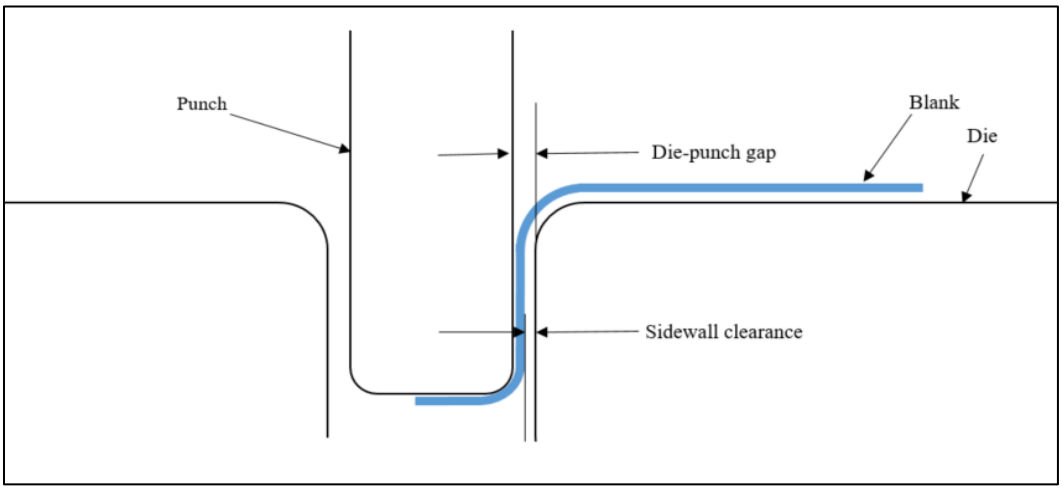

Figure 4.36: Representation of die-punch gap and sidewall clearance

Since the die-punch gap is different for each laminate thickness combination, the behavior of wall and flange angles is represented in terms of sidewall clearance in Figures 4.37 and 4.38. The variation is similar to that observed for monolithic aluminum sheets.

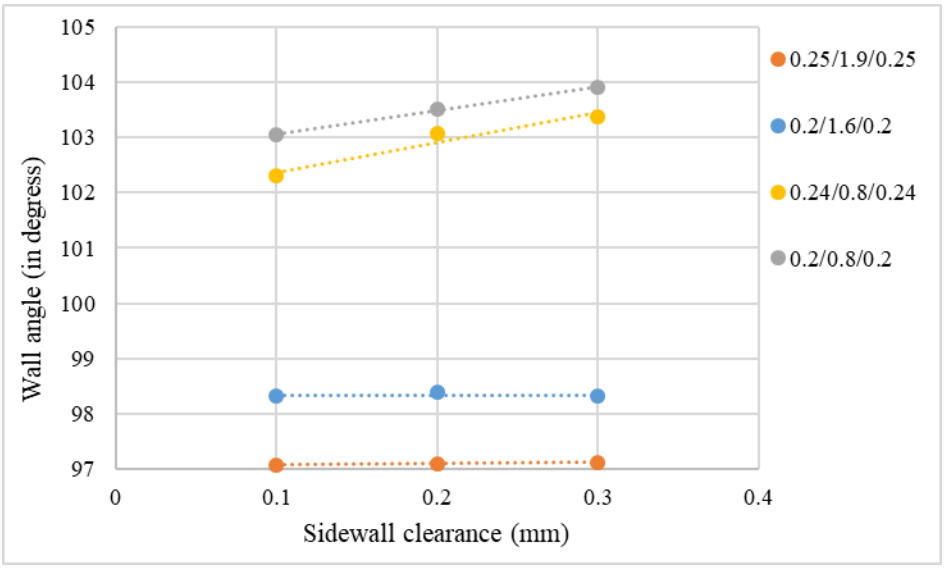

Figure 4.37: Effect of sidewall clearance on wall angle for different thickness combinations of the sandwich laminate

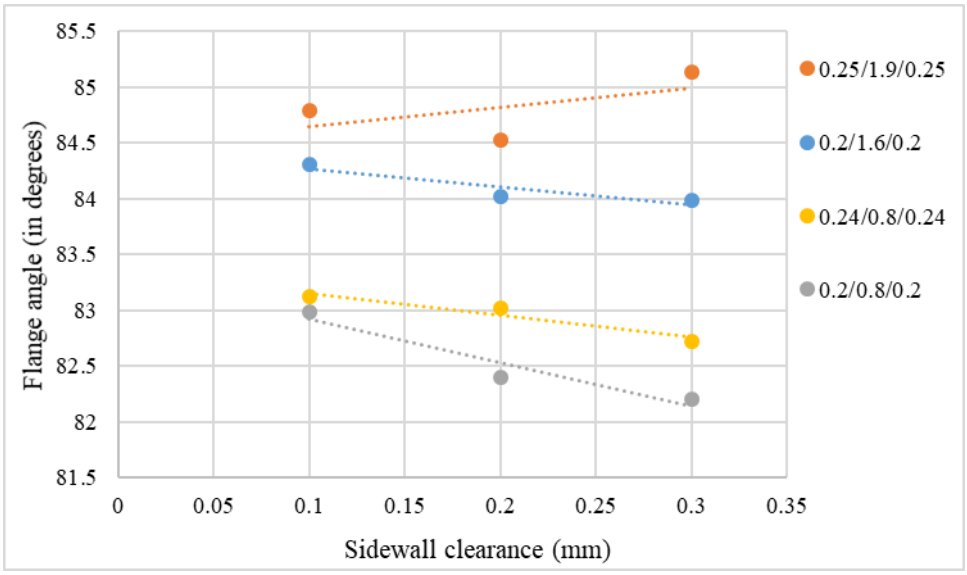

Figure 4.38: Effect of sidewall clearance on flange angle for different thickness combinations of the sandwich laminate

The wall angle increases as the sidewall clearance increases for the sandwich laminates with lower core thickness (0.8 mm). For the sandwich laminates of thickness combinations 0.2/1.6/0.2 and 0.25/1.9/0.25 the change in wall angle is insignificant.

The flange angle decreases with increasing sidewall clearance, i.e., as the gap increases in forming the flange exhibits more flexible behavior for the sandwich laminates with a core of 0.8 mm and 1.6 mm. The sandwich laminate with 1.9 mm core thickness shows no specific trend with changing punch-die clearance. Visually not much difference can be observed between the U-channel profiles after springback for the 0.2/1.6/0.2 mm laminate shown in Figure 4.39(b) for different sidewall clearance values, since the wall and flange angles are very close.

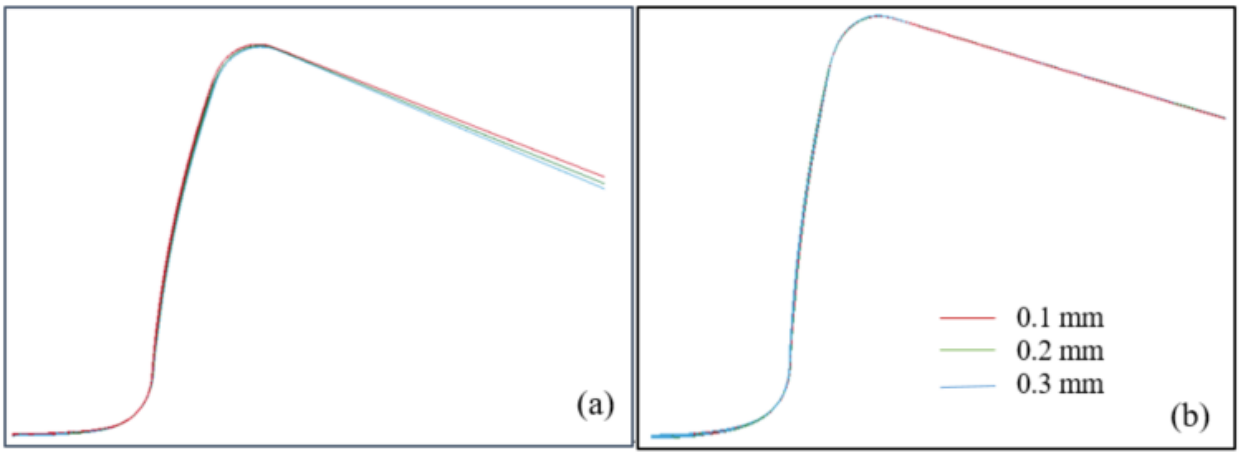

Figure 4.39: U-channel profiles after springback for punch-die clearance of 0.1, 0.2 and 0.3 mm. The thickness combinations are (a) 0.24/0.8/0.24 mm (b) 0.2/1.6/0.2 mm

The variation of radius of curvature with sidewall clearance (Figure 4.40) is very similar to the behavior of flange angle. The radius of curvature decreases with increasing sidewall clearance. However, for the 0.25/1.9/0.25 mm laminate, the radius of curvature of the wall remains almost the same when the sidewall clearance is increased from 0.1 mm to 0.2 mm and increases at 0.3 mm.

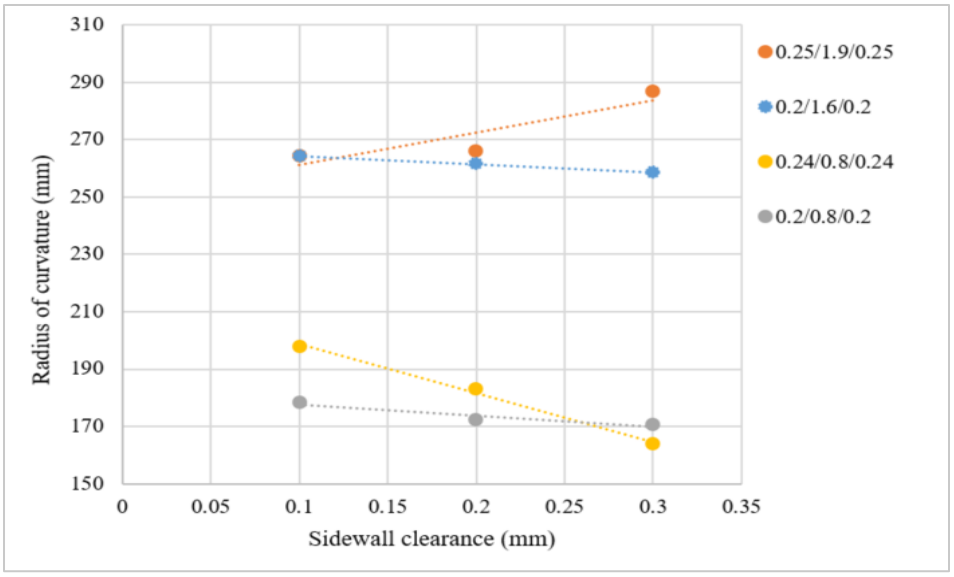

Figure 4.40: Effect of sidewall clearance on radius of curvature for different thickness combinations of the laminate

4.3.7 Effect of blank holder force

A study conducted by Mehran and Iman [24] on the influence of blank holder force (BHF) for DP-steel and AA5754-O shows an initial increase in springback behavior at low BHF followed by a decrease in springback at higher BHFs. Another study conducted by Tong and Nguyen [25] on U-draw bending of DP350 shows that wall and flange angles improve up to a BHF of 8 kN and do not show much change at higher BHFs. In both cases the punch radius was larger than the die radius and the BHF ranges from 2.5 kN to 25 kN. In comparing the springback results of a draw formed and crash formed part by experiment, Stein [22] found that the springback increased when the additional tension was applied using BHF and attributed it to the sidewall curl.

The effect of BHF on the springback of Al/PP/Al sandwich laminates is studied using four different blank holder forces, namely 500 N, 900 N, 1700 N and 2500 N. The die and punch radius is 8 mm.

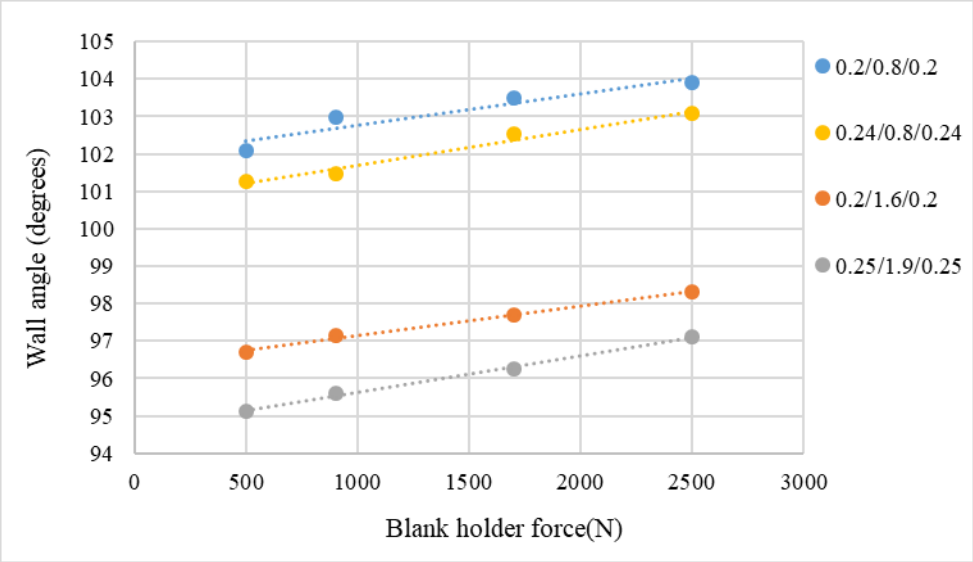

Figure 4.41: Effect of BHF on wall angle for various thickness combinations of sandwich laminates

The wall angle increases with increase in blank holder force for all thickness combinations (Figure 4.41). The flange angle first decreases and then increases with increasing blank holder force for the sheets with 0.8 mm core. A similar, but much smaller effect is seen with the 1.6 mm and 1.9 mm core thicknesses (Figure 4.42). Figure 4.43 shows the reduction in radius of curvature as the blank holder force increases. For a thickness combination 0.2/0.8/0.2 and 0.24/0.8/0.24 mm, the radius of curvature is almost unaffected by the blank holder force. Considering the effect of BHF on all three springback parameters, it can be concluded that BHF lower than 2500 N has a negative effect on the springback behavior of the SA5182/PP/SA5182 laminates. Blank holder forces at a higher range may be investigated to see if further increase in axial force during draw bending, shows any improvement in springback of aluminum/polypropylene/aluminum sandwich laminates

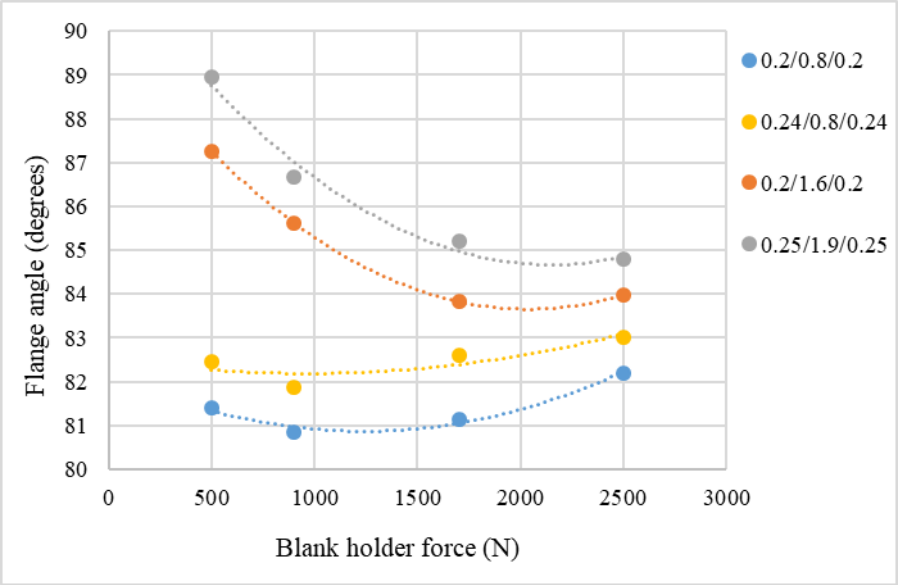

Figure 4.42: Effect of BHF on flange angle for various thickness combinations of sandwich laminates

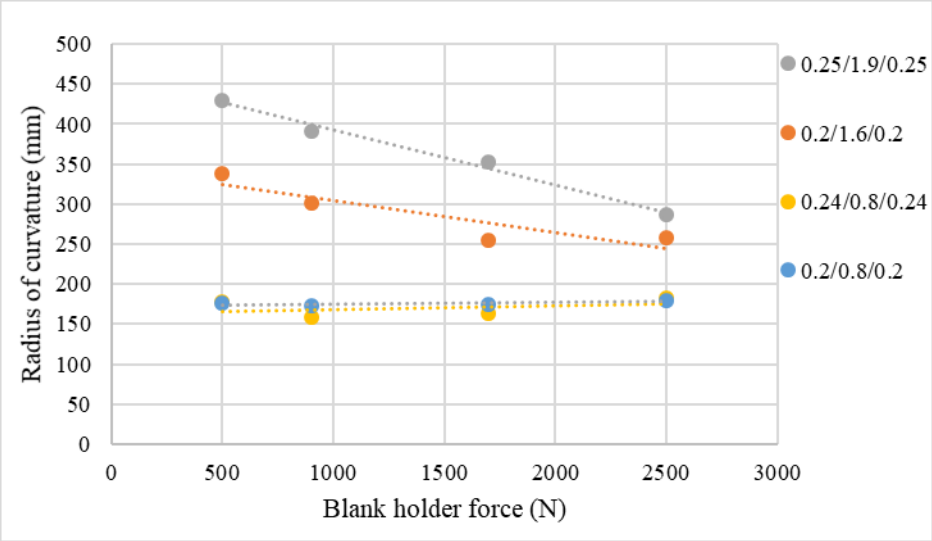

Figure 4.43: Effect of BHF on radius of curvature of the wall for various thickness combinations of the sandwich laminate

The load-displacement curves for increasing blank holder force are plotted in Figure 4.44. For a thickness combination of 0.24/0.8/0.24 mm as the blank holder force increases the punch load increases. A similar relationship between punch load and blank holder force is seen for all sandwich laminate thicknesses. The figure depicts the punch load only for a quarter model. The total punch load to draw the U-channel is four times the predicted load from the FE model.

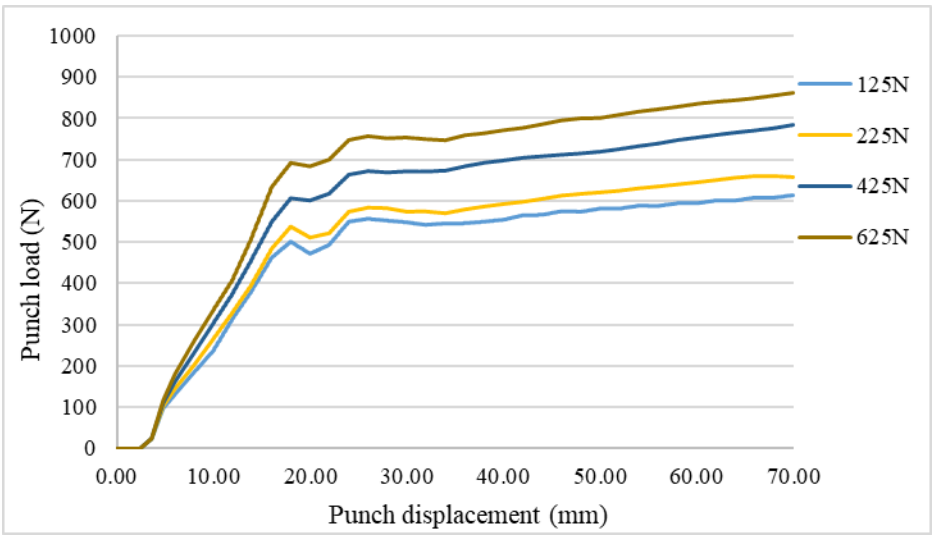

Figure 4.44: Load-displacement curves for varying blank holder force (0.24/0.8/0.24 mm)

4.3.8 Effect of friction

The effect of friction between the die, punch and blank surfaces on the springback angles of sandwich laminates is studied by varying the coefficient of friction value at the interfaces of these surfaces. The springback angles and the radius of curvature for different friction conditions are listed in Table 4.8.

Table 4.8: Springback angles and radius of curvature with different coefficients of friction between the die, punch and blank surfaces (0.2/0.8/0.2 mm sandwich laminate)

Coefficient of Friction (μ)	Wall angle (θ_1)	Flange angle (θ_2)	Radius of Curvature (mm)
0.08	103.024	81.151	159.788
0.15	103.9	82.206	179.582
0.30	101.44	83.875	245.794

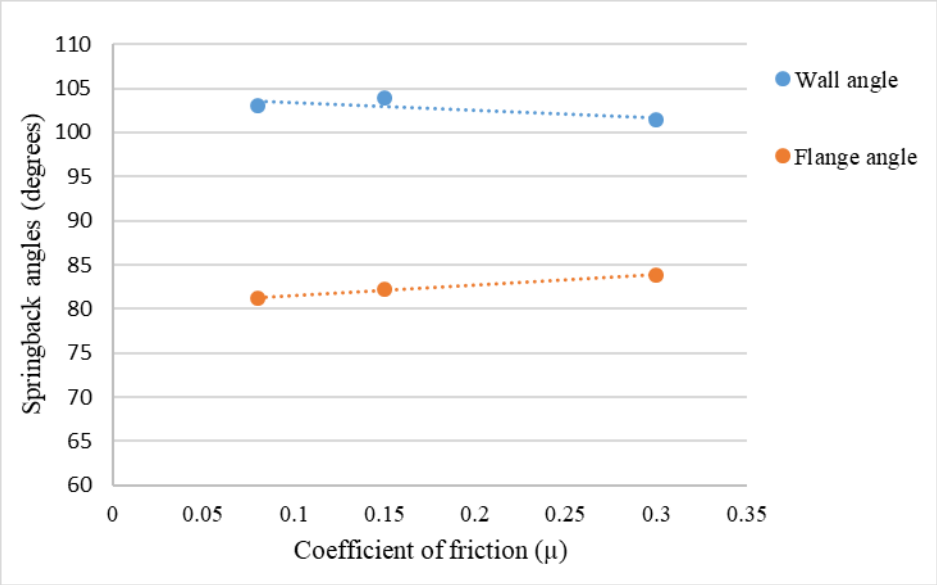

Figure 4.45: Effect of coefficient of friction on springback behavior of 0.2/0/8/0.2 mm Al/PP/Al sandwich laminate

From Figure 4.45 it can be seen that as coefficient of friction increases from 0.08 to 0.30, the flange angle increases and the wall angle decreases, showing an overall improvement in the springback response with increasing friction condition. However, at a very high coefficient of friction, such as at $\mu = 0.60$, the tensile strains in the aluminum skins exceed the failure strains of SA5182. The influence of friction on the springback of Al/PP/Al laminates is similar to that of monolithic aluminum with increasing coefficient of friction.

4.3.9 Effect of material model

The material models described in Section 4.2.1 are used in this section for springback simulations of sandwich laminates with 0.2/0.8/0.2, 0.24/0.8/0.24 and 0.2/1.6/0.2 mm thickness combinations. They are Mat_36 (IH +Barlat 89), Mat_125 (YU+Hill48), Mat_226 (YU+Barlat89) and Mat_133 (IH+Barlat2000). In Section 4.2.1, it is shown that springback prediction for single aluminum sheet depends on the material model selected for the simulation. As can be observed in Figure 4.46, there are also differences in the predicted profiles of the laminate U-channels at the end of

springback; however, the differences are much less than those for single aluminum profiles after springback (Figure 4.5).

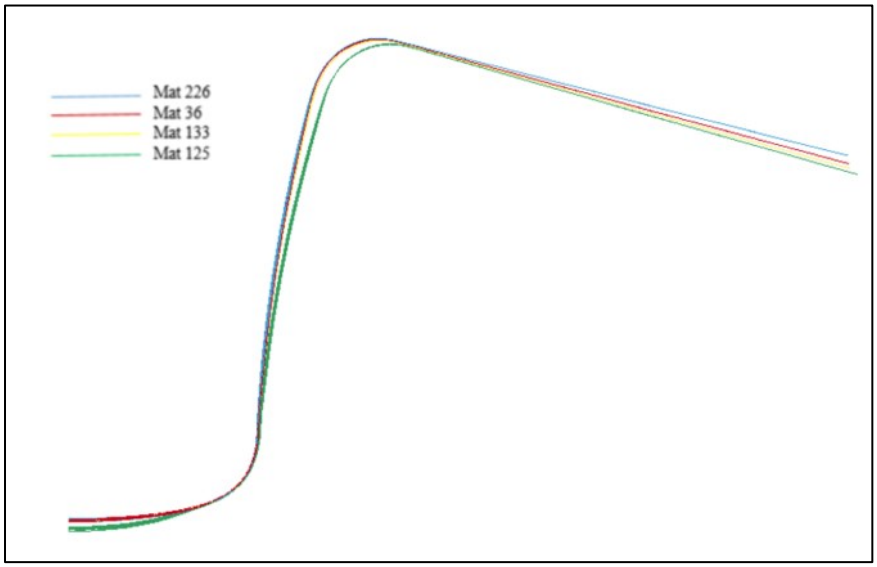

Figure 4.46: Springback profiles of 0.2/1.6/0.2 mm Al/PP/Al sandwich laminates as predicted by different material models

The wall angle predictions in Figure 4.47 show that increasing the core thickness from 0.8 to 1.6 mm for the laminates with 0.2 mm skin thickness and increasing the skin thickness from 0.2 to 0.24 mm for the laminates with 0.8 mm core thickness decrease the wall angle; however, they do not show any specific trend over the different thickness combinations. Material models 133 and 36, both containing the isotropic hardening model, show similar wall and flange angle values, indicating that not much difference is obtained between Barlat 89 and Barlat 2000 yield criteria. It is also observed that material model 125 shows greater sagging of the blank at the punch corner radius for the thicker core sandwich laminates (springback profile of Mat_125 in Figure 4.46). Material model 133 shows the closest value for wall angle to the experiment for sandwich thickness combination 0.2/0.8/0.2 mm. For the same thickness combination, Mat_125 has the closest prediction to the experimental flange angle, and the predicted wall angle is also quite close.

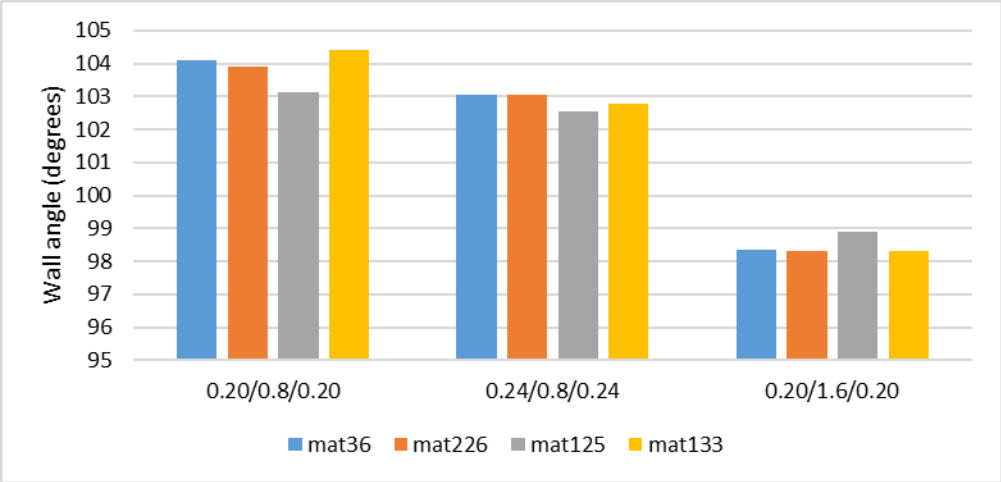

Figure 4.47: Wall angles after springback as predicted by different material models for the aluminum skins

The flange angles for each material model are shown in Figure 4.48. Material model 125 (YU +Hill 48) and 226 (YU+Barlat89) show similar flange angles, while material models 133 (IH+ Barlat2000) and 36 (IH +Barlat 89) show closer values.

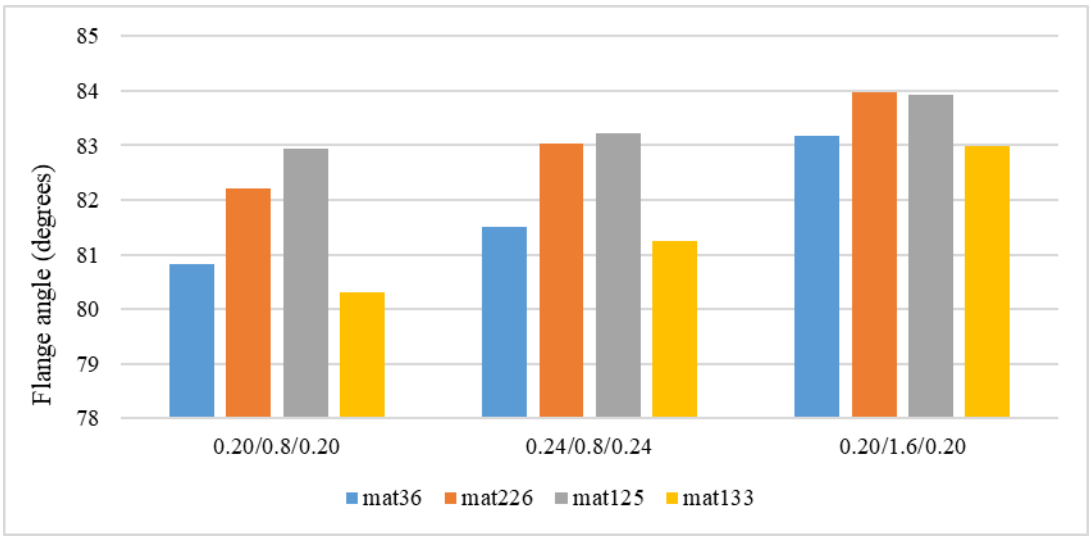

Figure 4.48: Flange angles after springback as predicted by different material models for the aluminum skins

Material model 133 using Barlat 2000 yield criteria is further explored by switching from isotropic hardening option to kinematic hardening option in the same material model. Both options are based on the the same yield criterion, but as can be observed in Table 4.9 and Figure 4.49, the

kinematic hardening rule shows a significantly different springback response from the isotropic hardening rule. The wall angle shows a larger difference for the thinner sandwich laminate (0.2/0.8/0.2) in comparison to the thicker sandwich laminate (0.2/1.6/0.2). The flange angle is significantly higher in both thickness combinations when the kinematic hardening rule is used. In Ref. [26] , a springback study conducted on the role of hardening rules on aluminum alloy AA6022 using Barlat 89 yield criteria shows similar results.

A large difference in the prediction of radius of curvature is also seen between the isotropic and kinematic hardening rules, with the latter showing a much stiffer response to springback. Hence, it can be concluded that the sidewall curl prediction is also dependent on the use of hardening model.

Table 4.9: Effect of isotropic and kinematic hardening rules on wall angle, flange angle and sidewall curl

Thickness Combinations (mm)	**Mat_133 with Isotropic Hardening (IH) Rule**			**Mat_133 with Kinematic Hardening (KH) Rule**		
	θ_1	**θ_2**	**P**	**θ_1**	**θ_2**	**ρ**
0.2/0.8/0.2	104.402	80.31	172.076	96.327	89.36	555.16
0.2/1.6/0.2	98.331	82.995	254.67	94.85	90	585.2

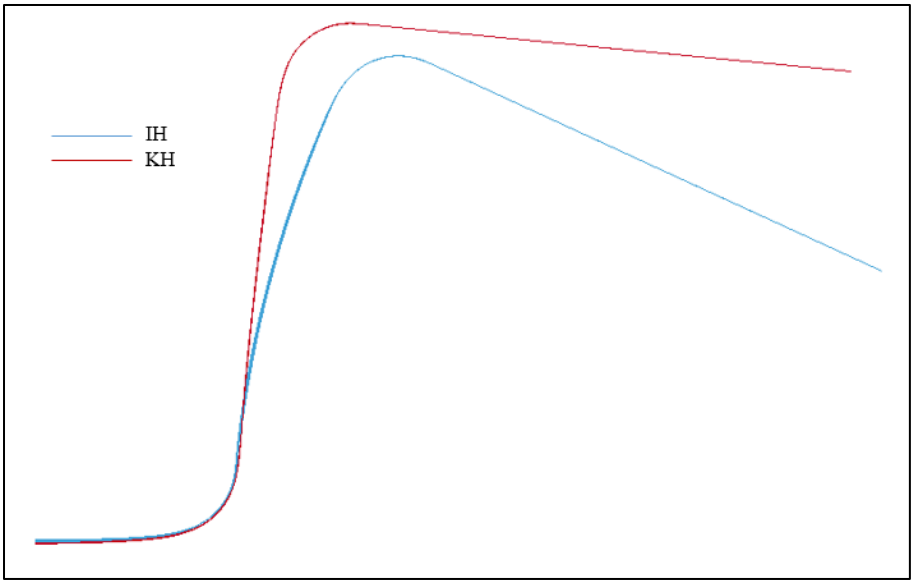

Figure 4.49: U-channel profiles after springback as predicted by Mat_133 material model with isotropic hardening (IH) and kinematic hardening (KH) hardening rules. Both uses Barlat 2000 Yield criteria

4.3.10 Effect of modelling approach

Two finite element modelling approaches are compared in this section. The first approach uses the Part_Composite model, which is explained in Section 4.2. The second approach uses a shell-solid-shell model in which the outer aluminum skins are represented by shell elements while the inner polymer core is modelled by solid elements. In this model, the polymer core is tied to the outer skins using tied nodes contact in LS-DYNA to simulate perfect bonding between the three layers of the sandwich laminate. To accommodate the thickness of the blank and avoid ironing, the gap between the punch and the die are adjusted appropriately and recorded in Table 4.5. The blank is drawn to a depth of 70 mm at a punch velocity of 200 mm/sec. A blank holder force of 2500 N (a reduced value of 625 N for quarter model) is used.

In the shell-solid-shell approach, the aluminum skins are modelled using fully integrated shell element formulation based on Reissner-Mindlin shell model. The polypropylene core is modelled using type-2 fully integrated solid elements. The polymer is modelled using piecewise

linear plasticity model (Mat_24) and the aluminum skins are modelled using Yoshida-Uemori hardening model including transverse anisotropy (Mat_125). The FE model is shown in Figure 4.50.

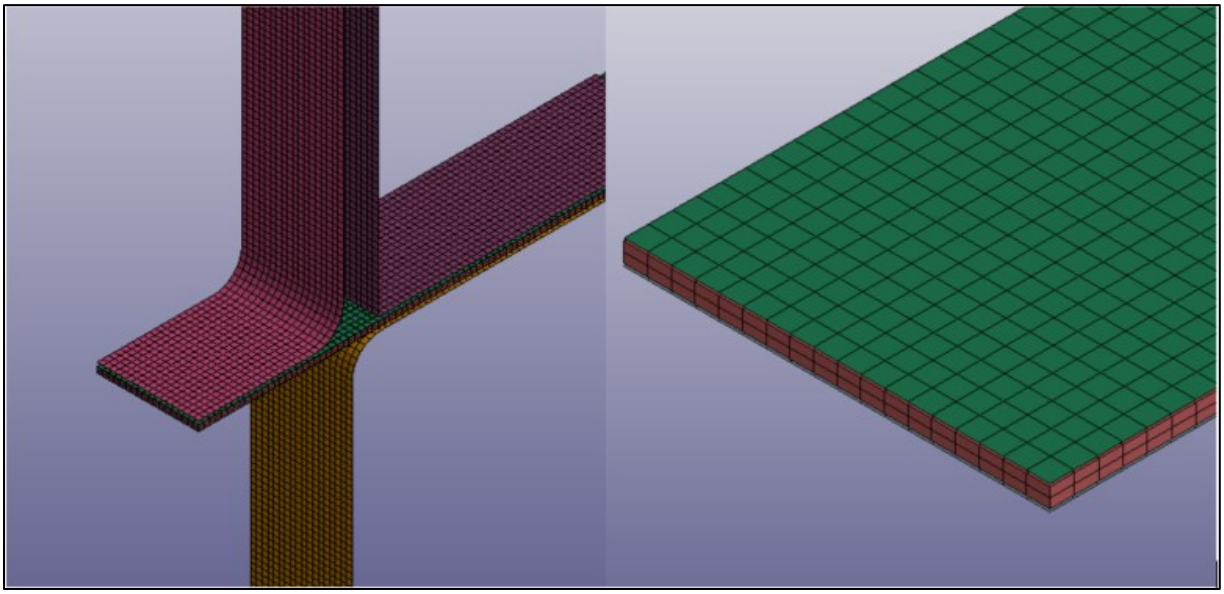

Figure 4.50: Finite element model with shell-solid-shell elements for the skin-core-skin

Springback is measured for different thickness combinations of the aluminum skin and polyproylene core. The sandwich laminates with a core thickness of 0.8 mm are modelled with two layers of solid elements through the thickness, resulting in four integration points through the thickness, while those with 1.6 mm core thickness are modelled using four layers of solid elements through the thickness. Three integration points are used for the shell elements that represent the skin.

To evaluate springback in the finite element model, the implicit solver in LS-DYNA is used. The deep drawn U-channel at the end of the explicit forming simulation with element stresses and strains is used as an input for the static implicit analysis. Automatic time step control is invoked and the U-channel is constrained at the node indicated in Figure 4.51 (a). The nodes are on the plane of symmetry as recommended for LS-DYNA springback inputs by Maker and Zhu [10] and

prevent rigid body translations and rotations. The sprung shape of one sandwich laminate (0.2/0.8/0.2) is shown in Figure 4.51(b) .

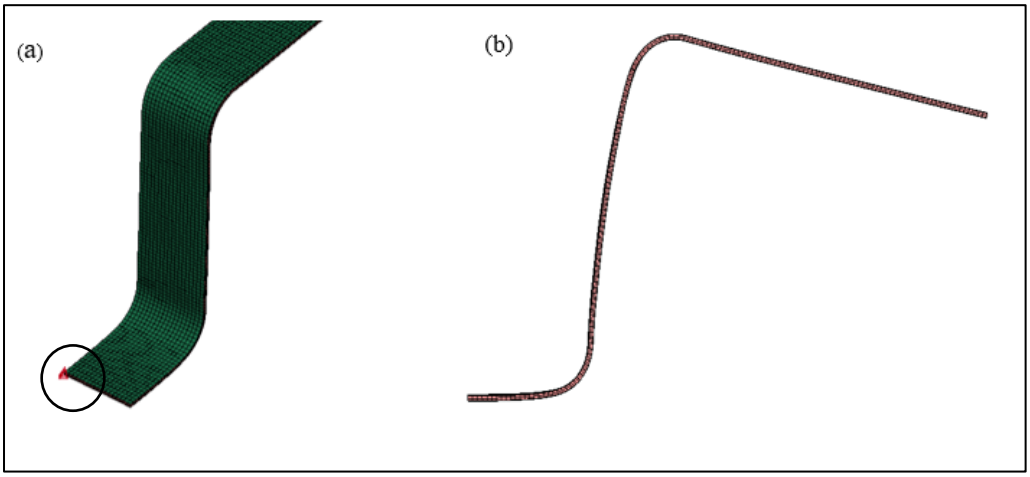

Figure 4.51: Shape of sandwich laminate (a) at the end of forming stage and location of rigid body constraints and (b) after springback

Using the same model parameters as Section 4.3 with a die and punch radius of 5 mm as well as 8 mm, a comparison between the two modelling approaches is made and tabulated in Table 4.10. It can be observed in this table that the Part_Composite model mostly shows more conservative values for wall angles. Overall, the springback angles determined using the two models are in close agreement with each other. The CPU time for processing shell-solid-shell model is more than the Part _Composite model (Table 4.11). Due to close agreement of the model's prediction to the experimental work along with its ease of model set up and lower run time, the Part_Composite model is recommended.

Table 4.10: Springback angles and sidewall curl predicted by two different finite element models

Thickness Combination (mm)	Shell-solid-shell model			Part _Composite model		
	θ_1 (°)	θ_2(°)	ρ (mm)	θ_1(°)	θ_2(°)	ρ (mm)
	Die and Punch Corner Radii = 5 mm					
0.20/0.8/0.20	99.3	85.99	226.552	98.682	83.74	228.5
0.22/0.8/0.22	98.55	86.9	259.25	98.18	83.046	228.685
0.24/0.8/0.24	97.8	87.62	325.511	95.752	85.007	327.947
0.22/1.6/0.22	95.77	86.8	373.698	92.477	89.577	410.118
0.24/1.6/0.24	95.59	88.09	441.032	92.083	89.895	509.895
	Die and Punch Corner Radii = 8 mm					
0.2/0.8/0.2	99.414	87.049	275.412	103.121	82.946	177.084
0.2/1.6/0.2	99.016	87.307	280.557	98.893	83.927	265.514

Table 4.11: CPU processing time for three sandwich thickness combinations with two different modelling approaches

Al/PP/Al Thickness combination (mm)	CPU Processing Time (seconds)	
	Shell-solid-shell	Part_Composite
0.2/0.8/0.2	6352	3084
0.22/1.6/0.22	7398	5520
0.24/1.6/0.24	7509	5650

4.3.11 Springback experiments

The springback behavior of SA5182/polypropylene/SA5182 sandwich laminates under draw-bending conditions is studied by experiment and described in this section. The experimental set up is based on Numisheet '93 [1] recommendations. A schematic of the setup along with dimensions is shown in Figure 4.52. In the initial experiments, the die and punch corner radii were 5 mm; however, since the sheet specimens in these experiments failed by crack formation at the punch corner within 10 mm of punch displacement, it was decided to increase both radii to 8 mm.

The simulation studies on the springback of the sandwich laminate reported in the previous sections are also done with 8 mm die and punch radii.

The draw bending tool consists of a rectangular punch attached to the moving crosshead (upper) and two die blocks attached to the fixed baseplate on an INSTRON 4469 testing machine. It is designed such that the die-punch gap can be adjusted to accommodate different sheet thicknesses. The blank holder force on each side of the sheet specimen is applied by tightening the bolts connecting the blank holder plates and the die blocks (Bolt A in Figure 4.52). A digital toque wrench with a minimum reading of 0.3 N-m was used for tightening the bolts on each side of the blank specimen. The torque calculation is described in Appendix B.

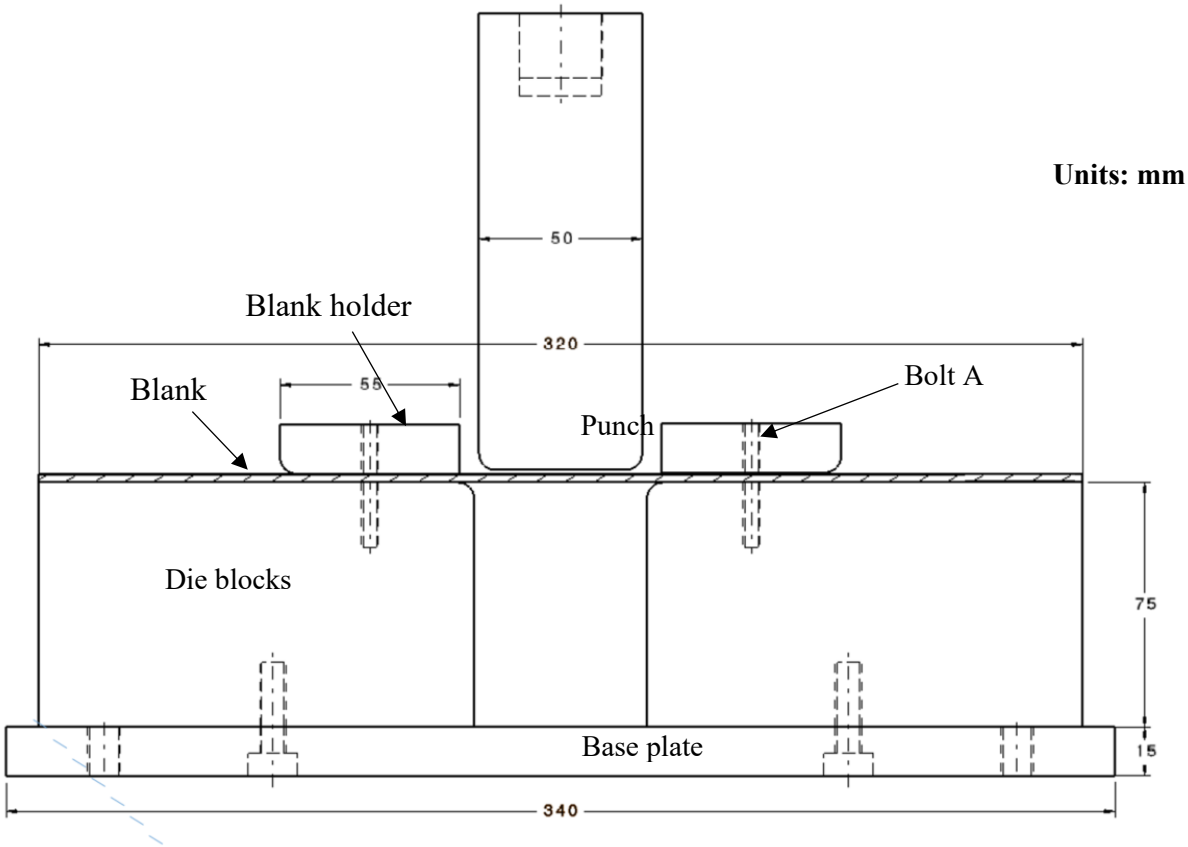

Figure 4.52: Schematic of the draw bending tool assembly for U-channel forming

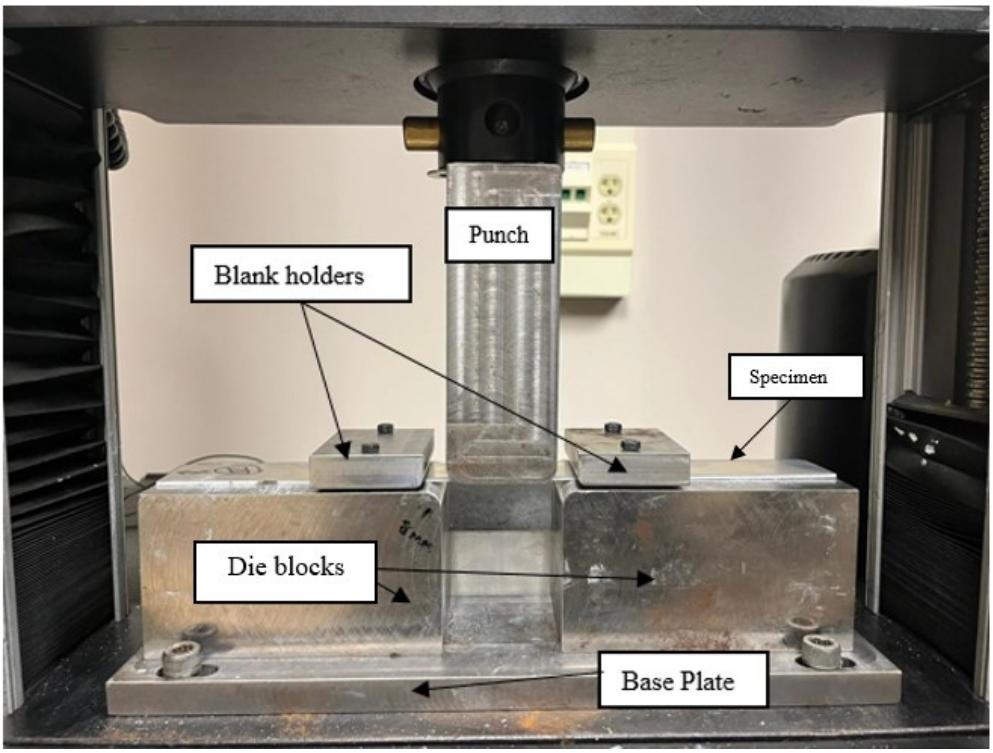

Figure 4.53: Experimental draw bending tool setup installed on Instron testing machine

The experiments are carried out for three different thickness combinations. The punch-die gap is adjusted to match the numerical simulations as recorded in Table 4.5. The punch displacement is controlled by moving the crosshead at 10 mm/min and is made to stop when it reaches 70 mm. A metal-to-metal working lubricant (White Lithium) is applied on all contact surfaces. The deep-drawn sheet when removed from the fixture springs back freely. The springback angles are calculated by tracing the final shape of the specimen on a paper and making the measurements following the prescribed method in Numisheet '93 [1]. Table 4.12 lists the springback angles measured from experiments.

Table 4.12: Experimental springback results

Thickness combination	Torque (N-m)	BHF (N)	Wall angle (θ_1) (°)		Flange angle (θ_2) (°)	
			Experiment	Simulation	Experiment	Simulation
0.2/0.8/0.2	0.46	2500	104.5	103.9	85.0	82.206
0.2/0.8/0.2	0.36	1700	102.5	103.494	85.0	81.134
0.2/0.8/0.2	Finger tightened	-	101.2	-	84.5	-
0.22/0.8/0.22	0.46	2500	102.5	103.106	85.0	82.415
0.22/0.8/0.22	0.36	1700	101.5	-	84.5	-

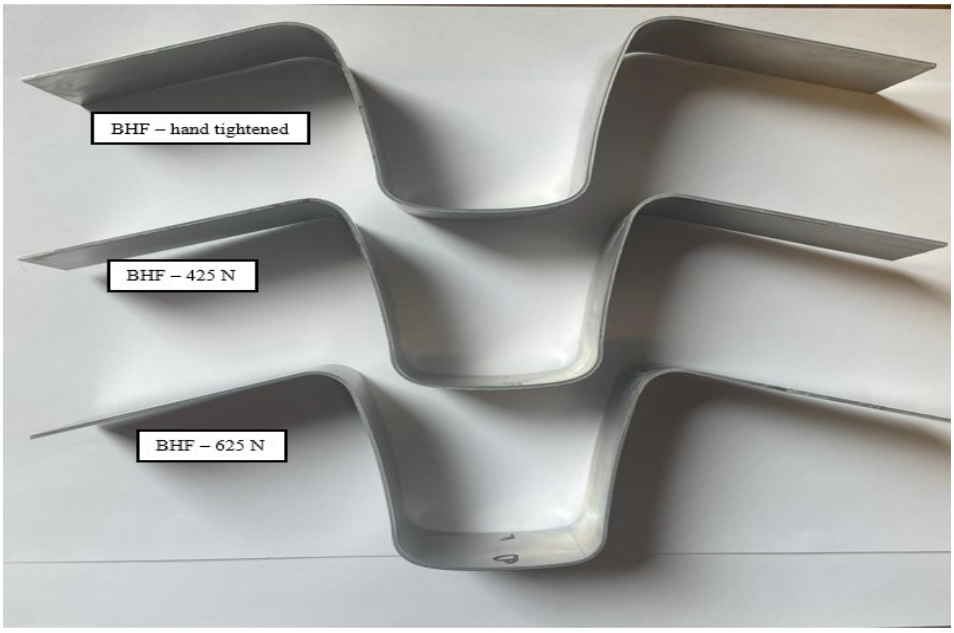

Figure 4.54: Profiles of Al/PP/Al specimens with 0.2/0.8/0.2 mm thickness combination after springback

The laminate specimens with 0.2/0.8/0.2 and 0.22/0.8/0.22 mm thickness combinations are drawn to 70 mm depth without failure at both 425 and 625 N blank holder forces. It can be observed in Figure 4.54 and also in Table 4.12 that as the blank holder force decreases, springback behavior decreases; this is also shown by simulation in Section 4.3.7.

Figure 4.55 compares the load vs. punch displacement curves for laminates with 0.2/0.8/0.2 and 0.22/0.8/0.2 mm thickness combinations. Both experimental and simulated curves are shown. The load curves obtained from simulation are almost identical up to a punch displacement of 12

mm, this is the period where the material is made to wrap around the punch and die radius. The differences in the load curve predicted by simulation and the experimental load curve is attributed to their difference in coefficients of friction. Figure 4.56 shows the progression of U-channel forming along the punch load-displacement curve. The blank is being drawn into the die cavity at a punch displacement of around 26 mm from this point the load continues to increase till the completion of drawing. Since the difference in total thickness of the specimens between Figures 4.55 (a) and (b) is only 0.04 mm, the punch loads do not show any significant difference over the entire forming process of the U-channel.

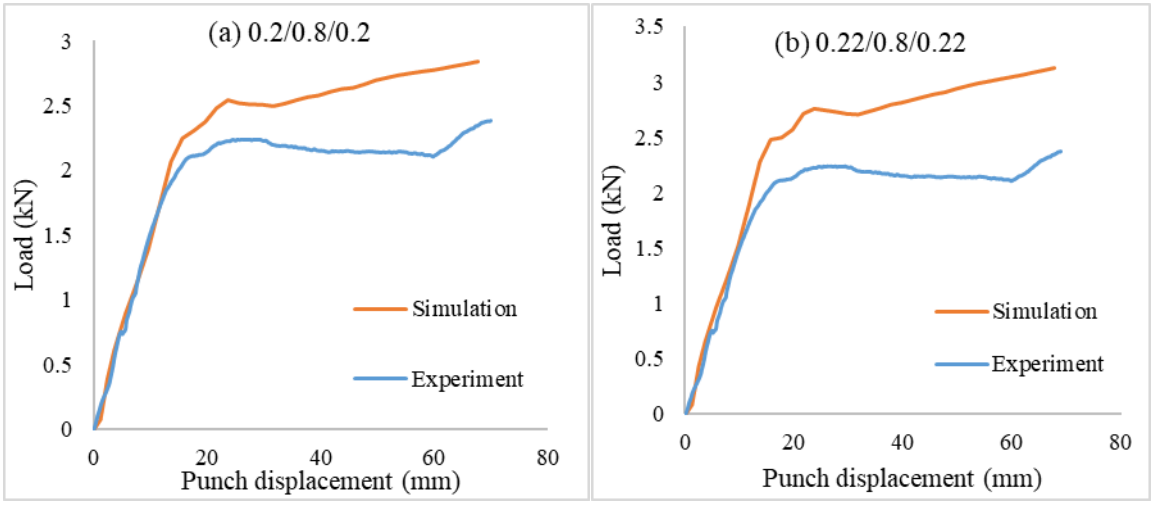

Figure 4.55: Comparison of load curves from experiment and simulation (a) 0.2/0.8/0.2 (b) 0.22/0.8/0.22

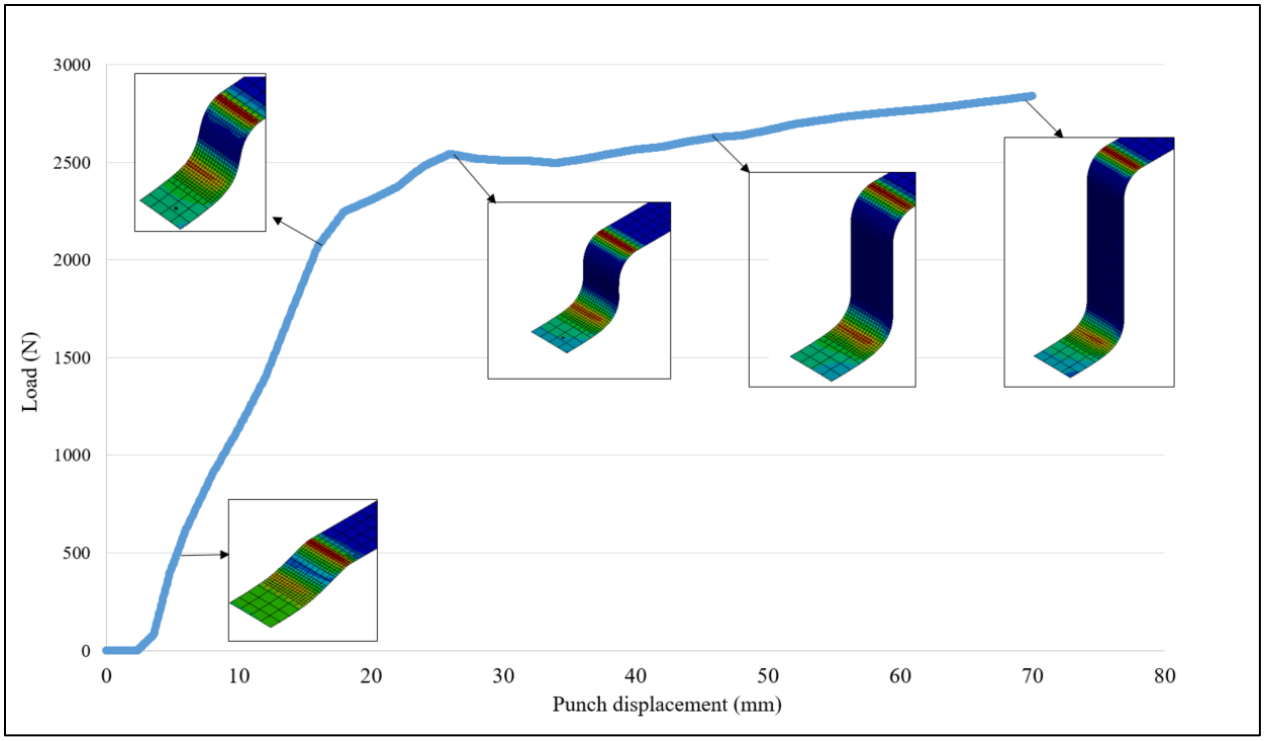

Figure 4.56: Stages of U-channel drawing along the punch load vs. displacement curve for the 0.2/0.8/0.2 mm sandwich laminate

For a die and punch radius of 8 mm, the sheet with thickness combination 0.2/1.6/0.2 (mm) fails at around 5 mm of punch displacement. The first onset of failure occurs in the lower aluminum skins at the punch corners. As the draw continues, failure in the upper aluminum skins at the die corner is observed. This is shown in Figure 4.57 (a). The load-displacement curve for the same specimen (0.2/1.6/0.2 mm) is shown in Figure 4.57 (b), each drop in punch load corresponds to the failure/crack in the aluminum skins. The load-displacement curve determined by finite element modeling does not show any drop in load since no failure strain is defined in simulation.

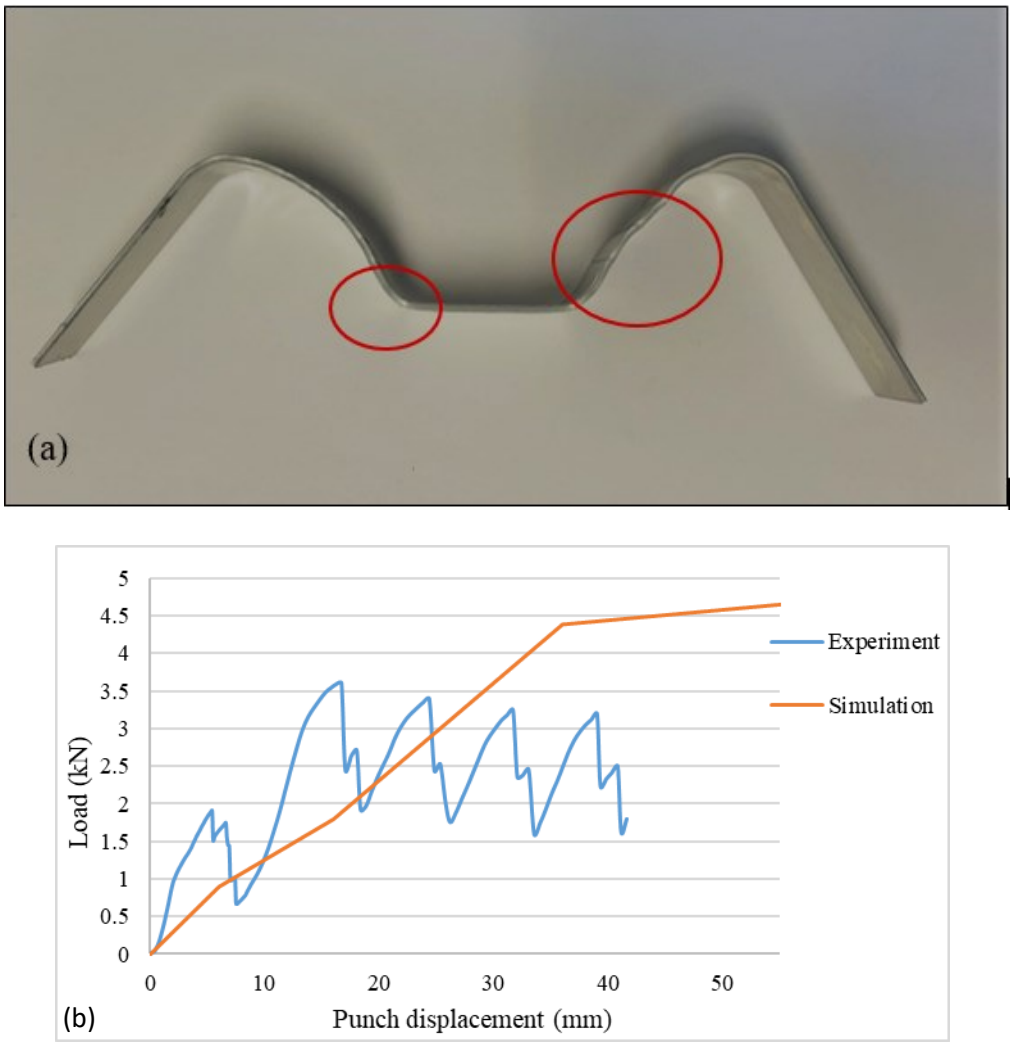

Figure 4.57: (a) specimen showing multiple crack formations and (b) load vs. punch displacement curve for 0.2/1.6/0.2 mm sandwich laminate

4.4 SPRINGBACK OF HA5182/POLYPROPYLENE/HA5182 SANDWICH LAMINATES

Sandwich laminates consisting of AA5182 aluminum alloy and polypropylene layers are constructed with two types of AA5182 in the skins, one with an annealed aluminum (AA5182-O) and the other with a hardened aluminum (AA5182-H18). This section explores the springback behavior of the sandwich laminates with AA5182-H18 in the skins. The hardened aluminum is referred to here as HA5182. The core is the same polypropylene as in the SA5182/PP/SA5182 laminates. The thickness combinations are 0.2/0/8/0.2, 0.22/0.8/0.2 and 0.2/1.6/0.2 mm.

The material properties HA5182 listed in Table 4.14 are taken from Ref. [18] which contains a detailed study of the tensile properties of Al/PP/Al sandwich laminates and each individual material of the sandwich.

Table 4.13: Mechanical properties of HA5182 aluminum alloy [18]

ρ (gm/cm^3)	E (GPa)	Poisson's ratio	K (MPa)	n	Y (MPa)	R0	R45	R90	M
2.89	69.6	0.33	581	0.07	425	0.51	0.95	0.98	8

Since the tension-compression stress-strain data for HA5182 were not available, Yoshida-Uemori parameters could not be determined for this material. The finite element model for HA5182/PP/HA5182 uses material model Mat_133 (Barlat 2000 yield criteria and isotropic hardening rule) for modelling the aluminum skins. All other simulation and process parameters are the same as in the finite element model for SA5182/PP/SA5182 sandwich laminates presented in Section 4.2. Barlat 2000 yield criteria requires the yield stress values in 0°, 45° and 90° directions and they are 425 MPa , 373 MPa and 395 MPa, respectively [18].

As can be observed in Figures 4.58-4.60, the wall angle of the sandwich laminates with HA5182 skins decreases with increasing sandwich thickness, but both the flange angle and the radius of curvature of the wall increase. This springback behavior is similar to that of the sandwich laminates with SA5182 skins. However, the sandwich laminates with HA5182 skins show higher springback values in comparison with the springback values obtained for the laminates with SA5182 skins. This is due to the higher yield strength of the hardened aluminum skins of HA5182.

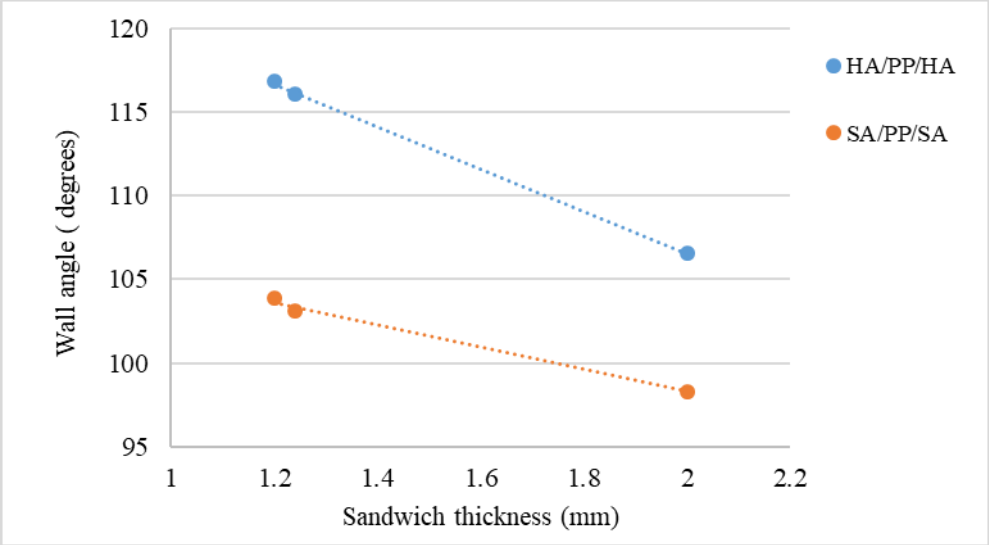

Figure 4.58: Variation of wall angles with sheet thickness for sandwich laminates with hard (HA) and soft (SA) aluminum skins

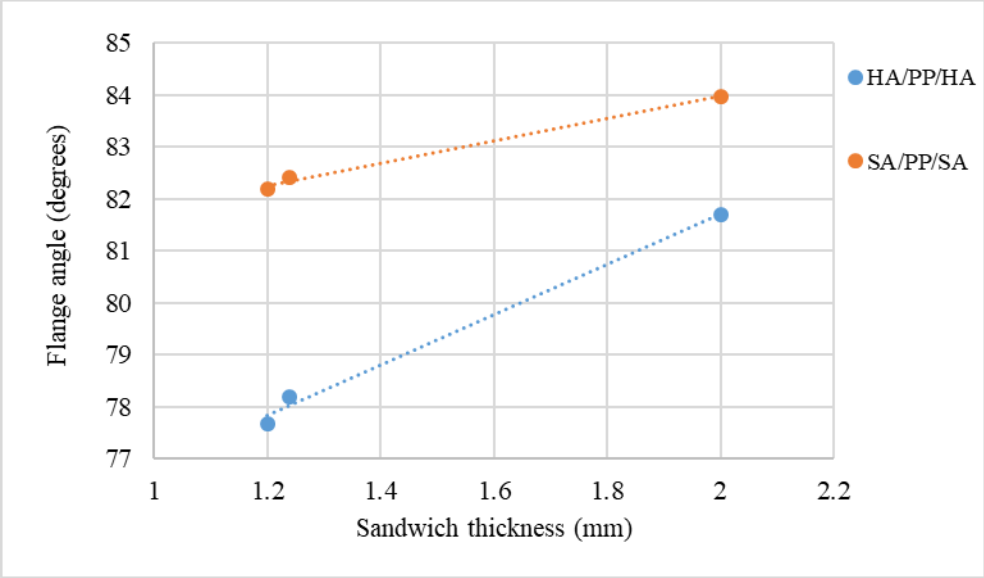

Figure 4.59: Variation of flange angle with sheet thickness for sandwich laminates with hard (HA) and soft (SA) aluminum skins

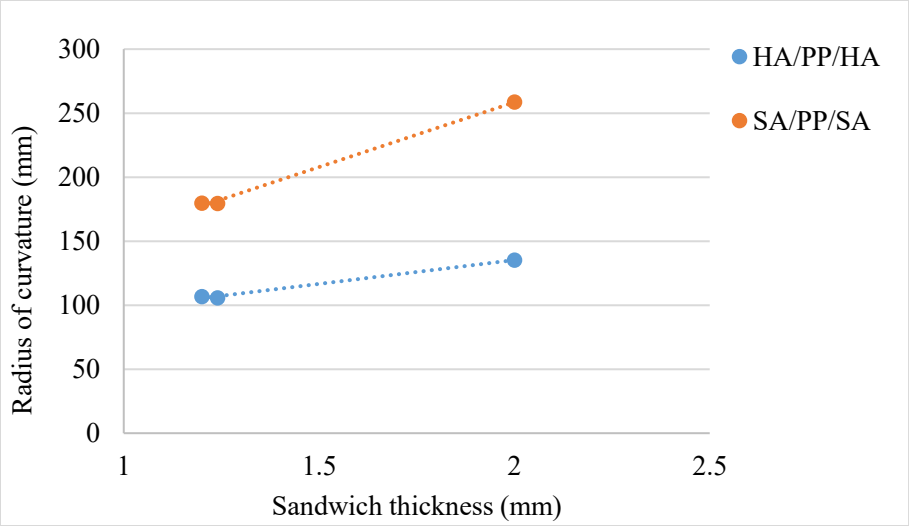

Figure 4.60: Variation of radius of curvature of the wall with sheet thickness for sandwich laminates with hard (HA) and soft (SA) aluminum skins

4.5 CONCLUSIONS

The springback behavior of aluminum-polypropylene-aluminum laminates under draw bending conditions is studied in this chapter using finite element simulations of the forming of U-channels following the Numisheet '93 guidelines. The springback behavior of single aluminum sheets is also studied under similar conditions to make comparisons. The springback parameters considered are the wall angle, flange angle and radius of curvature of the wall of the deep drawn U-channels.

In the study of single SA5182 (soft AA5182) sheets in the thickness range of 0.2 mm to 1.2 mm, it is seen that increasing the sheet thickness decreases the wall angle and increases both flange angle and radius of curvature of the wall, indicating that the springback behavior is improved. The Al/PP/Al sandwich laminate also shows lower wall angles, higher flange angles and higher radii of curvature of the wall with increase in laminate thickness. However, this is true up to a certain core thickness and then the laminate shows an increased springback behavior. When comparing a 1.2 mm thick SA5182/PP/SA5182 laminate with a thickness combination of 0.2/0.8/0.2 mm and a 1.2 mm thick single SA5182 sheet, the single aluminum sheet displays a

better springback behavior. This is because of the lower overall bending stiffness of the laminate compared to the single aluminum sheet. Based on available design dimensions, a combination of skin and core thickness can be used to show better springback behavior along with lower overall weight of the material. The laminates with hard aluminum skins exhibit higher springback behavior than the laminates with soft aluminum skins.

Draw bending experiments are conducted with a few SA5182/PP/SA5182 sandwich laminates to validate the finite element model. The soft aluminum laminates with 0.2/0.8/0.2 and 0.22/0.8/0.22 mm thickness combinations show springback values in close agreement with the current numerical model in this study. The 0.2/1.6/0.2 mm combination shows failure at the punch corner at the start of the blank being drawn into the wall of the cup. As the drawing progresses failure is seen at the die corner. This failure is only in the aluminum skins and does not propagate through the entire thickness of the sheet.

Keeping all other process parameters constant, the punch radius is varied from 5 mm to 12 mm. Increasing the punch radius shows an increase in wall angle and also in flange angle at all thickness combinations. For a constant punch radius of 8 mm, increasing the die radius from 8 mm to 12 mm shows that the flange angle increases and wall angle decreases over different thickness configurations of the sandwich laminate. The blank holder force (BHF) is varied between 500 N – 2500 N for four thickness combinations. With increasing BHF, the wall angle increases, the flange angle first decreases and then increases, and the radius of curvature of the wall either decreases or remains the same. This indicates that BHF has a negative effect on the springback behavior of the sandwich laminates. The wall angle increases and the flange angle decreases with increasing punch-die gap. With increasing coefficient of friction, the springback behavior decreases.

4.6 REFERENCES

[1] A. Makinouchi, NUMISHEET '93: proceedings of the 2nd International Conference of Numerical Simulation of 3-D Sheet Metal Forming Processes; verification of simulation with experiment, Isehara , Japan, 1993.

[2] L. Liu and J. Wang, "Modeling springback of metal-polymer-metal laminates," Journal of Manufacturing Science and Engineering, Transactions of the ASME, vol. 126, no. 3, pp. 599-604, 8 2004.

[3] F. Gardiner, "The springback of metals," Transactions of the ASME, vol. 79, no. 1, pp. 1-9, 1957.

[4] K. Ito, M. Kasajima and S. Furuya, "Bending and springback theory of metal-polymer sandwich laminates," Journal of Macromolecular Science, Part B: Physics, vol. 19, no. 4, pp. 773-791, 1981.

[5] M. Harhash, R. Rogin, S. Hartmann and H. Palkowski, "Experimental characterization , analytical and numerical investigations of metal / polymer / metal sandwich composites – Part 2 : Free bending," vol. 232, p. 111421, 15 January 2020.

[6] S. Kalpakjian and S. R. Schmid, Manufacturing Engineering Technology, Pearson Prentice Hall, 2005.

[7] J. Liu and W. Xue, "Unconstrained bending and springback behaviors of aluminum-polymer sandwich sheets," Internation Journal Advanced Manufacturing Technology, pp. 1517-1529, 2016.

[8] R. Ouled Ahmed and S. Chatti, "Simplified springback prediction of thick sandwich panel," Journal of Sandwich Structures and Materials, vol. 22, 2018.

[9] S. Mohammadi, M. Parsa and A. J. Aghchai, "Simplified springback prediction in Al/PP/Al sandwich air bending," Journal of sandwich structures and materials , vol. 17, no. 3, pp. 217-237, 2015.

[10] B. Maker and X. Zhu, "Input parameters for springback simulation using LS-DYNA," Livermore Software Technology Corporation, 2001.

[11] L. Chen, "Finite element simulation of springback in sheet metal forming," Applied Mechanics and Materials, Vols. 50-51, pp. 615-618, 02 2011.

[12] R. H. Wagoner, H. Lim and M. G. Lee, "Advanced issues in springback," International Journal of Plasticity , vol. 45, pp. 3-20, June 2013.

[13] W. Xu, C. Ma, C. Li and W. Feng, "Sensitive factors in springback simulation for sheet metal forming," Journal of Materials Processing Technology, vol. 151, pp. 217-222, 2004.

[14] B. Chongthairungruang, V. Uthaisangsuk, S. Suranuntchai and S. Jirathearanat, "Springback prediction in sheet metal forming of high strength steels," Materials and Design, vol. 50, pp. 253-266, 2013.

[15] B. Thaweepat and C. Jian, "Numisheet2005 Benchmark analysis on forming of an automotive underbody cross member: Benchmark 2," AIP Conference Proceedings, vol. 778, pp. 1113-1120, 2005.

[16] Z. Dongjuan, C. Zhenshan, R. Xueyu and L. Yuqiang, "Sheet springback prediction based on non-linear combined hardening rule and Barlat89's yielding function," Computational Materials Science, vol. 38, pp. 256-262, 2006.

[17] D. Banabic, Sheet Metal Forming Frocesses Constitutive modelling and Numerical Simulation, Springer , 2010.

[18] T. S. V. Somayajulu, "Vibration and Formability Characteristics of Aluminum Polymer Sandwich Materials," D. Eng. Dissertaion, University of Michigan, 2004.

[19] Y. Zhou and P. K. Mallick, "Effects of temperature and strain rate on the tensile behavior of unfilled and talc filled polypropylene Part I: Experiments," Polymer engineering and science, vol. 42, no. 12, pp. 2449-2460, December 2002.

[20] P.K.Mallick, Fiber reinforced composites Materials, Manufacturing and Design, third ed., Taylor & Francis Group, LLC., 2007.

[21] B. A. Chirita, "Factors of influence on the springback of formed metal sheets," in ESAFORM - The 5th International Conference on Material Forming, Krakow, Poland, 2002.

[22] J. J. Stein, "The effect of process variables on sheet metal springback," in International Body Engineering Conference and Exposition, Detroit, 1998.

[23] Y. Hu, "Simulating die gap effect on springback behavior in stamping processes," in SAE 2000 World congress, Detroit, 2000.

[24] M. Kadkhodayan and I. Zafarparandeh, "An investigation into the influence of blankholder force on springback in U-bending," Archives of Metallurgy and Materials, vol. 54, 2009.

[25] V.-C. Tong and D.-T. Nguyen, "A study on springback in U draw bending of DP350 high strength steel sheets based on combined isotropic and kinematic hardening laws," Advances in Mechanical Engineering, vol. 10, no. 9, pp. 1-13, 2018.

[26] B. Tang, X. Lu, Z. Wanga and Z. Zhao, "Springback investigation of anisotropic aluminum alloy sheet with a mixed hardening rule and Barlat yield criteria in sheet metal forming," Materials and Design, vol. 31, p. 2043–2050, 2010.

Chapter 5 - Residual Stresses After Springback

Residual stresses are internal stresses that arise due to the release of elastic strains after metal forming operations that involve non-uniform plastic deformations. They are lower than the yield strength of the material. Residual stress distributions contain both tensile and compressive stresses so that a static equilibrium condition exists in the formed part. Tensile residual stresses when added to the applied tensile stresses can cause early yielding or fatigue failure, and therefore, are not desirable, especially at or near the surfaces. Compressive residual stresses, on the other hand, are not considered detrimental since they will reduce the effect of the applied tensile stresses and may even improve the fatigue life of the part. In some applications involving fatigue loading, compressive residual stresses are intentionally induced on the surface, for example by shot peening, to increase the fatigue life of the material.

Residual stresses in single aluminum sheets and aluminum/polypropylene/aluminum sandwich laminates after springback are presented in this chapter. The formed part is a U-channel which is draw-bended from a flat sheet. As the punch load is released after the forming operation, the channel section not only shows springback due to the release of elastic strains, but also acquires a through-thickness residual stress distribution that varies along its length. Except for simple cases, such as a beam under pure bending loading, residual stresses are difficult to determine by analytical methods. More often, they are determined using experimental techniques, such as hole drilling method. In this study, they are numerically determined using finite element analysis, more specifically using LS-DYNA.

5.1 BACKGROUND

5.1.1 Residual stresses after pure bending

Figure 5.1 shows a plate of thickness *d* subjected to pure bending. As the bending moment is increased, the top and bottom surfaces of the plate which have the maximum normal stresses will first yield. With further increase in the bending moment, the yielded zone, which is called the plastic zone in Figure 5.2(a), on each side of the mid-thickness of the plate will spread into the interior of the plate. Assuming that *h* is the thickness of the plastic zone on each side of the mid-thickness, the thickness of the elastic zone is (*d-2h*). If the applied bending moment is now released, the elastic stresses will be recovered which will result in springback and the development of residual stresses through the thickness of the plate, which can be calculated by subtracting the elastic stresses from the elastic-plastic stresses due to bending at the time of their release.

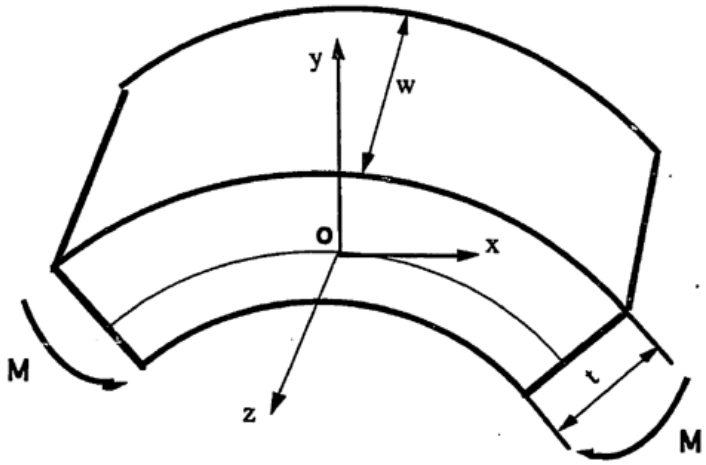

Figure 5.1: Pure bending of a beam [1]

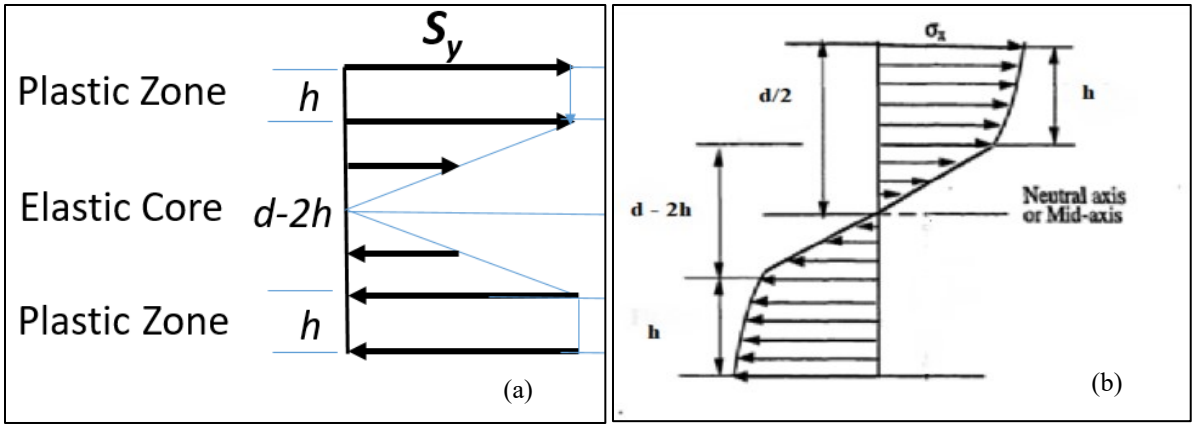

Figure 5.2: Distribution of bending stresses for (a) elastic, perfectly plastic material (b) elastic-strain hardening material

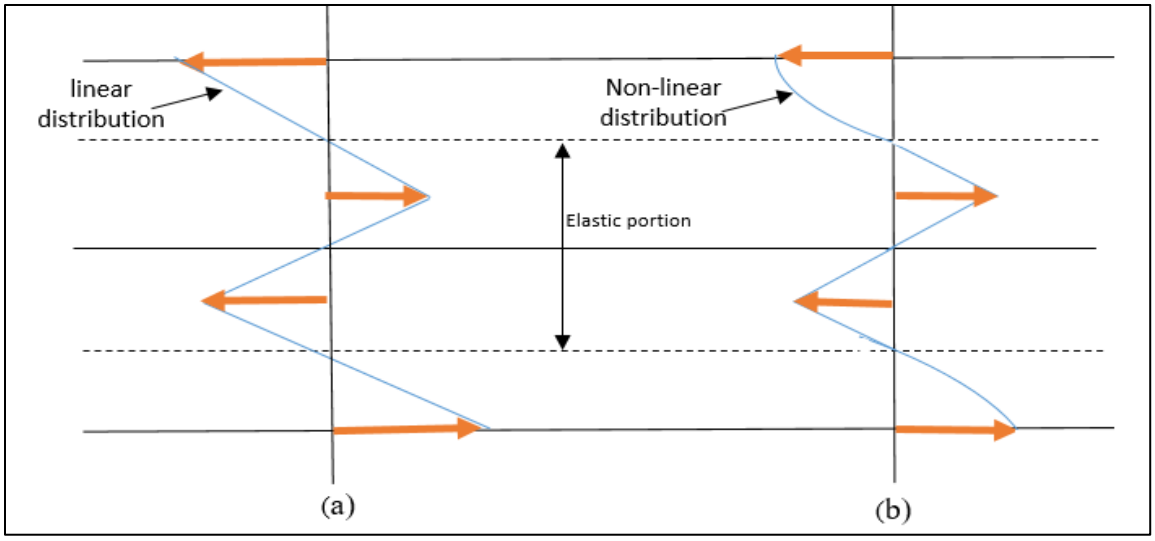

Figure 5.3: Distribution of residual stresses for (a) elastic, perfectly plastic material (b) elastic-strain hardening material

Residual stresses after pure bending of a plate of an elastic-perfectly plastic material can be calculated using the following equations [2] .

$$\text{Within the plastic zone: } \sigma_R = S_y\left(1-\frac{2y}{d}\left(1+\frac{2h}{d}\left\{1-\frac{h}{d}\right\}\right)\right) \qquad \text{Eq. 5.1}$$

$$\text{Within the elastic zone: } \sigma_R = S_y\left(\frac{2y}{(d-2h)}-\frac{2y}{d}\left(1+\frac{2h}{d}\left\{1-\frac{h}{d}\right\}\right)\right) \qquad \text{Eq. 5.2}$$

where, S_y = yield strength of the material

d = thickness of the plate

h = thickness of the plastic zone from each surface

y = distance from the mid-plane of the plate

A plot of Equations 5.1 and 5.2 in Figure 5.3(a) shows that the residual stress distribution in a plate of elastic, perfectly plastic material is linear in nature. It is also to be noted that the directions of the residual stresses on the surfaces are opposite to the directions of the stresses due to the application of the bending moment. For a plate of an elastic-strain hardening material, the bending stress distribution during loading will also contain an elastic zone in the interior of the beam and plastic zones on the top and the bottom of the elastic zone; however, as shown in Figure 5.2(b), the stress distributions in the plastic zones will now be non-linear due to the strain hardening of the material. On release of the bending moment, residual stress distribution will also be non-linear as shown in Figure 5.3(b). An analytical expression for the residual stress distribution in a material that follows the power-law equation, $\sigma = K\varepsilon^n$, after yielding is given by Tan et al. [3]. This expression, which was verified experimentally, shows that the residual stresses are not only a function of the plate thickness and yield strength of the material, but also its strain hardening parameters, K and n. Similar observations are made by Wang [1] in which it is concluded that residual stresses increase with increase with both K and n, decrease with increase in elastic modulus and Poisson's ratio, and are higher for wider sheets than narrower sheets.

Residual stress determination after forming processes, such as stretch bending and deep drawing, is much more complex than that after pure bending. In these forming processes, a combination of bending, stretching, and drawing deformations occur and may vary from location to location on the part being formed that are difficult to model analytically. Essa et al. [4] used finite element analysis to study the variation of residual stresses in an annealed SAE 1020 steel

sheet after a three-point bending loading. They observed that the maximum residual stress increases with increasing sheet width, which is due to a change in stress condition from plane stress at lower widths to plane strain at higher widths. Sherbiny et al. [5] presented a finite element simulation study on the residual stresses in deep-drawn round low carbon steel cups. Their study shows that the maximum residual stress increases with increasing blank thickness. It is also a function of die shoulder radius, punch nose radius and radial die-punch clearance. On the process parameter side, it is a function of blank holder force as well as friction condition between the surfaces in contact. With increasing blank holder force, the maximum residual stress first decreases, but after reaching the lowest value, it starts to increase.

5.1.2 Residual stresses after simultaneous bending and stretching

When a plate is subjected simultaneously to bending and stretching (Figure 5.4 (a)), the neutral plane is shifted from the mid-plane toward the compression side of the plate (Figure 5.4(b)). Since the combined tensile stress due to bending and tension is higher than that due to bending only, the plastic zone size on the tension side is larger than that on the compression side of the plate. The elastic recovery on the release of the applied loads will include elastic stresses due to the applied bending moment and elastic stresses due to the applied tensile force.

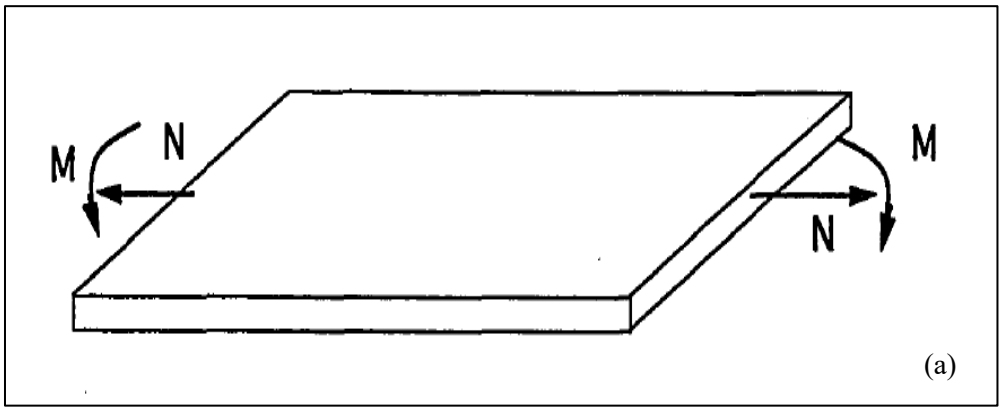

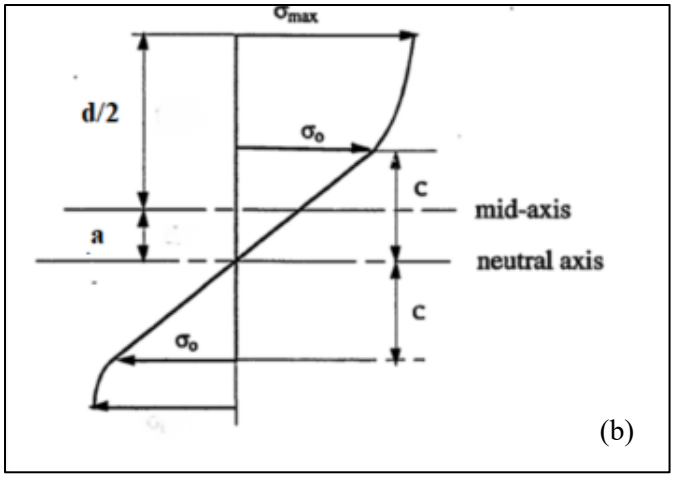

Figure 5.4: (a) Beam under combined bending moment and axial tension (b) Through-thickness stress distribution for an elastic-strain hardening material [1]

5.1.3 Residual stresses in a sandwich laminate

A 3-layered sandwich laminate is constructed of two different materials, a high modulus material in the upper and lower skins and a low modulus material in the core. Typically, the skin material will be a steel or an aluminum alloy and the core will be a polymer, which not only has a much lower modulus, but also a much lower yield strength than the skin material. Under a bending moment M, a longitudinal strain distribution in the beam is continuous, with the highest strains occurring at the upper and lower surfaces and reducing to zero strain at the mid-plane of the beam. However, because of the modulus difference of the skin and core materials, the stress distribution is discontinuous, as shown in Figure 5.5. The discontinuity occurs at the interfaces between the skins and the core. The elastic stresses in each layer can be calculated using the following equations.

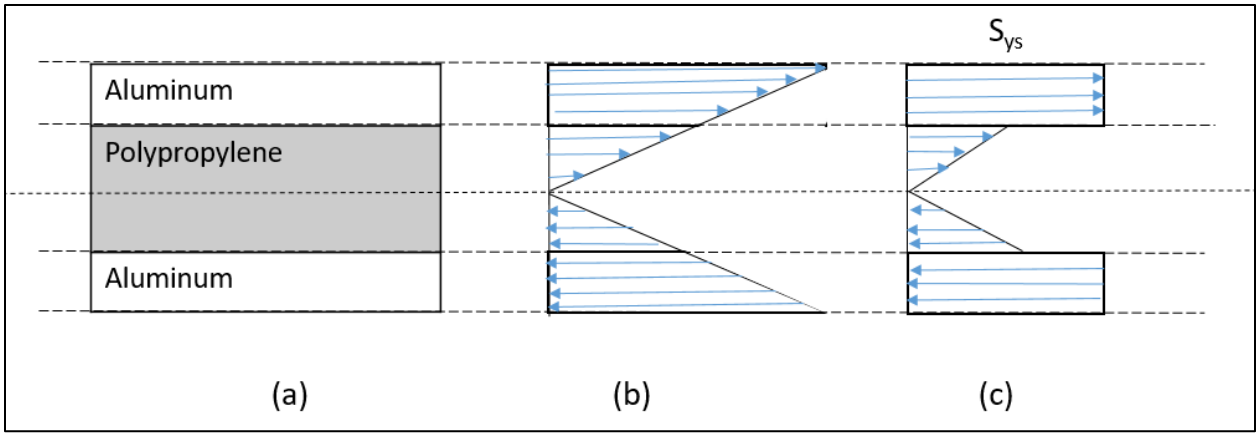

Figure 5.5: Cross-section of a three-layered laminate with core material modulus (E_c) lower than the skin material modulus (E_s) (a) sandwich laminate (b) strain distribution (c) stress distribution when the skins have yielded (assuming elastic-plastic behavior of the skin material)

$$\sigma_{skin} = \frac{My}{I_{eq}} \qquad \text{Eq. 5.3}$$

$$\sigma_{skin} = \left(\frac{E_c}{E_s}\right)\frac{My}{I_{eq}}$$

where, M = bending moment

E_c = elastic modulus of the core material

E_s = elastic modulus of the skin material ($E_s > E_c$)

y = distance from the mid-plane of the beam

$$Ieq. = \left(\frac{bt_s{}^3}{6}\right) + \frac{bt_s}{2}\{t_s + t_c\}^2 + \frac{E_c}{E_s}\left(\frac{bt_c{}^3}{12}\right)$$

t_s = skin thickness on each side of the laminate

t_c = core thickness

Assuming the skin thickness is much smaller than the core thickness, i.e., $t_s << t_c$,

$$I_{eq} \approx \frac{bt_c^2 t_s}{2} \qquad \text{Eq. 5.4}$$

The highest stresses in the laminate occur at the upper surface of the upper skin and lower surface of the lower skin, and they decrease linearly toward the interior. The highest stress in the core occurs at the interfaces of the core and the skins. As the bending moment is increased,

yielding will start first on the outer surfaces and then the plastic zone will move inward. The bending moment M_y corresponding to the first occurrence of yielding is given by the following equation.

$$M_y = \frac{S_{ys} b t_s t_c^2}{(2t_s + t_c)} \qquad \text{Eq. 5.5}$$

where, S_{ys} is the yield strength of the skin material.

With increasing bending moment, the plastic zones will spread through the skin thickness on each side of the laminate. Assuming that the core has much lower stresses than the skins so that it has not yet yielded, and it provides much less resistance to the bending moment than the skins, the bending moment M_{ys} at which skins will yield completely is

$$M_{ys} = S_{ys} b t_s (t_c + t_s) \qquad \text{Eq. 5.6}$$

Equation (5.6) assumes that the skin material behaves in an elastic-plastic manner and does not display strain hardening. The residual stress distribution in the skins can now be calculated as

$$\sigma_{residual} = S_{ys}\left[1 - \frac{2(t_c + t_s)y}{t_c^2}\right] \qquad \text{Eq. 5.7}$$

Equation 5.7 is plotted in Figure 5.6 to show the residual stress distribution in an aluminum/polypropylene/aluminum beam in which the aluminum skin thickness is 0.2 mm on the top and bottom side of a 0.8 mm thick polypropylene core. The aluminum has a modulus of 70 GPa and a yield strength 110.2 of MPa. The modulus and yield strength of the polypropylene are 2.4 GPa and 25 MPa respectively.

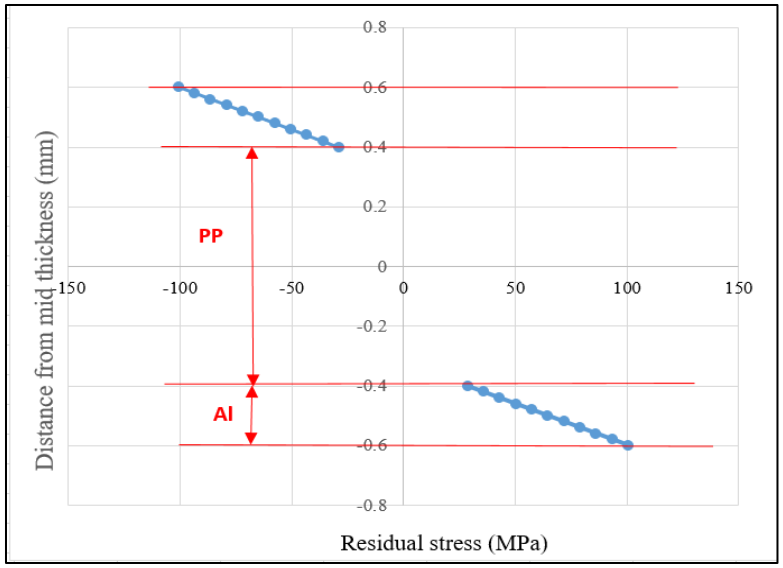

Figure 5.6: Residual stress distribution in the aluminum skins of a 0.2/0.8/0.2 mm Al/PP/Al sandwich laminate

5.2 Residual Stresses in U-Channels after Springback

Residual stresses in the U-channel are the internal elastic stresses that appear in its wall after the punch is retracted at the end of forming. Forming stresses in the channel wall at the end of the punch travel are rearranged due to the relaxation of the elastic stresses, which give rise to both springback and residual stresses. The finite element model used for determining residual stresses in the U-channels made of SA5182 aluminum and SA5182/PP/SA5182 sandwich laminate is the same as the one used for determining springback described in Chapter 4. The forming and finite element model parameters are summarized in Table 5.1.

Table 5.1: Forming and finite element model parameters used in residual stress determination in U-channels

Forming Parameters	
Sheet thickness	(1) SA5182: 0.6, 0.8, 1 and 1.2 mm (2) SA5182/PP/SA5182: 0.2/0.8/0.2, 0.22/0.8/0.22, 0.24/0.8/0.24. 0.2/1.6/0.2, 0.22/1.6/0.22 and 0.24/1.6/0.24
Blank aerial dimensions	320 mm x 35 mm
Die and punch diameters	52 mm and 50 mm
Die corner radius	5 mm and 8 mm for SA5182 and 8 mm for SA5182/PP/SA5182
Punch corner radius	5 mm and 8 mm for SA5182 and 8 mm for SA5182/PP/SA5182
Blank holder force	2500 N
Punch travel	70 mm
Punch travel speed	200 mm/s
Finite Element Model Parameters	
Element type	Shell for SA5182 and Part composite – shell for SA5182/PP/SA5182
Element size	1 mm by 1 mm
Material model	Mat_226 for SA5182 and Mat_24 for PP
No. of Integration Points	9 for SA5182 and 10 for SA5182/PP/SA5182

Irrespective of the forming force applied (without failure), the residual stresses are required to be in a state of static equilibrium at the end of springback. An example of the stress distribution is given in Figure 5.7. From this figure the force equilibrium condition can be verified by calculating the area under the curve and using the force balance equation,

$$A1 + A3 = A2 + A4 \qquad \text{Eq. 5.8}$$

and the moment balance equation,

$$A1.y_1 - A3.y_3 = A2.y_2 - A4.y_4 \qquad \text{Eq. 5.9}$$

where, y_1, y_2, y_3 and y_4 are the distances of the centroids of the areas A_1, A_2, A_3 and A_4, respectively, from the mid-plane of the beam.

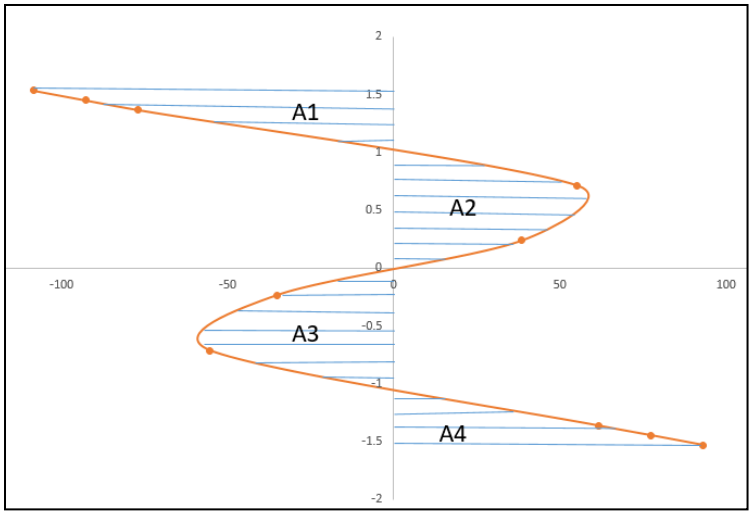

Figure 5.7: Example of residual stress distribution

5.3 Forming and Residual Stresses in Single SA5182 Sheets

5.3.1 Stresses at the end of forming

The forming stress distributions though the thickness of aluminum sheets at the end of forming the U-channels are shown in Figure 5.8. The stresses at each integration point are extracted from the simulation outputs and stress distribution plots are made for sheet thicknesses ranging from 0.6 mm to 1.2 mm. The stresses in Figure 5.8 are plotted at the die corner and punch corner which have a 5 mm radius and also at the mid-length of the vertical wall. At the die corner, the top surface is in tension and the bottom surface is in compression. At both die and punch corners, the stress at the mid-thickness is a positive tensile stress. The non-zero tensile stress at the mid-thickness is due to stretching of the sheet as it starts to form the vertical wall, at the end of bending and then unbending around die radius. At the mid-thickness of the die corner, the tensile stress is the highest for 0.6 mm thickness and the lowest for 1.2 mm thickness, while at the mid-thickness of the punch corner, the tensile stress is the lowest for 0.6 mm thickness and the highest for 1 mm thickness. At the punch corner, the top surface is in compression while the bottom surface is in tension. The neutral layer (i.e., the zero-stress layer) at the die corner occurs in the lower half of the sheet

thickness while the neutral layer at the punch corner occurs in the upper half of the sheet thickness. Thus, the neutral plane at the die corner shifts toward the lower surface on the compression side, and at the punch corner, shifts toward the upper surface or on the tension side. Both maximum tensile stress and minimum compressive stress increase with increasing sheet thickness and are the highest for the 1.2 mm thickness (Table 5.2). Also, to be noted is that the plastic zone size from the surfaces increases with increasing sheet thickness.

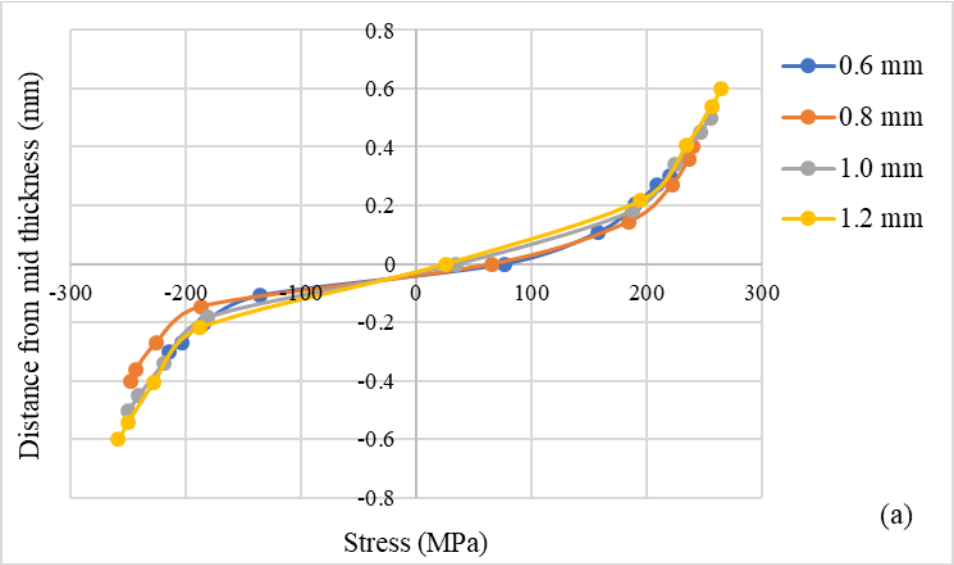

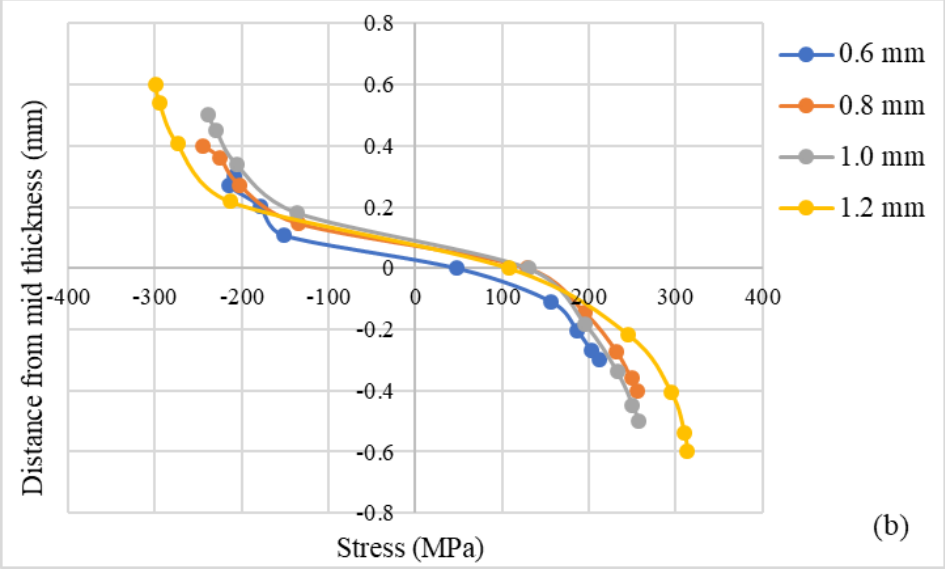

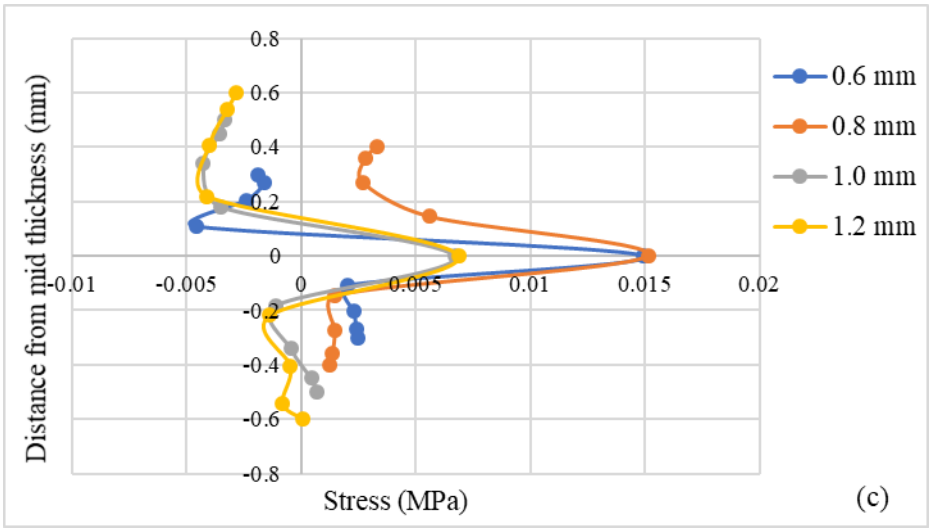

Figure 5.8: Forming stress distributions in SA5182 sheets for die and punch radii of 5 mm
(a) Die corner (b) Punch corner (c) Mid-length of the vertical wall

Additionally, the through-thickness stresses at the end of forming, when formed over a die and punch radius of 8 mm is shown in Figure 5.9. The stresses are plotted at the die corner, punch corner and mid-length of the vertical wall. The nature of the stress distributions at the die and punch corners are similar for both 5 mm and 8 mm die and punch corner radii; however, as can be seen in Table 5.2, the maximum tensile and compressive stresses on the outer surfaces are lower with 8 mm radii compared to 5 mm radii.

At the mid-length of the vertical wall, the stresses at the end of forming for both 5 mm and 8 mm die and punch radii are very close to zero. The stresses at the mid-thickness show higher values in comparison to the stresses at all other through-thickness locations. For the 8 mm die and punch radii, the stresses at the mid-plane are compressive and decrease with increasing sheet thickness. However, the mid-thickness stresses for the 5 mm die and punch radii at the mid-length of the vertical wall are tensile in nature. It can be concluded that the magnitude of the stresses at the mid-length of the wall are not significant. Due to the maximum tensile stress occurring on the

top surface at the die corner and on the bottom surface at the punch corner, it is possible that tensile failure may occur at these corners during forming.

Table 5.2: Stresses (MPa) in SA5182 sheets at the end of forming

Location	Through-thickness Location	Sheet thickness (mm)						
		0.6	0.8		1.0		1.2	
		Die and Punch Radii	Die and Punch Radii		Die and Punch Radii		Die and Punch Radii	
		5 mm	5 mm	8 mm	5 mm	8 mm	5 mm	8 mm
Die corner	Mid-thickness	76.89	65.91	65.789	35.16	63.403	25.42	51.082
	Top surface	220.02	236.55	207.07	255.45	223.95	265.15	250.85
	Bottom surface	-214.5	-248.29	-197.05	-250.02	-216.95	-258.93	-257.82
Punch corner	Mid-thickness	48.25	128.6	78.328	129.84	102.67	108.01	113.75
	Top surface	-214.72	-245.25	-235.6	-239.18	-242.12	-299.45	-238.33
	Bottom surface	212.11	255.56	243.18	257.32	251.42	313.28	256.81
Mid-length of the vertical wall	Mid-thickness	0.0145	0.0151	-0.0421	0.0067	-0.0259	0.0686	-0.0106
	Top surface	-0.0019	0.0033	-0.0004	-0.0033	0.0007	-0.0283	0.0031
	Bottom surface	0.0025	0.0012	0.0026	0.0007	0.0029	0.0001	0.0042

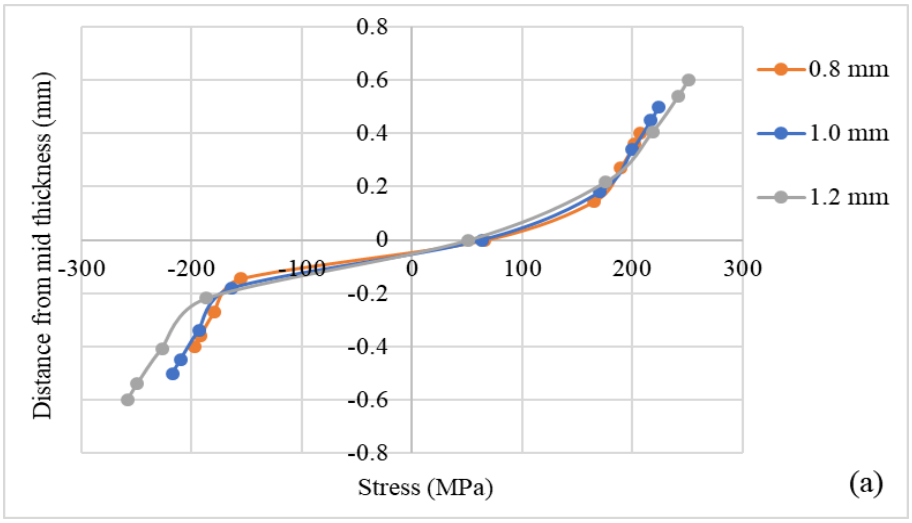

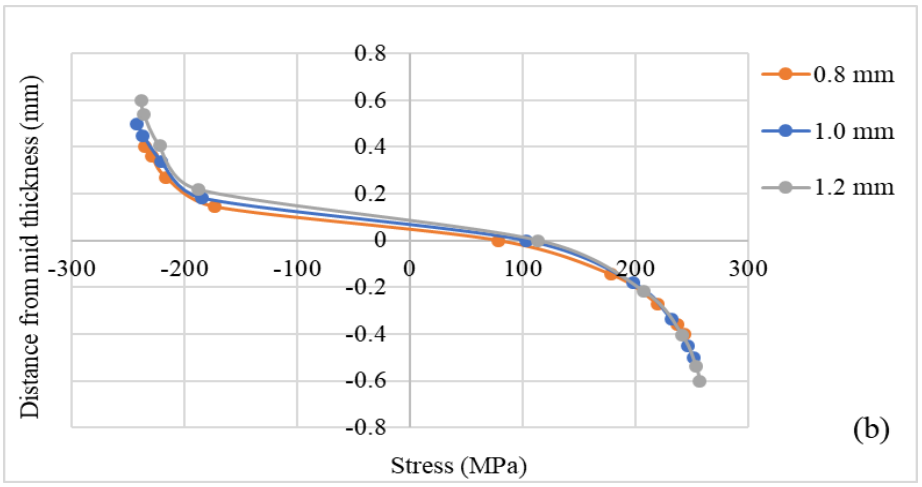

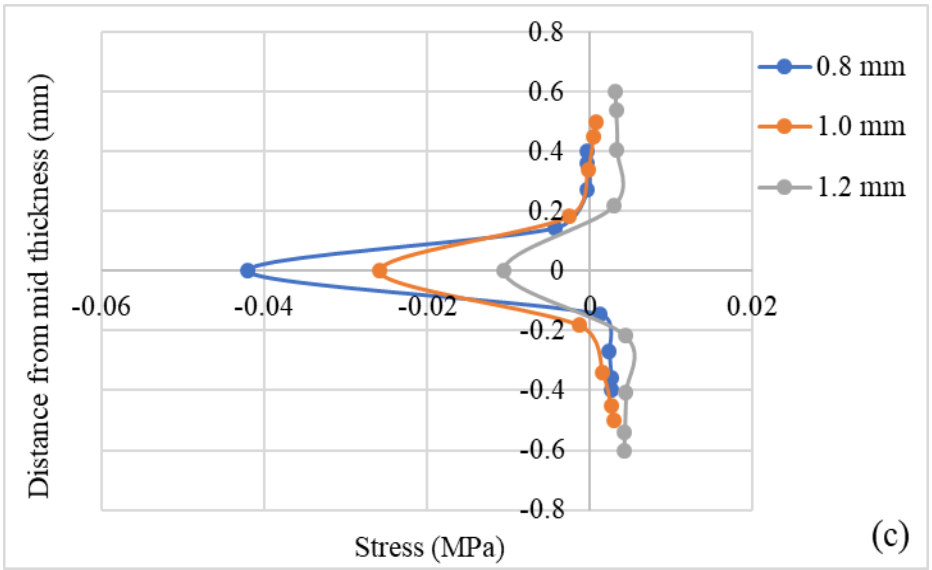

Figure 5.9: Stress distribution at the end of forming for an 8 mm die and punch radii at (a) Die corner (b) Punch corner (c) Mid-length of vertical wall

5.3.2 Residual stresses after springback

The residual stress distributions for single aluminum SA5182 of different thicknesses after springback are plotted in Figure 5.10. It can be observed in this figure that at the die corner, the residual stress is compressive on the top surface and tensile on the bottom surface, and the zero-stress location has moved toward the bottom surface. At the punch corner, on the other hand, the residual stress is tensile on the top surface and compressive on the bottom surface, and the zero-stress location has moved toward the top surface. The same behavior in stress patterns is observed in the U-channel drawn over an 8 mm punch and die radius (Figure 5.11) The maximum residual tensile stresses at these locations for both 5 mm and 8 mm tool radius are listed in Table 5.3. The effect of the axial force is more prominent at lower sheet thicknesses, i.e., the neutral layer moves closer to the mid-surface as the thickness increases at the die corner and the mid-length of the wall. At the punch corner, the mid-surface shows higher stresses with increasing sheet thickness.

The residual stresses at the mid-length of the vertical wall after springback are shown in Figure 5.10 (c) and 5.11 (c) for the 5 mm and 8 mm tool radius respectively. It can be seen that the residual stresses in the wall are greater than the stresses at the end of forming, whereas the residual stresses at the die and punch corners are lower than the forming stresses. This is because of the bending of flange areas of the U-channel as well as the sidewall curl that introduces stresses in the wall area. The residual stresses at the mid-thickness decrease with increasing sheet thickness. The stresses are tensile on the top surface and are compressive at the lower surface. The trend of the residual stress distribution at the mid-length of the wall is similar to that of the punch corner, but is much smaller in magnitude.

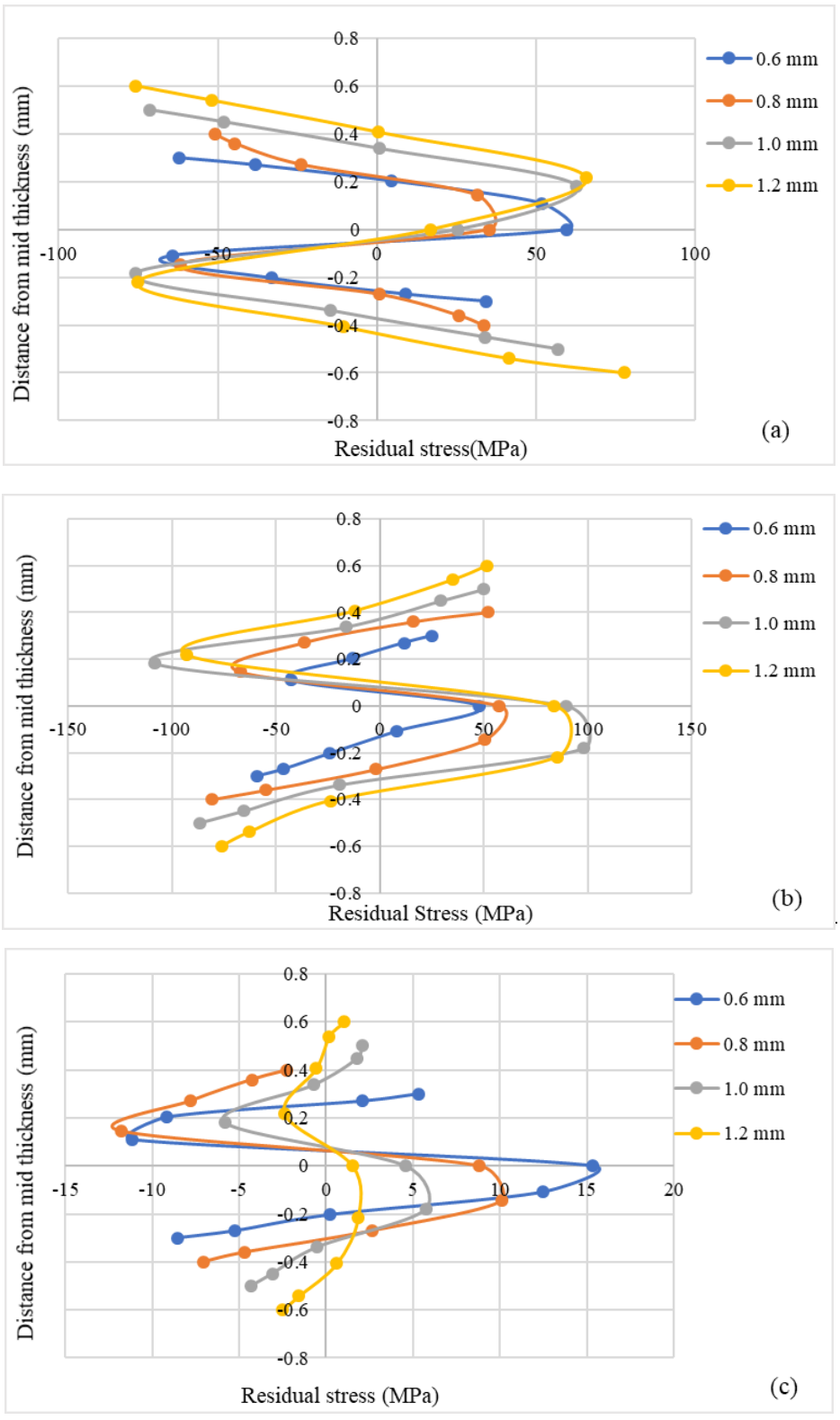

Figure 5.10: Residual stress distributions after springback in SA5182 sheets for 5 mm die and punch radii (a) Die corner (b) Punch corner, and (c) Mid-length of the vertical wall

Table 5.3: Residual stresses (MPa) in SA5182 sheets after springback

Location	Through-thickness Location	Sheet thickness (mm)						
		0.6	0.8		1.0		1.2	
		Die and Punch Radii	Die and Punch Radii		Die and Punch Radii		Die and Punch Radii	
		5 mm	5 mm	8 mm	5 mm	8 mm	5 mm	8 mm
Die corner	Mid-thickness	59.58	35.1	47.072	25.20	36.756	16.96	31.27
	Top surface	-62.20	-51.0	-64.307	-71.419	-76.402	-75.69	-75.233
	Bottom surface	34.38	33.4	46.579	56.918	46.45	77.49	73.78
Punch corner	Mid-thickness	47.568	57.4	43.8	89.429	54.696	83.667	67.177
	Top surface	24.849	51.704	22.332	49.739	49.663	51.446	28.469
	Bottom surface	-59.012	-80.771	-73.822	-86.433	-100.04	-76.125	-101.42
Mid-length of the vertical wall	Mid-thickness	15.316	8.823	4.075	4.548	3.23	1.512	0.2475
	Top surface	5.3165	-2.243	0.54487	2.0707	1.758	1.0307	1.3536
	Bottom surface	-8.566	-7.053	1.4327	-4.28	-2.54	-2.542	-2.42

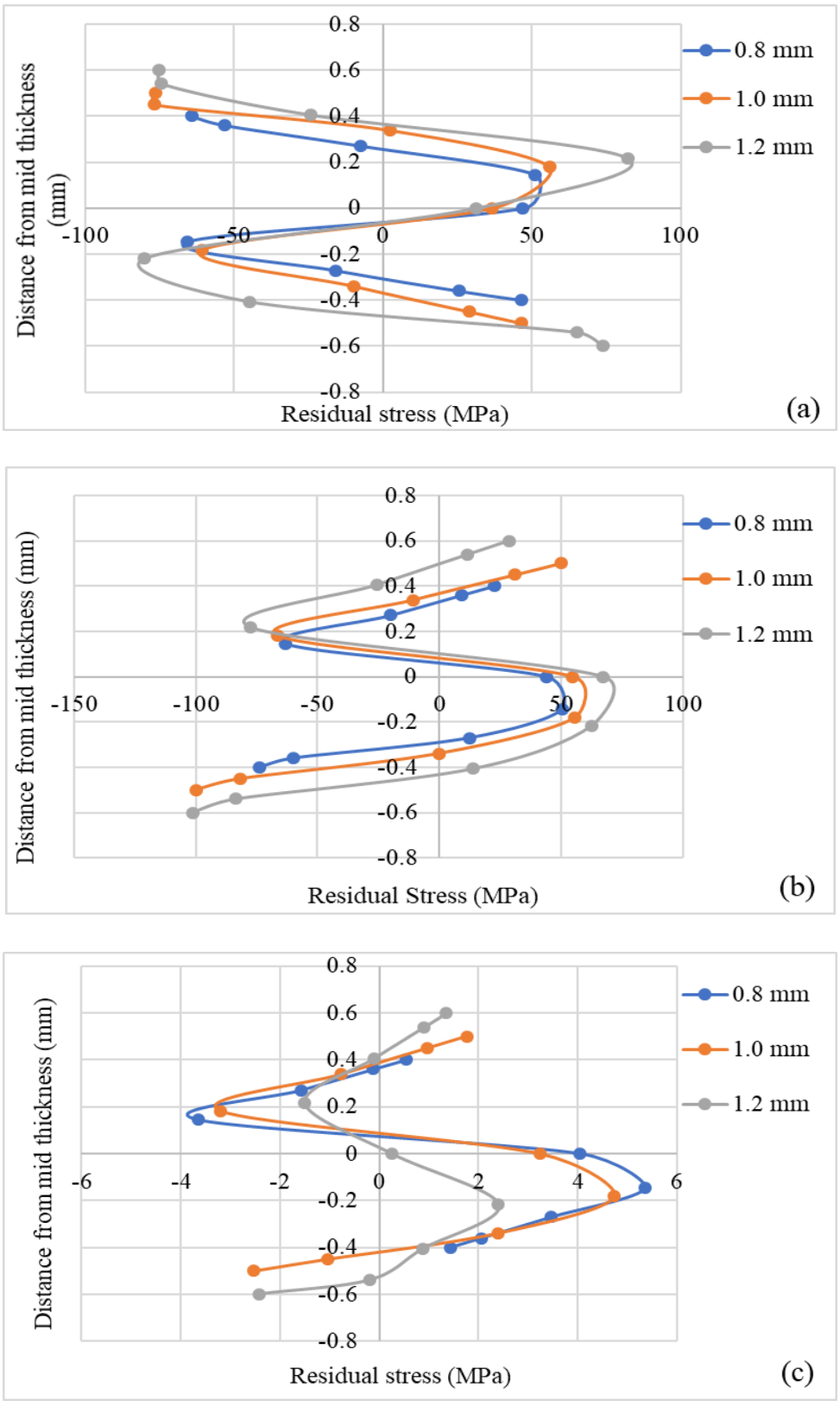

Figure 5.11: Residual stress distribution after springback in SA5182 sheets for 8 mm punch and die radii (a) Die corner (b) Punch corner (c) Mid-length of vertical wall

5.4 FORMING AND RESIDUAL STRESSES IN SA5182/POLYPROPYLENE/SA5182 SANDWICH LAMINATES

This section presents the distributions of forming and residual stresses at the die and punch corners and at the mid-length of the vertical wall in the formed U-channels of SA5182/PP/SA5182 sandwich laminates. Stresses are evaluated at three integration points each on the top and bottom aluminum skins and four integration points in the polypropylene core. Although the strain distribution is continuous through the thickness of the sandwich laminate, the stresses are discontinuous at the interfaces between the polypropylene core and aluminum skins.

5.4.1 Stresses at the end of forming

Figure 5.12 (a) shows the forming stress distributions through the thickness of SA5182/PP/SA5182 sandwich laminates with 0.2/0.8/0.2, 0.22/0.8/0.22 and 0.24/0.8/0.24 mm thickness combinations at the end of forming the U-channels. Figure 5.12 (b) shows the stresses at the end of forming for sandwich laminates with a constant core thickness of 1.6 mm and skin thicknesses of 0.2 mm, 0.22 mm, and 0.24 mm at the die corner. A large difference in stress levels is noted between the aluminum skins and the polypropylene core, since the majority of the load is carried by the aluminum skins. These stress values are evaluated at the die corner radius and show that the outer surface is in tension and inner surface is in compression. Majority of the stresses in the polypropylene core layer are above the yield stress value (25 MPa) and remain in a plastic stress state. The neutral layer or zero stress layer moves closer to the mid surface of the sandwich laminate as the core thickness increases. The stresses in the aluminum skins with the sandwich laminates of 1.6 mm core thickness show one or both the skins to have stresses higher than the UTS (280 MPa) of SA5182. For the laminates with core thickness 0.8 mm and 1.6 mm the stresses in the top and bottom surface increase with increasing skin thickness. The stresses in the

polypropylene layer at a constant core thickness remain almost the same with changing skin thickness.

At the punch corner, the stresses in the aluminum skins are lower than those at the die corner irrespective of core thickness (Figure 5.13). With increasing skin thickness, the stresses in the aluminum layers show a small increase and the stresses in the polypropylene remain almost the same. At the mid-length of the wall the upper aluminum skins are in compression while the lower aluminum skins are in tension for the laminates with 0.8 mm core thickness and in compression for the 1.6 mm core thickness (Figure 5.14). However, the magnitude of the stresses at the mid-length of the wall compared to those at the punch and die corner are negligible.

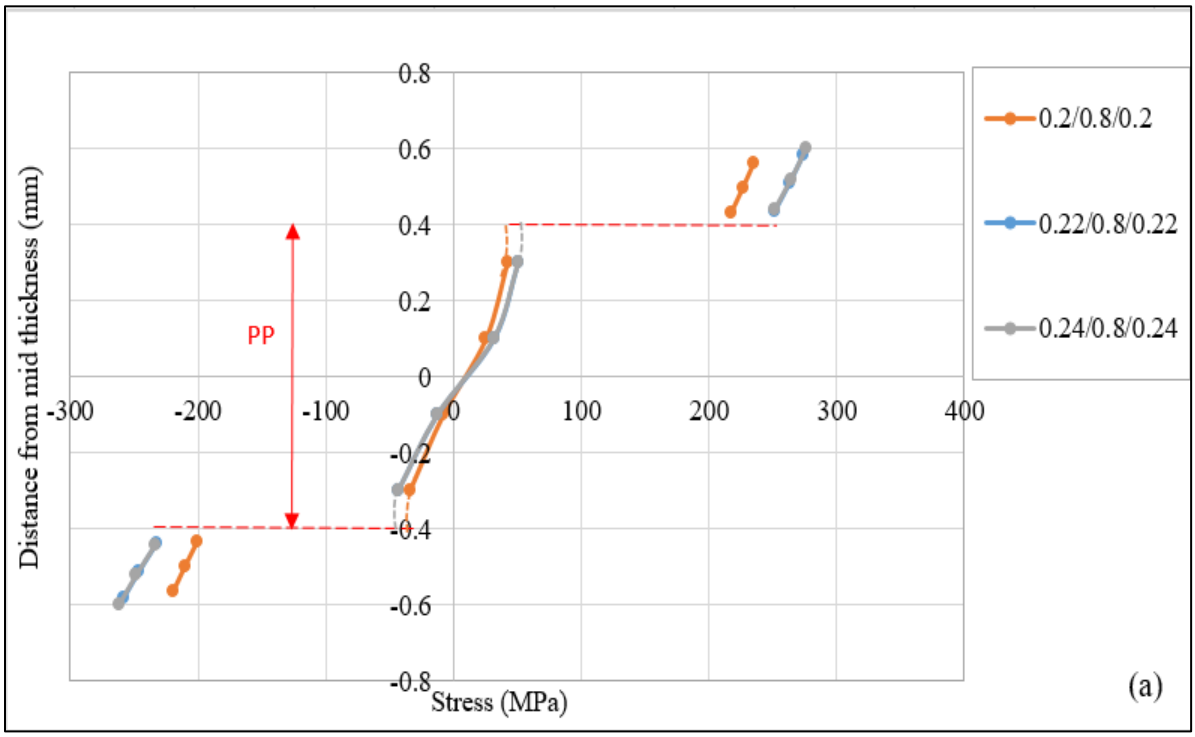

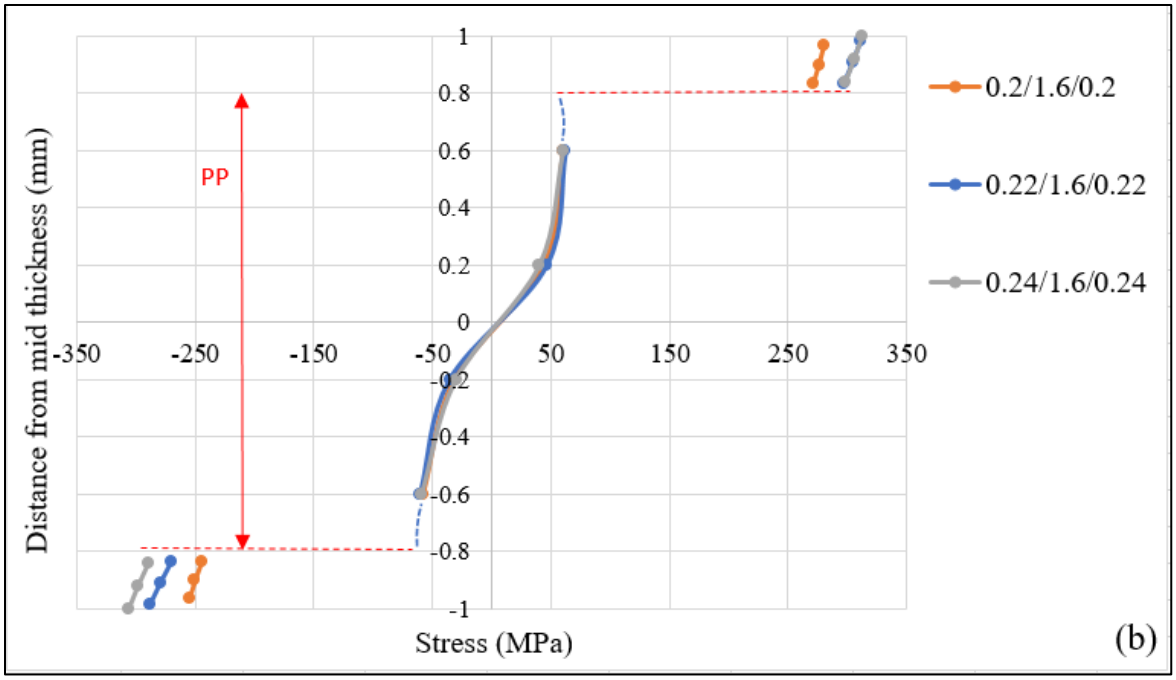

Figure 5.12: Through-thickness stress distribution at the die corner at the end of forming in SA5182/PP/SA5182 laminates with (a) 0.8 mm core (b) 1.6 mm core

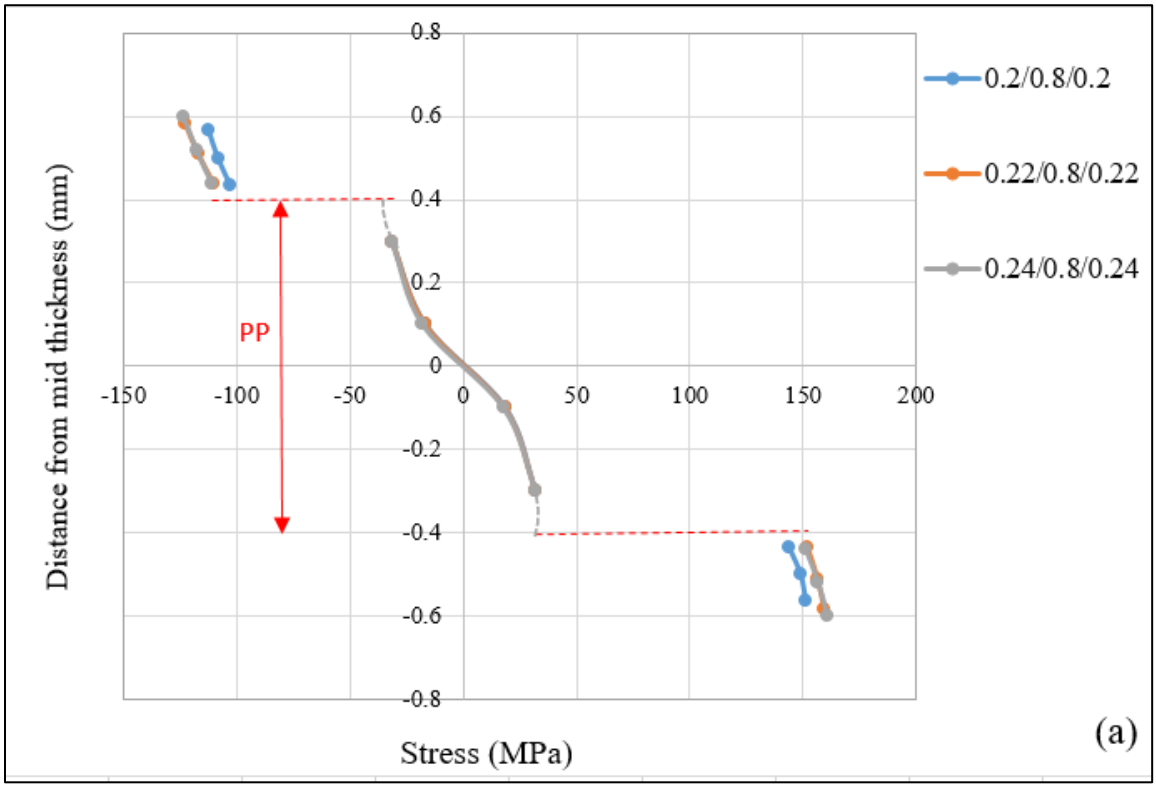

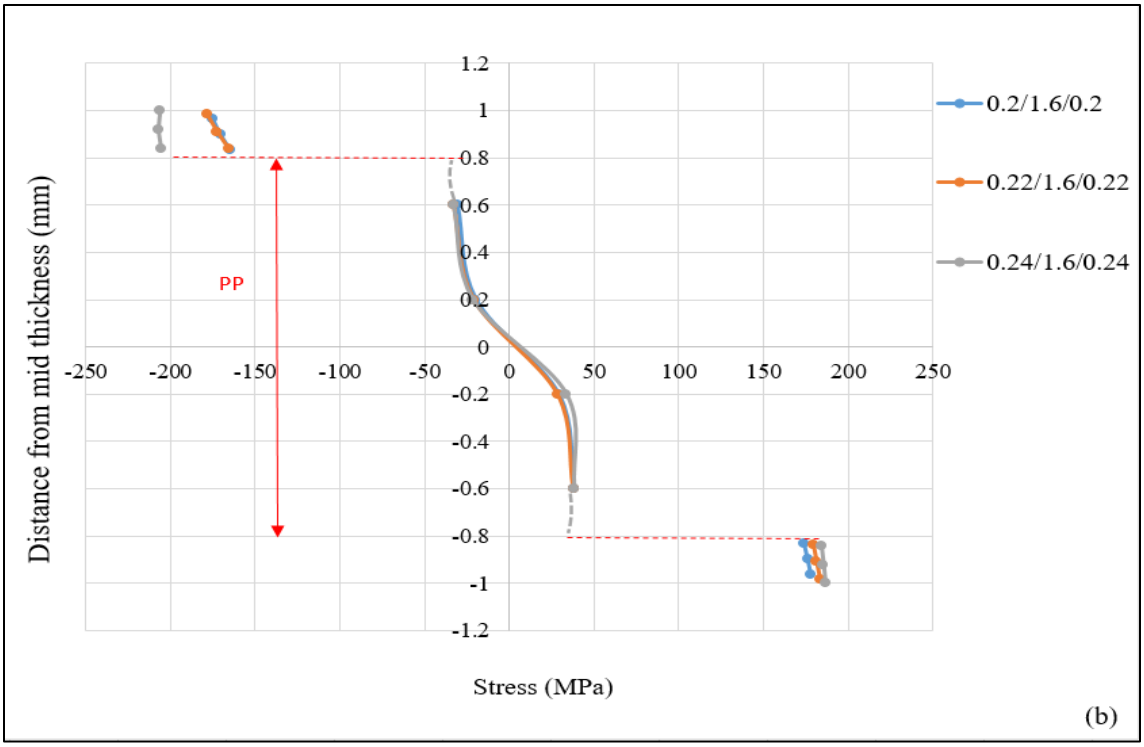

Figure 5.13: Through-thickness stress distribution at the punch corner at the end of forming in SA5182/PP/SA5182 laminates with (a) 0.8 mm core (b) 1.6 mm core

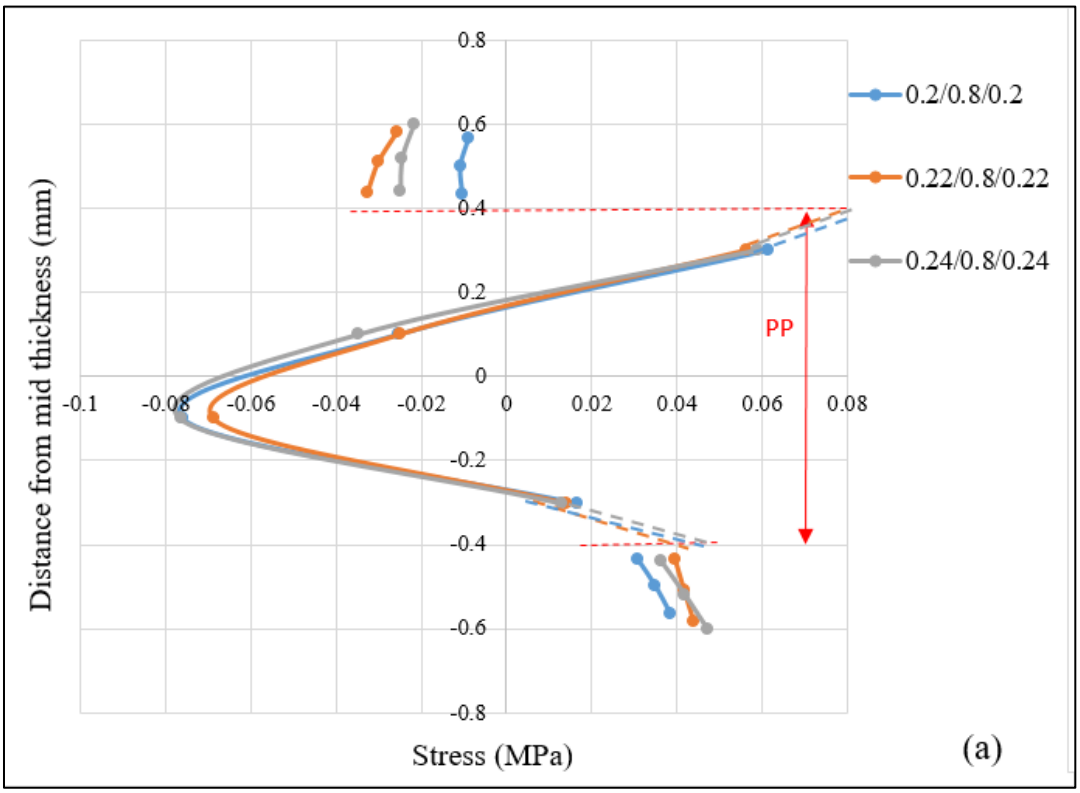

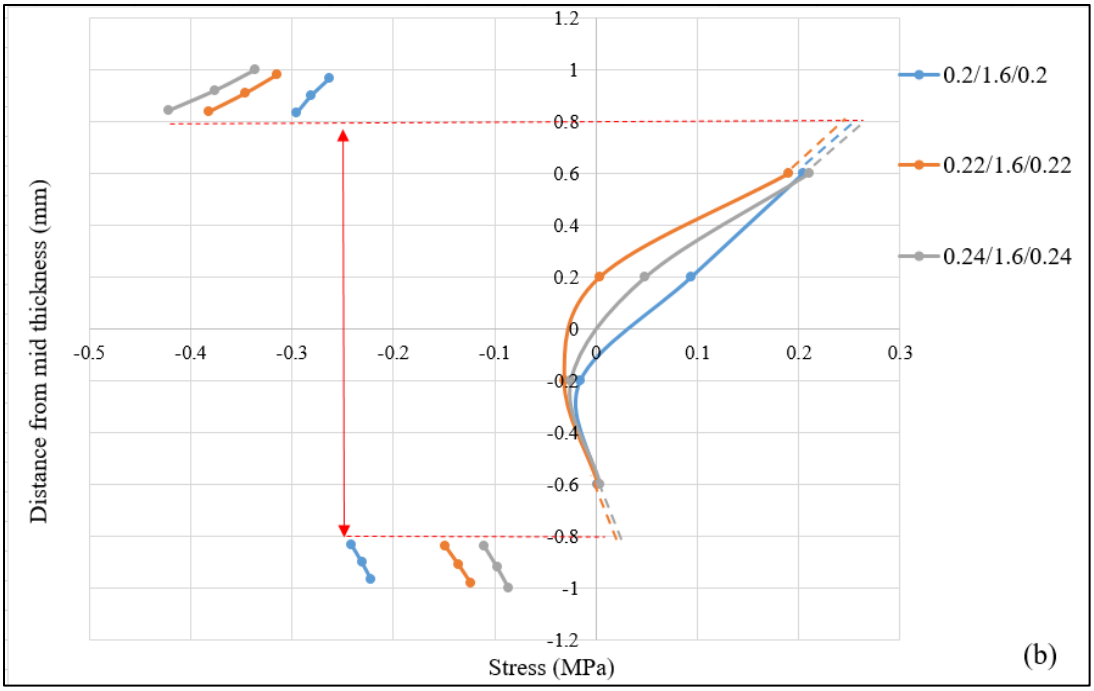

Figure 5.14 : Through-thickness stress distribution at the mid-length of the vertical wall at the end of forming in SA5182/PP/SA5182 laminates with (a) 0.8 mm core (b) 1.6 mm core

Table 5.4: Stresses in SA5182/PP/SA5182 laminates at the end of U-channel forming

Location		**Core thickness = 0.8 mm**			**Core thickness = 1.6 mm**		
		Skin thickness (mm)			**Skin thickness (mm)**		
		0.20	**0.22**	**0.24**	**0.20**	**0.22**	**0.24**
Die corner	Al - Upper skin	235.11	273.71	275.67	280.34	311.73	312.82
	PP – Top surface	41.982	51.11	50.83	60.24	62.189	60.48
	PP – Bottom surface	-33.59	-43.56	-43.63	-58.34	-59.77	-58.6
	Al - Lower skin	-219	-258.24	-261.34	-254.7	-287.44	-305.98
Punch corner	Al - Upper skin	-112.35	-122.52	-123.35	-174.98	-178.37	-205.86
	PP – Top surface	-31.46	-31.755	-31.67	-30.78	-32.714	-32.79
	PP – Bottom surface	32.18	32.163	31.98	38.167	37.94	38.285
	Al - Lower skin	151.408	159.12	160.82	178.19	183.38	186.7

Mid-length of vertical wall	Al - Upper skin	-0.009	-0.026	-0.022	-0.263	-0.314	-0.336
	PP – Top surface	0.061	0.056	0.059	0.204	0.190	0.211
	PP – Bottom surface	0.016	0.014	0.013	0.0016	0.003	0.004
	Al - Lower skin	0.038	0.044	0.047	-0.222	-0.124	-0.086

The evolution of forming stresses in each layer of the 0.2/0.8/0.2 mm sandwich laminate with increasing punch displacement is shown in Figure 5.15. The material in the upper skin at the die corner and the mid-length of the wall experiences tensile stresses, while the material at the punch corner is in compression (Figure 5.15 (a)). The stresses in the core layer are relatively small at all locations in the U-channel (Figure 5.15 (b)). The stresses in the lower aluminum skin show that the material passing over the die corner and the wall region is in compression while the material in the punch corner is in tension (Figure 5.15 (c)). At the die corner, the stresses in both upper and lower skins remain low until about 56 mm punch displacement, and then they start to increase to higher than the yield strength of SA5182. At the punch corner, the stresses in both upper and lower skins increase in the first 16 mm of displacement, reach a peak, and then reduces to a near constant value for the remaining punch displacement. The peak stress in the lower skin is slightly lower than the yield strength of SA5182. In the mid-length of the wall, the stresses are low for much of the punch displacement except at 36 mm when they peak in upper, lower and mid-layers. The U-channel shapes corresponding to 16, 36, 56, and 70-mm punch displacements can be seen in Figure 5.16.

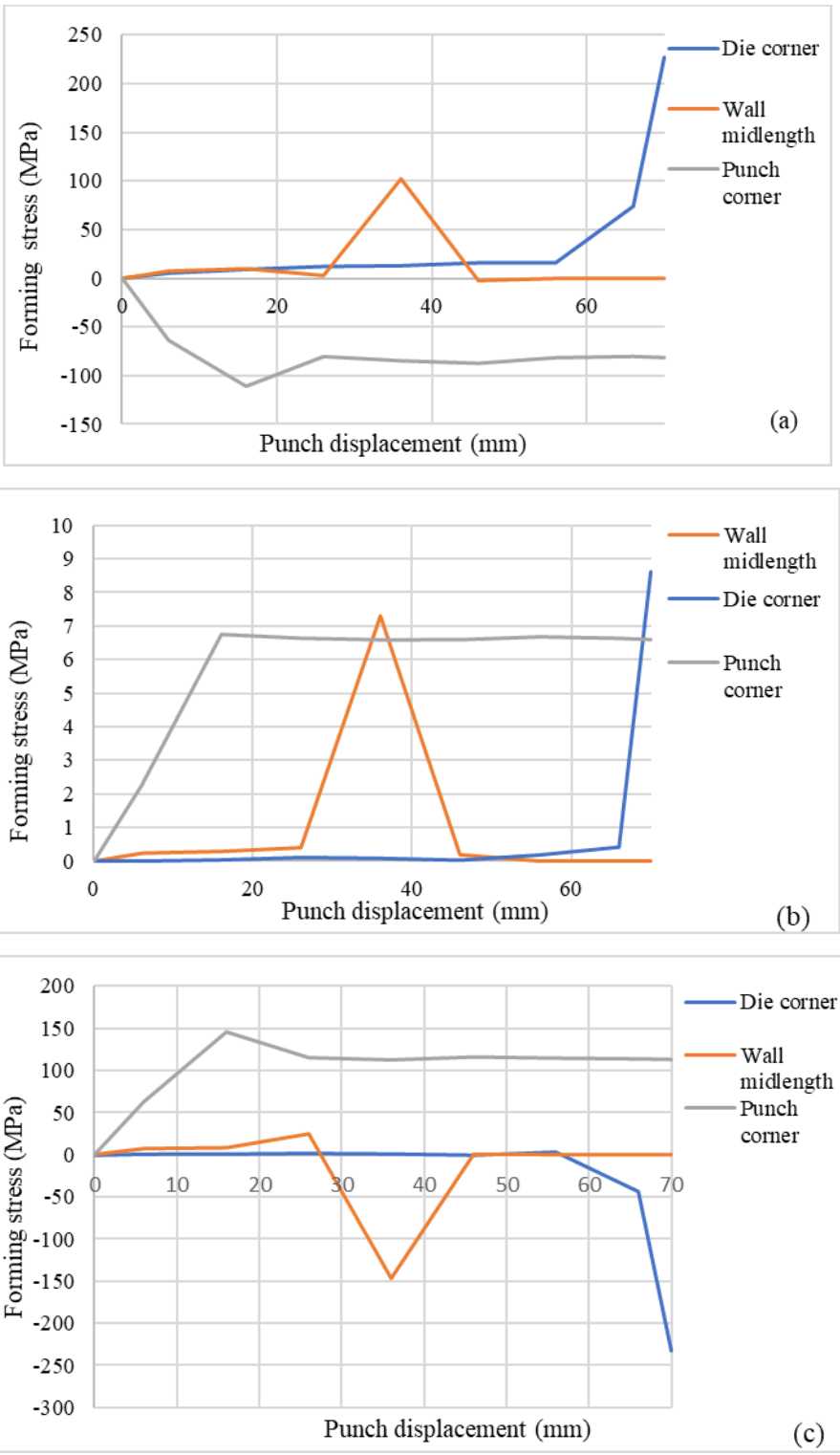

Figure 5.15: Evolution of forming stresses with increasing punch displacement - a) Upper aluminum skin (b) Polypropylene core, and (c) Lower aluminum skin

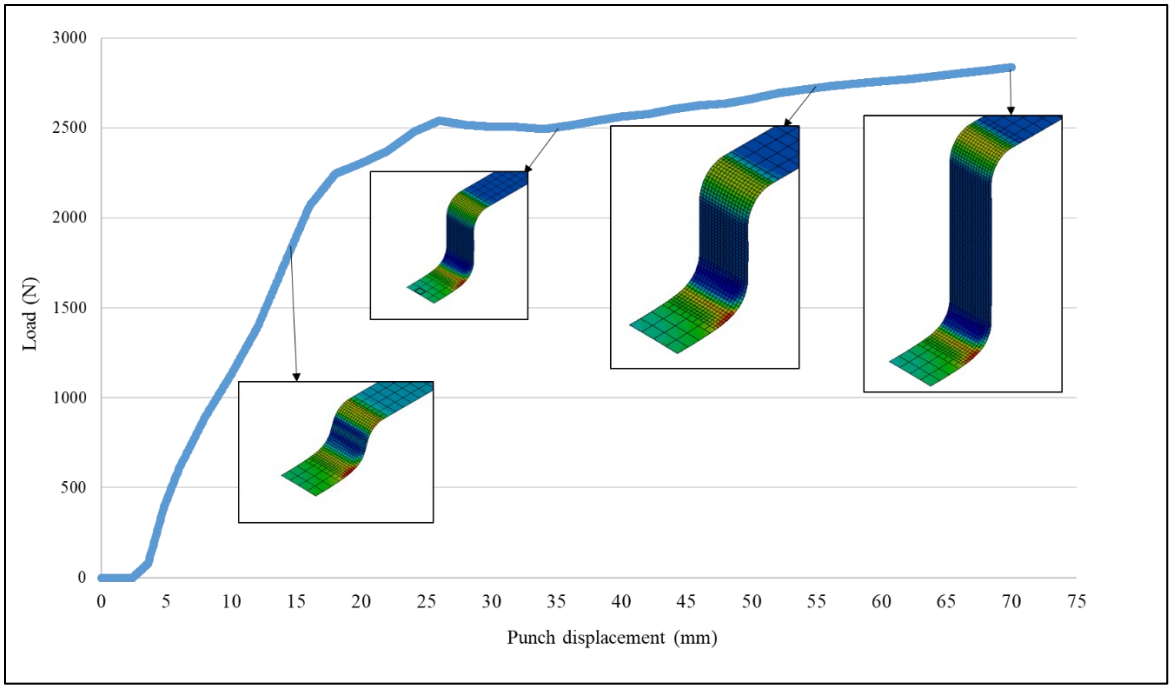

Figure 5.16: Shapes of the U-channel corresponding to 16 mm, 36 mm, 56 mm and 70 mm punch displacement

5.4.2 Residual stresses after springback

The residual stresses in SA5182/PP/SA5182 laminates are studied in this section. The residual stresses (at the end of springback) at the same integration points as in Figures 5.12- 5.14 are recorded and compared for different thicknesses at the die and punch corner and also at the mid-length of the vertical wall. At the die corner, the upper aluminum skin is in compression while for the lower aluminum skin, a portion of the aluminum is in compression and the rest in tension. The residual stresses in the polypropylene layer with 0.2 mm skin thickness are lower than the stresses in the polypropylene layer with 0.22 mm and 0.24 mm skins for the 0.8 mm core sandwich laminates. However, for the laminates with 1.6 mm core thickness, the stresses in the polypropylene layer are identical. The residual stresses in the aluminum skins are almost identical since the difference in their thicknesses is only 0.02 mm.

Another point to note is that the relaxation of the stresses in the polypropylene layer are controlled by the aluminum skins. Although major portion of the polymer core at the end of forming is in plastic stress state, with the stress relaxation in the aluminum skins, polypropylene also shows small amount of stress relaxation. Therefore, the stresses after forming and springback in the polypropylene layer are very close (Tables 5.3 and 5.4).

The residual stresses at the punch corner for the sandwich laminate (Figure 5.17) show that the upper aluminum skin is mainly in tension and the lower aluminum skin is mainly in compression. For the 1.2 mm thick laminates, the stresses in the polypropylene layer for the 0.2 mm aluminum skins are slightly lower than those of the 0.22 mm and 0.24 mm aluminum skins.

At the mid-length of the vertical wall, the distribution of residual stresses (Figure 5.19) shows that the stresses for both 0.8 mm and 1.6 mm core are quite low. The bottom skins are all in compression irrespective of core and skin thicknesses. However, the upper aluminum skins are in compression for the 0.8 mm core sandwich laminates and in tension for the 1.6 mm core sandwich laminates.

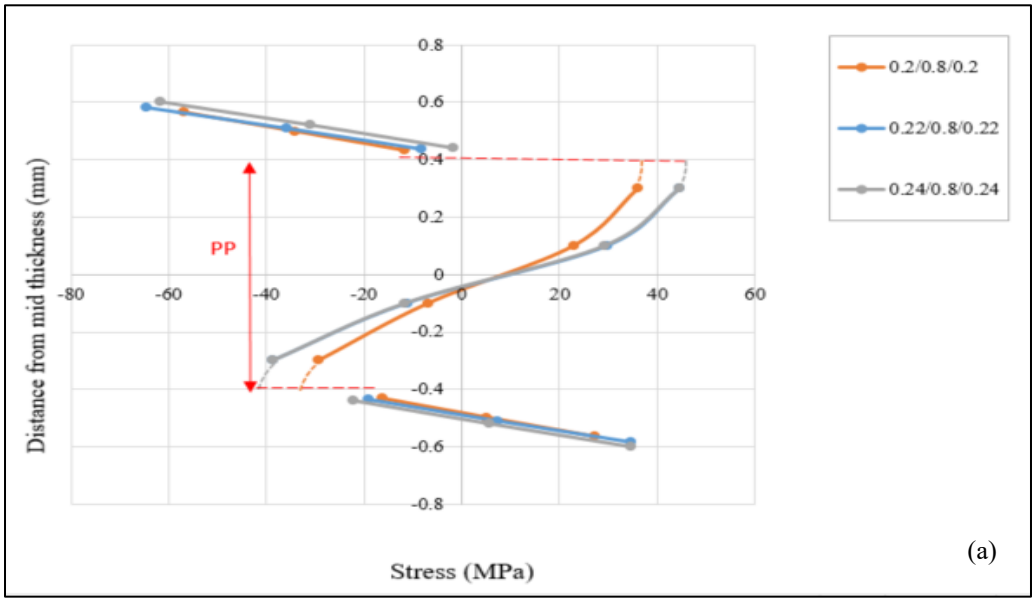

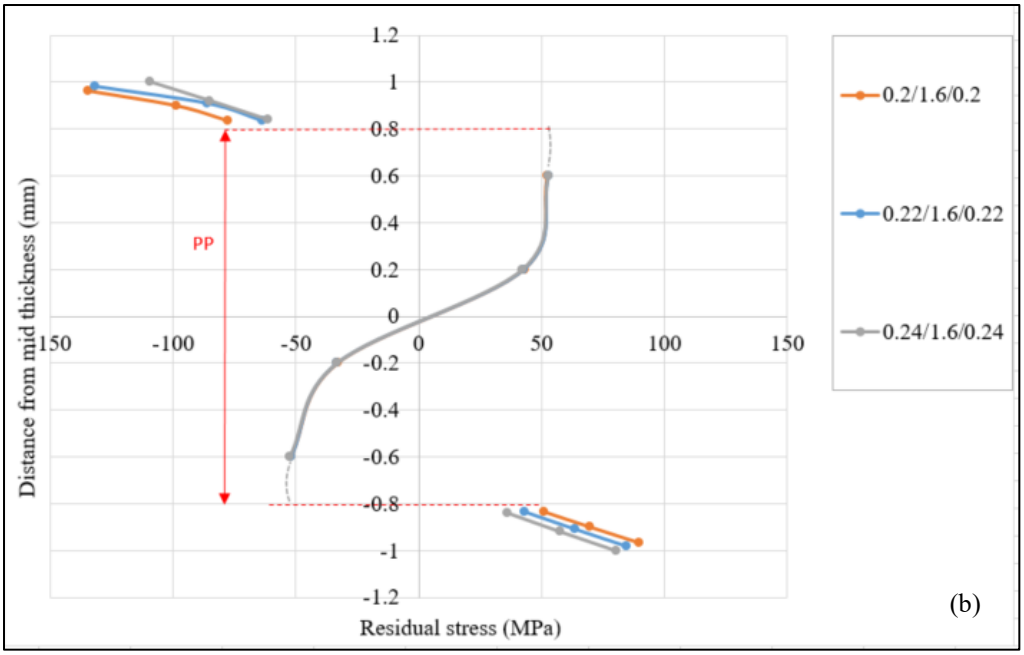

Figure 5.17: Through-thickness residual stress distribution in SA5182/PP/SA5182 at the die corner with (a) 0.8 mm core thickness (b) 1.6 mm core thickness

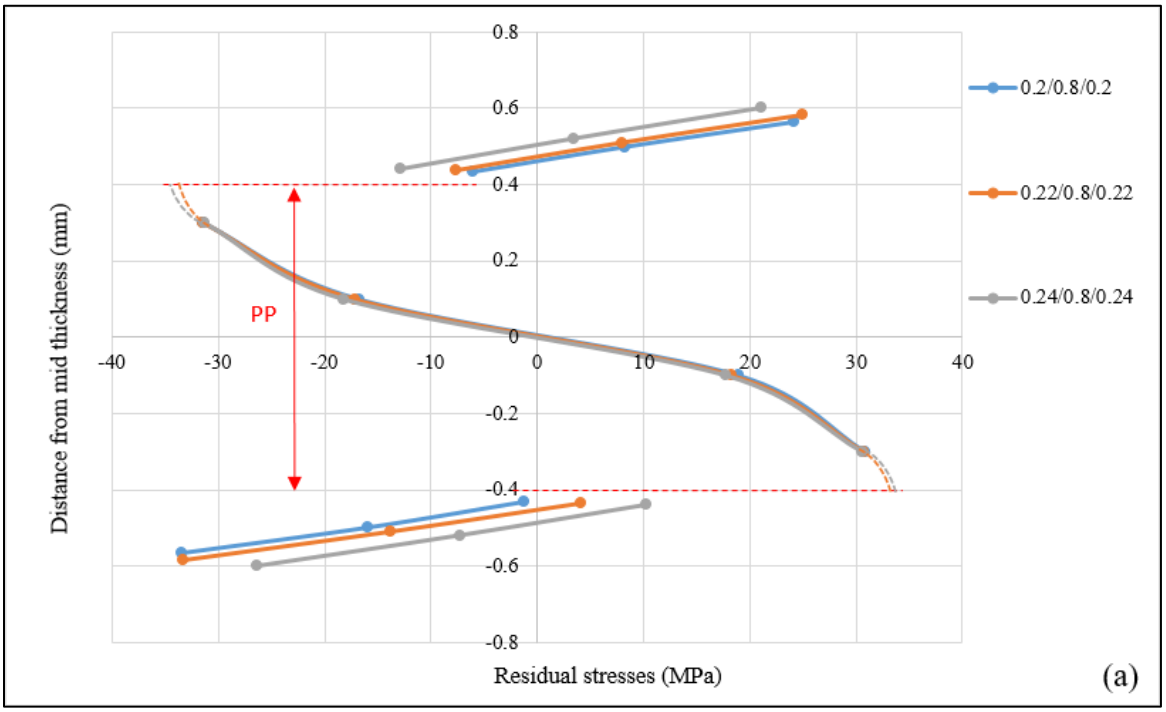

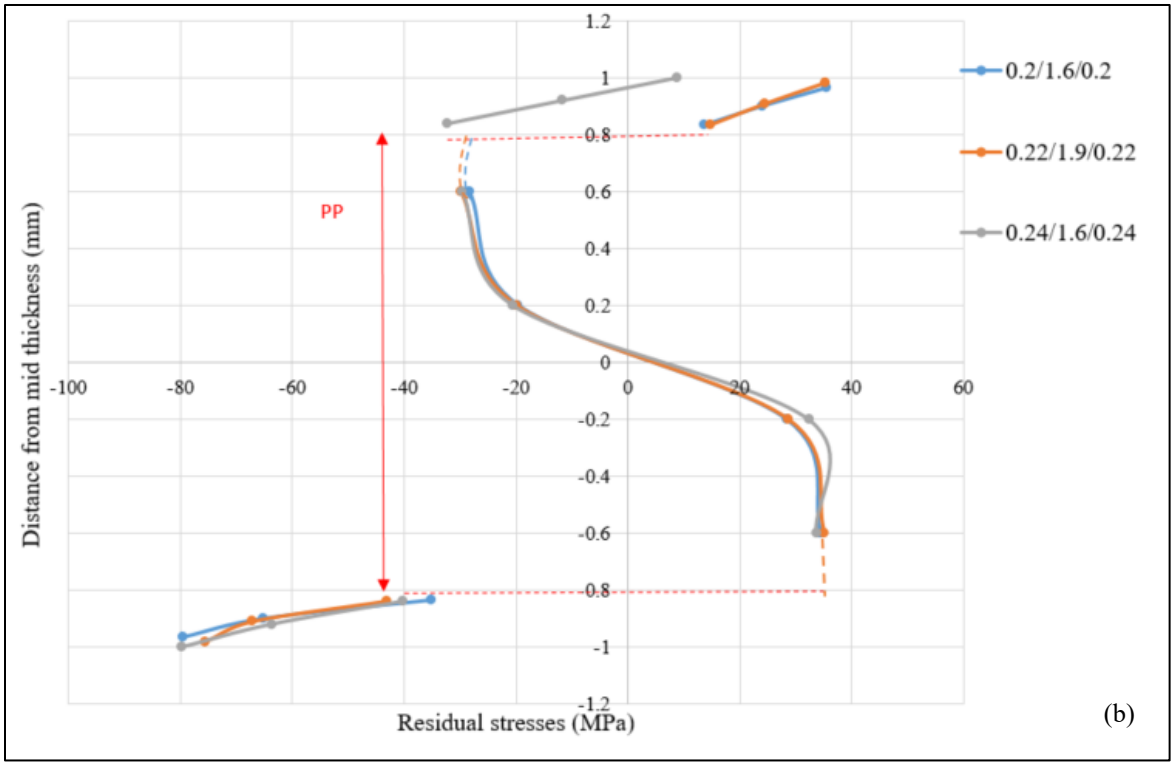

Figure 5.18: Through-thickness residual stress distribution in SA5182/PP/SA5182 laminates at the punch corner with (a) 0.8 mm core thickness (b) 1.6 mm core thickness

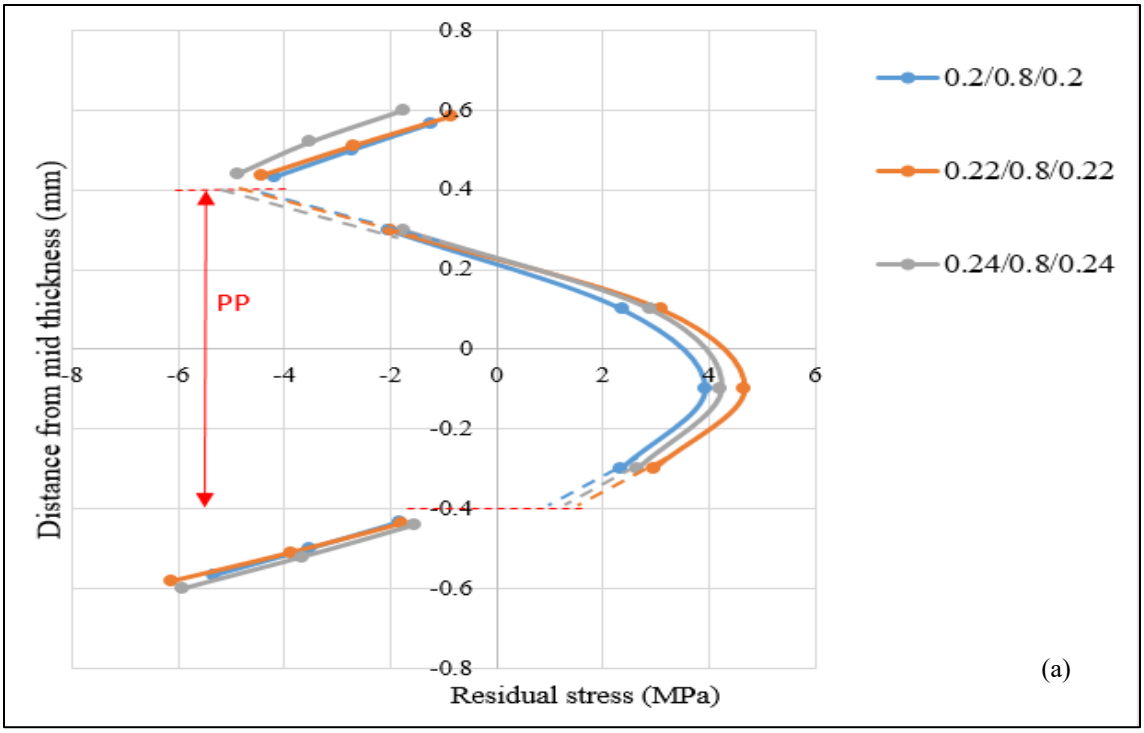

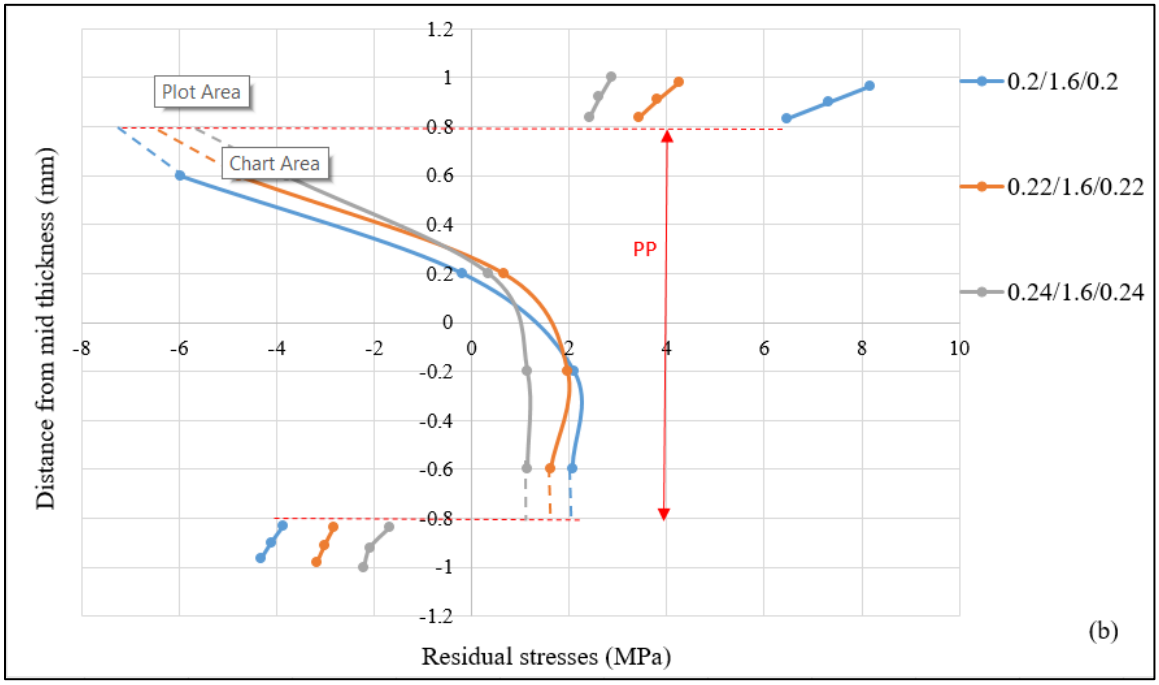

Figure 5.19: Through-thickness residual stress distribution in SA5182/PP/SA5182 laminates at the mid-length of the vertical wall with (a) 0.8 mm core thickness (b) 1.6 mm core thickness

Table 5.5: Residual stresses in SA5182/PP/SA5182 laminates at the end of springback

Location		Core thickness = 0.8 mm			Core thickness = 1.6 mm		
		Skin thickness (mm)			Skin thickness (mm)		
		0.20	0.22	0.24	0.20	0.22	0.24
Die corner	Al - Upper skin	-56.88	-64.591	-61.619	-134.3	-131.73	-109.39
	PP – Top surface	36.17	44.604	44.542	52.53	52.845	52.831
	PP – Bottom surface	-29.30	-38.61	-38.74	-51.82	-52.845	-52.26
	Al - Lower skin	27.356	34.526	34.774	89.79	84.826	80.55
Punch corner	Al - Upper skin	24.226	24.95	21.032	35.55	35.29	8.901
	PP – Top surface	-31.368	-31.369	-31.354	-28.38	-29.9	-29.517
	PP – Bottom surface	30.88	30.68	30.59	34.511	35.126	33.696
	Al - Lower skin	-33.45	-33.287	-26.29	-79.45	-75.794	-79.7
Mid-length of vertical wall	Al - Upper skin	-1.226	-0.851	-1.748	8.166	4.246	2.865
	PP – Top surface	-2.048	-1.982	-1.769	-5.96	-4.755	-3.788
	PP – Bottom surface	2.344	2.976	2.64	2.066	1.622	1.139
	Al - Lower skin	-5.322	-6.13	-5.90	-4.30	-3.177	-2.1995

The stress plots showing the distribution of stresses over the entire the U-channel for the upper and lower aluminum skins are shown in Figures 5.20 and 5.21. At the die corner for the upper aluminum skin, it is seen that the stresses are maximum and tensile in nature and change to compressive stresses with the bending of the wall and flange after springback. The opposite trend is noticed at the die corner of the lower aluminum skin.

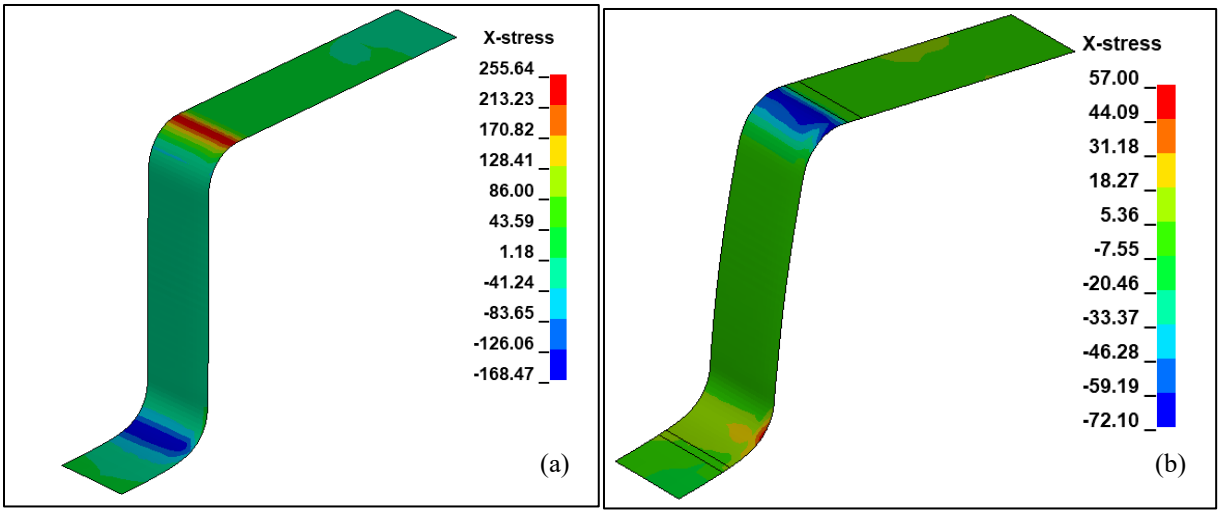

Figure 5.20: Stress plots in the upper aluminum skin (a) End of forming (b) After springback for 0.2/0.8/0.2 mm sandwich laminate

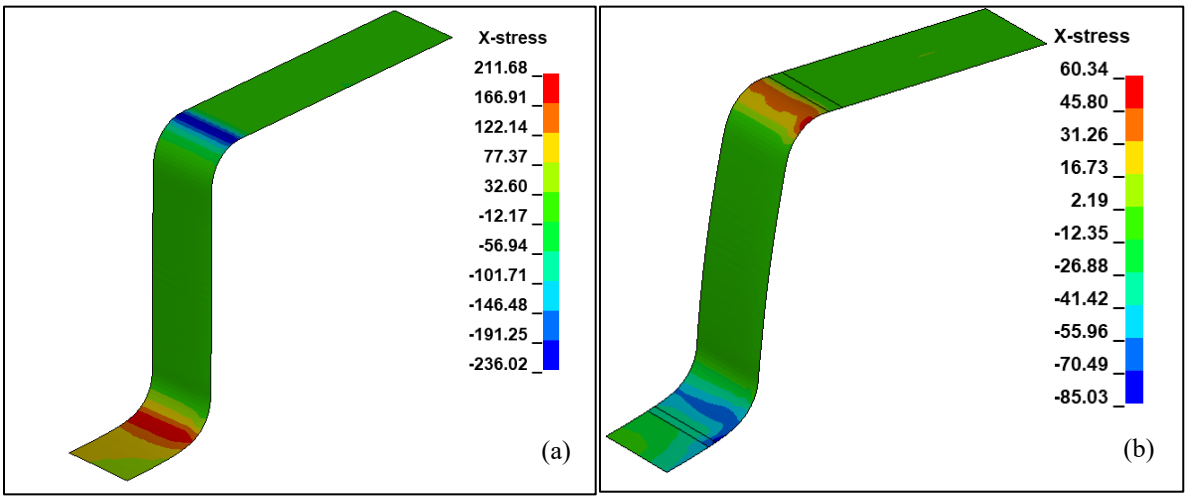

Figure 5.21: Stress plots in the lower aluminum skin (a) End of forming (b) After springback for 0.2/0.8/0.2 mm sandwich laminate

5.4.3 Effect of die and punch radii on forming and residual stresses

The distribution of through-thickness stresses at the end of forming for different die corner radii and at a constant punch corner radius of 8 mm are compared in Figure 5.22. It is observed that the stresses in the aluminum skins show no significant difference at the die corner but show a significant difference at the punch corner. The maximum forming stress at the punch corner

increases with decreasing die corner radius. After springback, the residual stresses in the polypropylene layer at the punch corner decrease with increasing die radius (Figure 5.). The residual stresses at the die corner do not show much variation.

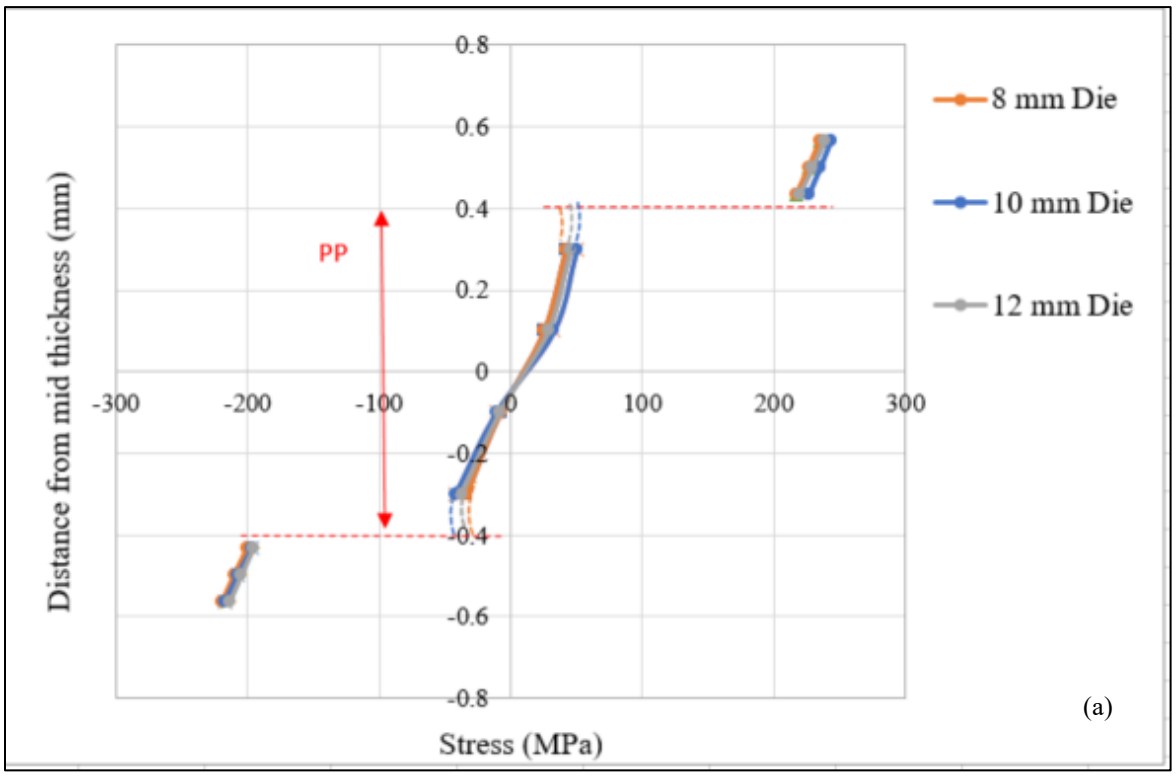

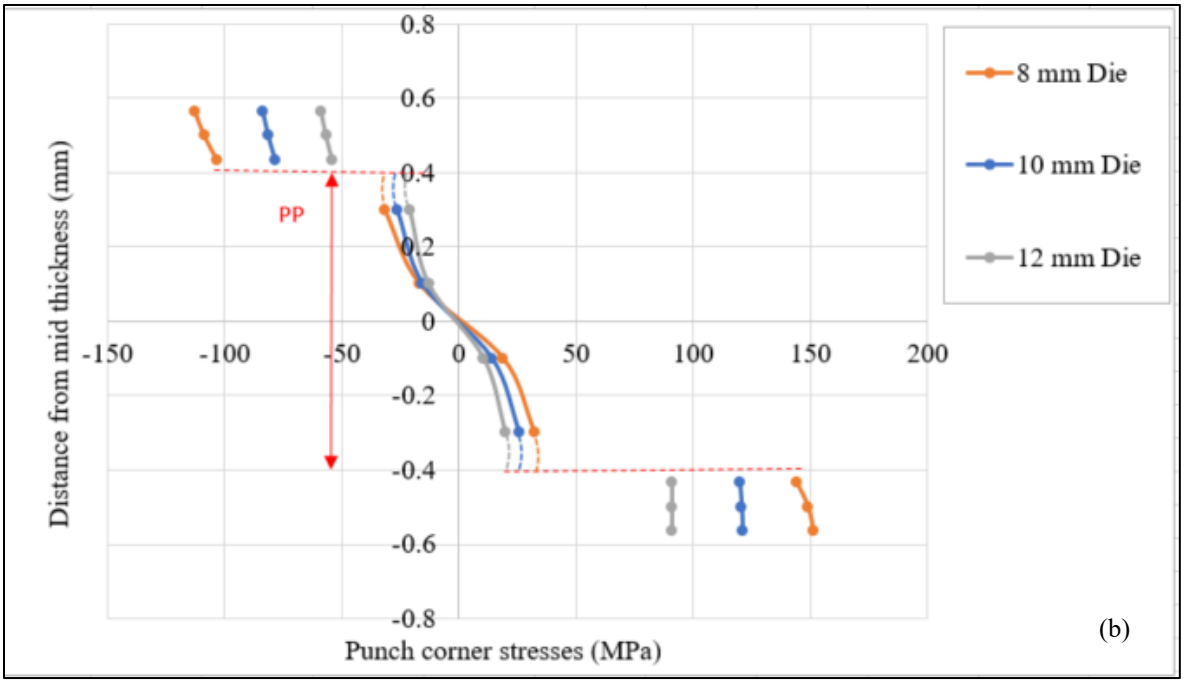

Figure 5.22: Stress distributions at the end of forming for different die corner radii and constant punch radius of 8 mm for 0.2/0.8/0.2 mm laminate at (a) Die corner (b) Punch corner

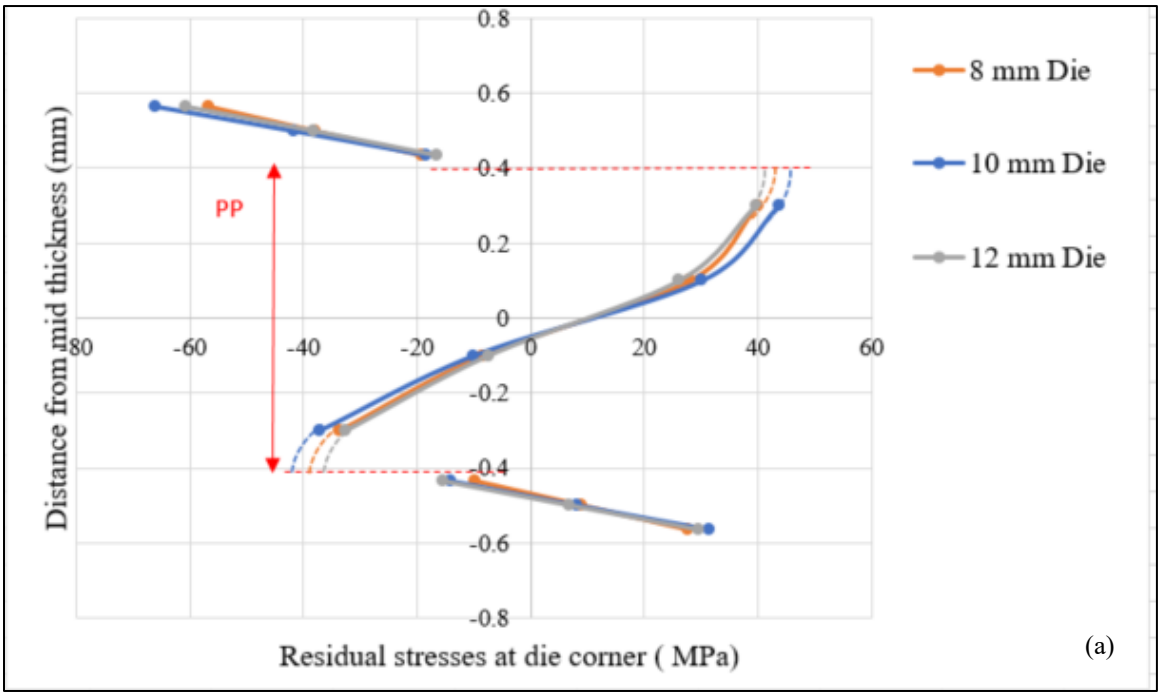

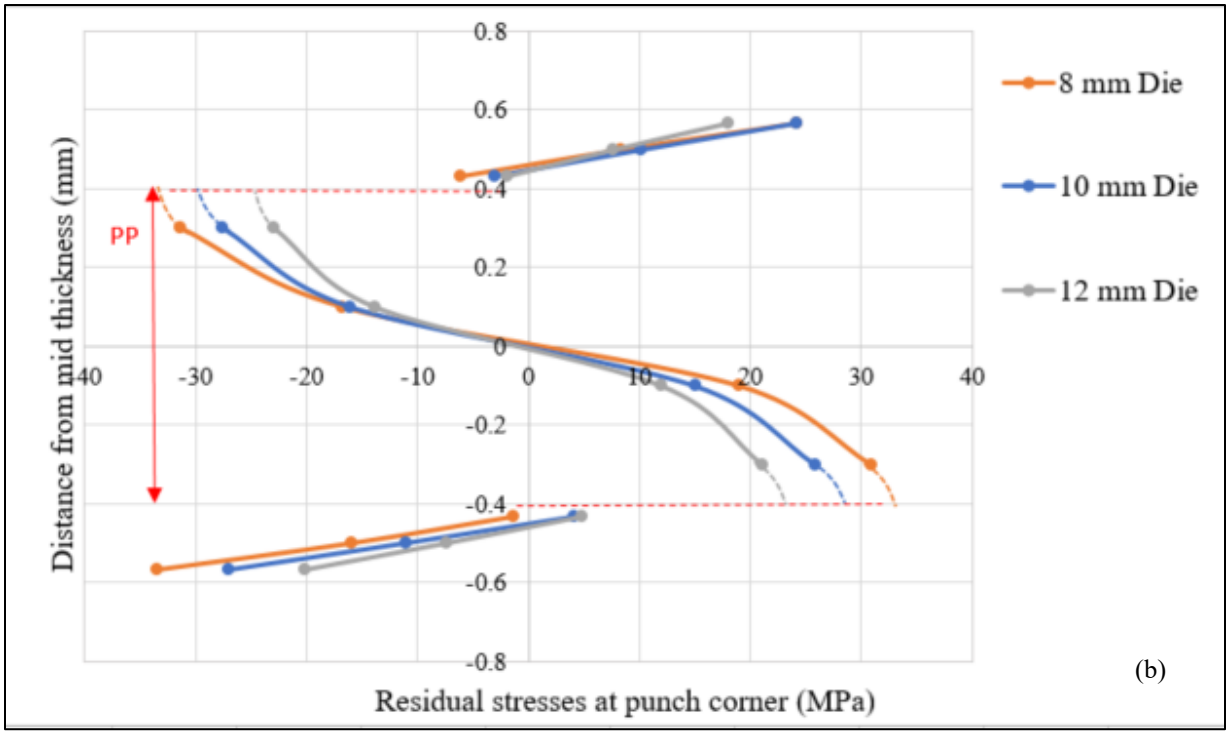

Figure 5.23: Residual stress distributions after springback for different die corner radii and a constant punch radius of 8 mm for 0.2/0.8/0.2 mm laminate at (a) Die corner and (b) Punch corner

Similarly, the through-thickness stress distribution for sandwich laminates with varying punch radius is plotted in Figure 5.24. The stresses at the end of forming are lower at the punch corner in comparison to the stresses at the die corner. As the die radius is maintained at a constant value of 8 mm, the main variation in the residual stresses is observed in the lower aluminum skin at the punch corner causing the differences in springback (Figure 5.25).

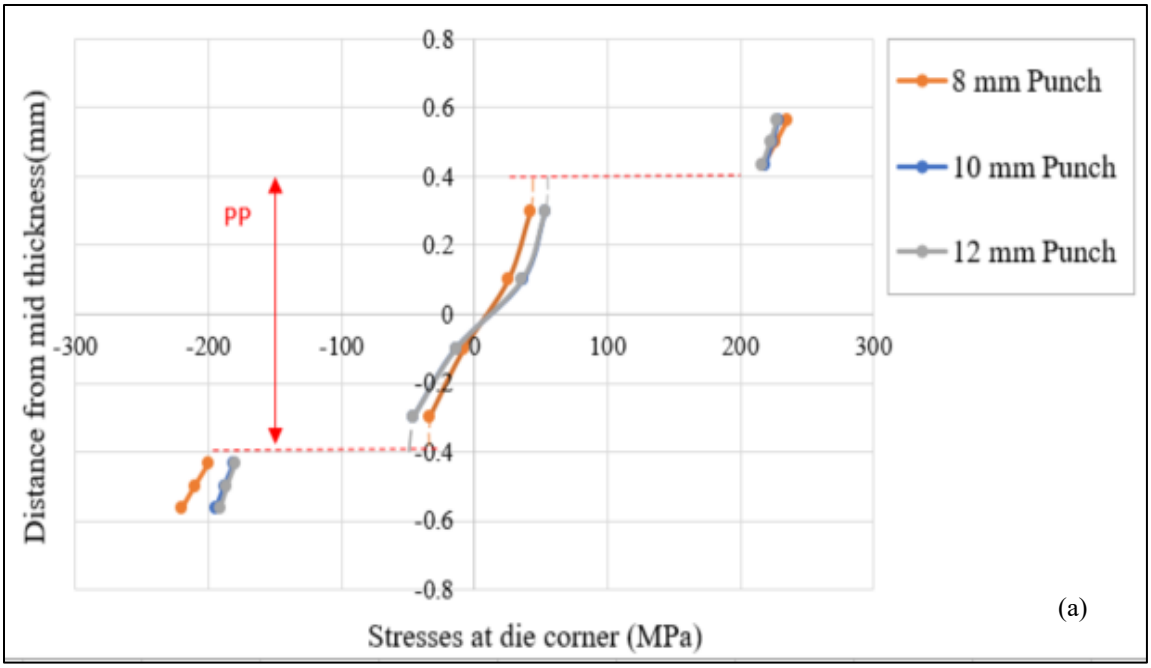

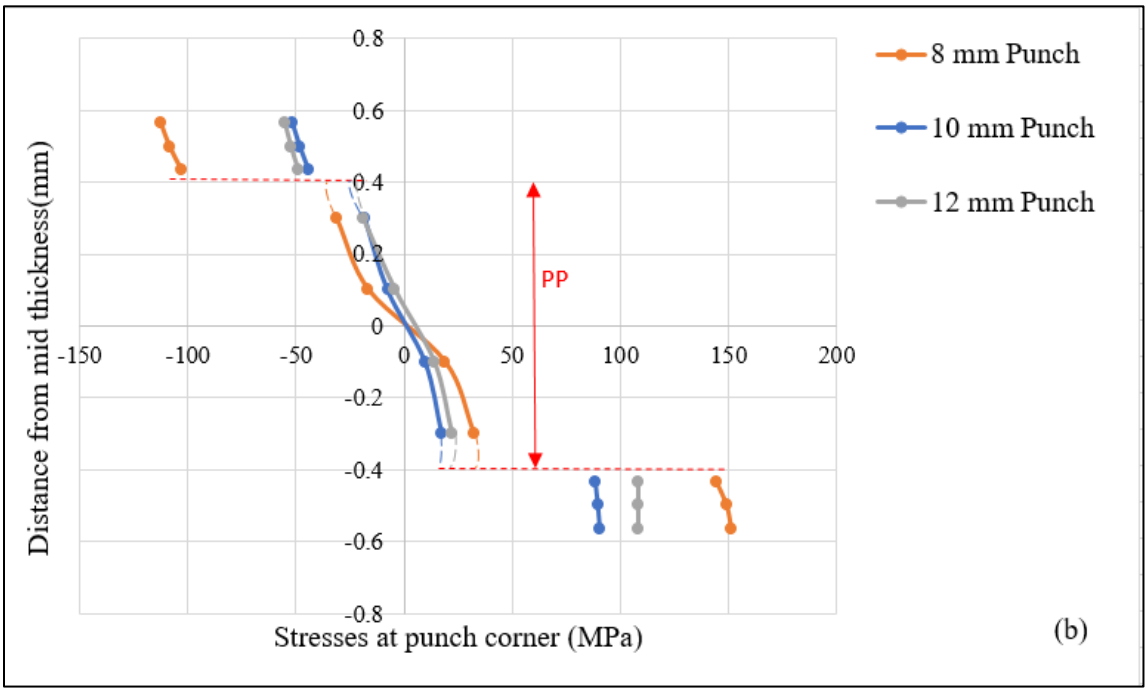

Figure 5.24: Stress distributions at the end of forming for different punch radii and a constant die radius of 8 mm for 0.2/0.8/0.2 mm laminate at (a) Die corner and (b) Punch corner

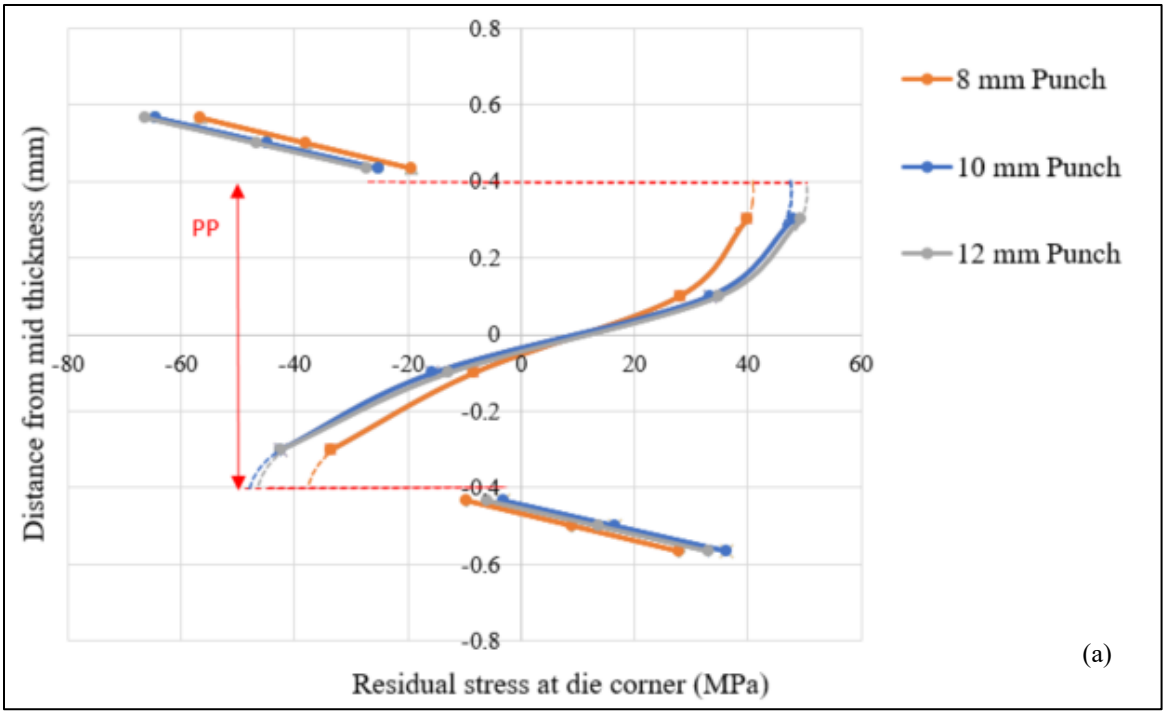

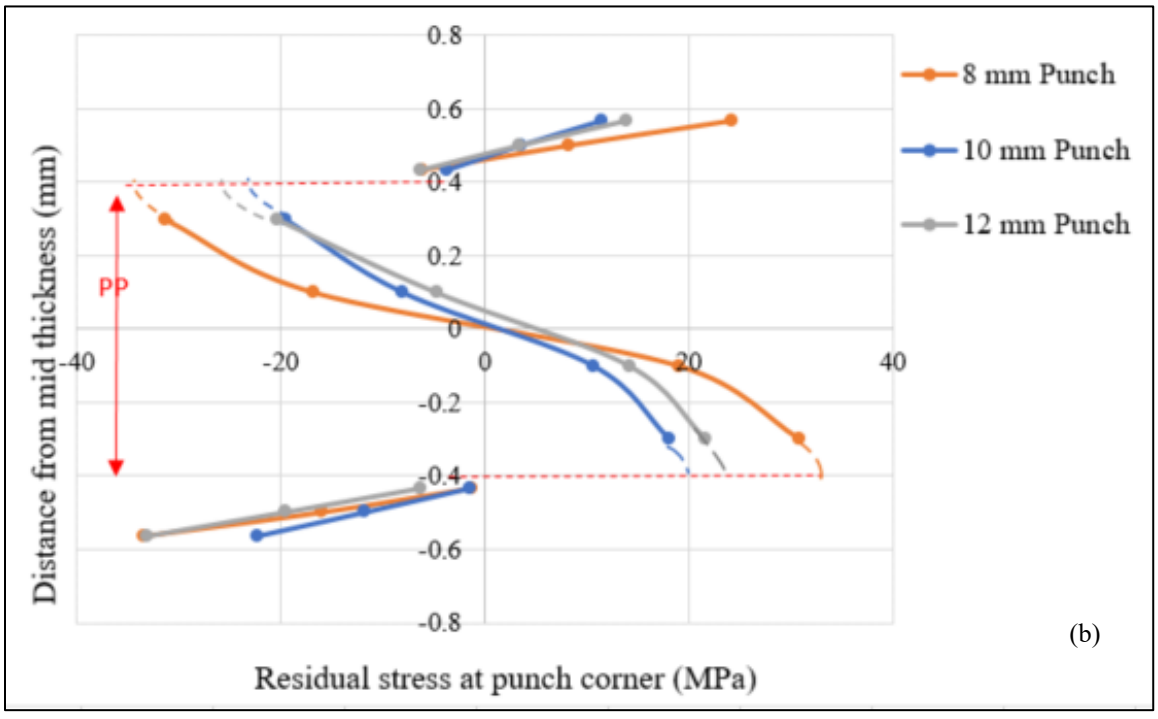

Figure 5.25: Residual stress distributions after springback for different punch radii and a constant die radius of 8 mm for 0.2/0.8/0.2 mm laminate at (a) Die corner (b) Punch corner

5.4.4 Comparison of stresses in single aluminum and sandwich laminate sheets

In Figure 5.26, the forming stress distributions through the thickness of the sheet are compared for single aluminum sheet and sandwich laminate of equivalent thickness. The single aluminum sheet is 1.2 mm thick, while the sandwich has a configuration of 0.2/0.8/0.2 mm (total thickness of 1.2 mm). This figure shows that during forming, the plastic zone in the single aluminum sheet has extended to approximately 0.45 mm from each surface and the rest of the cross-section is in elastic condition. For the sandwich laminate, the aluminum skins show stresses higher than the yield strength of SA5182 at the die corner for all three integration points at the end of forming, indicating that both aluminum skins are in plastic zone. However, at the punch corner, the forming stresses in the aluminum skins of the sandwich laminate are lower than the stresses in the single aluminum sheet and the upper aluminum skin have not completely yielded.

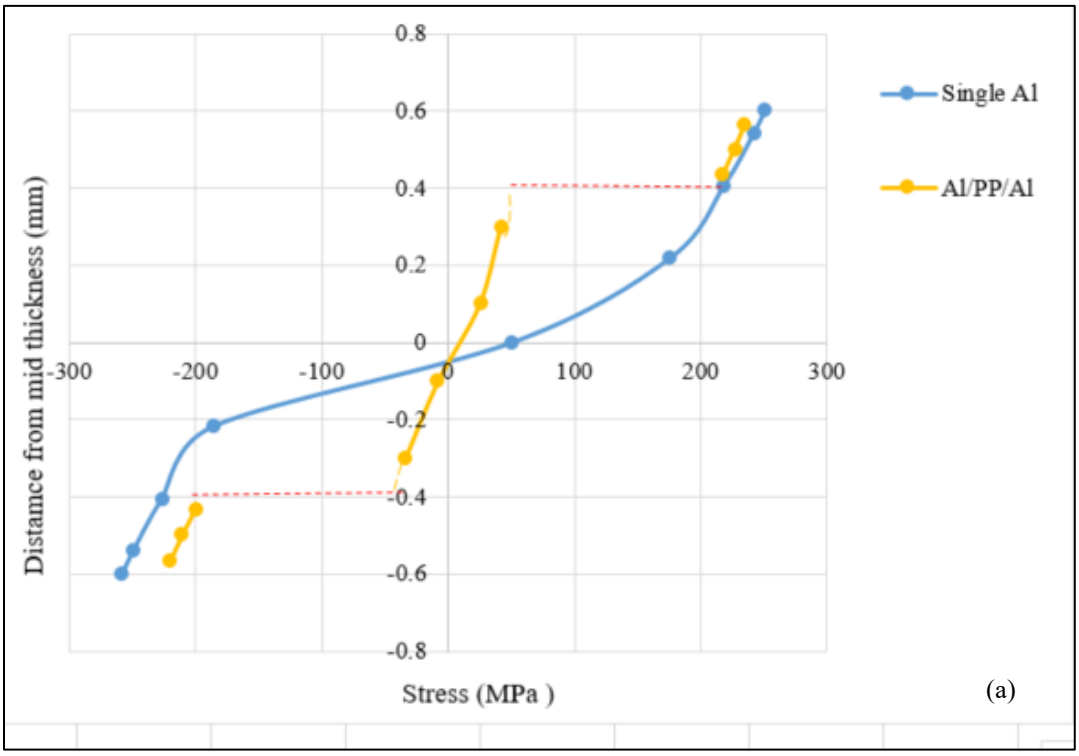

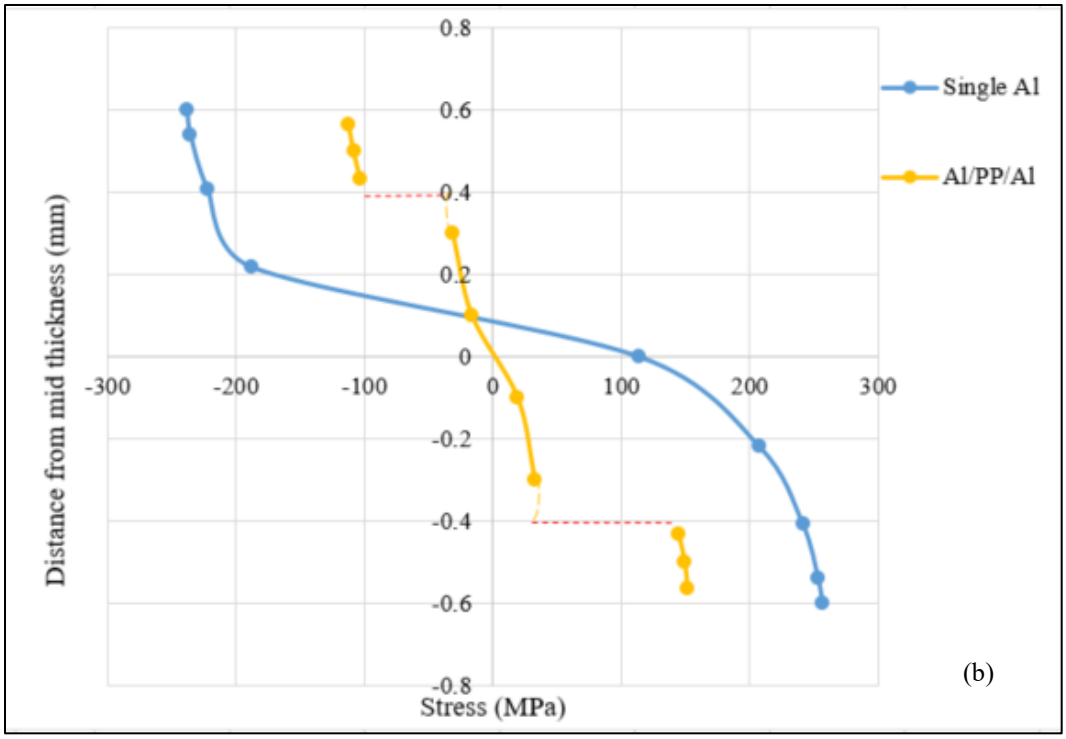

Figure 5.26: Stress distributions at the end of forming - single SA5182 (1.2 mm) vs SA5182/PP/SA5182 sandwich laminate (0.2/0.8/0.2 mm at (a) Die corner (b) Punch corner

The residual stresses at the end of springback of the U-channel for the single aluminum sheet and the sandwich laminate are compared in Figure 5.27. The maximum residual stresses in the single aluminum sheet are much higher in comparison to the maximum residual stresses in the sandwich laminate. The mid-layer stress at the end of springback is also higher in the single aluminum sheet. It can be seen that the neutral or zero stress layer at the die corner for the single aluminum sheet and the laminate are almost coincident Figure 5.27 (a). However, this is not the case at the punch corner. The neutral axis at the punch corner for the single aluminum sheet is closer to the upper surface while it is close to the mid-thickness for the sandwich laminate.

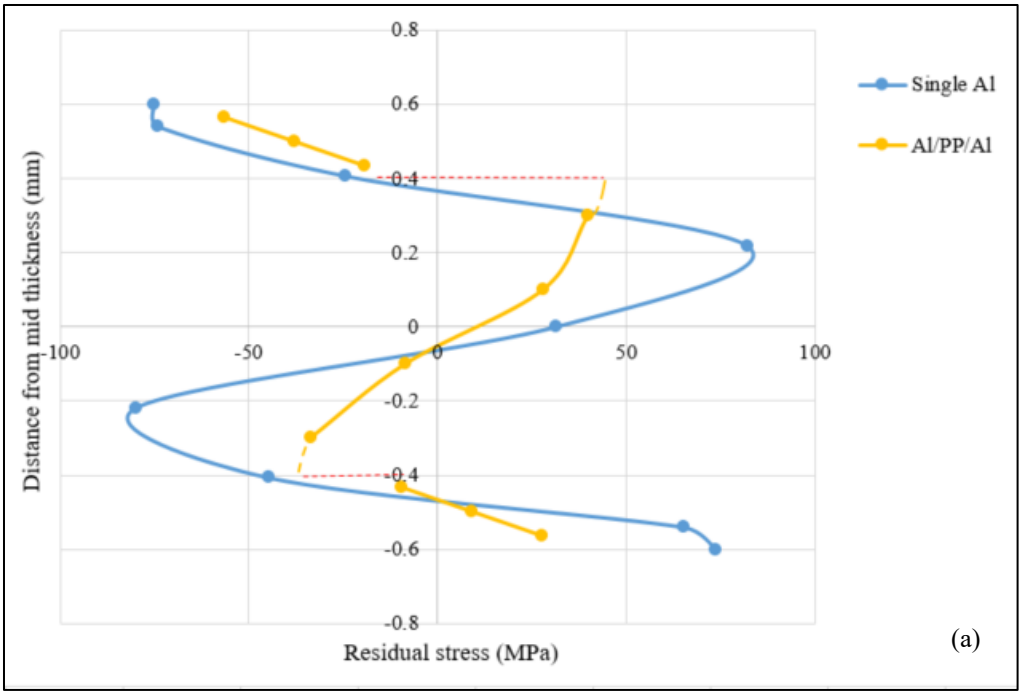

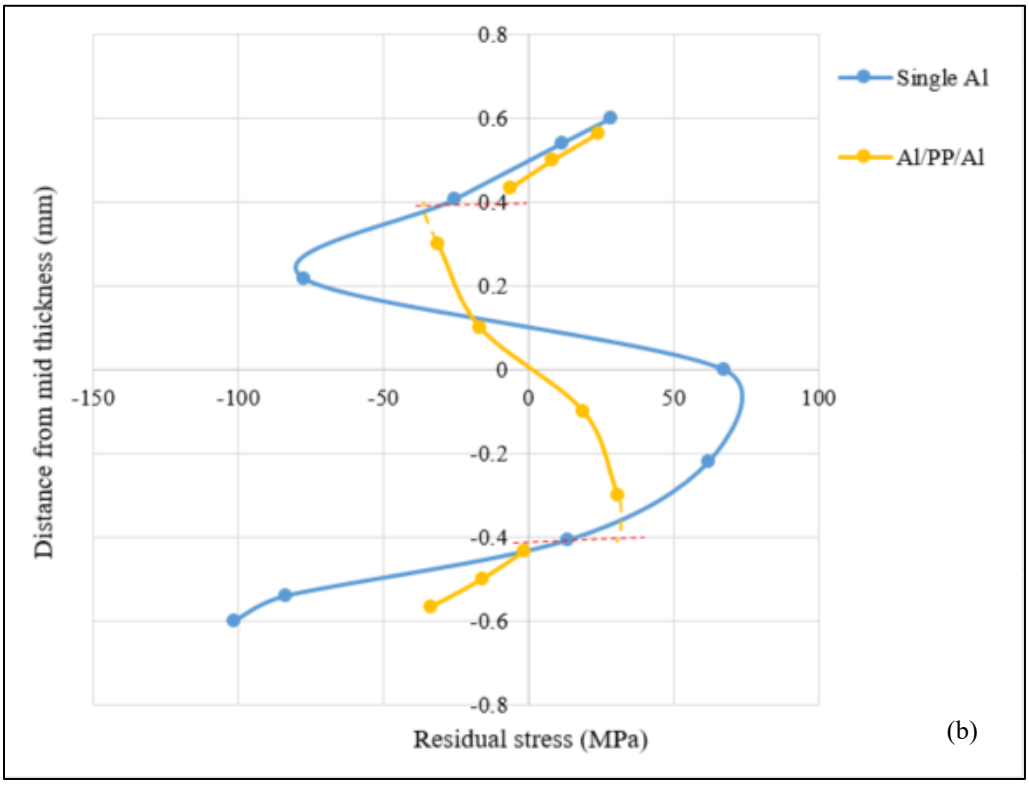

Figure 5.27: Residual stress distributions after springback – SA5182 (1.2 mm) vs. SA5182/PP/SA5182 sandwich laminate (0.2/0.8/0.2 mm) at (a) Die corner (b) Punch corner

5. 5 CONCLUSIONS

The stress distribution through the thickness of the U-channel is studied at different locations at the end of the forming and after springback. The residual stresses in the formed part after elastic recovery (springback) are critical to the performance of the formed final part and estimation of the nature of these stresses is important. In case of pure bending, the neutral axis coincides with the mid surface of the plate subjected to the bending moment. When an additional axial tension is applied along with bending moment, the neutral or zero stress layer in the plate shifts towards the lower or upper surface. Therefore, the residual stresses in draw-bending conditions depend on the elastic recovery of the bending stresses as well as the elastic recovery of the axial stresses.

For single aluminum AA5182-O sheets, the forming and residual stresses are studied for two sets of punch and die radii. The stresses at the end of forming with 5 mm radii are in general higher than those with the 8 mm tool radii. The stresses at the mid length of the vertical wall are much smaller in magnitude compared to the stresses in the die and punch corner. At the die corner, the neutral axis moves toward the lower surface and the opposite occurs at the punch corner.

The residual stresses in the single aluminum sheets are opposite in nature to the stresses at the end of forming i.e., at the punch corner the upper surface is in compression at the end of forming but moves to the tension side after springback. At the die corner the residual stresses on the top surface are in compression while the residual stresses at the bottom surface are in tension. The stresses at the mid surface of the die corner, decrease with increasing thickness and at the punch corner, they increase with increasing thickness. The residual stresses for the 8 mm die and punch radii are mostly higher than the residual stresses for the 5 mm die and punch radii at the top and bottom surfaces. The residual stresses at the mid surface do not exhibit any particular trend with varying die and punch radii.

For the aluminum-polypropylene-aluminum laminates the stresses in the polypropylene layer are much lower than the stresses in the aluminum sheets. The polypropylene layers of equal thickness show small amount of variation in stresses with changing skin thickness.

For the laminate with constant punch radius and increasing die radius the stresses at the end of forming vary only at the punch corner and not the die corner. The major difference in residual stresses with varying die radius is observed in the polypropylene layer and the aluminum skins show nearly identical stresses. The same behavior is seen when the die radius is kept constant, and the punch radius is increased. It is concluded that the effect of die and punch radii on the stress distribution is mostly observed at the punch corner.

The stresses at the end of forming for the Al/PP/Al sandwich laminate are observed to be lower than the stresses in the single aluminum sheet. A larger difference is stresses between single aluminum and sandwich laminates is seen at the punch corner. The residual stresses in the sandwich laminate are lower than the residual stresses in the single aluminum sheet, a larger difference in residual stresses is noticed between lower aluminum skin and the lower surface of the single aluminum sheet.

5.6 REFERENCES

[1] C. T.Wang, "Mechanics of Bending, Flanging, and Deep Drawing and a Computer-Aided Modeling System for Predictions of Strain, Fracture, Wrinkling and Springback in Sheet Metal Forming," Phd Dissertation, Ohio State University, 1993.

[2] D. Rees, Mechanics of Solids and Structures : 2nd edition, Imperial College Press, 2016.

[3] Z. Tan, B. Li and B. Persson, "On analysis and measurement of residual stresses in the bending of sheet metals," *Internation Journal of Mechanical Siences ,* vol. 36, no. 5, pp. 483-491, 1994.

[4] A. Essa, M. Nasr and M. H. Ahmed, "Variation of the residual stresses and springback in sheet bending from plane-strain to plane-stress condition using finite element modelling," in *International Conference on Applied Mechanics and Mechanical Engineering At: Military Technical College*, Cairo , 2016.

[5] N. Simon, H. Erdle, S. Walzer, J. Gibmeier, T. Böhlke and M. Liewald, "Residual stresses in deep-drawn cups made of duplex stainless steel X2CrNiN23-4," *Forschung im Ingenieurwesen,* vol. 85, no. 3, pp. 795-806, 2021.

Chapter 6 - Conclusions

6.1 Summary and Conclusions

Forming and springback behaviors of aluminum-polypropylene-aluminum sandwich laminates are studied in this dissertation. Such laminates are being considered in many automotive applications because of their weight reduction capabilities and high specific modulus. Among the various types of sandwich laminates available, this research focuses on three-layered symmetric laminates of AA5182 aluminum skins and a polypropylene core. Two types of aluminum AA5182 skins, soft or annealed and hard or cold worked, are studied.

The forming behaviors of monolithic Al sheets, Al/Al laminates and Al/PP/Al laminates are characterized by their forming limit curves (FLCs) determined by numerically modeling the Nakazima formability tests in a commercial finite element software (LS-DYNA). For the Al/Al and Al/PP/Al laminates, the FLC obtained using the upper aluminum layer is considered as the FLC of the entire laminate since it gives a more conservative FLC than the lower aluminum skin, specifically on the tension-tension side of the forming limit diagram. In comparing a single aluminum sheet (0.22 mm), the Al/Al (0.22/0.22 mm) laminate and the Al/PP/Al (0.22/0.8/0.22 mm) laminate, the highest limit strain in the plane strain condition (FLC_0) is obtained for the Al/Al laminate. Between the single aluminum sheets and the sandwich laminates, small improvements in FLC_0 are observed for the soft skin aluminum sandwiches. For a constant core thickness, small improvements in all limit strains are seen when increasing the skin thicknesses in the order of 0.02 mm. Keeping the skins at a constant thickness and doubling the core thickness of the sandwich

showed large improvements in limit strains on the tension-tension side of the FLC, while not much difference was observed on the tension-compression side. For the hard skin aluminum sandwich laminates, the limit strains improve only on the tension-compression side of the forming limit diagram when the thickness of the polypropylene layer is increased.

Springback behavior of monolithic Al sheets and Al/PP/Al laminates are studied by draw-bending flat blanks into U-channels, a method defined in Numisheet '93. The study includes numerical and experimental work. The drawn U-channel when removed from the tools shows an angular change in the vertical wall and flange area along with a sidewall curl. Lower wall angle, higher flange angle and higher radius of curvature indicate an improvement in springback. Since springback changes the final dimensions of a formed part, it is an undesirable phenomenon and optimal parameters that show a reduction in springback are sought after.

For the Al/PP/Al sandwich using annealed aluminum skins, the following conclusions are derived. With increasing laminate thickness, the springback behavior decreases; however, at very high thicknesses, a very small change is observed. At a constant core thickness, increasing the skin thickness by a small amount shows improved springback behavior. For a constant skin thickness, increasing the core thickness initially reduces the springback; but at very high core thicknesses, the springback increases. This is attributed to very high effective plastic strains in the skins, which in turn causes higher elastic recovery and higher springback. For equal bending stiffness, the sandwich laminate shows higher springback than single aluminum sheets.

Comparing two finite element modeling approaches used in the springback study, the Part_Composite feature using a single shell mesh and a model including shell elements for the skins combined with solid elements for the core layer shows that the former model gives values closer to the experimental results and includes lower computation time. In comparing material

models, the material model using isotropic hardening with Barlat 2000 yield, shows the closest wall angle to the experiment. Material model using Yoshida-Uemori hardening with Hill 1948 yield criteria shows flange angle closest to experimental values. The finite element model predictions of springback values are in close agreement with the experimental springback values.

A larger die radius-and higher friction can be used to reduce the springback of an Al/PP/Al sandwich laminate. Since the punch radius only has a positive effect on springback in the flange angle and radius of curvature, it may be used as a factor to control springback in parts where the dimensional tolerance of the wall is high. The core thickness must be below a value of 1.6 mm to have reduced springback when using skins in the thickness range of 0.2 mm – 0.25 mm. The skin thickness can be increased to attain lower springback. Sandwich laminates with cold-worked skin will exhibit higher springback behavior in comparison to laminates made with annealed skins. Therefore, the use of cold-worked aluminum is not recommended for tight tolerance applications.

Much of the forming and residual stress distributions in the Al/PP/Al laminates is similar to that of the single aluminum sheets, with the main difference being the discontinuity in the stress distribution at the interface of the aluminum skin and polypropylene core. With increasing skin thickness, at a constant core thickness, the stresses at the end of forming show an increasing trend at both the die and the punch corner. Doubling the core thickness, with a constant skin thickness also increases the surface stresses. At the mid-length of the vertical walls, the higher stresses are located in the polypropylene layer. However, through the entire thickness, the stresses are very close to zero and can be ignored. Residual stresses at the surfaces of the aluminum skins increase significantly when the core thickness is doubled. For constant core thickness, the stresses in the aluminum skins are nearly equal for the 0.2, 0.22 and 0.24 mm skins. Residual stresses in the aluminum skins at the punch corner are much lower than the residual stresses at the die corner.

The residual stresses in the polypropylene layer show a decrease with an increase in skin thickness at constant core thickness. At the die and punch corner, the residual stresses in a single aluminum sheet are slightly higher than the stresses in the Al/PP/Al laminate of equal thickness.

6.2 Intellectual Merit and Future Scope of Work

The findings of this research can be helpful in selecting the optimal process and computational parameters as well as core and skin thickness combinations when building sandwich laminates to achieve lower springback, and therefore, high dimensional accuracy of the formed parts. The residual stress behavior provides insight into the load carrying capabilities of the formed parts during their applications. Desired formability of the sandwich laminates can be achieved by adjusting the thickness combinations of the skin and core layers. The advantages of sandwich laminates of the type investigated here are their weight saving potential and high stiffness-to-weight ratio compared to the over the monolithic skin material. By controlling the core-to-skin ratio in the sandwich laminates, it will be possible to maintain these advantages, yet achieve higher formability, better dimensional accuracy, and lower residual stresses.

Future work should aim to study the change in forming and springback behavior of sandwich laminates that include a higher volume fraction of the skin material. Such laminates may contain viscoelastic layer that can be used in noise and vibration attenuation. Investigations can be made into the draw-bending characteristics when steel skins are used in place of aluminum. Shear stress distributions through the thickness of the laminate after draw bending of the U-channel can also be explored further. An optimization study can be done to determine the core-to-skin thickness combinations in the sandwich laminates that are light in weight and give high formability and low springback.

Appendices

Appendix A Determination of Finite Element Parameters for Springback Analysis

The process of finding the finite element model parameters that can give an accurate prediction of springback values and residual stress distributions after draw-bending of U-channels with single aluminum (AA5182-O) sheets is described. The parameters investigated are the number of through-thickness integration points, integration rule, adaptive meshing and mass scaling. Five different cases are considered, each for a 1.2 mm thick single aluminum sheet. The finite element model is the same for these case studies, except for the parameters that are being investigated. It is described in Chapter 4. Residual stress distributions are displayed and the force equilibrium condition to validate the residual stress distribution in each case is checked.

Case I: This model contains 7 through-thickness integration points, uses Gauss quadrature integration rule, and does not use adaptive meshing, mass scaling is included.

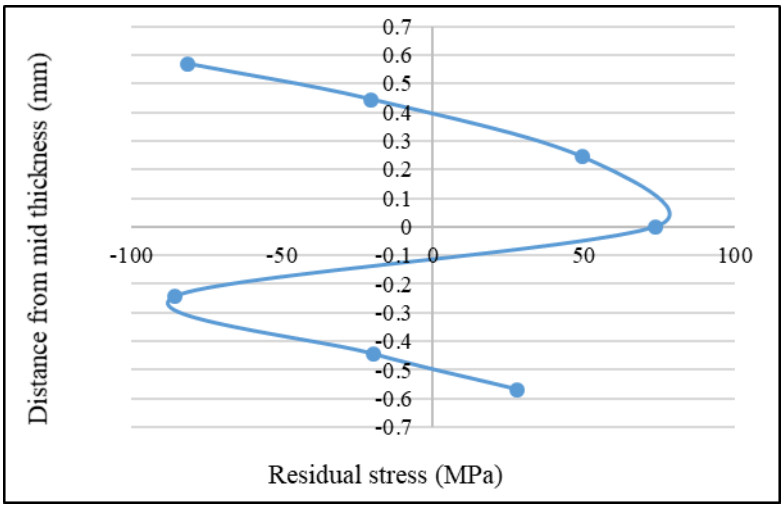

Figure A-1: Residual stress distribution - Case I

Case II: This model contains 9 through-thickness integration points, uses Gauss quadrature integration rule, and does not use adaptive meshing and mass scaling.

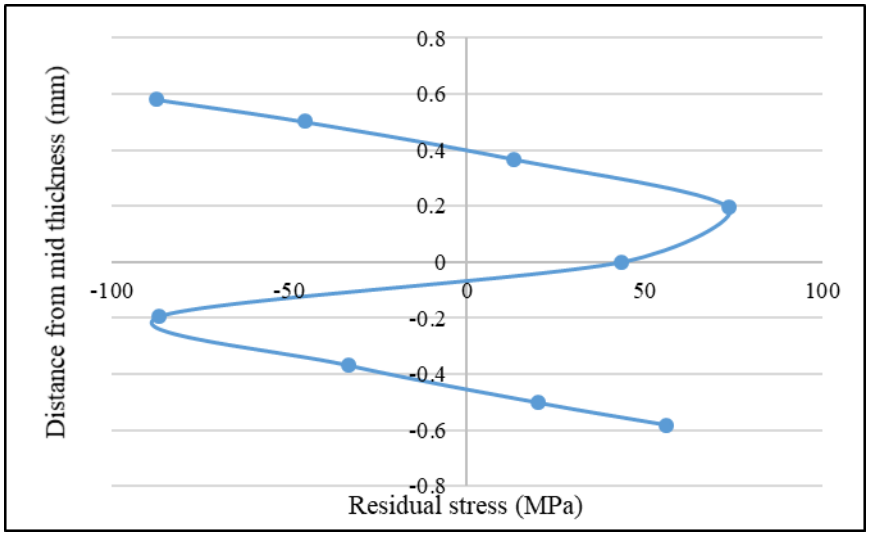

Figure A-2: Residual stress distribution - Case II

Case III: This model contains 9 through-thickness integration points, uses Gauss quadrature integration rule, includes adaptive meshing, does not use mass scaling.

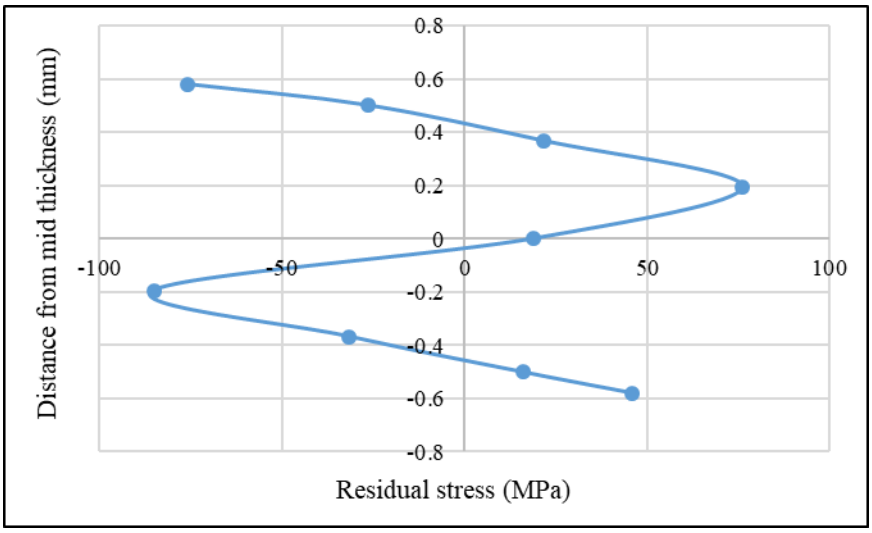

Figure A-3: Residual stress distribution - Case III

Case IV: This model contains 9 through-thickness integration points, uses Lobatto integration rule, includes adaptive meshing and does not use mass scaling.

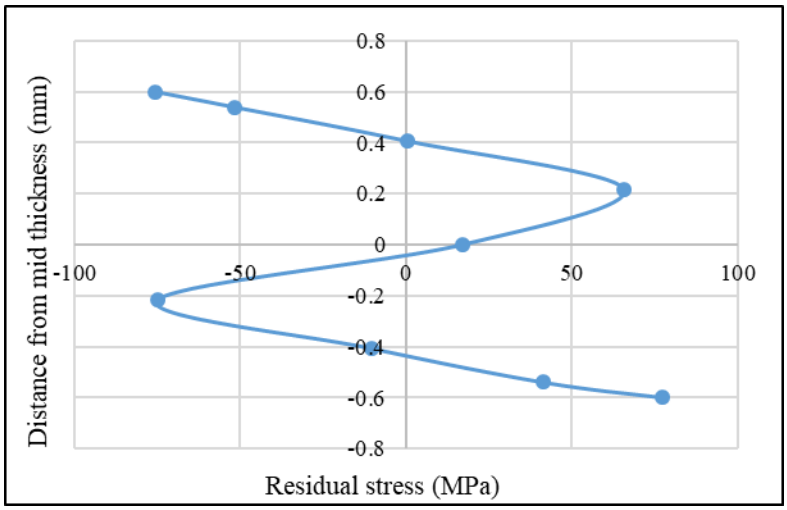

Figure A-4: Residual stress distribution - Case IV

Case V: This model contains 9 through thickness-integration points using Trapezoidal integration rule, includes adaptive meshing and does not use mass scaling.

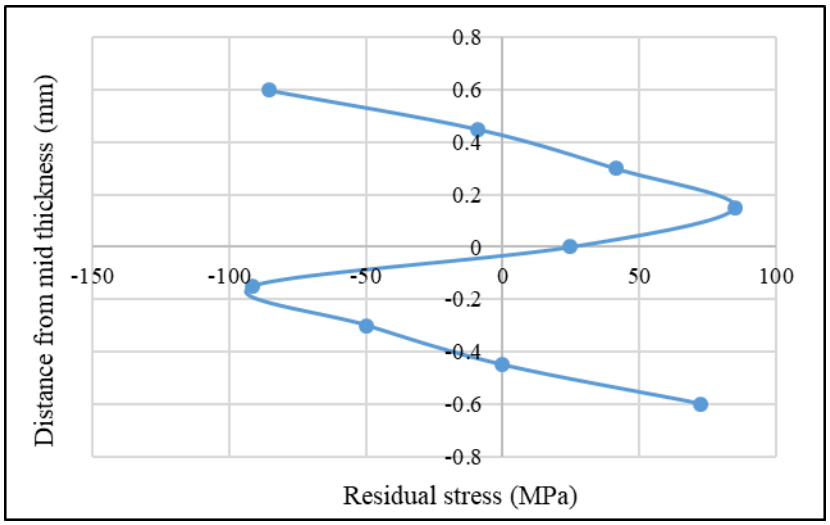

Figure A-5: Residual stress distribution - Case V

The condition for equilibrium is checked for each of the five cases. The force balance is checked such that the difference in areas under compression and tension (Figure A-6) are equal proving the accuracy of the springback results. The quality of the results is quantified by the

fraction of area unaccounted for under the residual stress-strain curve. The results are tabulated in Table A-1

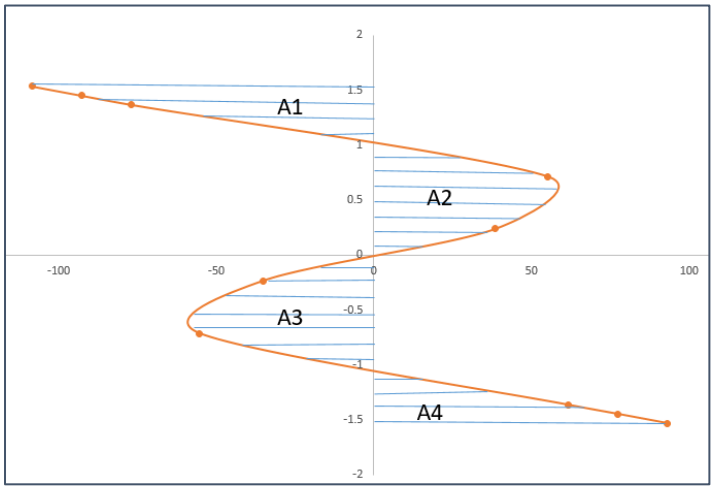

Figure A-6: Area sub-division under residual stress distribution

From figure A-6, we have

$$A1 + A3 = Ac \text{ and } A2 + A4 = At$$

where, Ac is the area under compression and At is the area under tension, and for equilibrium,

$$Ac = At$$

Table A-1: Check for equilibrium condition for different case studies

Case	Ac	At	Difference (d)	Percentage of area unaccounted (d/ Ac+At) x 100
I	23.646	22.8357	0.8103	1.74%
II	25.4921	24.9195	0.5726	1.13%
III	23.6225	23.983	0.3605	0.75%
IV	22.37	21.8059	0.564	1.27%
V	26.087	24.415	1.672	3.31%

Based on the results obtained in Table A-1, all cases are near equilibrium. The most accurate result is attained from case III, which uses Gaussian integration rule. The Gauss quadrature rule does not include integration points at the outer surfaces of the shell element. The

location of the integration points through the thickness of the shell element is based on the integration rule. The location of these points in LS-DYNA are as defined in Table A-2.

However, since it is of importance for this analysis to know the stress values at the surface extremes, using Lobatto integration is more suitable. Therefore, Case 4 is used as the final model.

Table A-2: Location of integration points (LS-DYNA) for a 1.2 mm thick shell element

Integration Rule	Lobatto 9 points	Gaussian 9 point	Gaussian 7 points	Trapezoidal 9 points
1	-0.6	-0.58089612	-0.5694648	-0.6
2	-0.5398548	-0.50161866	-0.44491872	-0.45
3	-0.40631178	-0.36802284	-0.24350712	-0.3
4	-0.2178705	-0.19455204	0	-0.15
5	0	0	0.24350712	0
6	0.2178705	-0.19455204	0.44491872	0.15
7	0.40631178	-0.36802284	0.5694648	0.30
8	0.5398548	-0.50161866		0.45
9	0.6	-0.58089612		0.6

Table A-3: Comparison of springback angles

Case	Integration points	Integration rule	Adaptive Mesh	Theta 1	Theta 2
I	7	Gaussian	×	98.507	80.92
II	9	Gaussian	×	102.768	79.564
III	9	Gaussian	✓	99.228	82.998
IV	9	Lobatto	✓	98.639	83.017
V	9	Trapezoidal	✓	98.841	81.389

Since case III and case IV are very close in predicting springback wall and flange angles, the use of case IV is considered reasonable.

Appendix B Bolt Torque Calculation

Calculation of the torque required to apply the blank holder force through the clamping load on each bolt is explained in Appendix B. All tools are made of steel. Zinc coated M5 bolts connect the blank holder to the lower die. A sufficient width is present so that the specimen slides between blank holder and lower dies without lifting off the tool. Force applied by the weight of the blank holder is calculated below.

Density of the material used for blank holder

$$\rho = 7.8\ g/cc = 0.0078\ g/mm^3$$

Dimensions of the blank holder are 55 mm* 70 mm* 15 mm.

Mass m = ρ* V where, V = volume of the blank holder

$$m = 0.0078*55*70*15 = 450.45\ g$$

Weight w = $m * g = 450.45g * 980\ mm/s^2 = 4.41\ Kg\text{-}m/s^2$

Therefore, Force $F = 4.41\ N$

Load on each bolt, $P = 625\text{-}4.41 = 620.59\ N$

The torque (T) needed to apply the bolt load P on each bolt is given in Ref. [1] and is calculated below.

$$Torque\ (T) = \mu * P * D = 0.15 * 620.59 * 0.005 = 0.465\ N\text{-}m$$

where, D = Diameter of the bolt used and μ = Coefficient of friction

Reference

[1] J. Greenslade, “What is the proper torque to use on a given bolt.” Zero Products Inc., [Online].Available: https://www.zerofast.com